STUDIES OF THE WALL JET CELL AS A

DETECTOR FOR HIGH PRESSURE LIQUID CHROMATOGRAPHY

by

Haritharan Gunasingham   B.Sc. A.R.C.S.

A Thesis Submitted for the Degree of Doctor of Philosophy

of the University of London

Chemistry Department   May 1978

Imperial College of Science and Technology

London SW7 2AY

ABSTRACT

This thesis is concerned with the evaluation of the wall-jet cell with particular reference to its use as a voltammetric detector for high pressure liquid chromatography.(HPLC).

Suitable electrode materials are investigated for use as electrode materials and the effects of the surface state on electrode performance are studied.

The hydrodynamic parameters of the wall-jet cell are calculated and the equations for the hydrodynamic boundary layer and diffusion layer thickness derived. Experimental verification of the limiting current equation is given.

Finally the efficacy of the wall jet cell in HPLC detection is demonstrated. A number of specific determinations are given in environmental and biomedical analysis. The use of non aqueous solvents is demonstrated.

i

ACKNOWLEDGEMENTS

H. Gunasingham

TABLE OF CONTENTS

PREFACE

PREFACE

The development of continuous monitoring electrochemical detectors requires consideration of a number of factors:

i) the electrode material; bearing in mind the need to couple high electrocatalytic activity (high exchange currents) with stability and reproducibility.

ii) electrode geometry; affording maximum mass transfer under well defined laminar flow conditions.

iii) compatibilty with system to which it is to be coupled; in this case, high pressure liquid chromatography.

iv) instrumentation ; namely, potentiostatic control, with fast response times and high signal/noise capabilities.

The work that is presented in this thesis attempts to investigate the first three of these points. (iv) having been already dealt with by earlier workers has been given little comment.

That two chapters have been devoted to aspects of solid electrode voltammetry must reflect the importance of the working electrode material. In fact it could be said that it is the heart of any electrochemical detector, for not only is/it required to have an electrode reaction take place but it must take place reproducibly over long periods of use (as would be required in HPLC detection). In this context the state of the electrode surface becomes a critical factor. Thus the first two chapters is basically a study of the influence of the electrode surface on the electrode reaction. In particular, the study considers glassy carbon (chosen for its superior electrocatalytic properties) surface phenomena.

1

The third chapter investigates the hydrodynamic parameters of the wall-jet cell. Though a limiting current equation has been derived for a general wall-jet configuration, there has been no attempts at calculating the boundary layer and diffusion layer thickness. This has been attempted in this chapter.

Finally, the remaining chapters of the thesis are devoted to examining the efficacy of the wall-jet cell as a detector for HPLC. A number of specific determinations have been given in order to demonstrate the range of its application.

One possible criticism is that some of the chromatograms are not as well resolved as would have been hoped. This has been due to the constraints of having a limited supply of the correct columns.

Apart from this it is hoped that the objective of showing the wall-jet cell to be ideally suited to HPLC detection has been achieved,

CHAPTER I   SOLID ELECTRODE VOLTAMMETRY

1.1 Introduction

Considering the analogy with heterogeneous chemical reactions, an electrode may be viewed as a catalyst with the added function of serving as a source (during electronation) or sink (during de-electronation) for electrons. The term electrocatalysis has been coined to describe this phenomena.

There has been some evidence that the solid state properties of electrode materials exert an influence on its electrocatalytic activity (1-4). For instance in the case of the noble metals the exchange current density for the oxidation of ferrocyanide has been found to be related to the work function of the metal (4).

Another factor which may influence the rates of electrode processes is the state of the electrode surface. The electronic and structural properties of the surface can vary significantly from the bulk material. This is mainly due to the termination of the solid crystal lattice resulting in surface atoms with unsatisfied valencies (dangling bonds). These atoms can serve as reactive sites for impurities, products of electrolysis etc. While in many cases adsorption of material on electrode surfaces leads to inhibition of the electrode process, there are several examples where it has resulted in enhancement. This is examined in more depth in the next chapter.

This chapter investigates the surface phenomena of glassy carbon. This new form of carbon (made first in 1963 (5)) has good electrocatalytic properties and is well suited for continuous monitoring

applications. An interesting feature of glassy carbon surfaces is due

to the presence of covalently bonded redox centres formed as the result

of oxygen chemisorption. These centres have been found to have a

significant influence on the electrode process.

1.2 Problems of Solid Electrode Voltammetry

1.21 Surface Contamination

One of the advantages of the dropping mercury electrode

lies in a readily renewable surface. In the case of solid electrode

materials prolonged use invariably results in inhibition of the

electrode reaction and at times leads to total passivation.

Contamination is most often due to the chemisorption of

substances on the electrode surface. We can, for the sake of convenience,

distinguish between four different types of chemisorption which can

lead to inhibition of the electrode process:

> (i) adsorption of products of electrolysis
>
> (ii) polymeric film formation
>
> (iii) oxide film formation
>
> (iv) doping

In (i) and (i), inhibition results primarily as a consequence

of having less surface available for further electron transfer. Polymeric

film formation is common in phenol oxidation (6,7).

The formation of oxide films can be treated separately from

(i) and (ii) as it is in effect a reaction of the electrode surface with

water, dissolved oxygen etc. The degree of surface oxidation depends on

the pH , oxidation potential and the nature of the solution. In the case

4

of massively oxidised electrodes total passivation of the electrode process can occur.

Doping can be considered to be a mechanism by which surface states are introduced into the electronic band structure of the surface by the adsorption of trace amounts of material. This is a common mechanism for semiconductor electrodes.

1.22 Capacitance

In comparison with mercury, solid electrodes generally have a higher double layer capacitance. This can be related to the build up of point charges on uneven surfaces. In the case of mercury, being a liquid, cohesive forces produce smooth surfaces resulting in very much less charge build up.

The limitation of high capacitance is in the main restricted to time dependent techniques such as cyclic voltammetry and pulse methods. In the case of time independent techniques such as hydrodynamic voltammetry this is not such an important consideration.

1.23 Potential Limits

Whereas solid electrodes have the advantage of a large anodic range, on the cathodic side a low hydrogen overpotential (in aqueous solutions) precludes their use for most electroreductions.

One technique which has proved satisfactory in extending the cathodic potential range involves plating insitu a thin film of mercury onto the solid substrate. This approach appears to work well in the case of Anodic Stripping Voltammetry (8,9). It has also been used in HPLC detection(10).

5

1.3 Choice of Electrode Material

In continuous monitoring applications an ideal electrode material must couple high electrocatalytic activity with long term stability and reproducibility.

In a study by Fleet et. al. (11), the conclusion was that glassy carbon gave higher current densities for the oxidation of ferrocyanide than any other electrode material. This view has been corroborated by some workers (12,13) and contradicted by others (14). The discrepency must be attributed to variations in the type of glassy carbon used by the different groups.

In this work it was found that while oxidation of ferrocyanide resulted in slightly higher exchange currents for platinum electrodes, in the case of organic oxidations involving proton transfer,(for example the oxidation of hydroquinone) glassy carbon proved to be a better material .. The same was found to be true for a number of ireversible organic electrode reactions (for example, oxidation of phenols in acid media). This is discussed in greater detail in chapter 2.

Practically, long term stability and reproducibility means minimum surface contamination. The biggest cause for concern is surface oxidation. In the case of the noble metals (platinum or gold), if the electrode potential is greater than +0.6 V vs SCE rapid oxidation of the surface occurs which can lead to passivation of the electrode. Glassy Carbon in contrast forms oxides only at edges of graphite planes. As a result it shows a very much better stability of response. This is discussed in greater detail in chapter 2.

Table 1-1 summarizes the working characteristics of some electrode materials. It can be seen that glassy carbon has the best all round characteristics for continuos monitoring applications.

Electrode	Anodic Range	Cathodic Range	E_p / $Fe(CN)_6^{4-}$	Comments
Pt	+1.25	–	0.35	rapid oxidation of surface at potentials $>0.6V$
Au	+1.5	−0.2		
glassy carbon	+1.5	−0.5	0.33	
graphite	+1.19	−0.24	0.35	
carbon paste	+1.30	−0.90		cannot use in non aqueous solvents
B_4C	+1.13	−0.90	0.35	
Pd	+1.4		0.40	

pH= 1

Table 1-1

1.4 A Study of Glassy Carbon Surface Phenomena.

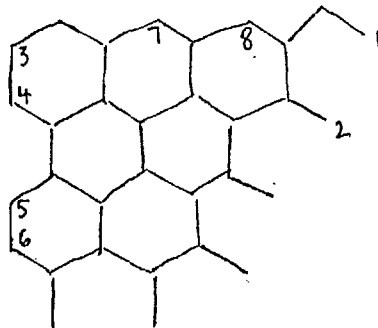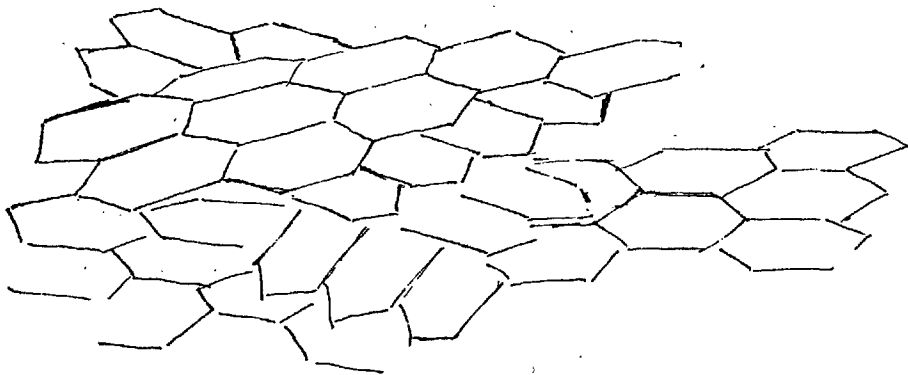1.41 The Structure of Glassy Carbon.

Figure 1-1

Diamond and graphite are two forms of carbon which have been completely characterised. Graphite structure can be described as a system of infinite layers of fused hexagons, held together by weak Van der Walls forces. In contrast, glassy carbon has been described as consisting of packets of randomly orientated graphite like structures (15). The extreme hardness and strength is attributed to tetrahedral cross linkages between the hexagonal layers (16). The growth of cone structures within the graphite lattices has been described but can be presumed unlikely in the case of glassy carbon owing to the compact nature of the material.

Functional group formation is found at free valence carbons at the edges of graphite layers (17-19). Free valencies may also be formed by the rupture of adjacent carbon-carbon bonds due to mechanical grinding. Three types of boundary situations can be distinguished at the edges of garphite layers (see figure 1- 1):

i) isolated unpaired electrons in sp^2 trigonal orbitals at the tails of boundary atoms 1 or 2.

8

ii) the straight edges distort and pairs of adjacent atoms are displaced inwards to form linear boundaries- for example atoms 3 and 4 or 5 and 6. The previously described sp^2 hybrid orbitals now become $2p_x$ atomic orbitals and can be paired together to form an additional bond. Thus edge bonds may acquire a partial triple bond character.

iii) isolated edge atoms, for example atoms 7 or 8, may revert to a divalent state acquiring s^2p^2 character.

THE RANDOM STRUCTURE OF GC.

Figure 1-2

1.42 Electronic Properties

Graphite has been described as a semi metal in which the highest filled valence band overlaps the lowest empty conduction band by 50 - 60 meV (20). Glassy carbon however apparantly shows semiconductor properties (21-22) with valence and conduction bands separated by a few milli electronvolts.

9

The electrons around the carbon nuclei are arranged into two bond types; namely, s^2p^2 hybridized orbitals (σ bonds) in the basal plane and p_z orbitals (π bonds) in the c plane.

It is well established, both experimentally and theoretically that the valence band of graphite (and thus glassy carbon) arises from bonding π orbitals and the conduction band from anti bonding π^* orbitals (23).

1.43 The Nature of Surface Groups

The studies into C-O surface functionalities of various carbon material, including carbon black, pyrolytic carbon and glassy carbon have been reviewed by Panzer and Elving (24). Since then there has been only a few more papers which have been published on this topic.

The existance of quinone, hydroquinone, semiquinone, phenolic, carboxyl and lactone functionalities have been mentioned as occuring on carbon surfaces (25-39). Under special conditions hydrogen bonded interlayer groupings have also been suggested.

One of the early accounts of structures of C-O functionalities is due to Boehm (25). In this work it was suggested that the oxidation of microcrystalline graphite at elevated temperatures leads to the formation of acidic surface oxides or in the presence of water, hydroxides. four types of acidities were described: strongly acidic, weakly acidic, phenolic and carbonyl, (see figure 1-3).

Additionally Hennig (26) proposed the existence of carbonyl and ether groups (see figure 1-4).

10

I&II carboxyl

III phenolic

IV carbonyl
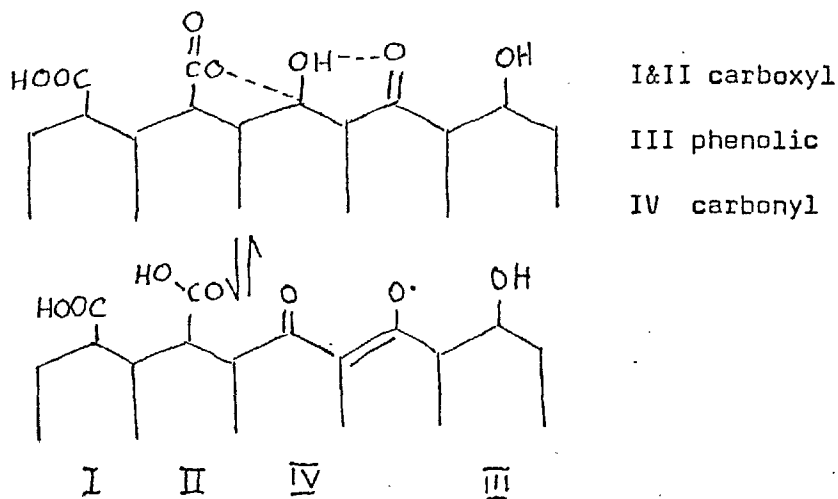
Figure 1-3 (From Boehm (25))

Figure 1-4 (From Hennig (26))
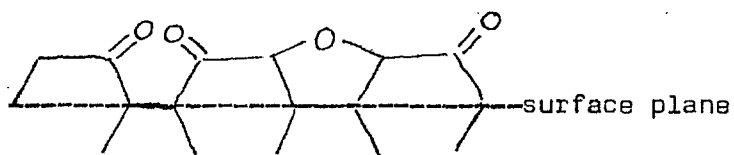
1.44 Experimental Evidence for the Existance of C-O Functionalities

The quinone/hydroquinone couple

The existance of quinone functionalities on carbon surfaces has been one feature of carbon surface activity which has gained considerable comment, Electrochemical evidence for the existance of a quinone/hydroquinone redox couple has been given by several workers (29-35).

11

The overall redox couple may be represented by the following equation.

$$Q + 2H^+ + 2e \rightleftarrows H_2Q$$
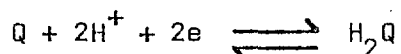
In a recent paper Laser and Ariel (29) substantiated the existance of this couple by cyclic voltammetry. In fact two distinct oxidation and reduction regions were identified.

i) a redox couple due to the chemisorption of oxygen (the quinone/hydroquinone couple) represented by:

$$C + H_2O \longrightarrow C(O)_{CHEM\ ADS} + 2H^+ + 2e$$

$$C(O)_{CHEM\ ADS} \xrightleftharpoons{H^+ + e} C(OH)_{CHEM\ ADS}$$

(the quinone couple)
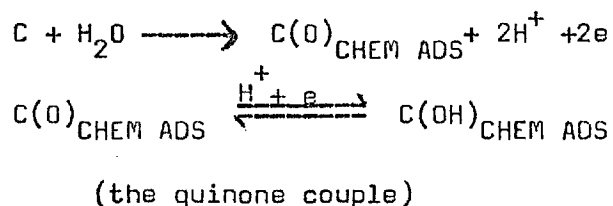
ii) an irreversible couple due to the reaction of existing surface groups.

Among the conclusions that were arrived at was that once the reversible couple was formed by electrode oxidation it is not removable by reduction. The magnitude of couples i and ii depends on how positive the anodic scan is taken.

Other functional groups

Evidence for the formation of other functionalities, most notably carboxyl groups, has been given by Boehm (36). These groups are however not easily discernable by electrochemical techniques and studies were based mainly on chemical and spectroscopic methods (37). These groups are probably formed under more severe oxidation conditions.

12

It may well be that the irreversible couple of Laser and Ariel, mentioned earlier, is due to the formation of carboxyl groups.

The occurance of lactone groups has also been described by Blurton et. al. (38,39). The formation of these groups was believed to result in the broadening of the cyclic voltammogram of the glassy carbon. In this work it was found that such broadening occured under more severe oxidation conditions.

Broadening of cyclic voltammograms could also be due to hydrogen bonding between surface functionalities.

Chronopotentiometric Studies

The technique of constant current charging known as chrono-potentiometry has provided some of the most convincing evidence for the presence of oxygen films on platinum electrodes (40,41). In view of this the anodic and cathodic 'charging characteristics' of glassy carbon were studied to establish conditions for the formation of surfacegroups.

The charging currents used were 10 uA and less. Low charging currents were used in order to minimize the effect of double layer charging.

Experimental:

Chronopotentiometric studies were carried out with glassy carbon supplied by Plessy (England) and Tokai (Japan). The diameters of the carbon was 3mm and 2mm respectively.

A model PAR 173 potentiostat was used as the current source together with a model 178 electrometre probe to follow the potential.

All reagents were of analar grade and used without further purification. Solutions were bubbled with purified nitrogen for an average of fifteen minutes before each run. During the course of the run an atmosphere of nitrogen was maintained above the solution.

Glassware had been previously cleaned with concentrated nitric acid and leached with distilled water for 24 hrs.

All potentials were measured against the saturated calomel electrode.

Results and Discussion

Study of Platinum:

A study of oxide formation on Pt is first given for the sake of comparison with studies of glassy carbon.

The nature of the interaction of oxygen with Pt surfaces has been the subject of a number of studies (40-43). One widely held view is that the adsorbed oxygen film is made up of hydrated oxide molecules such as PtO and PtO_2. In this work it was found that the constant current anodic curve shows two arrests: one at about 0.6 V and the other at +1.1 V (see figure 1-5). Following the reasoning of El. Waked end Emra (42) this corresponds to the formation of PtO and PtO_2 resp. Close to 0 V we have arrests corresponding to hydrogen desorption.

On the cathodic charging curve (figure 1-6) only one large arrest at about 0.5 V is evident. This arrest can be related to the reduction of Pt oxides formed during the anodic charging. The presence of only one arrest points to the instability of PtO_2 (42).

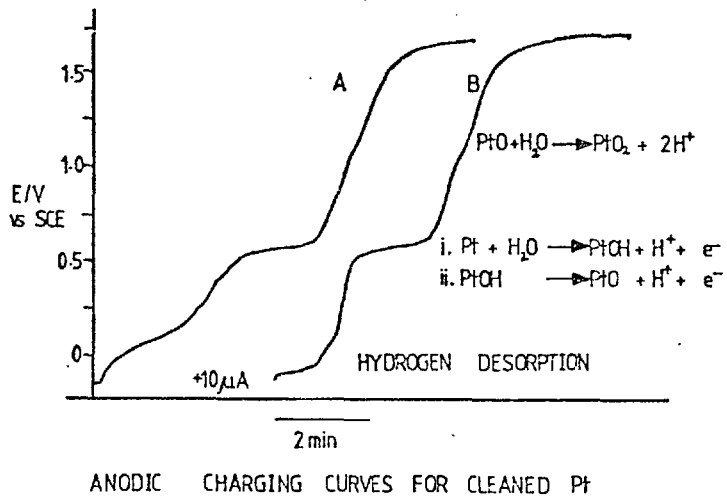ANODIC   CHARGING   CURVES FOR CLEANED Pt

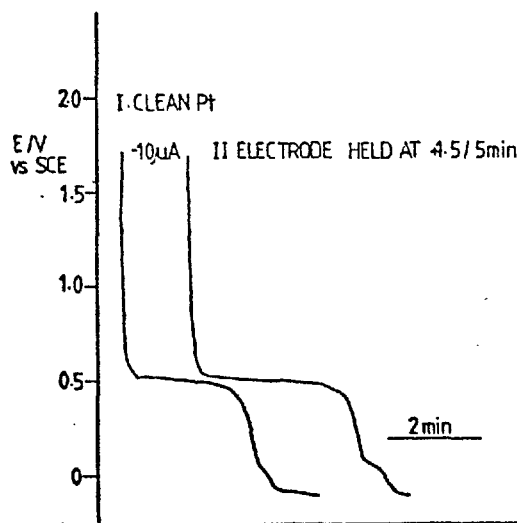Figure 1-5

TYPICAL   CATHODIC CHARGING CURVES

Figure 1-6

15

From the above chronopotentiograms it can be seen that the
use of small currents improves anodic and cathodic charging transients
as it reduces the effect of capacitance charging and the irreversibility
of the Pt-O redox system.

Study of Glassy Carbon

It is shown below that the surface activity of glassy carbon
depends to a large extent on the type of glassy carbon and the degree of
surface oxidation. Some glassy carbons are highly compact with a
higher degree of cross linking between adjacent graphite planes. In
such cases oxidation of surfaces is less likely as less free valence
carbons are available for reaction. Unfortunately the exact structure of
the glassy carbon used in this work was not available. However, it was
found that the glassy carbon made by Tokai was very much harder and more
difficult to polish than the Plessy GC. On this basis it is plausible
to assume that the former has a greater degree of cross linking and
thus a more compact structure. We would therefore expect a lesser degree
of surface C-O functionalities. This is in fact what was found.

Figure 1-7 shows anodic and cathodic charging curves of a
Plessy GC (GC 2) previously oxidised at +1.5 V vs SCE.

The ahodic charging curve is relatively simple showing a sharp
arrest at about +500 mV and a shallow arrest starting at +1250 mV. The
oxygen evolution potential begins at about 1800 mV.

The cathodic charging curve shows two arrests; at +900mV
and +400 mV before reaching hydrogen evolution potential at -800 mV.

ANODIC AND CATHODIC CHARGING CURVES FOR OXIDISED GC 2.
5M H₂SO₄
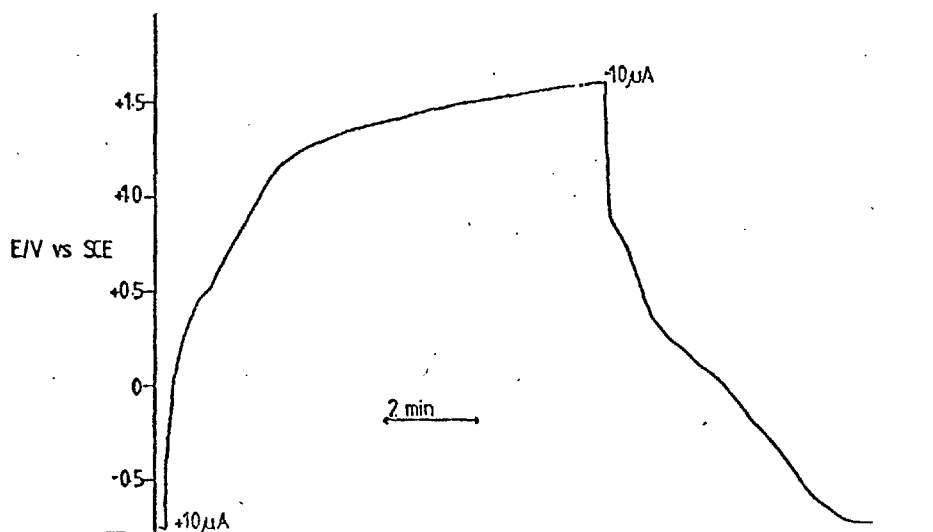
Figure 1—7

These results may be explained as follows:

i) the arrest at +500mV on the anodic charging curve and the arrest on the cathodic curve at +400 mV correspond to the quinone/ hydroquinone couple.

ii) the arrest starting at +1250 mV due to the irreversible oxidation of existing surface groups (cf. Laser and Ariel (29)) leading to the formation of carboxyl and lactone groups.

iii) the arrest at +900 mV was only noticed occasionally.

17

ANODIC AND CATHODIC   CHARGING   CURVES   FOR GC OXIDISED AT +1.5 V/ 3 min
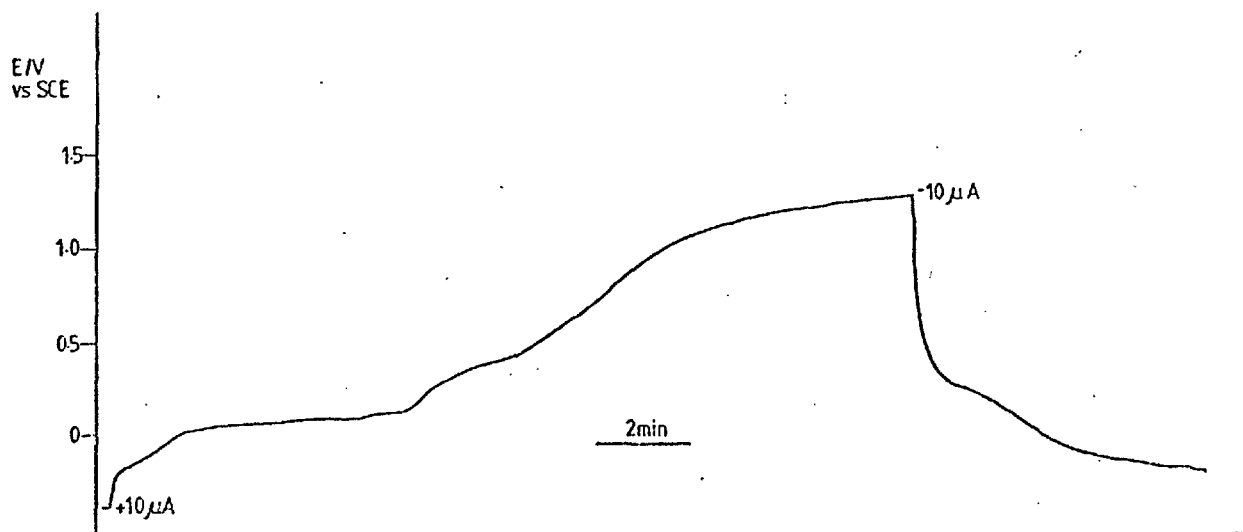5M H$_2$SO$_4$

Figure 1-8

The above figure shows the anodic and cathodic charging

curves obtained for a Plessy GC cut from a different stock piece to

the previous one (GC2). The electrode had been previously oxidised

at +1.5 V. The following points summarize the differences between

the two carbons:

i) the two arrests on the anodic charging curves found for

GC2 are greatly increased. Additionally the start of both arrests are

shifted to less positive potentials; namely 425 and 1125 mV.

ii) in contrast with the earlier case, two arrests are evident

close to 0 V on the anodic charging curve. These are probably due to

the desorption of adsorbed hydrogen.

iii) the cathodic charging curve reveals an arrest at +325 and a broad arrest starting at -200 mV. The former is probably due to quinone reduction and the latter due to hydrogen adsorption.
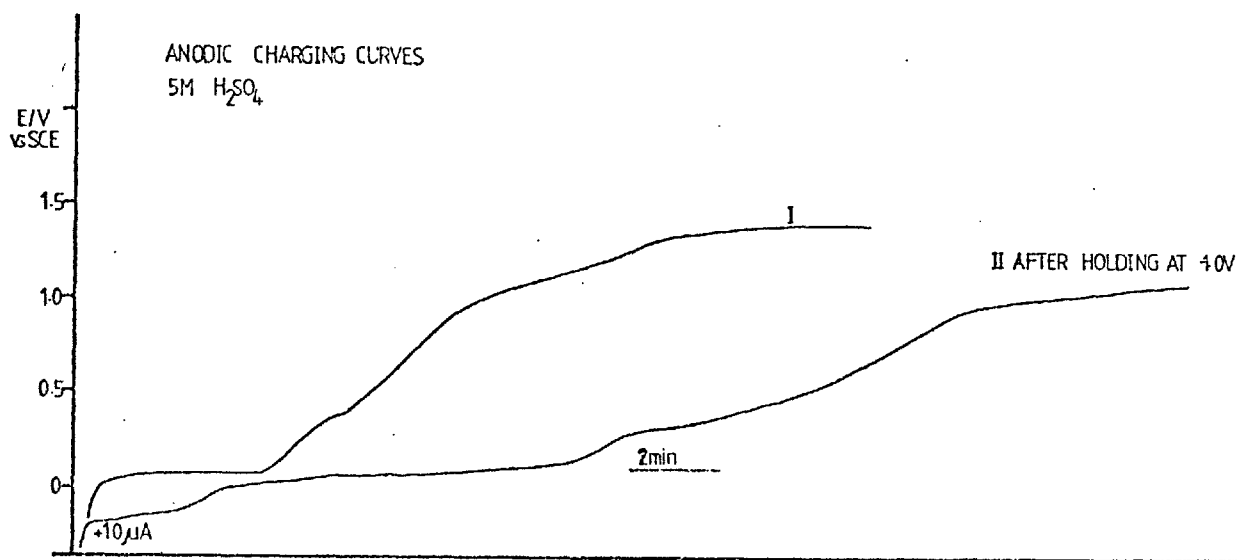
PLESSY GC 3

Figure 1-9

Effect of Hydrogen Adsorption:

In figure 1-9 above we have two cathodic charging curves; I oxidised at a potential of +1.5 V and II after holding at -1.0 V (i.e past the potential for hydrogen evolution). It can be seen that arrests due to the oxidation of hydroquinone groups and the irreversible oxidation of existing groups are greatly increased. Additionally, the two arrests due to the desorption of hydrogen are also increased.

19

TYPICAL ANODIC AND CATHODIC CHARGING CURVES FOR GC OXIDISED AT POTENTIALS >2.0V
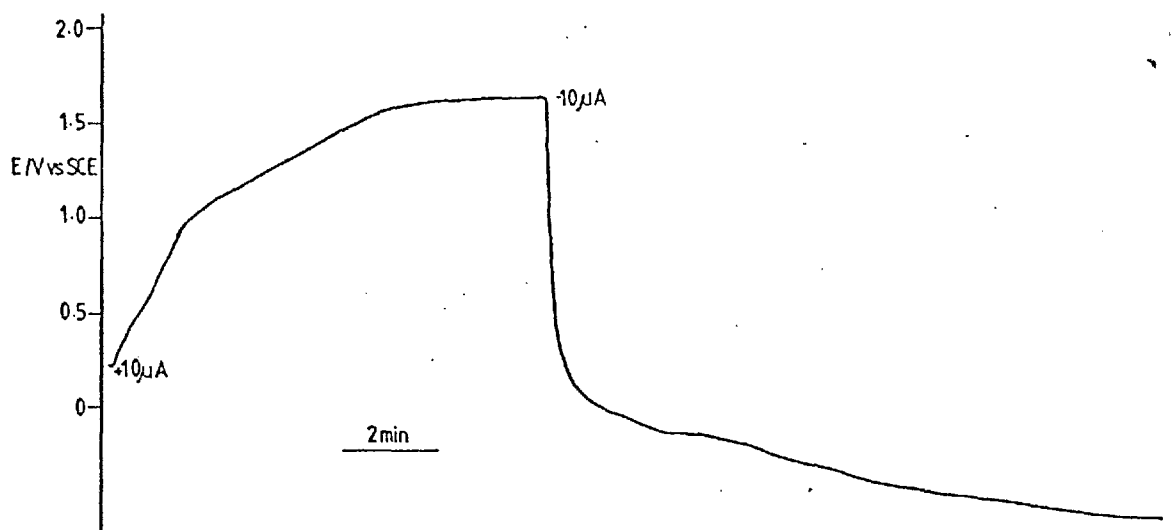
Figure 1-9b

Effect of Oxidation Beyond Oxygen Evolution Potential:

Oxidation of the GC surface at potentials greater than that for oxygen evolution (potentials greater than 1.8V) results in a distinct change in the cathodic charging curve.(see figure 1-9b). The arrest due to the reduction of quinone groups seems to be shifted, to more negative potentials giving a broad arrest starting at about 0 V.

The reason for this could be due to the addition of molecular oxygen to the double bond of the quinone structure to form peroxides as suggested by Garten and Weiss (27).

The duration of the cathodic arrest depends on how long the electrode is kept at the oxidising potential (see figure 1-10).

Figure 1-10

I POTENTIAL HELD AT +2.0V FOR
1min BEFORE CATHODIC CHARGING
CURVE RECORDED

II POTENTIAL HELD AT
+2.0V FOR 2 min

III POTENTIAL HELD
AT +2.0 V FOR 3min
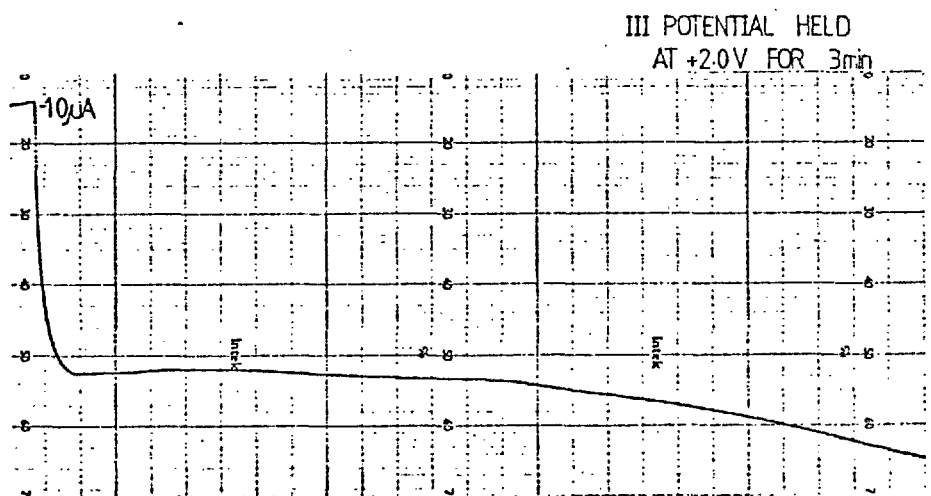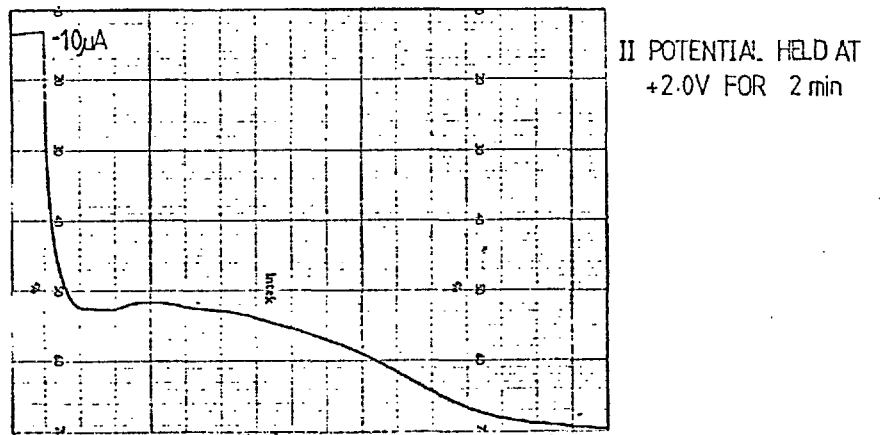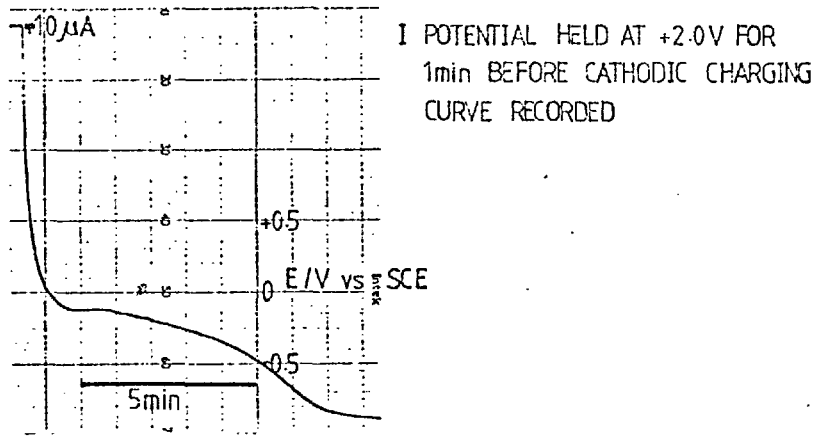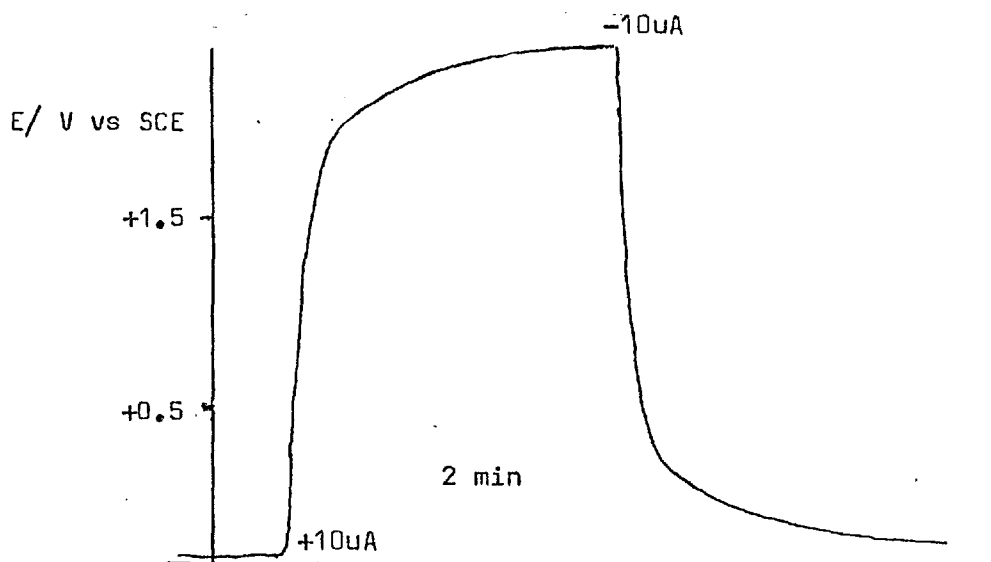
Anodic and Cathodic Charging Curves For Glassy Carbon(Tokai)

Electrode previously held at +1.5 Volts for 2 min.

Figure 1-11

The anodic and cathodic charging curves for the Tokai GC reveal very little surface functionalities. Additionally no arrests corresponding to hydrogen adsorption are apparant.

Cyclic Chronopotentiometry(CCP)

In this study chronopotentiograms were recorded in cyclic form (see figure 1-12).

From the fifth cycle, successive CCP's had the cathodic transient started st less positive potentials.

The first cyclic potentiogram shows on the anodic charging curve, arrests due to hydroquinone oxidation and the irreversible region before reaching the oxygen evolution potential. On the cathodic side a broad arrest starting at +200 mV is seen.
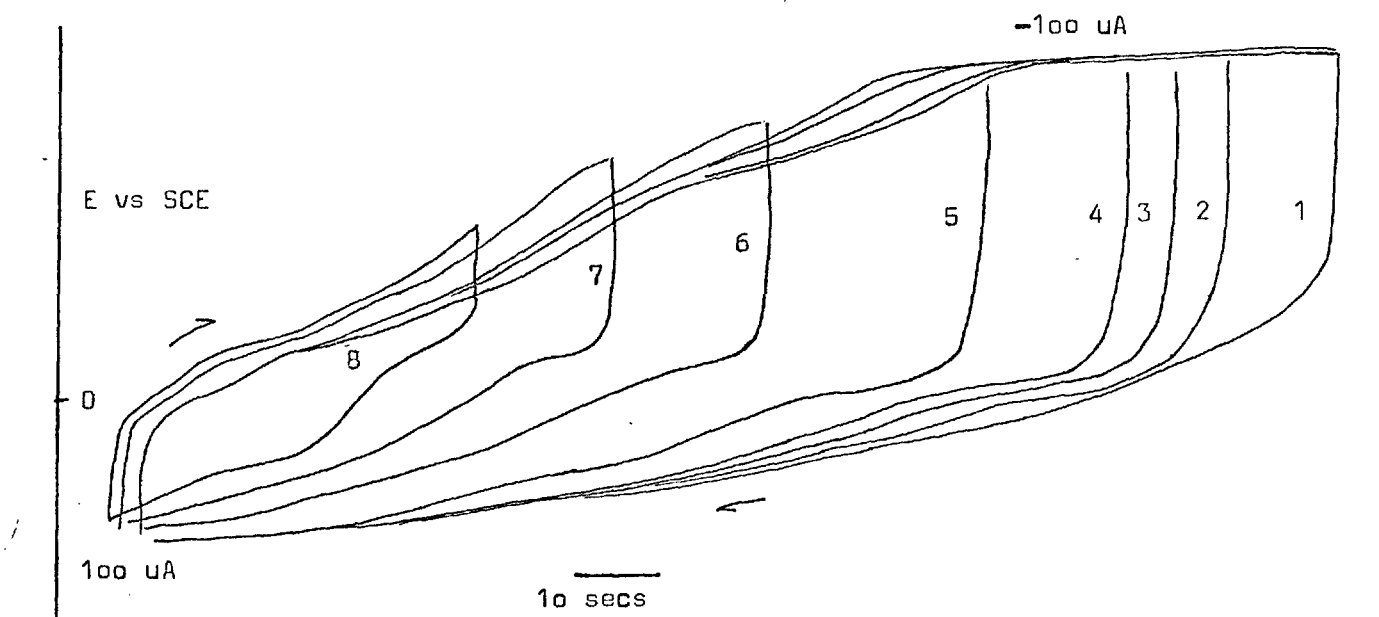
Figure 1-12

With successive CCP's (2-5) the cathodic arrest goes below
0 V and the anodic transient shows decrease in its arrests.

If the cathodic transients are started at less positive
potentials (CCP's 6-8) it is seen that the cathodic transient increases,
to the potential for reduction of quinoidal functionalities (about 400
mV).

The CCP's clearly show how oxidation at the potential of
oxygen evolution affects the cathodic charging curve. The mechanism of
peroxide formation seems a reasonable explanation for the effect. That
the cathodic transient reverts to its normal form when started below
oxygen evolution potential is probably due to the irreversible reduction
of the peroxide on the previous cathodic transient.

23

Cyclic Voltammetry

Experimental

Cyclic voltammograms were obtained using a model PAR 174 polarograph. Other experimental conditions were the same as for the chronopotentiometric work.

Cyclic Voltammetry of Glassy Carbon
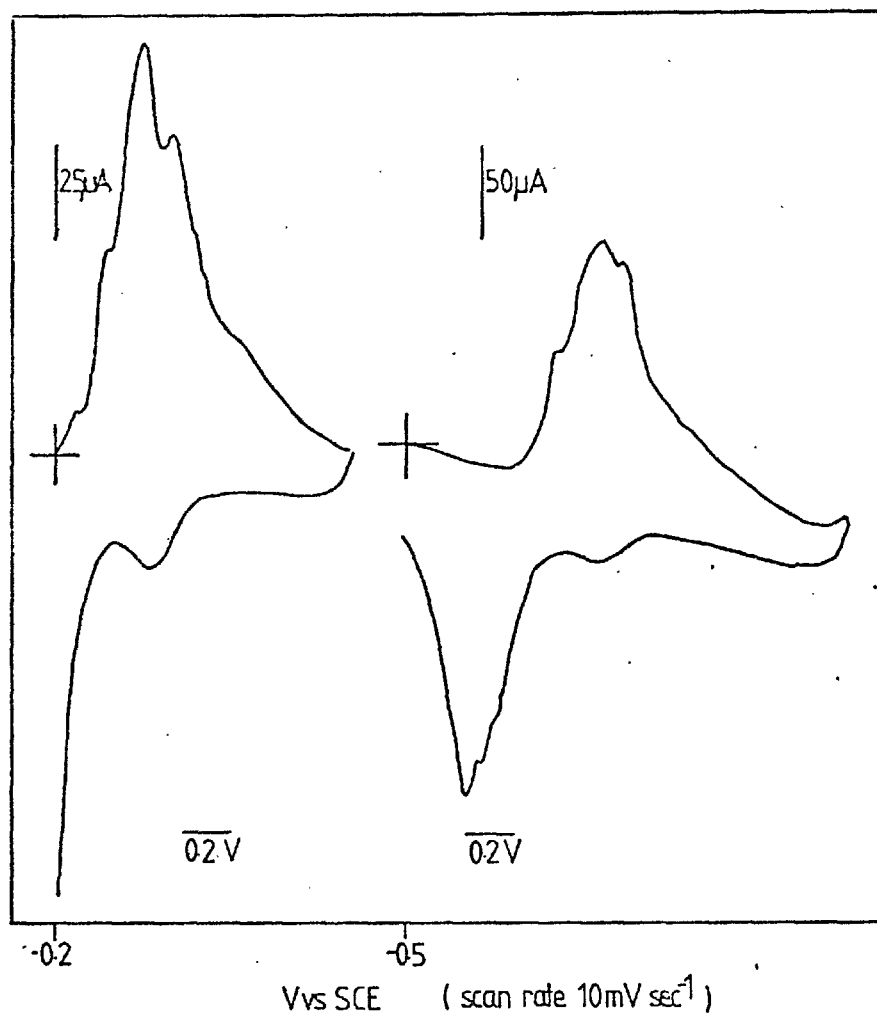
Figure 1-13

Cyclic Voltammogram of a Highly Surface Active
Glassy Carbon in 0.1 M H_2SO_4 (GC1)

Figure 1-13 shows a cyclic voltammogram of a highly oxidised glassy carbon (GC 1). The large number of peaks (0-0.3 V) are probably due to adsorbed hydrogen, lactone formation and hydrogen bonding. The two peaks due to the quinone/hydroquinone couple are barely seen.

The large peak starting at about 0 volts in the reverse, negative scan is due to the desorption of hydrogen; this correlates well with the earlier chronopotentiometric studies. The peak can be seen to be made up of actually 3 components. This could mean that hydrogen exists in a number of adsorbed forms (cf Pt),
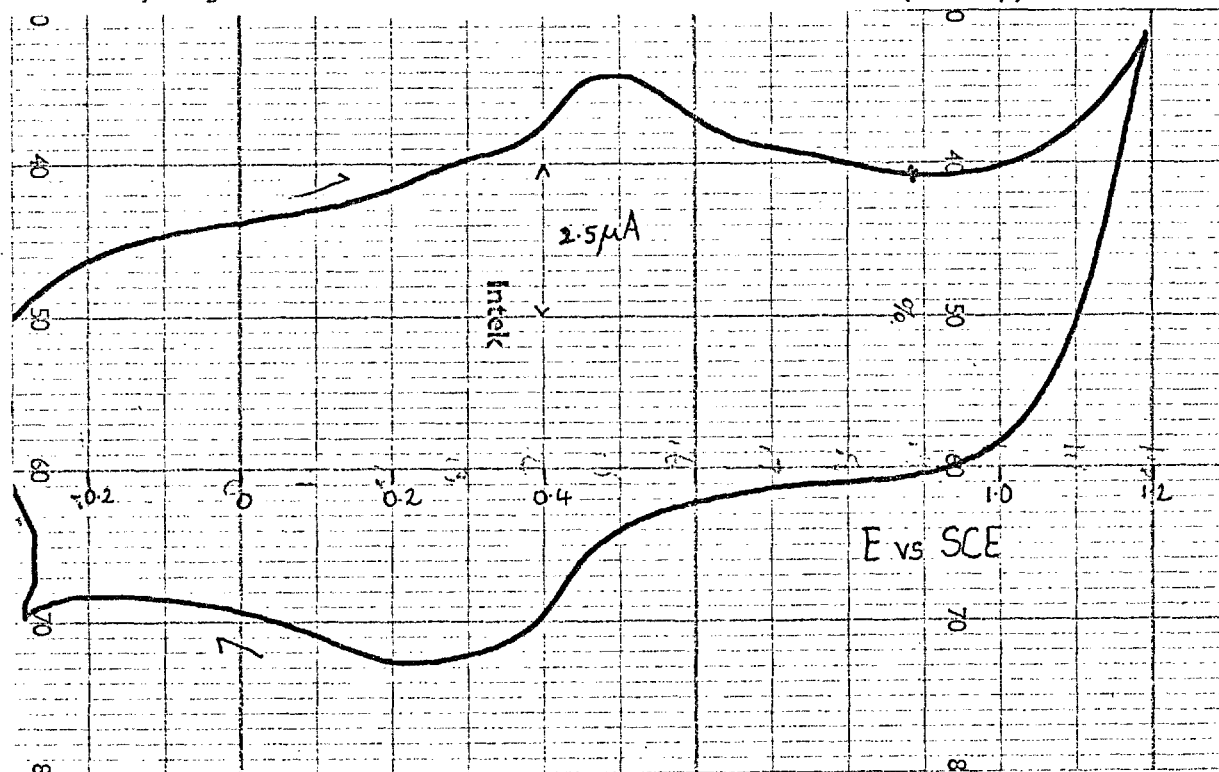
Figure 1-14

Cyclic Voltammogram of oxidised Plessy GC 2

1.0 uA

0.0

0.2V vs SCE
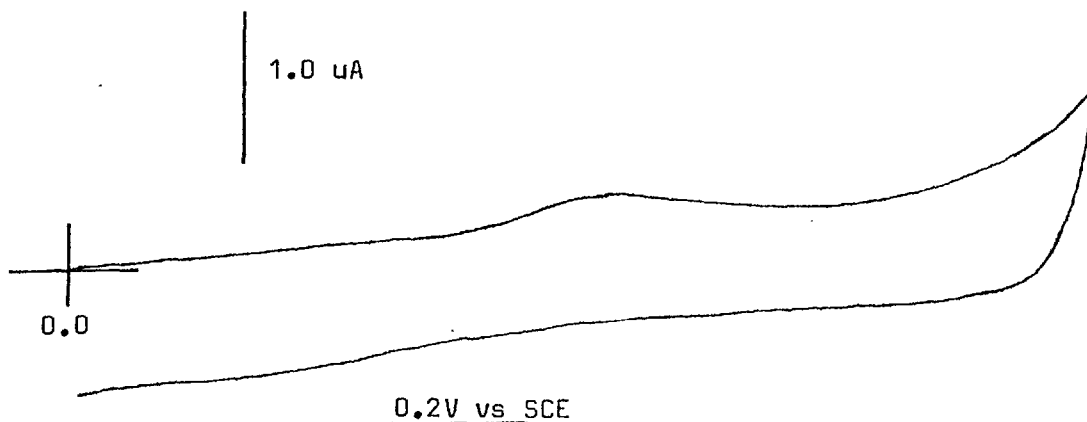
Cyclic Voltammogram of Tokai GC
20 mV/sec

The cyclic voltammogram of the Tokai GC, taken in 0.5M H_2SO_4 shows very little surface activity. This corresponds with the cathodic and anodic charging curves given earlier.

Conclusion

The surface activity of glassy carbon therefore depends both on the type of electrode material (i.e. degree of cross linking) as well as the degree of oxidation.

Tokai carbon shows very little surface activity compared to the Plessy GC. This has been described as being due to a higher degree of cross linking between graphite layers; as a result it has less free valencies at the edges of the graphite planes for oxygen chemisorption. This is further confirmed by the fact that Tokai GC is har der than Plessy GC.

One phenomena which was interesting is the change in the cathodic charging curve of Plessy GC when oxidised at potentials greater than that for oxygen evolution. This has been explained as being due to peroxide formation.

26

1.5 Double Layer Charging

One of the techniques which were devised to reduce effects
of surface adsorption was the use of an asymmetric pulse wave form
where the leading pulse is set at the working potential followed by
a pulse of shorter duration at the opposite polarity. The idea is to
strip off the adsorbed products of electrolysis (see chapter 2).

In this context it is important to investigate the influence
of surface groups on the charging current. This is attempted in this
section.

The time taken to charge a double layer is of the order of
10microseconds (41). Therefore, a plausible technique for assessing the
charging current is to measure the instantaneous current when a potential
is applied.

Figure 1-15 shows charging current decay curves obtained
for different glassy carbon electrodes. GC1 (the cyclic voltammetry
of which corresponds to figure 1-13) shows a very much higher capacitance
current when compared with the other GC's and Pt. The effect is clearly
due to the oxidation of surface functionalities and the desorption of
hydrogen. Thus the charging current consists largely of a faradaic
contribution.

The magnitude of the other charging decay curves reflect the
degree of surface oxidation and hydrogen adsorption. GC 2 , the surface
as shown earlier, has mainly quinoidal functionalities and very little
hydrogen adsorption(cf. figure 1-14) has a low charging current
which decays to the residual level in a very much shorter time.

CURRENT DECAY CURVES FOR ELECTRODES
CHARGED TO 0·8V vs SCE IN 0·1M H_2SO_4
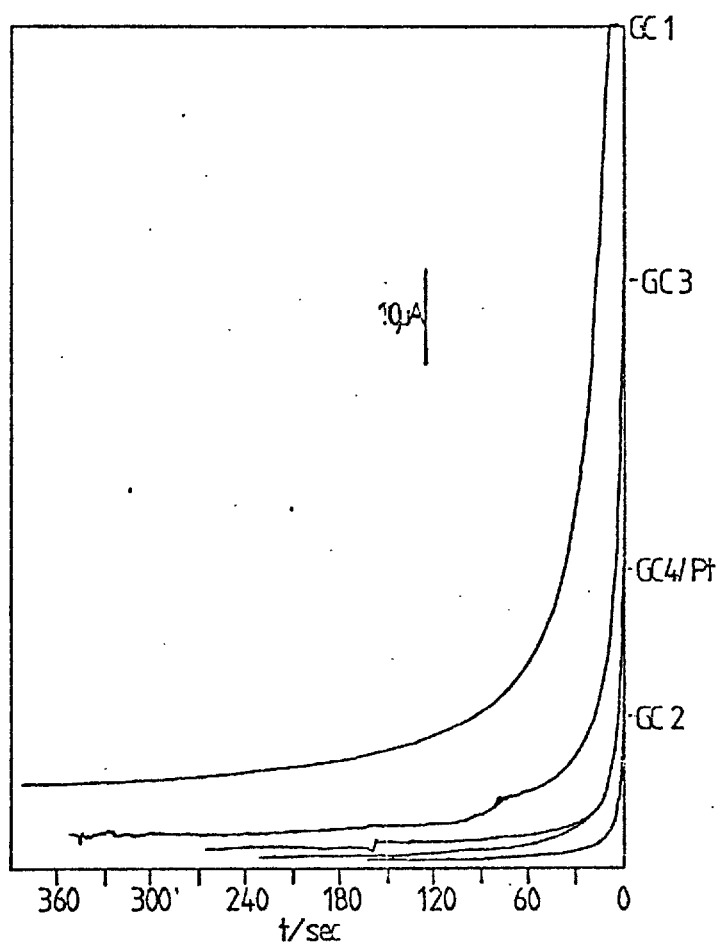
Figure 1-15

The variation in the instaneous charging current (i_{cap}) with

change in potential was next investigated. Figure 1-16 gives plots of i_{cap}

vs potential. It is seen that holding the electrode at -0.8 V results

in an increase in the charging current. This again reflects the faradaic

contribution due to the oxidation of hydroquinone and adsorbed hydrogen

formed as a result of holding the electrode at -0.8V.
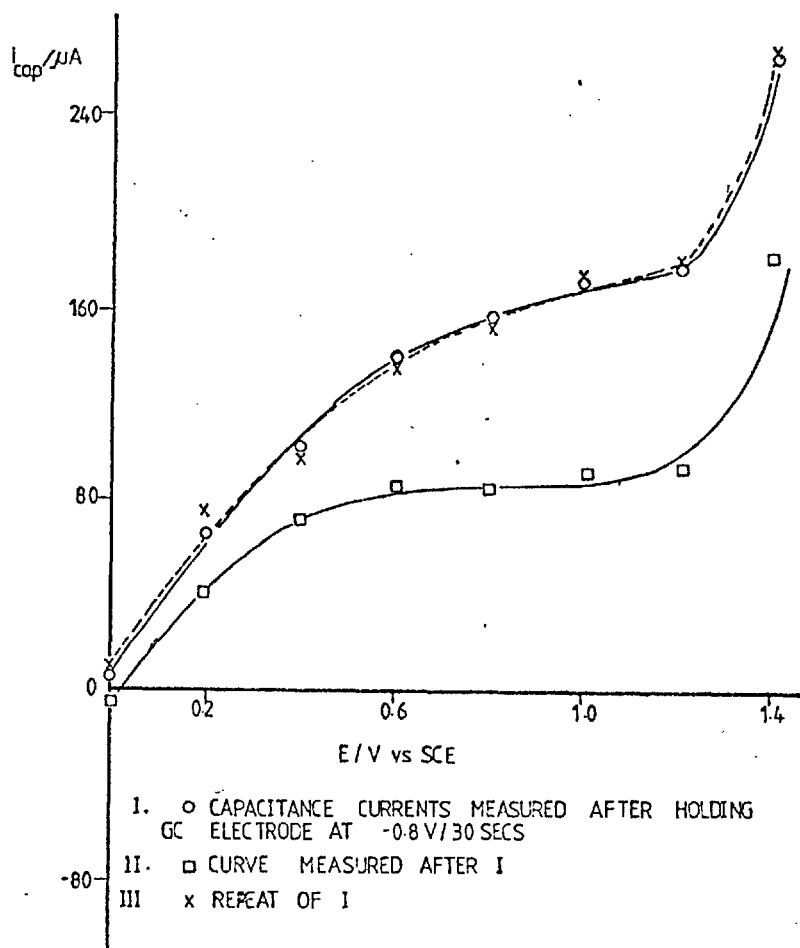
Figure 1-16

Figure 1-17 gives plots of the instantaneous charging

current measured over a wider potential range to include the cathodic

side.

The first curve (I) was obtained for an electrode that had

been previously held at + 1.5 V vs SCE. The faradaic contribution, due

to the reduction of oxidised functionalities and the adsorption of

hydrogen are the primary reasons for the high value of i_{cap}. Hydrogen

evolution occurs at about −0.8 V.

29

Curve II was obtained after holding the electrode at −0.8 V

for thirty seconds. It can be seen that the instantaneous charging currents

are greatly reduced. This is again probably due to the reduction of

surface groups and adsorption of hydrogen during reduction at −0.8 V.
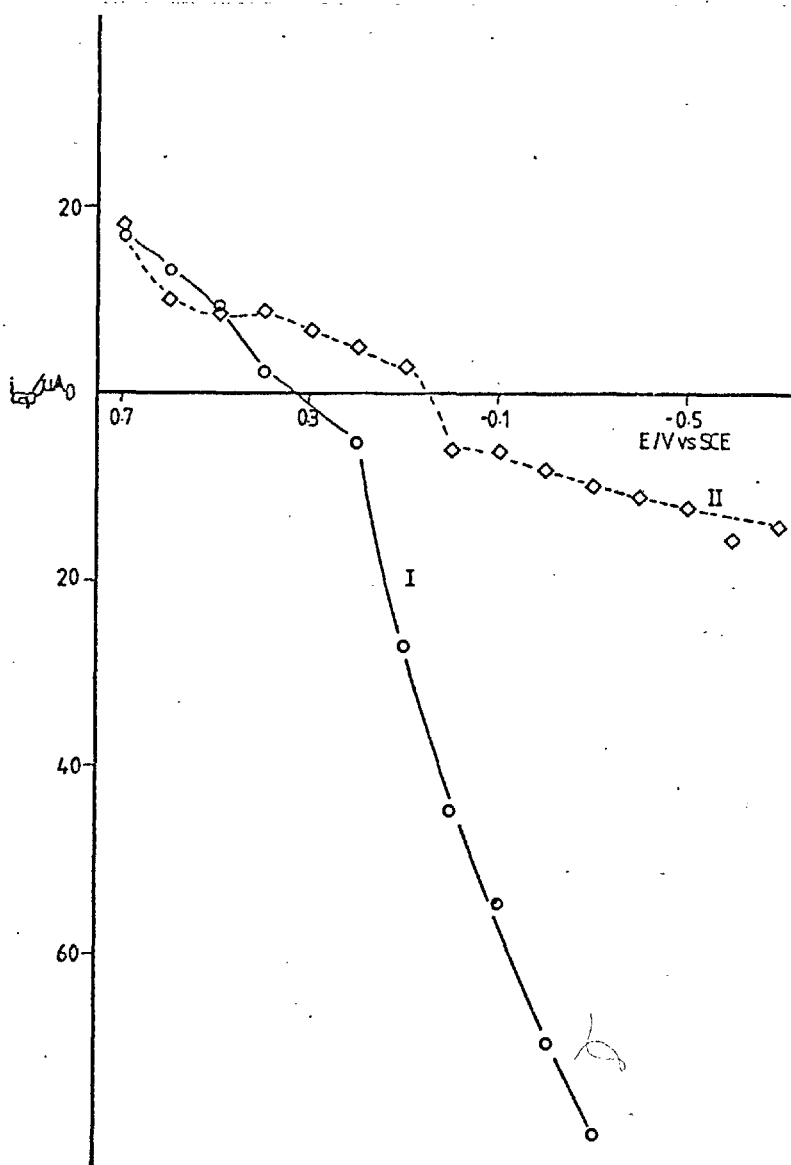
Figure 1–17

Note: i_{cap} measured from positive to negative potentials.

1.52 Discussion

From the analysis of the above experimental results it
becomes evident that the use of a cleaning pulse is limited by the
faradaic contribution to the charging current of surface functionalities
and adsorbed hydrogen.

For this reason it was found that in aqueous solutions,
and in the case of a positive working potential, the maximum cleaning
pulse that could be used without having intolerable background currents
was about −0.3 V. In actual fact this value depends to a great extent
on the state of the electrode surface. For a newly polished electrode
for example, the cleaning potential could be extended to −0.5 V.

1.6 The Effect of pH

For reactions involving the species H_2O and H^+ we can write
the equation

$$aA + bB + cH_2O + mH^+ + Ze = 0$$
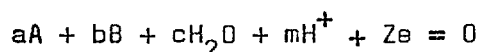
in which a substance A is changed into a substance B, the only other
species involved being water, hydrogen ions and electrons.

The equilibrium condition takes the form:

$$E = E^O - \frac{0.059m}{Z} pH + \frac{0.059}{Z} (alogA + blogB)$$

If we have the condition that (alogA + blogB) =0, we obtain
a straight line having an intercept of E^O on the potential axis and
a slope of $\frac{0.059m}{Z}$ volts per pH unit. For the special case in which no
electrons or H^+ ions are involved, the lines will be parallel to the
potential or to the pH axis respectively.

1.61 Experimental

Chemicals

Analar grade chemicals were used throughout. The following
buffer solutions were used:

      i) H_2SO_4 0.5M pH 0.8

      ii) Citrate buffer – citric acid/sodium citrate

        pH2.2 – 6.2

      iii) Phosphate buffer – Na_2HPO_4/NaH_2PO_4 ; pH 5.8 – 8.0

      iv) Sodium Borate + NaOH

        pH 9.2 – 10.8

      v) NaOH + Na_2HPO_4

        pH 10.9 – 12.00

All glassy carbon disks were of radius = 1.5mm (Plessy).
Open circuit potentials were measured using a Corning – EEL model 112
pH metre. Chronopotentiograms were obtained using a model PAR 173
potentiostat/galvanostat.

Purified nitrogen was used to deareate solutions.

1.62 Open circuit Potential vs pH

In figure 1-18 we have plots showing the variation of the
open circuit potential with pH for two different glassy carbons(GC 2
and GC 1 – see section 1.44).

Curve I corresponds to GC 2 which is characterized mainly by
quinoidal surface activity. The slope in the pH range 0-7 is about
60 mV/ pH unit. This reflects the response of the reversible quinone/
hydroquinone redox centres (chemisorbed on the carbon surface) to pH.
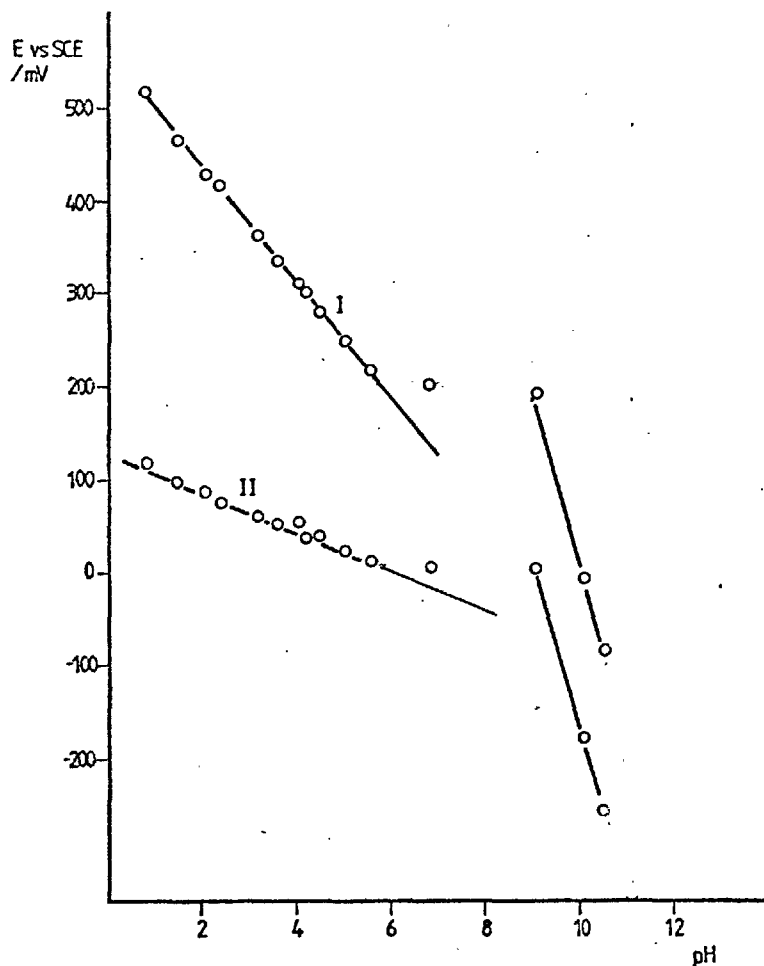
Figure 1-18

At higher pH the slope increases greatly. It is not clear why this occurs. However the large slope indicates that, whatever the change taking place, it is highly pH sensitve.

Curve II was obtained with a highly oxidized electrode (GC 1). the small slope indicates that the reaction at the surface inolving H^+ is irreversible. This is possible if it is considered that the surface is dominated by carboxylic and lactone groups. At high pH the slope once again increases(parallel to the previous plot (I)).Again no explanation is offered to explain this large slope.
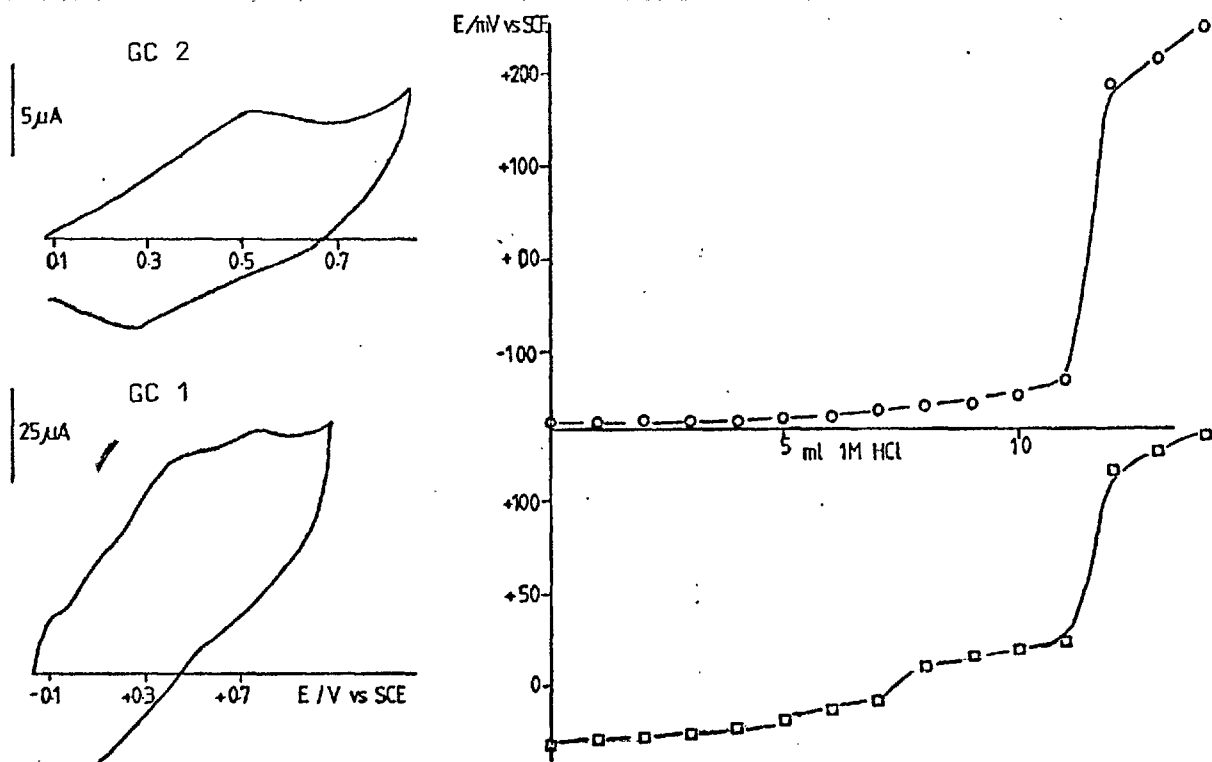
Figure 1- 19

THE USE OF GLASSY CARBON AS AN INDICATOR ELECTRODE IN ACID-BASE

TITRATION

The use of carbon electrodes as indicators in acid-base

base titrators has been described (28,43). The reponse of the carbon

electrode was related to surface quinoidal groups.

In figure 1-19 we have two acid base titrations using

two different glassy carbons as the indicator electrodes. The cyclic

voltammogram describing the state of the electrode prior to use is

given next to the respective tiration curve. It can be seen that the

more highly oxidised electrode (GC1) shows a smaller change in the

open circuit potential at the end point. This is consistent with the

theory that the highly oxidised carbon is dominated by lactone and

carboxylic acids.

34

Effect of pH on Chronopotentiograms

According to Vetter (49) the anodic and cathodic charging curves for platinum are of the same shape regardless of pH. The only difference is that corresponding points on the charging curve are shifted by 59.2 mV/pH.

In figure 1-20 we have anodic charging curves obtained at different pH. It can be seen that as the pH increases the charging curve becomes broader with arrests less well defined.
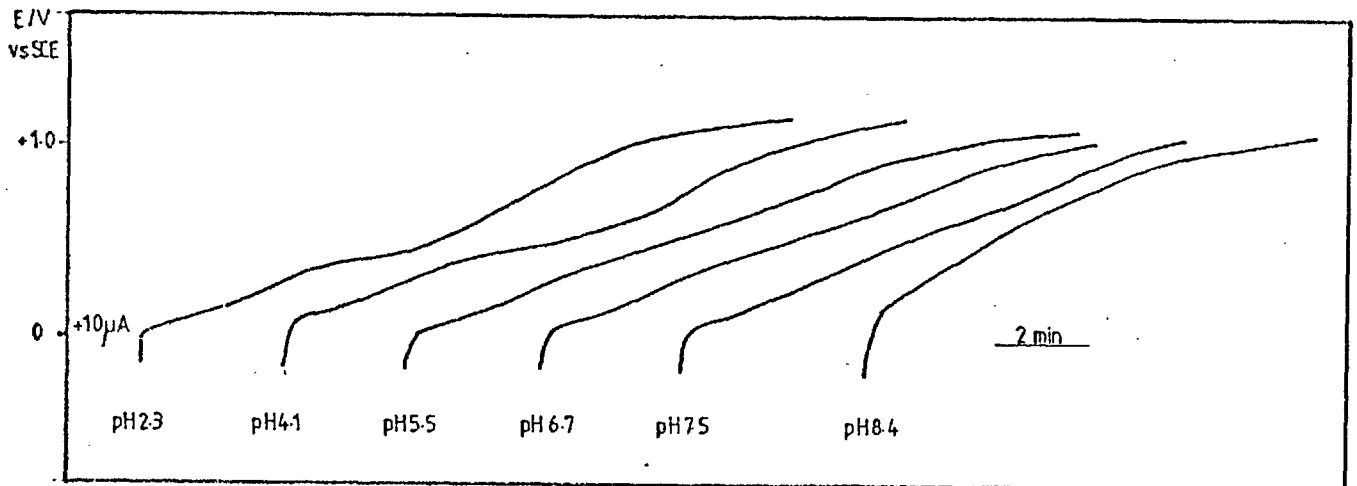
EFFECT OF pH ON ANODIC CHARGING CURVE OF GC EXPOSED TO AIR

Figure 1-20

35
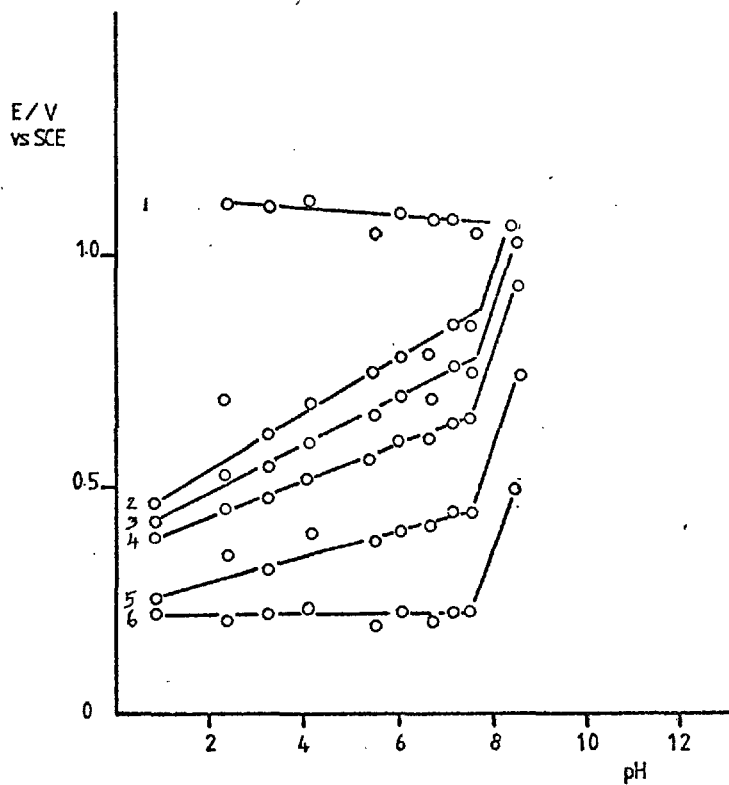
Figure 1-21

A plot of corresponding points on the charging curve
with pH reveals interesting trends.

In the potential region in the vicinity of the reversible
quinone-hydroquinone couple the potential vs pH plot slope is about
60 mV/pH. The slopes become less as we go to less positve potentials
(plots 3-6); 6 is parallel to the pH axis indicating that it is
indipendent of pH. This could be due to the region being purely
double layer charging.
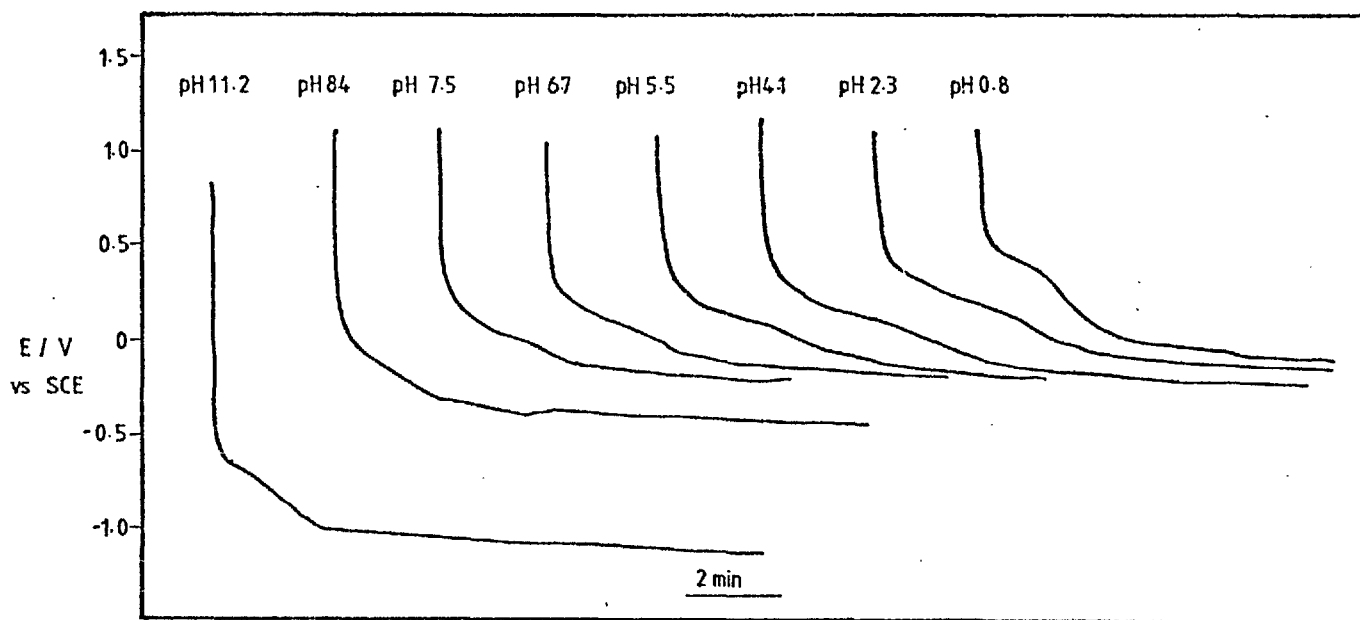
EFFECT OF pH ON CATHODIC CHARGING CURVE OF A GC ELECTRODE LEFT EXPOSED TO AIR

Figure 1-22

In the above figure the cathodic charging curves obtained at different pH is shown. As the pH is increased the cathodic transients appear to become more drawn out with arrests becoming less well defined. At higher pH the catodic transient goes to very much more negative potentials than in the case of transients obtained in the lower pH range. This correlates with the transition found in the open circuit potential vs pH plot as well as the anodic charging curves given earlier.

A plot of corresponding points on the cathodic transients with pH reveals trends which are similar to that obtained with the anodic transients (see 1-23).
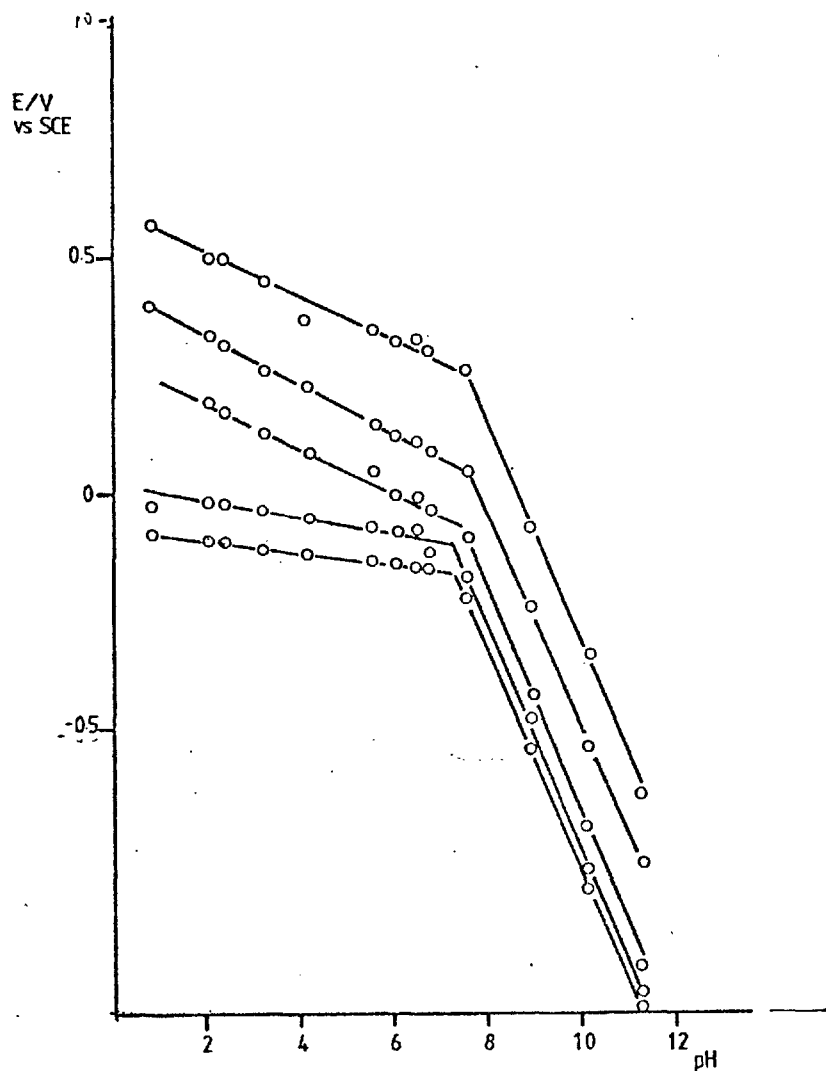
Figure 1-23

In the region of the reversible quinone-hydroquinone couple the slope at low pH is about 6o mV/ pH unit. Close to 0 V the slope is about 15 mV/ pH unit. Two reasons can be put forward for such a low slope:

i) due to double layer charging

ii) due to the desorption of hydrogen which, as it has been shown earlier, is a irreversible process (unlike in the case of Pt).

It is most probable however, that the small slope results
from a combination of (i) and (ii) and not for any one reason.

Discussion

The response of glassy carbon electrodes thus appears
to be highly dependent on the pH of the solution. While it is possible
to correlate this response to the surface quinoidal, carboxyl and
lactone functionalities at low pH, at high pH it seems to be dominated
by another mechanism.

On account of the fact that the potential vs pH slope
is large (about 250 mV/pH unit), the mechanism can be assumed to be
less dependent on electron transfer and more on pH.

There is a possibility that this effect could be related
to changes in the basal planes; perhaps due to the interaction
of hydroxyl species with the electron system of the basal planes, in
the form of charge transfer complexes.

CHAPTER II APPROACHES TO IMPROVING ELECTRODE PERFORMANCE

2.1 General

Whether a reaction is reversible, quasireversible or

irreversible depends to a large extent on the ease of formation

of the preferred transition state for electron transfer. Two energy

barriers which must be surmounted in order to form the transition

state involves ionic reorganistion and solvent redistribution. A

free energy profile may drawn to represent this.
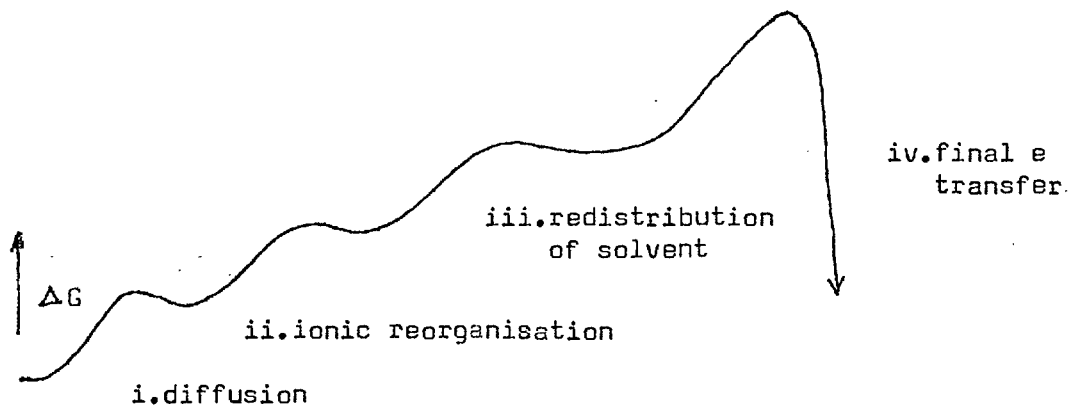
Figure 2-1 From Albery(45)

According to Hale (46) for such an electrode reaction,

the heterogeneous rate constant may be written as:

$$k = \kappa\, Z \exp\left(\frac{-\Delta G^{\neq}}{kt} \right)$$

where $\quad G^{\neq} = w^{\neq} + \dfrac{(\lambda + w - w^{\neq} + e(E - E_i^0))^2}{4\lambda}$

Z = thermal energy of the reacting particles

$w^{\neq}$ = work required to transport reactant to plane at

which electron transfer occurs

λ = work required to reorganize environment about reactant

κ = transmission coeficient

Having formed the prferred transition state, the next step
is electron transfer. Following Gersicher (47), we can distinguish
between three cases, dependent on the interaction of the reactant
species with the electrode surface. These are tabulated below.

Interaction	Location of e Transfer
i) none or weak	from solution within double layer
ii) strong	interface
iii) very strong chemical bonds	surface only

Table 2-1

Very little is known about the actual act of electron
transfer, but by analogy with the Frank Condon effect, it is a
very rapid adiabatic process occuring in a time interval significantly
less than that for the formation of the transition state. According
to Vetter and Gerischer (48,49), electron transfer is very much more
likely by quantum mechanical mechanism (electron tunnelling) than
by quasi thermodynamic considerations. The only requirement here is
that, e transfer occurs between states at the same energy level.

The effect of the electrode material on the rate of the
electrode process is small when the electroactive substance is not
adsorbed (case (i) in table 2-1). In such cases it is related only
to a change in the diffuse double layer since the charge of the electrode
as well as the value E_z (the potential of zero charge) depends on
the electrode material(50). Thus in the oxidation of ferrocyanide,
though the heat of activation is independent of the electrode work
function, the exchange current density is found to be proportional to it (4).

In electrocatalysis where adsorbed species participate
in the electrode process, a strong dependence on the electrode
material is observed. This is due to the considerable differences
in the strngth of the chemisorptive bond between the reacting particle
and the electrode.

2.2 The Role of Surface Adsorbed Material on Kinetics and Adsorption

The presence of adsorbed material on electrode surfaces
can effect the kinetics of electrode processes by several mechanisms.

It has been shown by Gerischer (51) that adsorbed molecules
can be represented as providing new donor or acceptor levels in the
band structure at the surface of semiconductors. This can result in
an additional exchange of electrons at the energies of these levels.
This mechanism can predominate as the means of electron transfer
in the case of semiconductor materials with large band gaps (52). In
the case of glassy carbon however, this mechanism must be presumed only
partially responsible for the exchange current as the band gap is
very small.
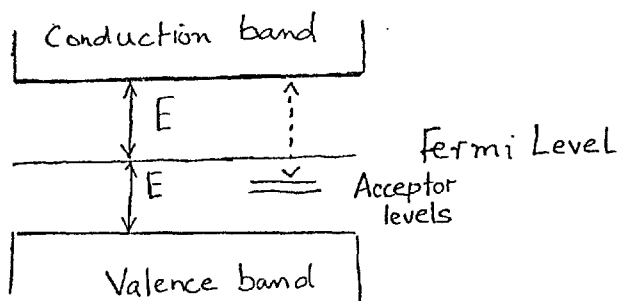
Figure 2-2

The C-O functionalities are good electron withdrawing
groups and as such can create acceptor states in the surface electronic
band structure (see figure 2-2).

Surface Potential Gradients

There is usually a large potential drop between the surface
of a metal and a solution. In the case of semiconductors a drop is still
present but a significant part of the potential drop occurs across the
space charge region of the semiconductor.

If the density of surface states is high enough an effect
which is analogous to contact adsorption on metal electrodes is observed
(4, 53). The semiconductor then behaves more like a metal and the
major part of the potential drop occurs across the solution double layer.

2.22 Direct Interaction of Adsorbed material with Reactants

It has been long known that freshly anodized platinum
electrodes behave more reversibly towards certain redox systems than
one which has not been preanodized (54,55). According to Davis (55),
the anodization produces an adsorbed oxygen film which facillitates
electron transfer across oxygen bridges.

In contrast, according to Vaselovski and co-workers (56), the
electrochemical oxidation of a reducing agent in solution occurs mainly
through chemical oxidation by the adsorbed oxide film. This involves
an interaction of the reducing species with the oxide layer and implies
a change in the concentration ratio of the redox system.

A similar theory for transition metal oxides has been put
forward by Fleishman and co-workers (57,58).

43

The scheme for such an oxidation mechanism is given
below:

$$OH^- + \text{lower oxide} \underset{\longleftarrow}{\overset{k'e}{\longrightarrow}} \text{higher oxide} + H_2O + e$$

$$\text{higher oxide} + \text{organic substrate} \xrightarrow{k} \text{lower oxide} + H_2O + e$$

$$\text{intermediate} \longrightarrow \text{product} + (n-1)e$$
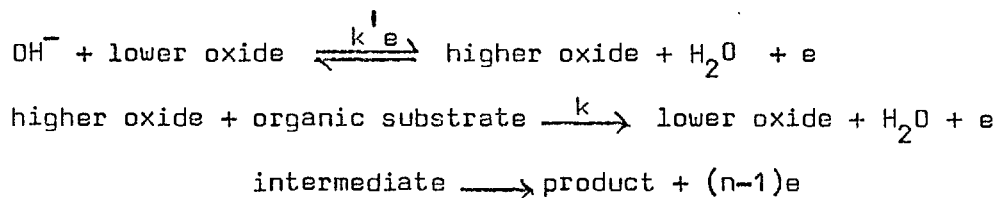
In favour of such a scheme, it has been found that reverse
peaks are missing in the cyclic voltammograms obtained at low sweep
rates.

In the context of the above, the direct interaction of C-O
functionalities with reactant is one possibility which can be
considered.

Quinoidal groups can be pictured as acting as bridges between
the glassy carbon surface and the reactant. Electron transfer could
proceed/the π molecular orbitals of the bridges.

However, according to Coughlin and Esra (59), commenting on
the adsorption of phenol on carbon, as surface groups are found at edges
of layer planes they would not be expected to interfere. Therefore it
was proposed that the C-O functionalities serve to localize electrons
in surface states thus removing them from the π e system of the basal
planes. Adsorption is then due to the interaction of the phenol π e
system and the π band of the graphite plane resulting in donor acceptor
complexes.

Walker (60) described a similar mechanism affecting the
thermo-electric properties of carbon materials.

44

In this chapter the effect of surface groups on glassy carbon on some selected electrode processes are examined. Additionally it is attempted to improve electrode performance by chemically modifying these groups.

2.23 Cyclic Voltammetry of ParaPhenylene Diamine (PPD)

EFFECT OF SURFACE CONDITION ON CYCLIC VOLTAMMOGRAM OF PPD
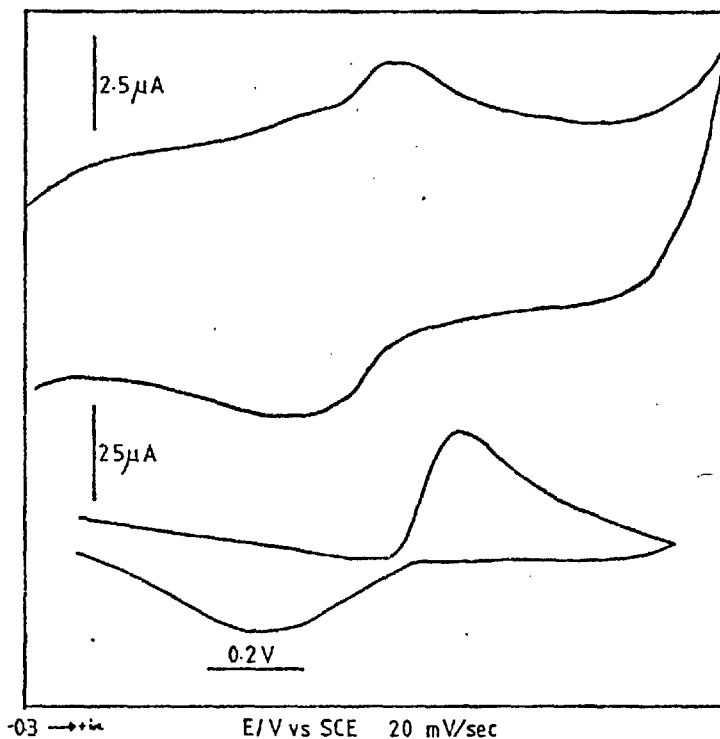
Figure 2-3

The oxidation of paraphenylene diamine (PPD) in acidic medium is a a two-electron process giving the diimine(61). In figure 2-3 above, the first cyclic voltammogram is of a glassy carbon showing mainly quinoidal activity. The peaks due the reversible quinone/hydroquinone couple is evident.

PPD   PPI
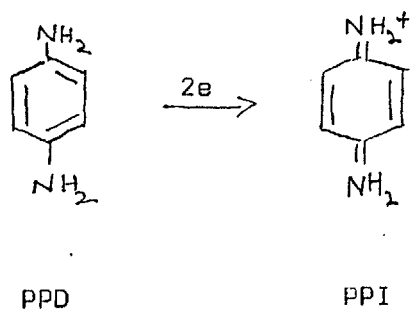
The cyclic voltammogram of PPD, obtained using the above GC shows a hihg degree of irreversibility with $\Delta E_p = 400$ mV.

a. CYCLIC VOLTAMMOGRAM OF GC SURFACE 5M H_2SO_4

b. (effect of adsorption)
  CV OF PPD 5mM/.5M H_2SO_4

E/V vs SCE

Figure 2-4

46
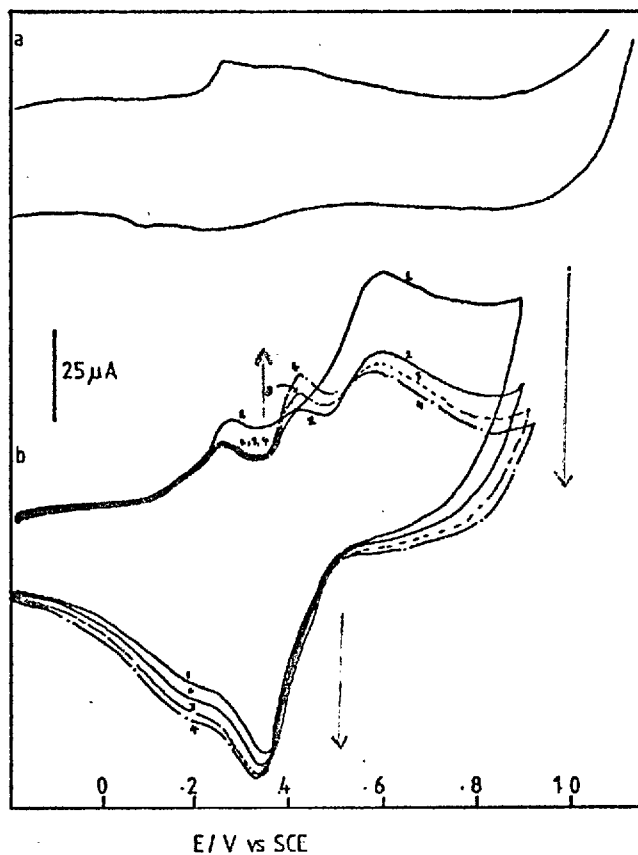
When the glassy carbon is oxidised at +2.0 V for 1 minute, a dramatic change in the cyclic voltammogram of PPD occurs, (see figure 2-4). The first voltammogram is of the GC; it shows that surface activity is greatly enhanced when compared with figure 2-3. In the case of the CV of PPD, the following points can be made:

i) the first peak on the anodic scan is due to the oxidation of surface hydroquinone groups (cf 2-4b).

ii) the second peak on the anodic scan is due to the adsorption of products of electrolysis (62). This peak increases with successive scans (as would be expected in adsorption).

iii) the third peak on the anodic scan is due to the oxidation of PPD. This peak decreases with successive scans. There could be two reasons for this:

   a) due to adsorption of reactant (62)

   b) due to the reduction of oxidised surface groups with each scan

iv) the cathodic peak is greatly enhanced. Additionally peak height increases with successive scans.

2.24 The Effect of Surface Condition on the Reduction of Nitrobenzene

The reduction of nitrobenzene has been outlined as follows(63):
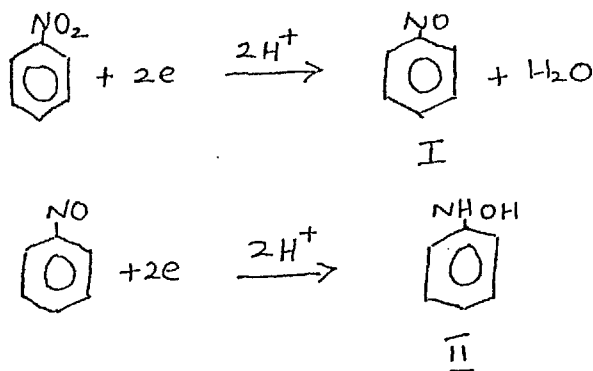
Nitrosobenzene occurs as an intermediate but as it reduces at more positive potentials a peak corresponding to its reduction is not seen.

Phenyl hydroxylamine (II) may rearrange to p-aminophenol or undergo further reduction at a more negative potential to give analine.

According tp Snowdon (64) however, in an aqueous/ethanol solution and acetate buffer (the solution system used in this experiment) the following reaction may occur:

$$\text{C}_6\text{H}_5\text{NO} + \text{C}_6\text{H}_5\text{NHOH} \longrightarrow \text{C}_6\text{H}_5-\overset{\overset{\text{O}}{|}}{\text{N}}=\text{N}-\text{C}_6\text{H}_5$$

III

$$\text{C}_6\text{H}_5-\overset{\overset{\text{O}}{|}}{\text{N}}=\text{N}-\text{C}_6\text{H}_5 + 2e + \text{H}_2\text{O} \longrightarrow \text{C}_6\text{H}_5-\text{N}=\text{N}-\text{C}_6\text{H}_5 + 2\text{OH}^-$$

azobenzene

$$\text{C}_6\text{H}_5-\text{N}=\text{N}-\text{C}_6\text{H}_5 + 2e + \text{H}_2\text{O} \longrightarrow \text{C}_6\text{H}_5-\text{NH}-\text{NH}-\text{C}_6\text{H}_5 + 2\text{OH}^-$$

IV
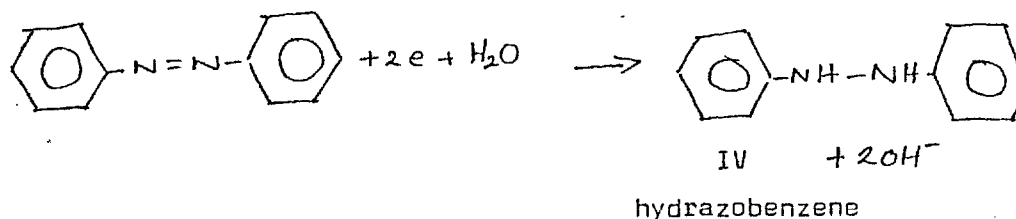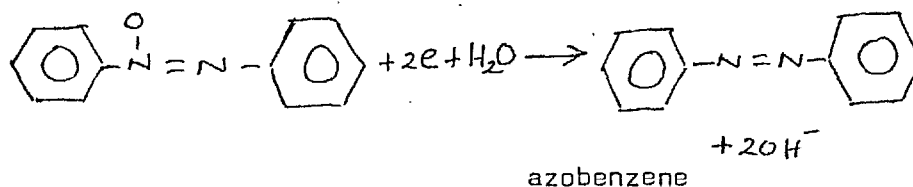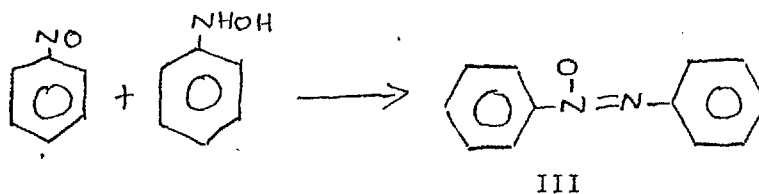
hydrazobenzene

In figure 2-5 we have a cyclic voltammogram of nitrobenzene taken with a polished glassy carbon. The second peak on the cathodic scan is probably due to the formation of hydrazobenzene (IV) via the four-electron process described above.

48

a) INITIAL CONDITION
OF GC ELECTRODE

5μA

E vs SCE   20 mV/sec

0   ·2   ·4   ·6   ·8   1·0   1·2   1·4

b) REDUCTION OF
NITROBENZENE
10% EtOH. ACETATE BUFFER

50μA

0   -·2   -·4   -·6   -·8   -1·0   -1·2   -1·4
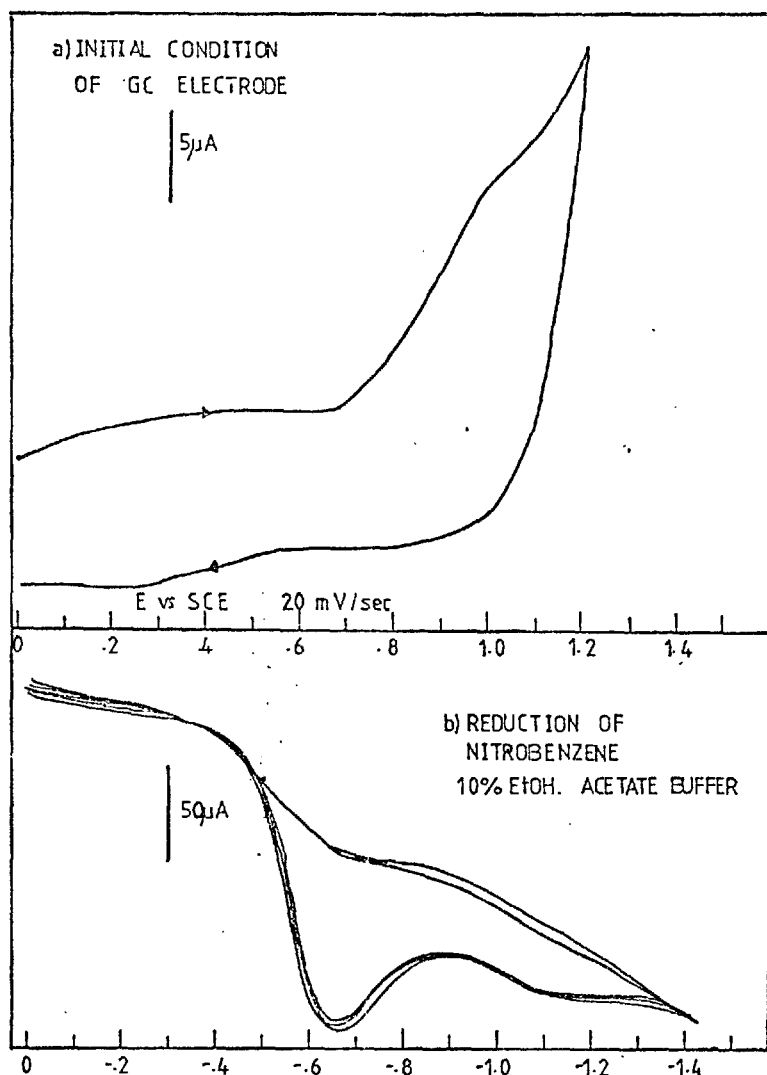
Figure 2-5

As it can be seen, the reduction is completely irreversible.

The GC electrode was next held at -2.0 V for 1 minute. This was followed by holding the electrode at +0.3 V for 2 minutes in order to remove any adsorbed hydrogen. Cyclic voltammogram of the electrode taken in 0.5M H_2SO_4 (figure 2-6a) shows increased surface activity. The effect on the CV of nitrobenzene is seen in figure 2-6b.
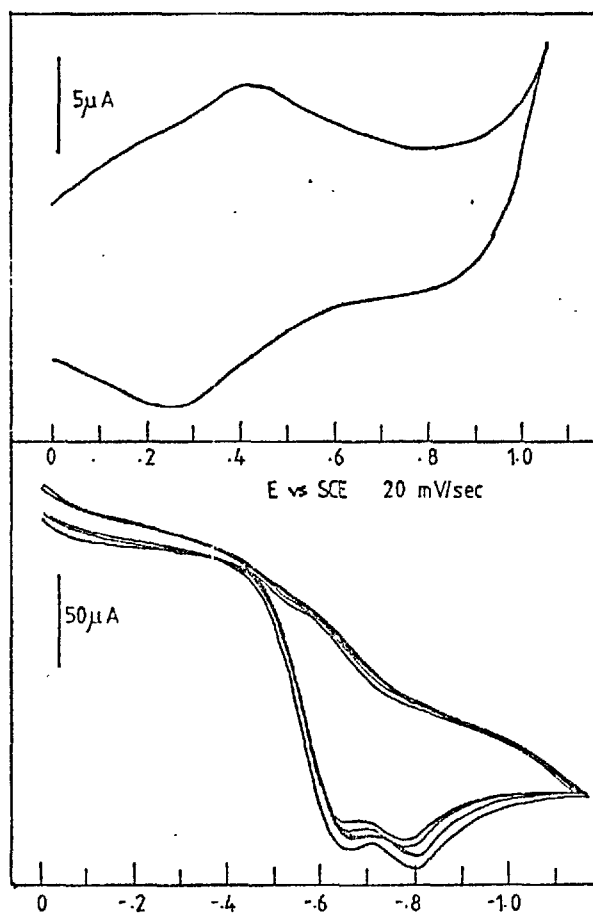
Figure 2-6

With reference to figure 2-6b, it can be seen that while the first reduction peak due to the primary reduction of nitrobenzene remains the same. the second peak however is shifted to a less negative potential.

On oxidising the glassy carbon at +2.0 V it is found that the second peak on the CV of nitrobenzene is greatly enhanced (figure 2-7).

50

The peak however reduces rapidly back to its original level. The
reduction in the peak with successive cathodic scans can be atributed
to reduction of the oxidised surface functionalities (formed during
oxidation at +2.0).

The first cathodic peak due to the primary reduction of
nitrobenzene does not appear to be affected by the oxidation of the GC.

a) STATE OF GC AFTER OXIDATION   +2.0 V

b) C.V. OF NITROBENZENE ON SAME GC SURFACE
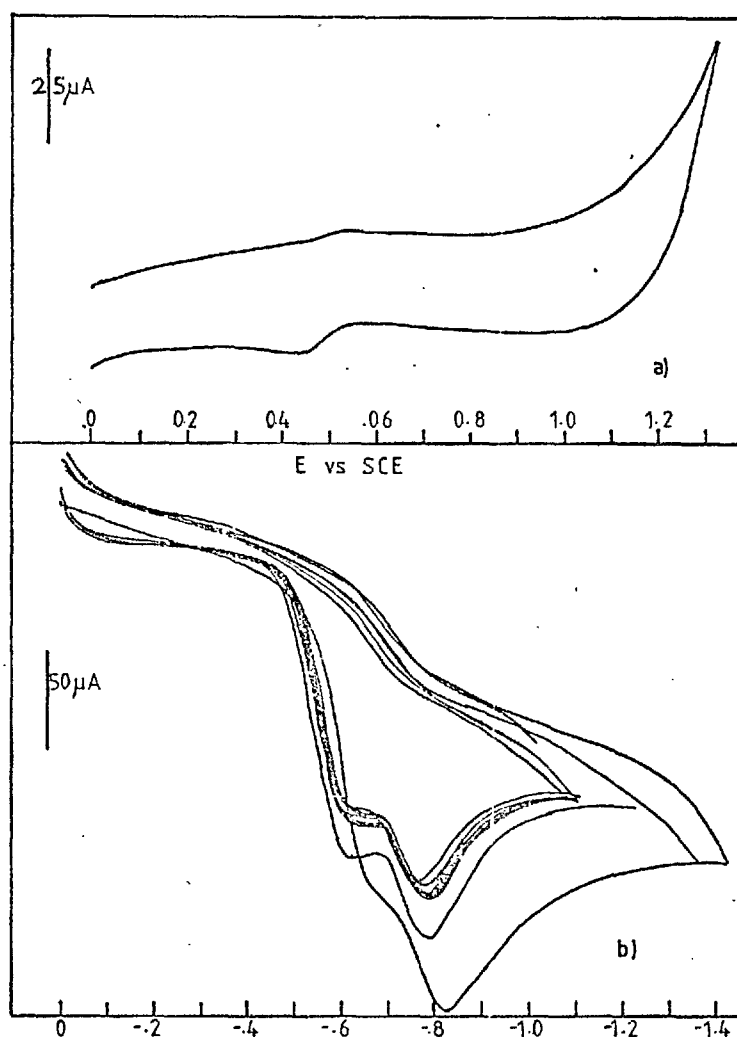
Figure 2-7

2.25 The Adsorption of Phenols

In order to examine the effect of surface groups on adsorption, isopropyl phenol and m-cresol were separated using an ODS Permaphase column (see chapter IV) with methanol/water/0.1M KNO_3 as the eluent; the wall jet cell was used as detector . Pt, Plessy GC and Tokai GC were used as the electrode material. The working potential was +1.0 V vs Ag/AgCl.

Isopropyl phenol and m-cresol were used as they are known to adsorb on the electrode surface and have a very much less tendancy for polymerisation than phenol.

Adsorption on Pt
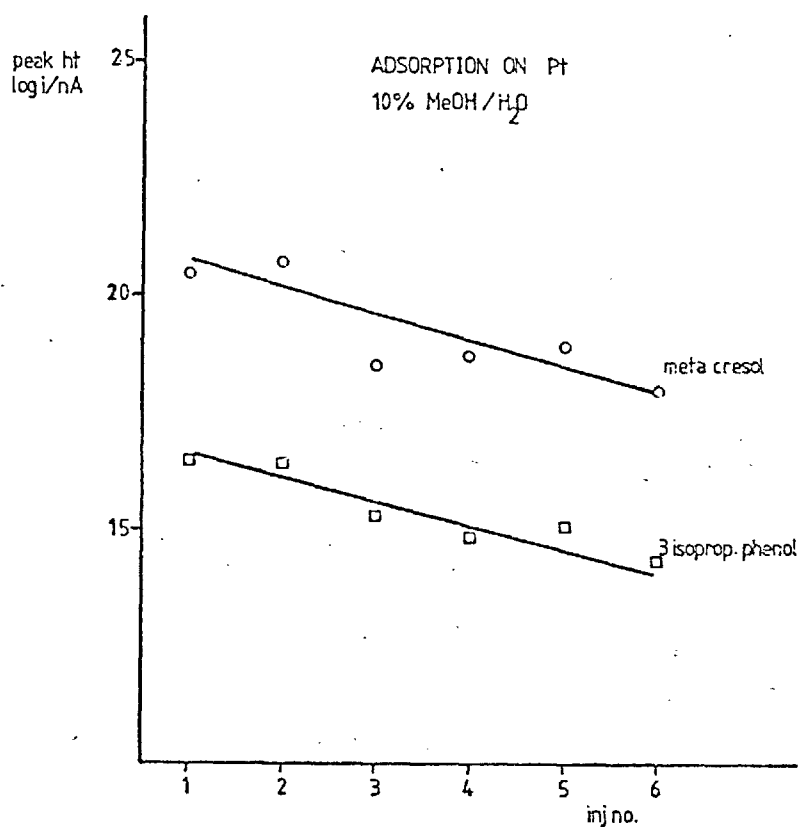
Figure 2-8

Adsorption on Plessy Glassy Carbon
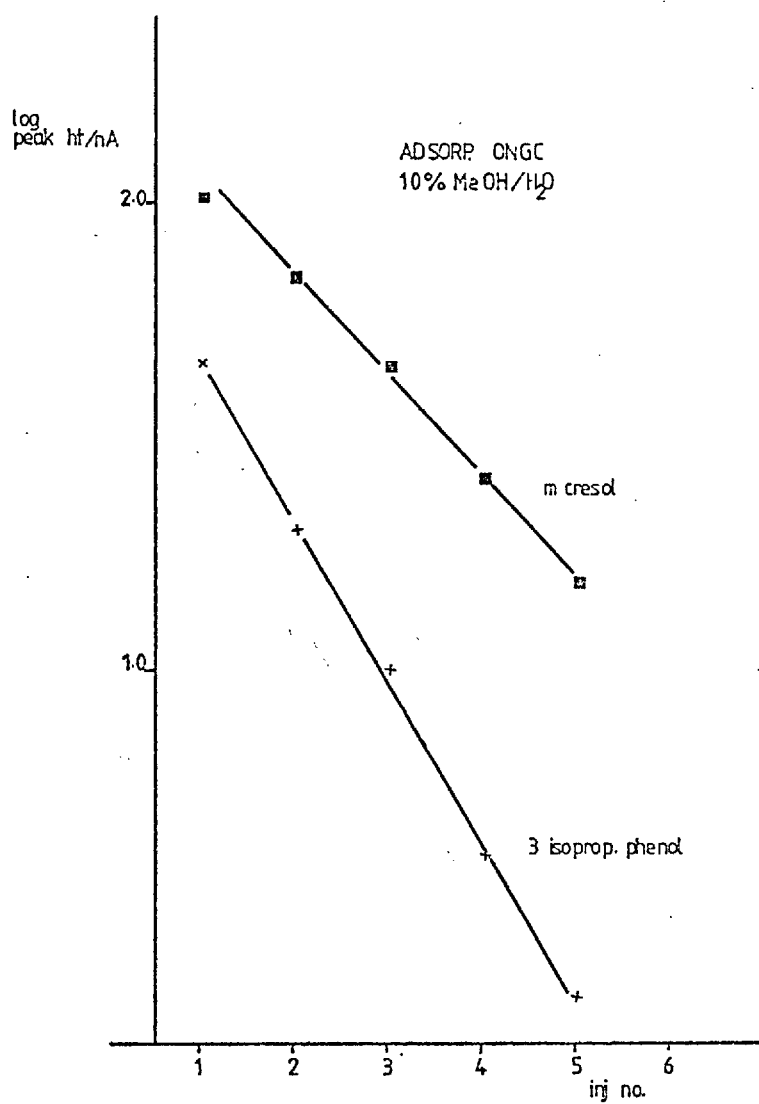
Figure 2-9

Adsorption on Tokai Glassy Carbon
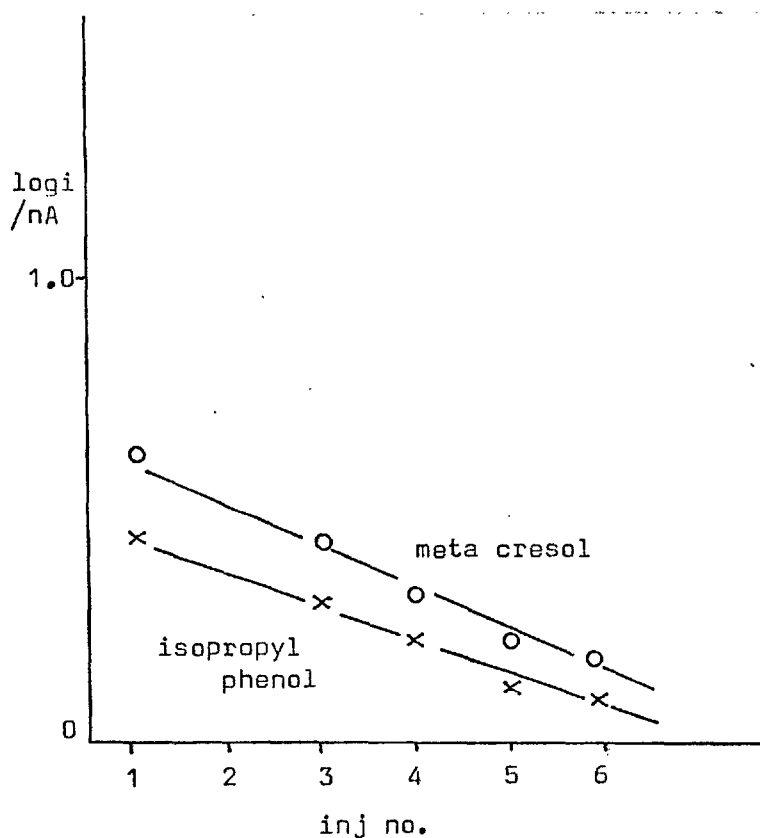
Figure 2-10

From the above plots it can seen that in the case of Plessy GC (characterized by high surface activity), the phenols adsorb more strongly than on Pt or Tokai GC (characterized by low surface activity). Pt shows least amount of phenol adsorption.

In figure 2-11 the effect of using a non aqueous solvent is seen. The working electrode was the Plessy GC used above. The slope for isopropyl phenol is singificantly less than with the methanol/H_2O eluent (figure 2-9). According to Kissinger (65) the effect of the non aqueous solvent is to reduce polymerisation.

ADSORPTION OF PHENOLS ON
OXIDISED GC - HEXANE /EtOH ELUENT
1μg / 5μl injs.
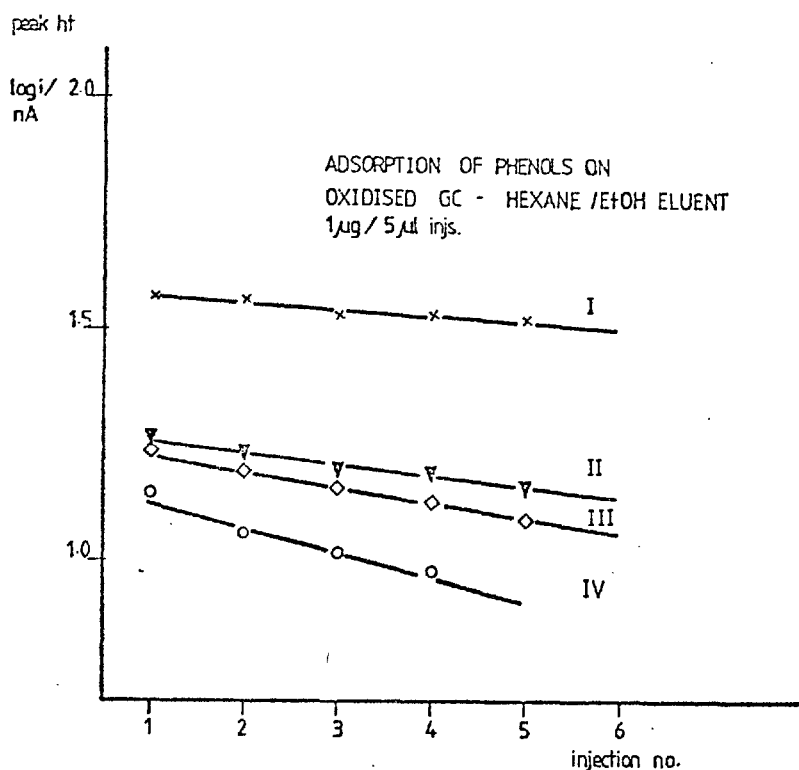
I p-amino phenol
II o-amino phenol
III phenol
IV 3 isopropyl phenol

Electrolyte: 0.05M Tetrabutyl ammoniumfluorobrate
Working potential = +0.8V

Figure 2-11

2.3 Chemical Modification of Glassy Carbon Surfaces

Attempts at chemically treating carbon surfaces dates back
to 1948 when Villars and co-workers (66) treated carbon black with
Grignards reagent and diazomethane.

More recently Murray and co-workers (67,68) attempted
modification with 2,4 dinitrophenyl hydrazine and organo silane reagents.

55

Clem (69) reported the use of diazomethane, lithium aluminium hydride and amines in order to reduce the loss of hydrogen overvoltage. The acidic oxide groups apparantly act as a source for hydrogen ions in the catalytic evolution of hydrogen.

In this work glassy carbon surfaces were treated with hydrazine and hydroxylamine reagents. The electrocatalytic activity of these chemically modified carbons were then compared with that of untreated carbons, Pt and Au.

2.31 Experimental

Treatment with Hydrazine

The glassy carbon (mounted as described in chapter 3) was immersed in hydrazine for twenty-four hours. The electrode was rinsed in distilled water and then placed in a beaker of distilled water for 2 hrs. The electrode was then placed in an ethanol wash for 2 hrs followed by further rinsing with distilled water

Hydrazine adds on to carbonyl groups as follows:

$$\text{C=O} + NH_2NH_2 \longrightarrow \text{C=N–NH}_2 \quad \text{a Hydrazone}$$
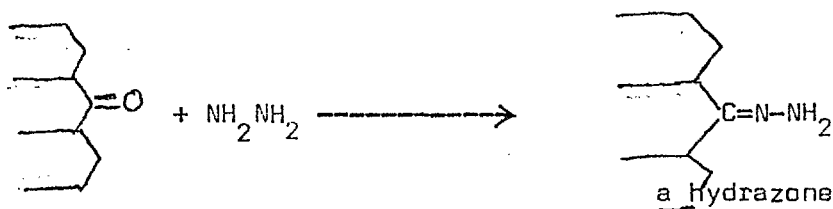
Treatment with Hydroxylamine

1 gm of hydroxylamine was dissolved in 10mls of distilled water. The glassy carbon electrode surface was immersed in this solution and the solution heated to 50° C for five hours. The electrode was then rinsed with distilled water and left overnight in a beaker of distilled water.

56

Hydroxylamine adds on to carbonyl groups according to the following mechanism:(70):

$$\text{C=O} \quad + \quad \ddot{N}H_2OH \quad \underset{\longleftarrow}{\overset{\longrightarrow}{\rightleftharpoons}} \quad \underset{NHOH}{\overset{OH}{C}} \quad \xrightarrow{-H_2O} \quad C=NOH$$
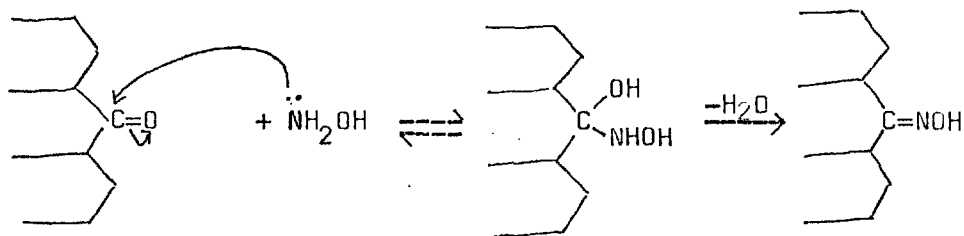
2.32 Results and Discussion

In figures 2-12(a) and 2-12(b) we have cyclic voltammograms, obtained in the anodic potential region, of hydrazine and hydroxylamine treated glassy carbons respectively. In both cases the first scan (I) shows oxidation of unreacted reagent, and any other derivatives which may have been formed.

After the first scan however a reproducible cyclic voltammogram is obtained (scan II). Both scans were obtained in 0.5 M H_2SO_4.

Comparism of the two voltammograms shows that the one obtained with the hydrazine treated carbon corresponds more to that of an untreated glassy carbon. The hydroxylamine treated glassy carbon in contrast shows the cathodic peak at about 0.15 V (as compared with 0.35 V in the case of the hydrazine treated carbon). The anodic peaks however are about the same.

Effect of Chemical Treatment on Hydrogen Overvoltage

It has already been mentioned that Clem (69) has described the loss of hydrogen overvoltage due to the presence of C-O surface gps.

(a)
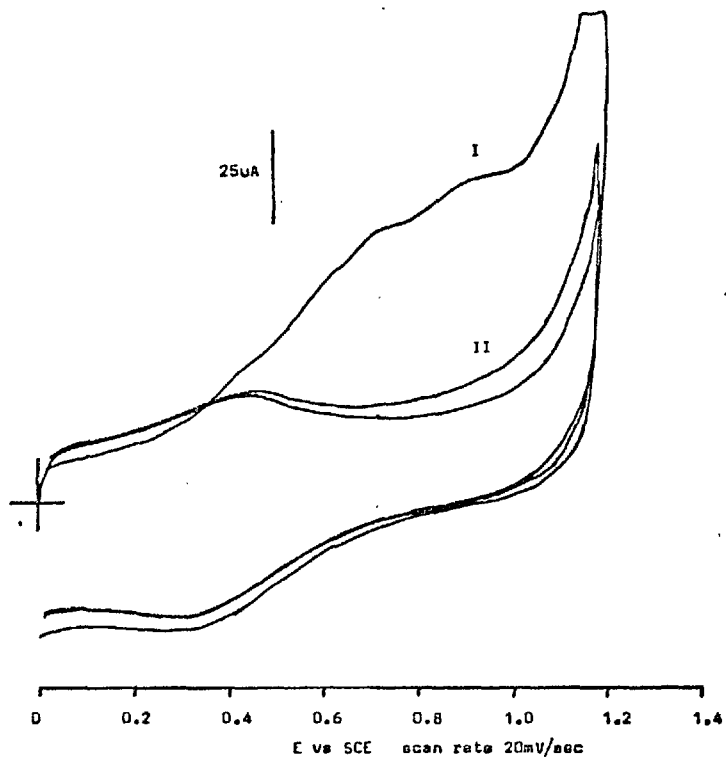
CYCLIC VOLTAMMETRY OF HYDRAZINE TREATED GLASSY CARBON
I. OXIDATION OF IMPURITIES AND HYDRAZINE DERIVATIVE
II. REVERSIBLE COUPLE

25uA

I

II

E vs SCE   scan rate 20mV/sec

(b)
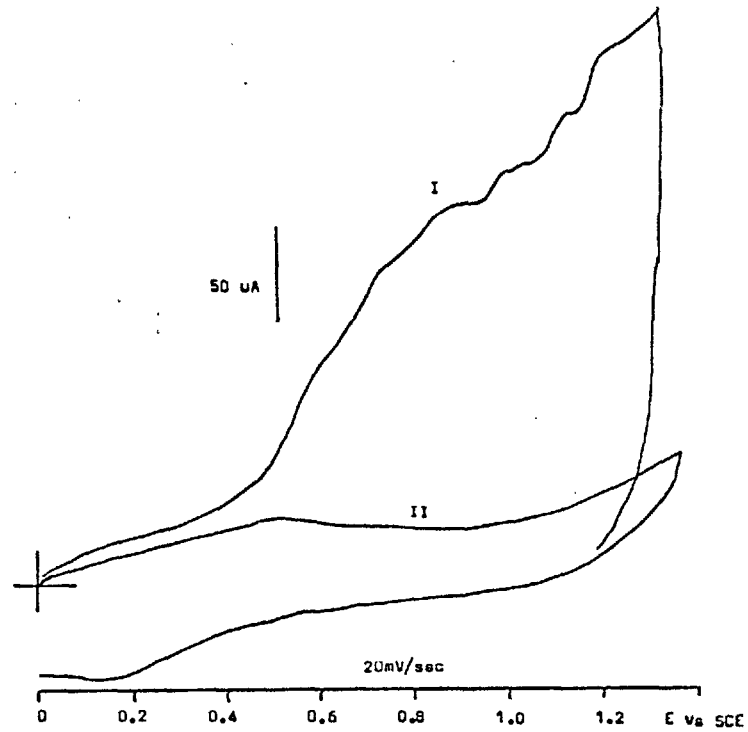
ANODIC CYCLIC VOLTAMMOGRAM OF HYDROXYLAMINE
TREATED PLESSY GLASSY CARBON

50 uA

I

II

20mV/sec

E vs SCE

Figure 2-12

Two basic reaction paths have been suggested in the process of hydrogen evolution (71,72):

i) discharge followed by chemical desorption given by:

$$M(e) + H_3O^+ \longrightarrow MH + H_2O \qquad 1$$

$$2MH \longrightarrow 2M + H_2 \qquad 2$$
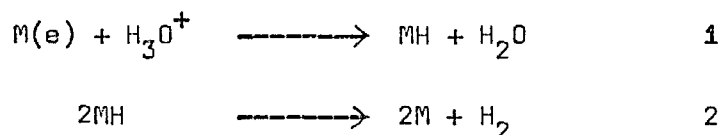
and ii) discharge followed by electrodic desorption:

$$M(e) + H_3O^+ \longrightarrow MH + H_2O \qquad 3$$

$$MH + H_3O^+ + M(e) \longrightarrow 2M + H_2O + H_2 \qquad 4$$
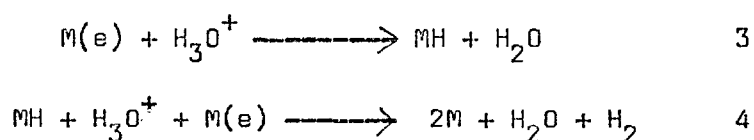
On the basis of equations 1-4 it is possible to imagine that acidic C-O functionalities serve as sources of H^+.

In figure 2-13 we have current potential curves obtained for a polished glassy carbon electrode and for an electrode which had been oxidised at +2.0 V. It can be seen that the hydrogen overvoltage occurs at a significantly less negative potential in the case of the carbon electrode oxidised at +2.0 V (figure 2-13(b).

SSV = Steady State Voltammetry, a technique developed by Blaedel and Jenkins (73) because of the high charging current contribution from surface groups; In SSV, currents are allowed to reach their steady state before measuring them for voltammetric purposes.

Figure 2-14 gives cathodic current - potential curves for the two treated glassy carbons. It can be seen that the hydrogen overpotential begins at potentials comparable to the electrode oxidised at +2.0 V.

59

Figure 2-13

(a)

SCAN RATE 20 mV/SEC

50 uA

SSV TAKEN AFTER
1MIN

-1.0   -0.8   -0.6   -0.4   -0.2   0

E vs SCE/ Volts

CURRENT POTENTIAL CURVES OBTAINED FOR UNTREATED AIR
OXIDISED PLESSY GLASSY CAEBON

(b)

50 uA

SSV TAKEN AFTER 1MIN

SCAN RATE 20 mV/SEC

-1.0   -0.8   -0.6   -0.4   -0.2   0

E vs SCE
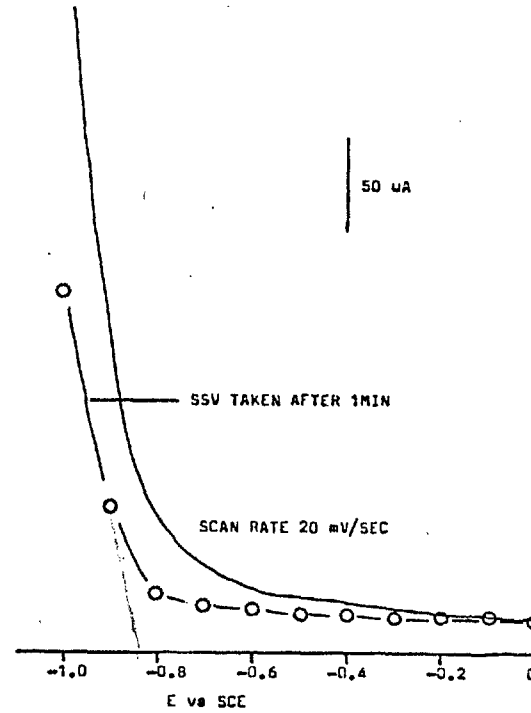
CATHODIC CURRENT POTENTIAL CURVES OBTAINED FOR UNTREATED
PLESSY GLASSY CARBON OXIDISED AT +2.0 V FOR 10 SECS

Figure 2-14

(a)

50 uA

SCAN RATE 20 mV/SEC

SSV TAKEN AFTER 1MIN

-1.0   -0.8   -0.6   -0.4   -0.2   0

E vs SCE
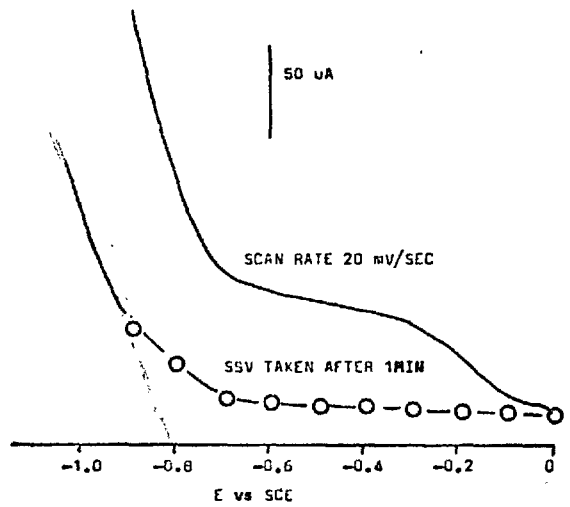
CATHODIC CURRENT POTENTIAL CURVES OBTAINED FOR
HYDROXYLAMINE TREATED PLESSY GLASSY CARBON

(b)

50 uA

SCAN RATE 20 mV/SEC

SSV TAKEN AFTER 1MIN

-1.2   -1.0   -0.8   -0.6   -0.4   -0.2   0
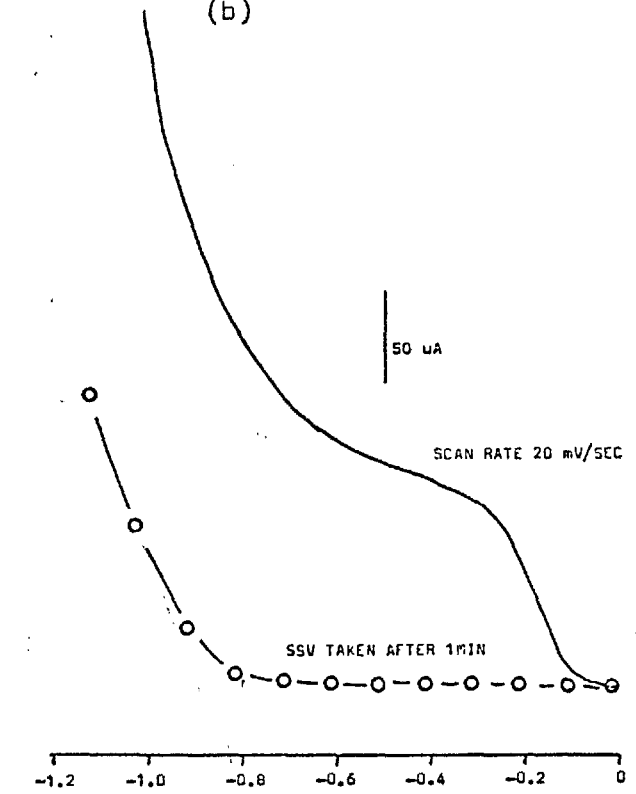
CATHODIC CURRENT POTENTIAL CURVES OBTAINED FOR HYDRAZINE
TREATED PLESSY GLASSY CARBON

Effect of Chemical Treatment on Oxygen Overpotential

The oxygen evolution reaction:

The rate determining step in the potential range up to
+ 1.8 V vs SCE is the oxidation of the hydroxyl ion or the water
molecule (74).

$$OH^-(ads) \xrightarrow{\text{slow}} OH(ads) + e \qquad 1$$

$$or \quad H_2O(ads) \xrightarrow{\text{slow}} OH(ads) + H^+ + e \qquad 2$$
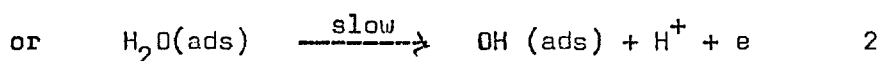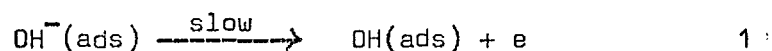
This step is followed by fast processes, either

$$2OH(ads) \longrightarrow O(ads) + H_2O \qquad 3$$

$$or \quad OH(ads) \longrightarrow O(ads) + H^+ + e \qquad 4$$

$$and \quad 2O(ads) \longrightarrow O_2 \qquad 5$$
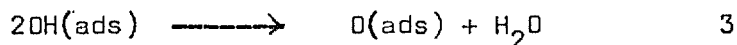
The manner in which surface C–O functionalities could
influence the oxygen evolution reaction must therefore be related
steps 1 and 2.

Considering the electron withdrawing properties of the
C–O groups, it is plausible to imagine that the removal of electrons
from the πe system of the basal planes (see section 2.2) thus
creating acceptor states, enhancing steps 1 and 2.

In figure 2-15 we have two anodic current potential
curves: (a) for Tokai GC and (b) for Plessy GC. It can be seen that
the overpotential for the Tokai GC occurs at very much more positve
potentials than the oxidised Plessy GC.

2.5 uA

100mV/SEC

20mV/SEC

SSV TAKEN AFTER 1 MIN

0.2   0.4   5.6   0.8   1.0   1.2   1.4   1.6   1.8
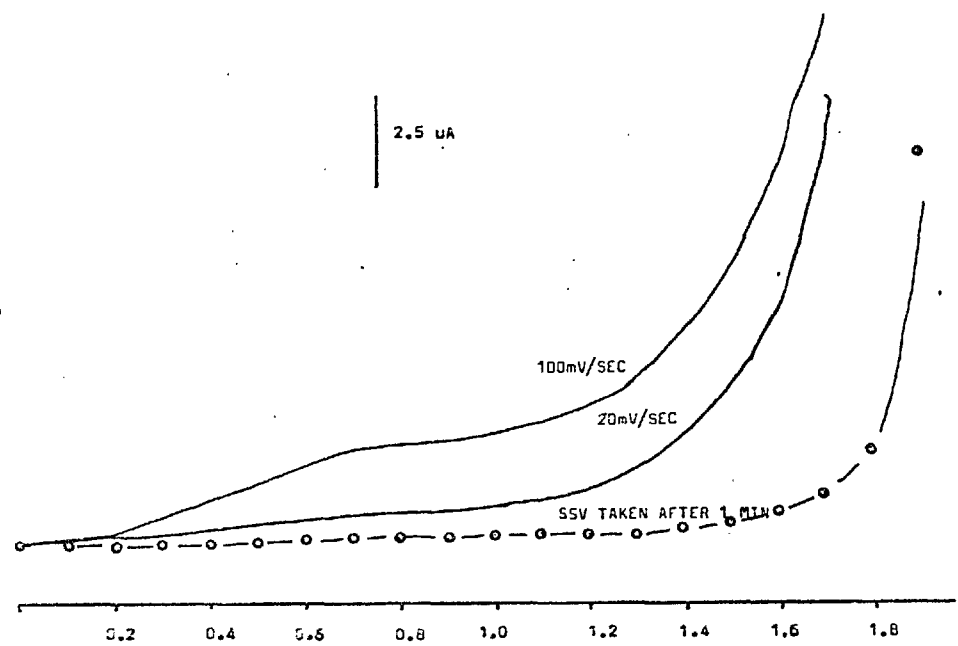
ANODIC CURRENT POTENTIAL CURVES OBTAINED FOR TOKAI GLASSY CARBON

15% H_2SO_4

a

25 uA

20 mV/SEC

SSV TAKEN AFTER 1 MIN

0   0.2   0.4   0.6   0.8   1.0   1.2   1.4   1.6   1.8

E/V vs SCE
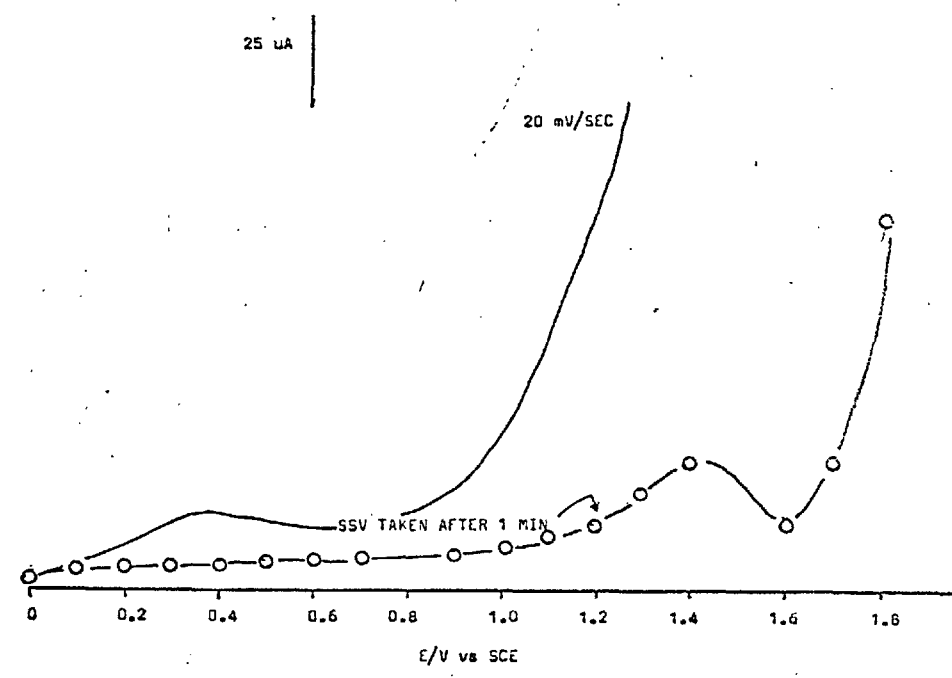
ANODIC CURRENT VOLTAGE CURVE FOR AN UNTREATED PLESSY GLASSY CARBON

b

Figure 2-15

In figures 2-16(a) and 2-16(b) we have the anodic current potential curves obtained for the hydroxylamine and hydrazine treated glassy carbons respectively. The oxygen overpotential corresponds to that of the oxidised Plessy GC described earlier.

From the above results it can be concluded that the oxidation of glassy carbon surfaces results in a loss of hydrogen overvoltage and oxygen overvoltage. Chemically treated surfaces show a response similar to a severely oxidised electrode. Tokai GC having relatively little surface activity has the largest overpotential.

Cyclic Voltammogram of Ferrocyanide

The oxidation of ferrocyanide is a simple electron transfer process involving very little solvent reorganiztion. The electrode reaction can be written as follows:

$$Fe(CN)_6^{4-} \rightleftharpoons Fe(CN)_6^{3-} + e$$

The reaction has been generally described as a reversible process.

Figure 2-17 gives cyclic voltammograms of ferrocyanide on a platinum electrode before and after electrochemical pretreatment. The pretreatment procedure involved holding the electrode at +1.5 V for 30 secs followed by 1 min at 0.4 V.

It can be seen that there is a dramatic change in the cyclic voltammogram after pretreatment: i) the reversibility of the reaction is increased as ΔE_p is decreased ii) the peak currents are increased.

64

ANODIC CURRENT POTENTIAL CURVES FOR HYDROXYLAMINE TREATED PLESSY GLASSY CARBON

15 % H₂SO₄

Figure 2-16(a)

CURRENT POTENTIAL CURVES FOR HYDRAZINE TREATED PLESSY GLASSY CARBON

15% H₂SO₄

Figure 2-16(b)

65
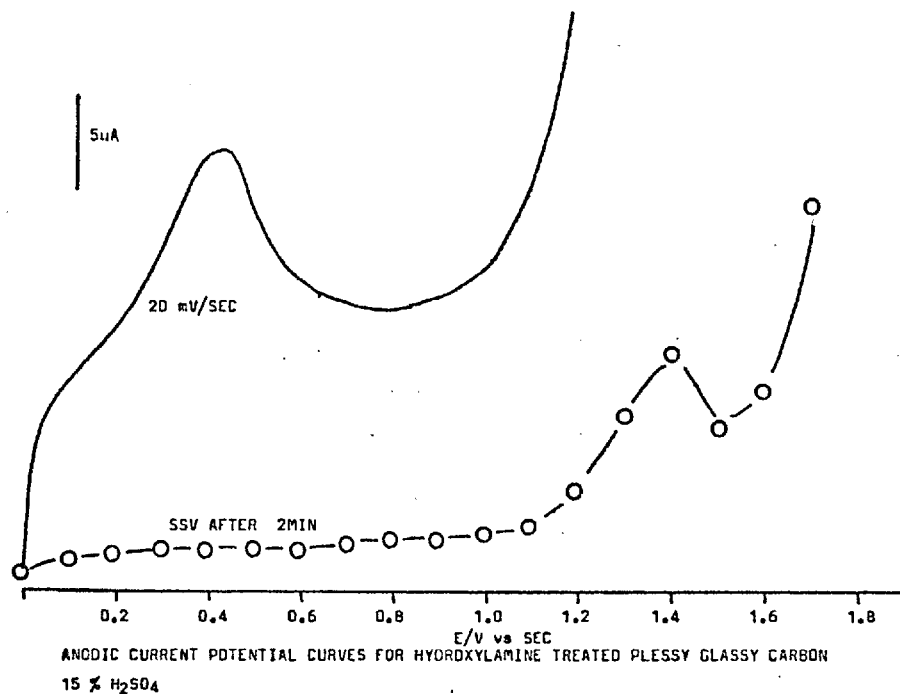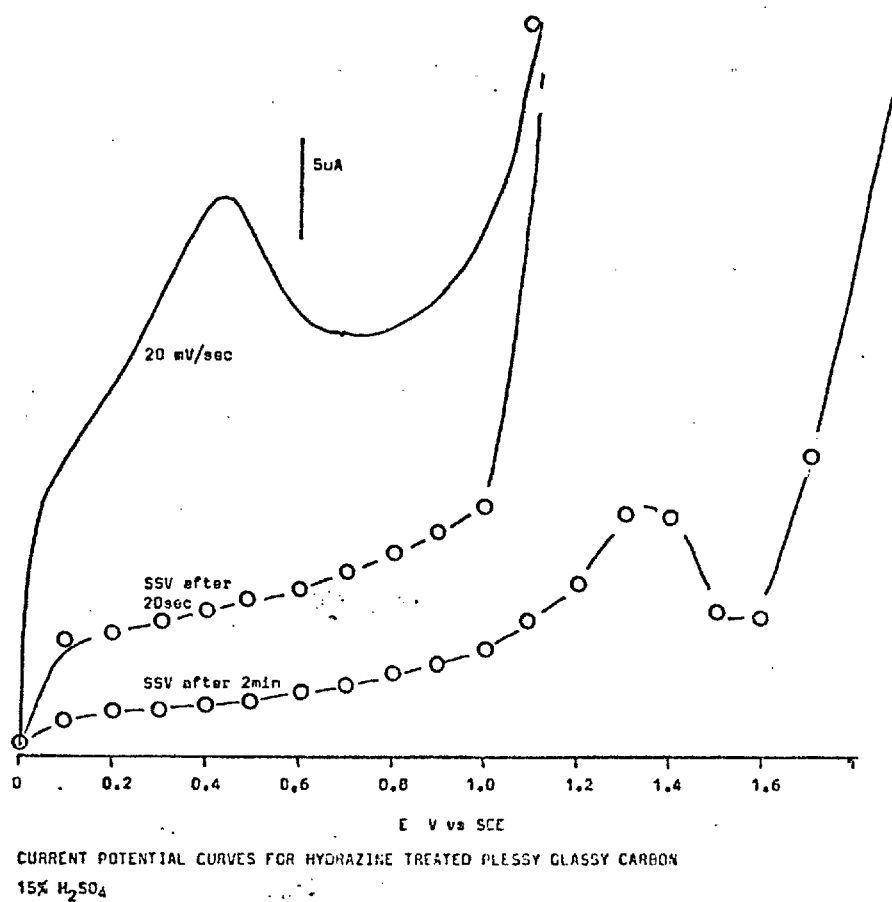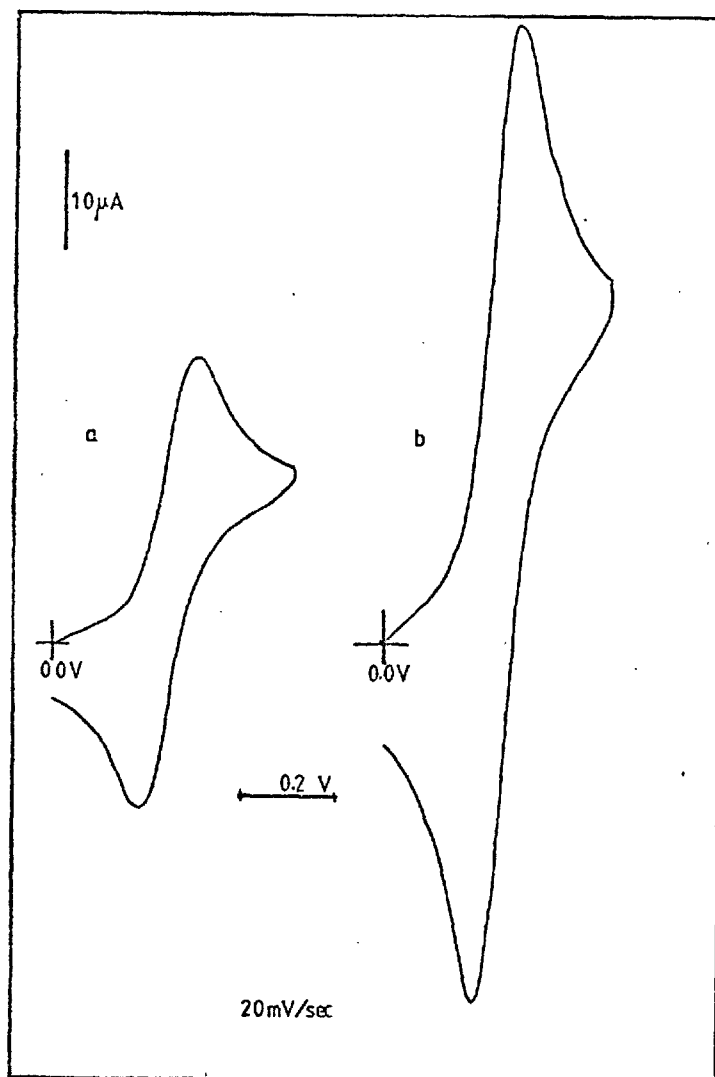
CYCLIC VOLTAMMOGRAM OF 5mM FERROCYANIDE
Pt
a, cleaned with HNO_3 b, after e/c pretreatment

Figure 2-17

The cyclic voltammograms obtained with the various (treated
and untreated) glassy carbon electrodes are given in the next figure
(figure 2-18). The voltammograms all show a lesser degree of reversibility
than the electrochemically treated Pt electrode. The chemically treated

carbons show only a slight improvement over the oxidised, untreated one with the hyrdroxylamine treated GC the best. The Tokai glassy carbon shows a very poor response.

a,Plessy GC   b,Hydrazine treated   c,Hydroxylamine treated   d,Tokai GC

CV OF 5mM FERROCYANIDE   20mV/sec
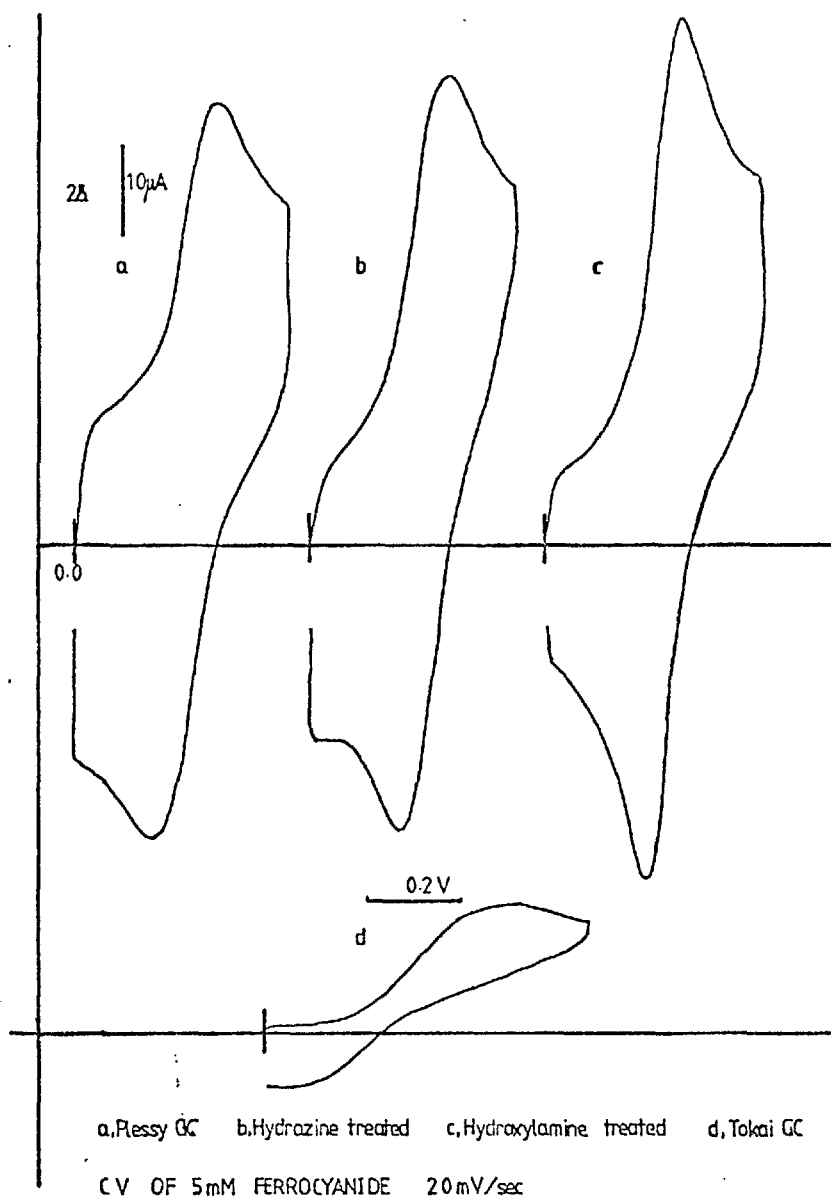
Oxidation of Fe^{2+}

In figure 2-19 below the cyclic voltammograms of Fe^{2+} ~~that~~
were obtained /are shown. Compared with the cyclic voltammograms of ferrocyanide

these can be seen to show a greater degree of irreversibility. This

can be related to the fact that a much greater level of solvent

reorganization is required. This is reflected in a lower rate constant

than in the oxidation of ferrocyanide. (75).

OXIDATION OF 5 mM Fe^{2+}
pH = 0.3

10 uA

UNTREATED
PLESSY CC

PLESSY CC
TREATED WITH
HYDRAZINE

0.0 V

0.0V

SCAN RATE 20 mV/sec

0.2V vs SCE

TOKAI
CC   100mV/sec

0.0V

Figure 2-19

68
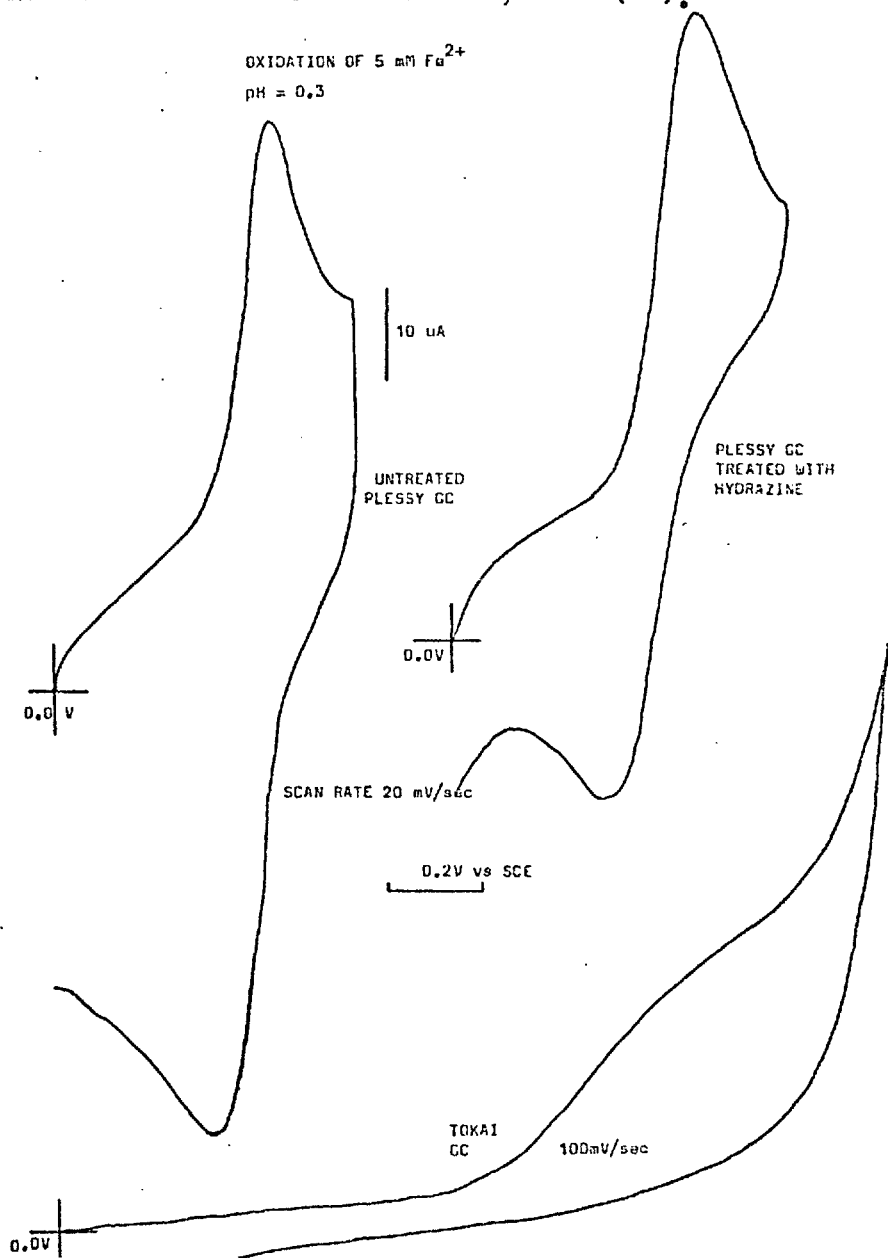
In the case of Fe^{2+} oxidation the Tokai GC performs
even worse than before. The cyclic voltammogram for the Tokai GC was
obtained at a scan rate of 100mV/sec. At lower scan rates the
oxidation peak was very much smaller. There was no peak observed in
the cathodic scan for all scan rates.

Cyclic Voltammetry of Hydroquinone

According to Adams (76) the cyclic voltammetry of hydroquinone
on solid electrodes suggests a high degree of irreversibility.
The overall reaction is a two electron transfer as given below.

In figure 2-20 we have a number a cyclic voltammograms
obtained with different electrode materials. The scan rate is quite
slow; 5mV/second.

It can be clearly seen that the reaction is most reversible
for the chemically treated Plessy GC. The voltammogram obtained with
the untreated Plessy GC shows a smaller peak current as well as less
reversibility.

Voltammograms obtained with Tokai GC, Au and Pt show a
very high degree of irreversibility with the cathodic peak missing
in the case of Pt.
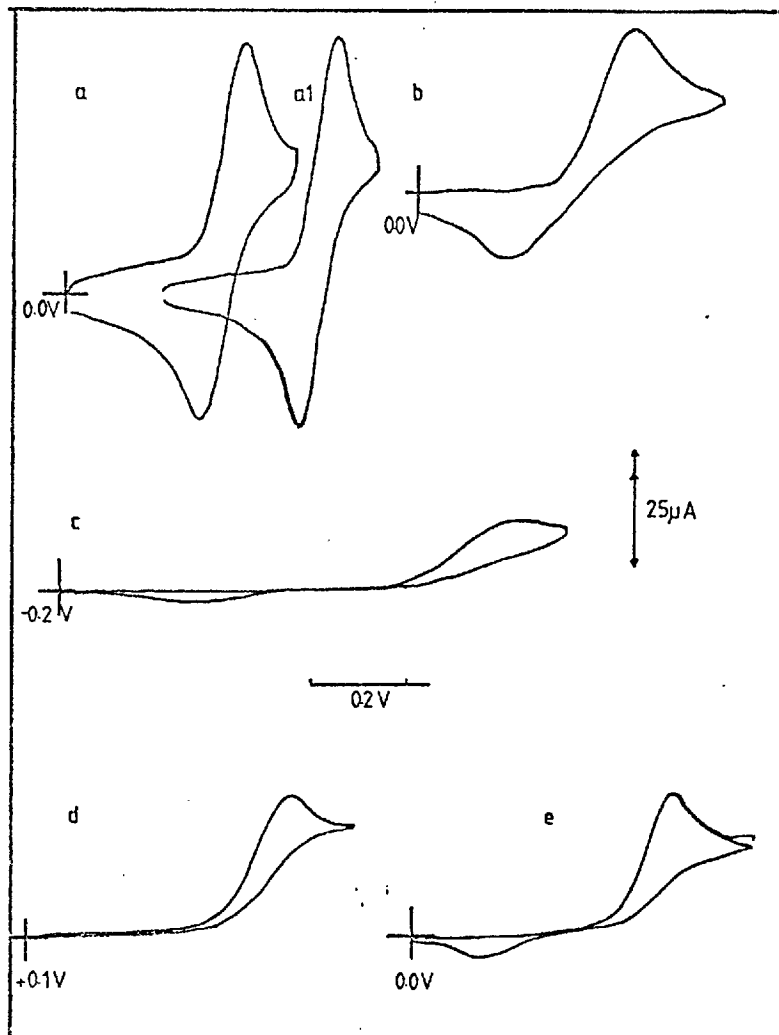
CYCLIC VOLTAMMOGRAMS OF 5mM HYDROQUINONE /pH 2·2
5mV/sec

a. Oxidised Plessy GC treated with Hydrazine;a1. with Hydroxylamine
b. Oxidised Plessy GC untreated
c. Tokai GC
d. Pt
e. Au

Figure 2-20
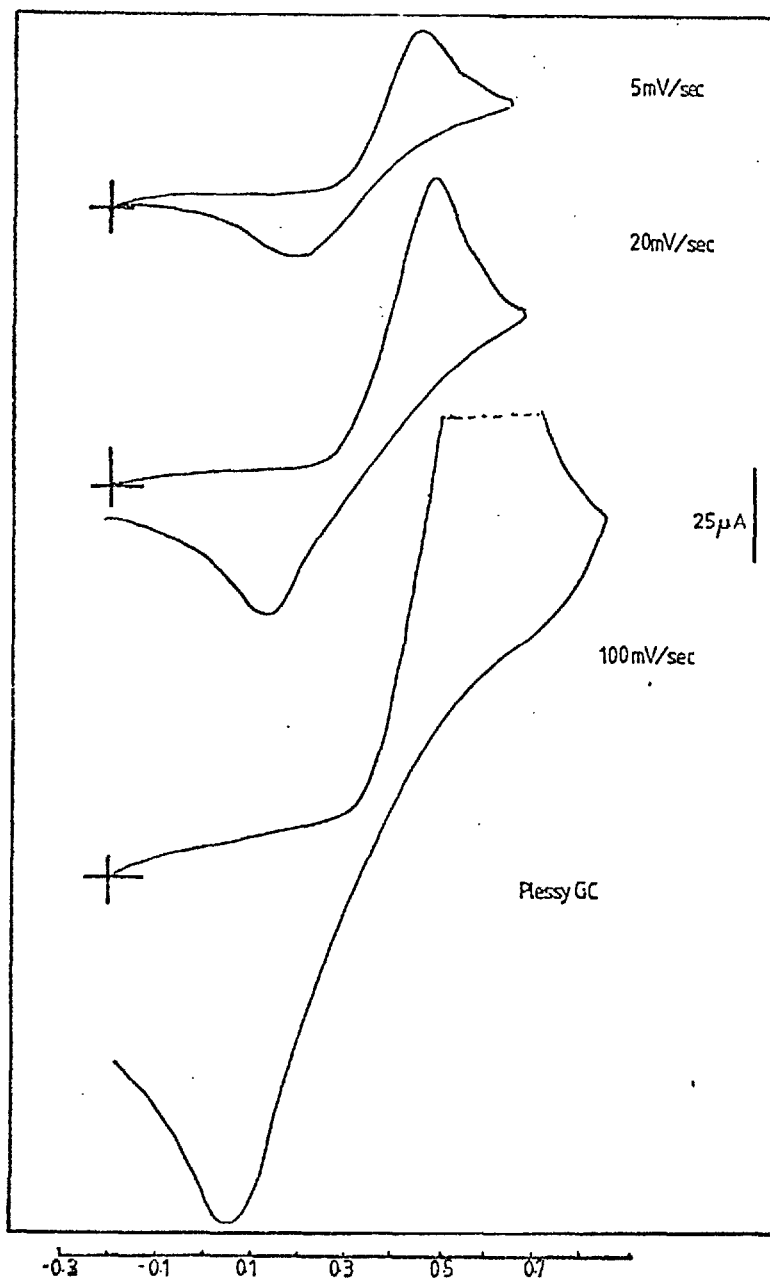
Figure 2-21

In the figure above the effect of scan rate on the cyclic voltammogram of hydroquinone (pH 2.2) obtained with an untreated Plessy GC.

5mV/sec

20mV/sec

2 5μA

100mV/sec

5mV/sec

20mV/sec

25μA

EFFECT OF SCAN RATE ON CYCLIC
VOLTAMMOGRAM OF H_2O (Pt)
pH 2.2

100mV/sec

-0.2   0.2   0.6   1.0

-.2   0.2   0.6   1.0
E /V vs SCE
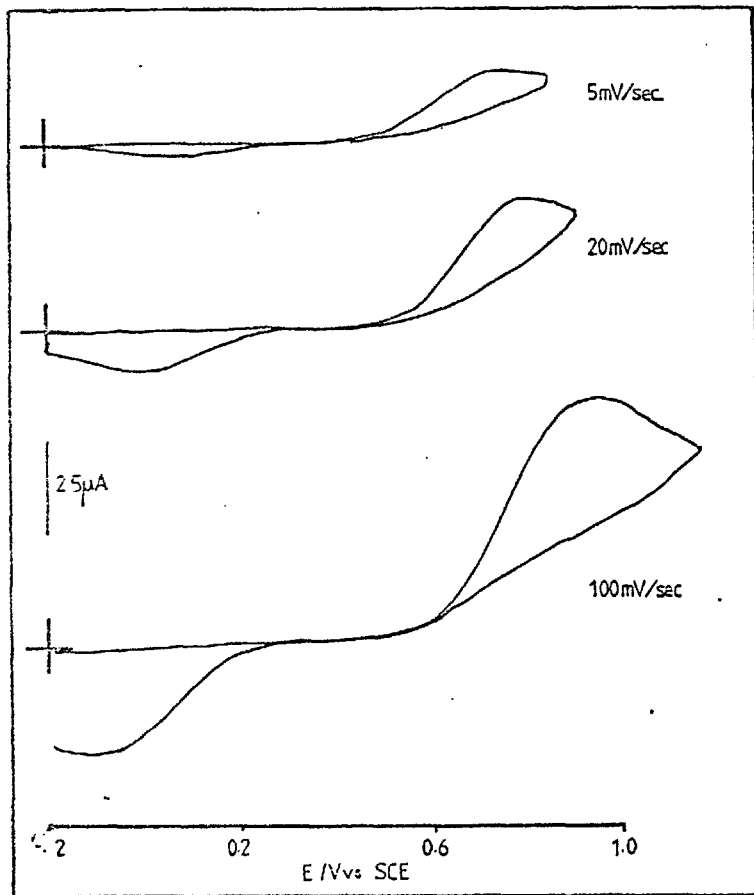
EFFECT OF SCAN RATE ON CV OF HYDROQUINONE
TOKAI GC
pH 2.2

(a)
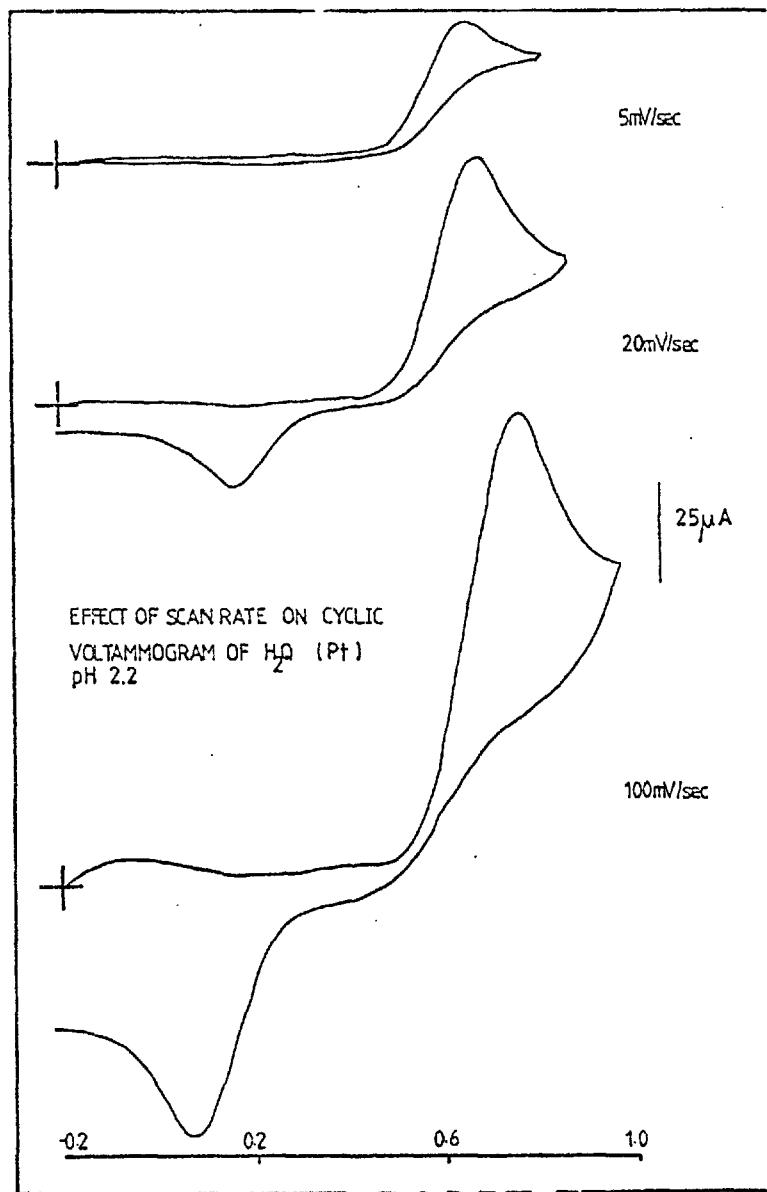
(b)

Figure 2-22

If the electron transfer rate is sufficiently high to maintain Nernstian equilibrium at the electrode surface (the reversible case), then the peak current density follows the following relationship (the Randles Seevcik equation (77,78))

$$I_p = 2.71 \ 10^5 \ n^{3/2} \ D_0^{\frac{1}{2}} \ c_0 \ v^{\frac{1}{2}}$$

Howvever, if the reaction is sufficiently slow compared with the potential sweep rate, v, that the surface concentrations of the electro active species can no longer follow the Nernstian values, the peak characteristics change and the following limiting behaviour is approached at high sweep rates

$$I_p = 3.01 \ 10^5 \ n_\alpha (\alpha n_\alpha)^{\frac{1}{2}} \ D_0^{\frac{1}{2}} \ c_0 \ v^{\frac{1}{2}}$$

where n_α is the number of electrons transferred up to and including the rate determining step.

In figure 2-23 we haves plots of i_p vs $v^{\frac{1}{2}}$. It shows that the hydrazine treated glassy carbon has the most linear slope. Pt and Au show the most curved plot . Interestingly the untreated Plessy GC and Tokai GC show indentical response.

This deviation from linearity must reflect that the reaction is sufficiently slow compared to the sweep rate. On this basis it is plausible to assume that reaction on hydrazine treated carbon is significantly faster.

Another parameter which can be of use in analysing reactions is the peak separation ΔE_p, which is $\frac{o.o59}{n}$ volts for a reversible (fast) process and independent of sweep rate.
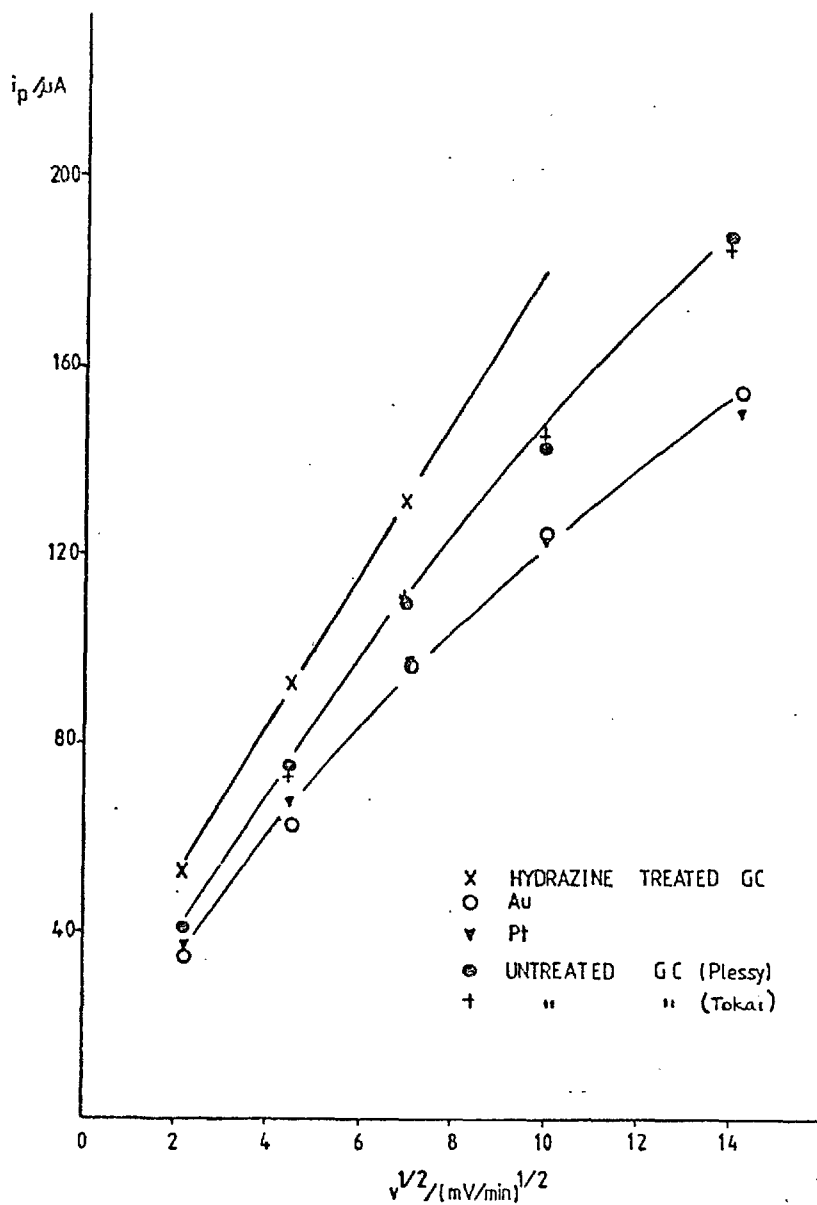
Figure 2-23

Figure 2-24 shows the variation of E_p with scan rate.
It can be seen that Tokai GC has the largest peak separation.
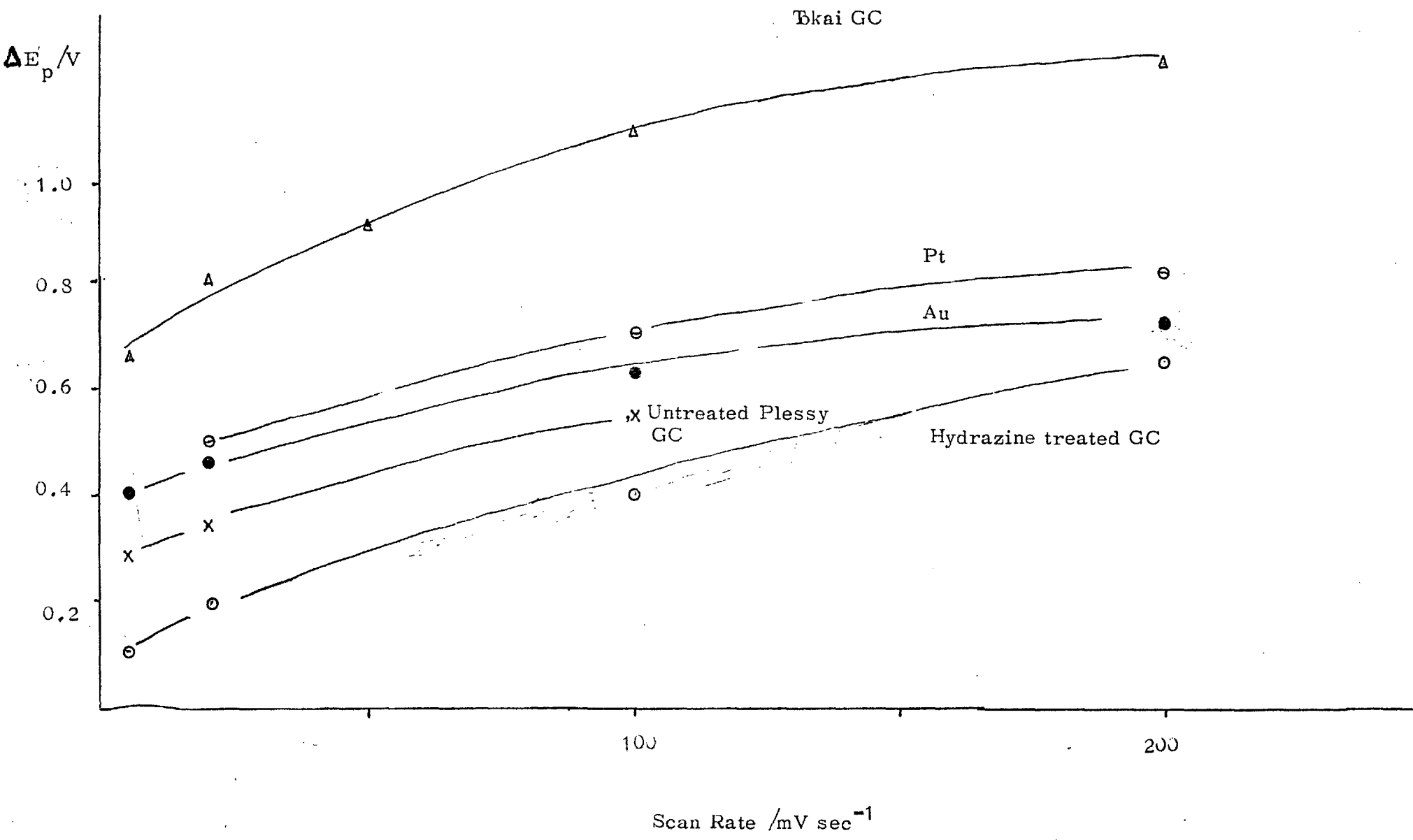
Figure 2-24

The Effect of pH

In the following cyclic voltammograms the effect of using buffer solutions of different pH is shown. The buffer solutions used have already been described in section 1.61.

10 uA

0.0V

-0.2V

m   -0.3V

-0.3V

Platinum Electrode

0.2V vs SCE

pH 0.3   pH 2.2   pH 6.0   pH 10.8
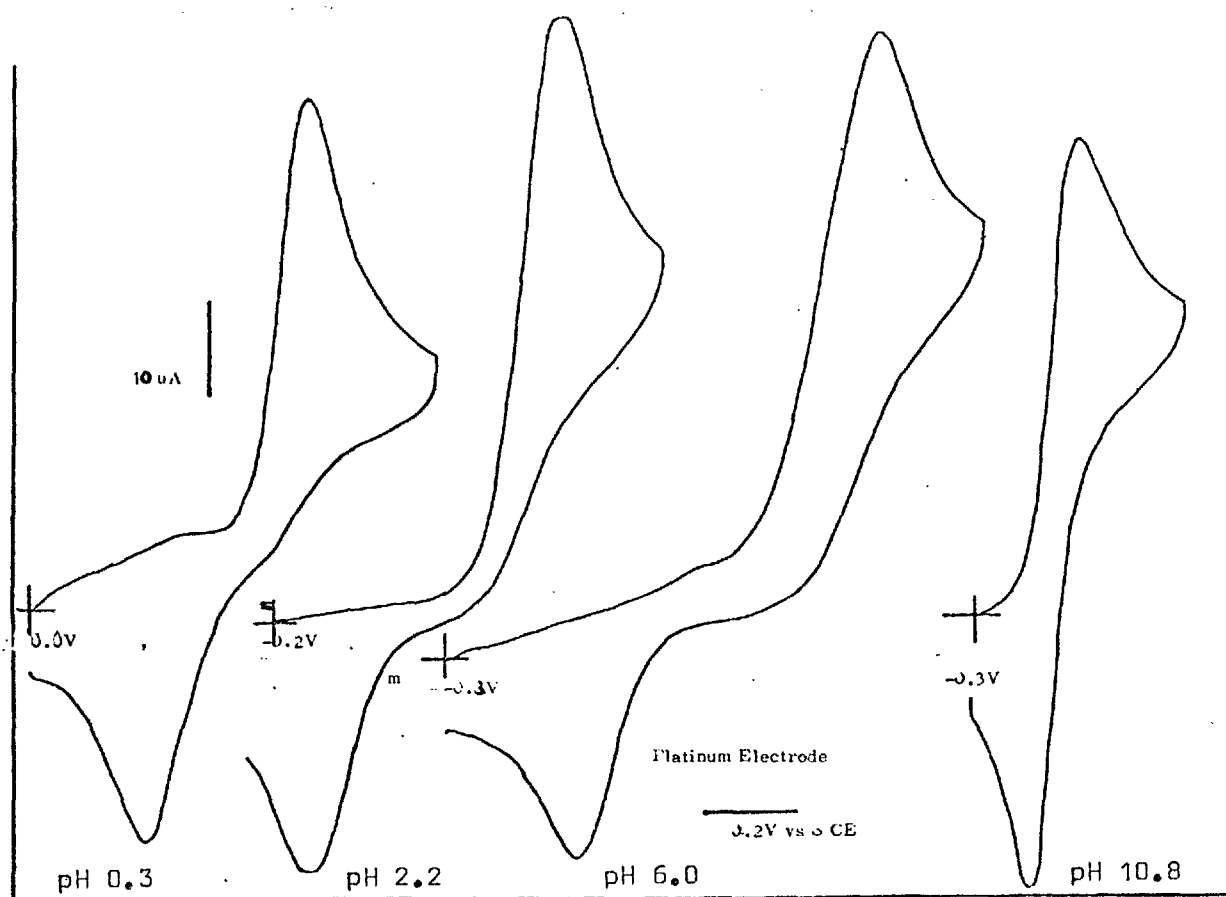
Figure 2-25

Cyclic Voltammograms for Pt Electrode
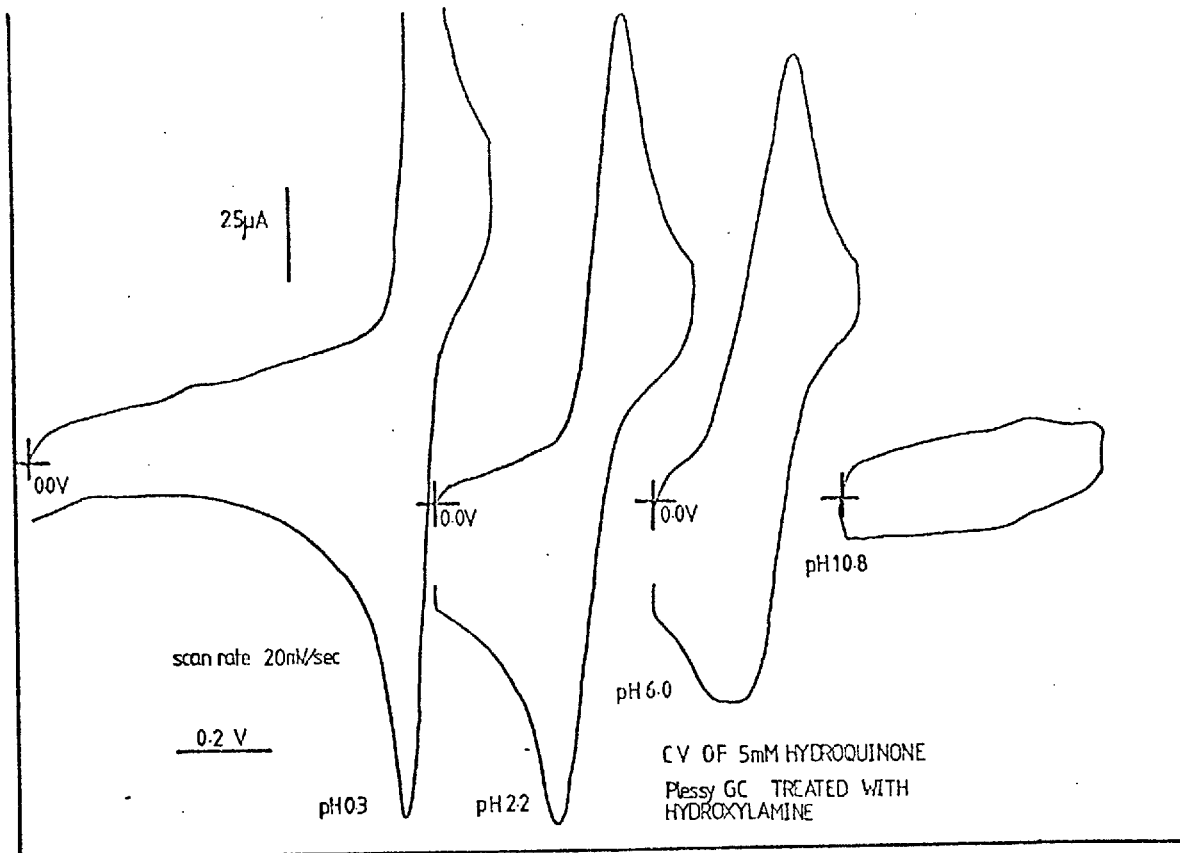
Figure 2-26
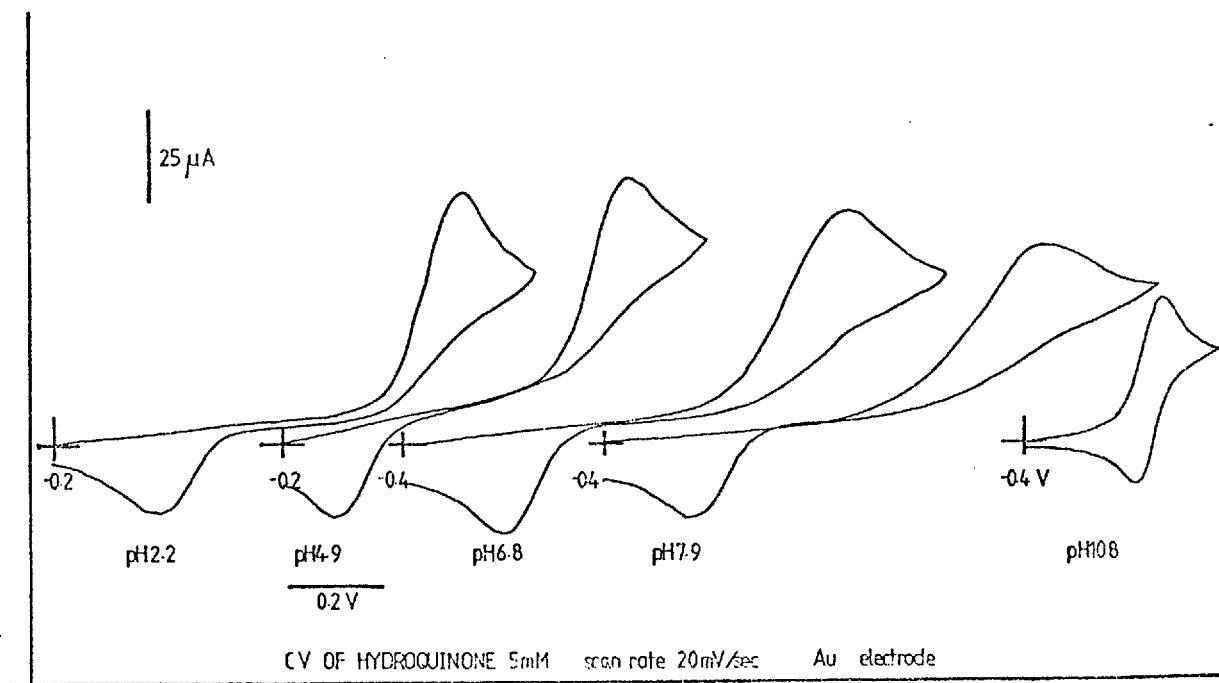
Figure 2-27

77
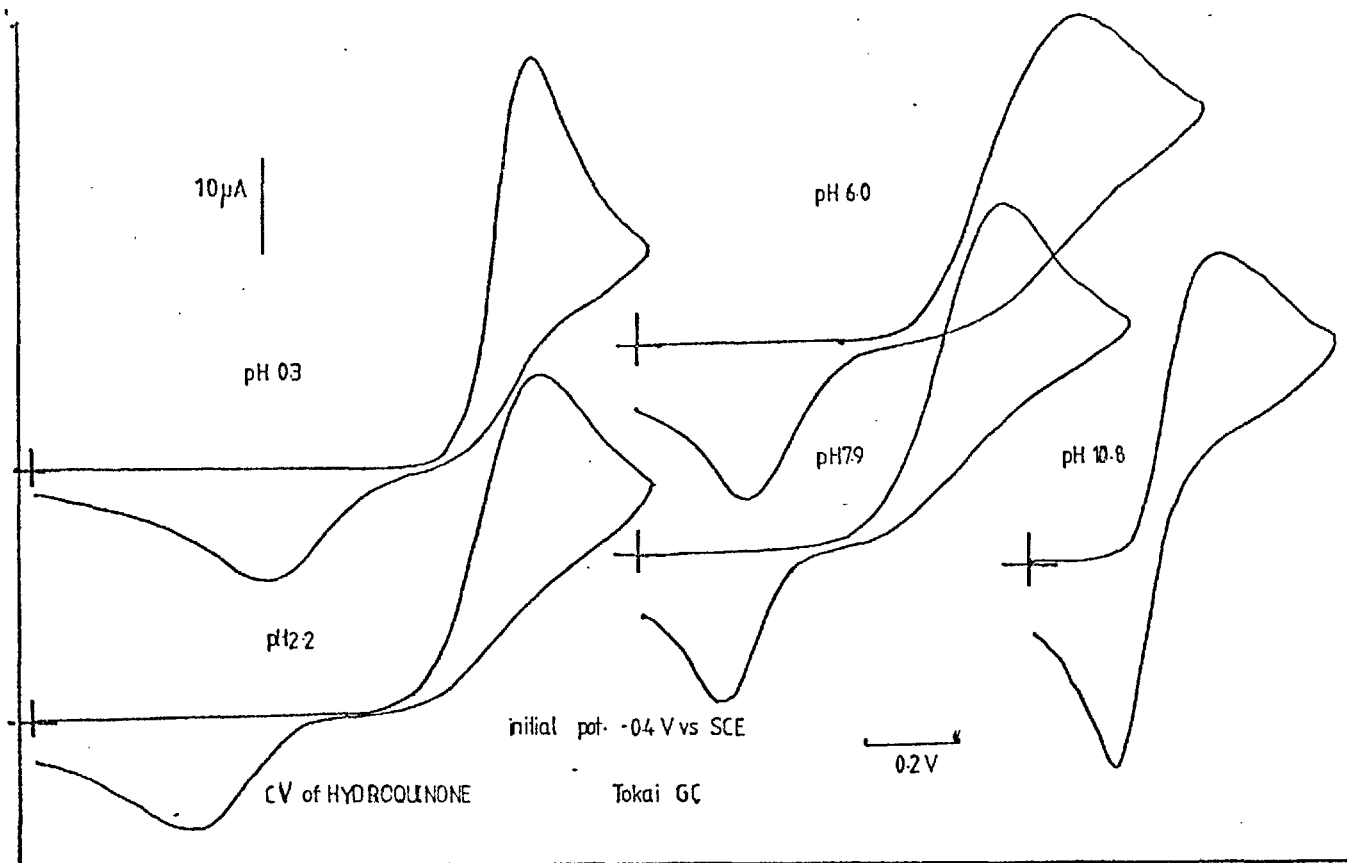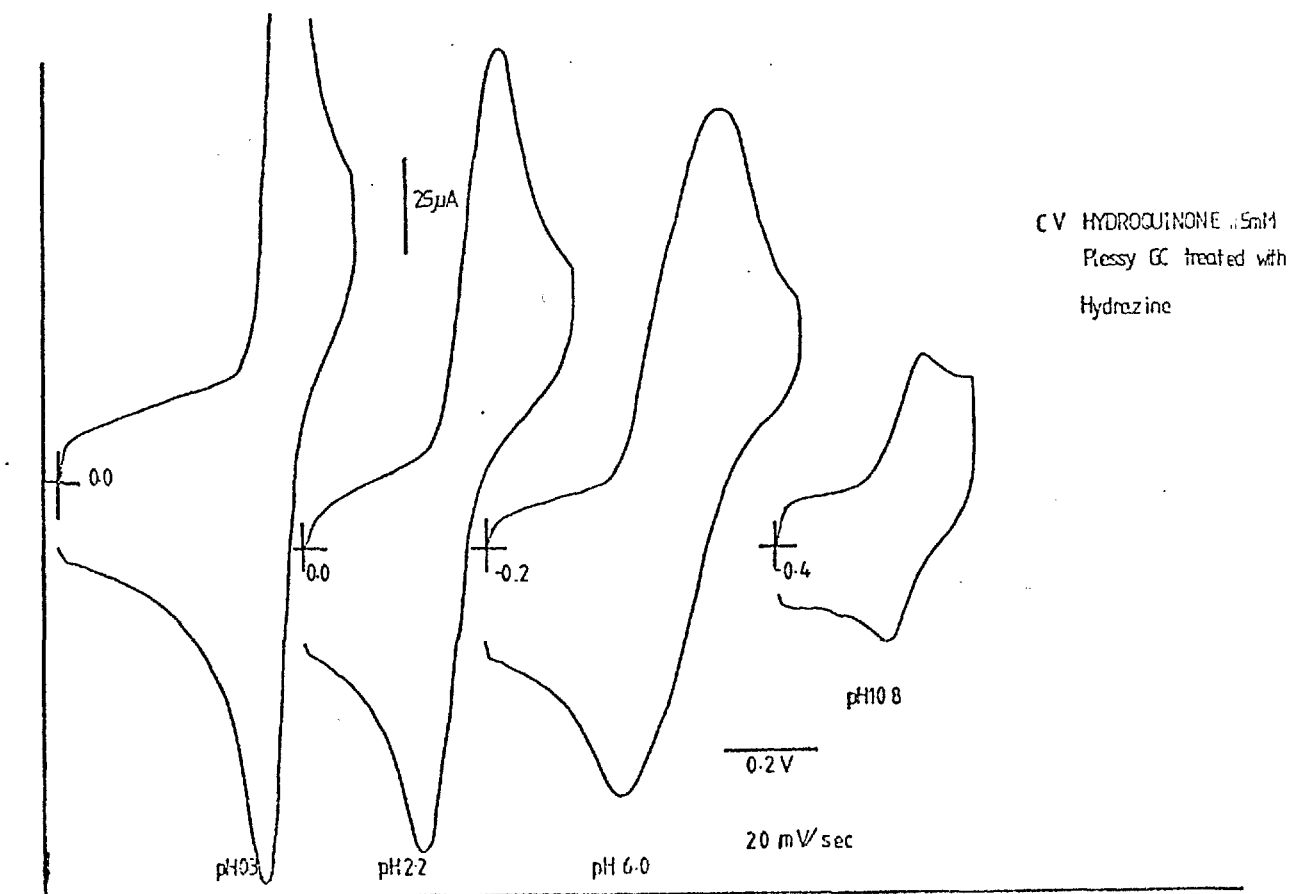
Figure 2-28

Figure 2-29
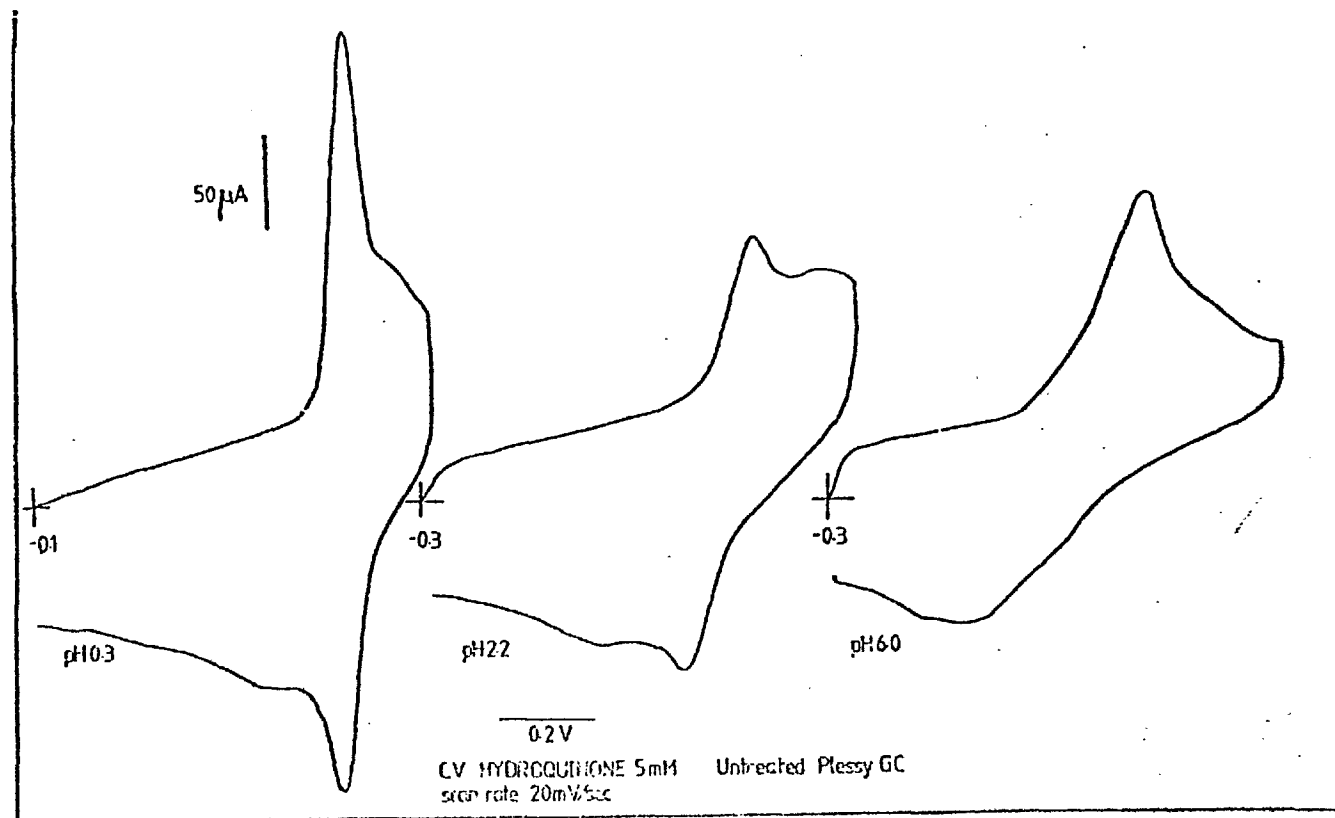
Figure 2-30

The effect of buffer solutions of different pH on the cyclic voltammogram of hydroquinone could be ascribed to two reasons:

i) anion effect (i.e. citrate and phosphate)

ii) susceptibility of the eloctrode surface to change with pH; for example, due to ionisation of C-O groups on glassy carbon.

From the above figures the following points can be made:

i) for the Tokai GC, Pt and Au, as the pH is increased, the CV of hydroquinone does not appear to change shape as much as in the case of the treated and untreated Plessy GC.

ii) Tokai GC appears to be the least susceptible to pH change.

iii) As the pH is increased the peak potentials become more negative (figure 2-31 & 2-32). This has been described by Adams (76). The slight deviation at pH 6 is due to the anion effect; of changing from citrate to phosphate buffers.

iv) From the E_p- pH plots it can be seen that Pt, Au and Tokai GC behave similarly, in contrast with the Plessy GC's.

79

Figure 2-31

GRAPH SHOWING VARIATION OF CATHODIC PEAK CURRENT

WITH pH

⊖ Au
○ Pt
✗ Tokai GC
⊛ Plessy GC (Untreated)
▽ Plessy GC (Treated with Hydrazine)

Peak Currents Obtained at a Scan Rate = 20 mV/sec

E_p/V vs SCE

pH
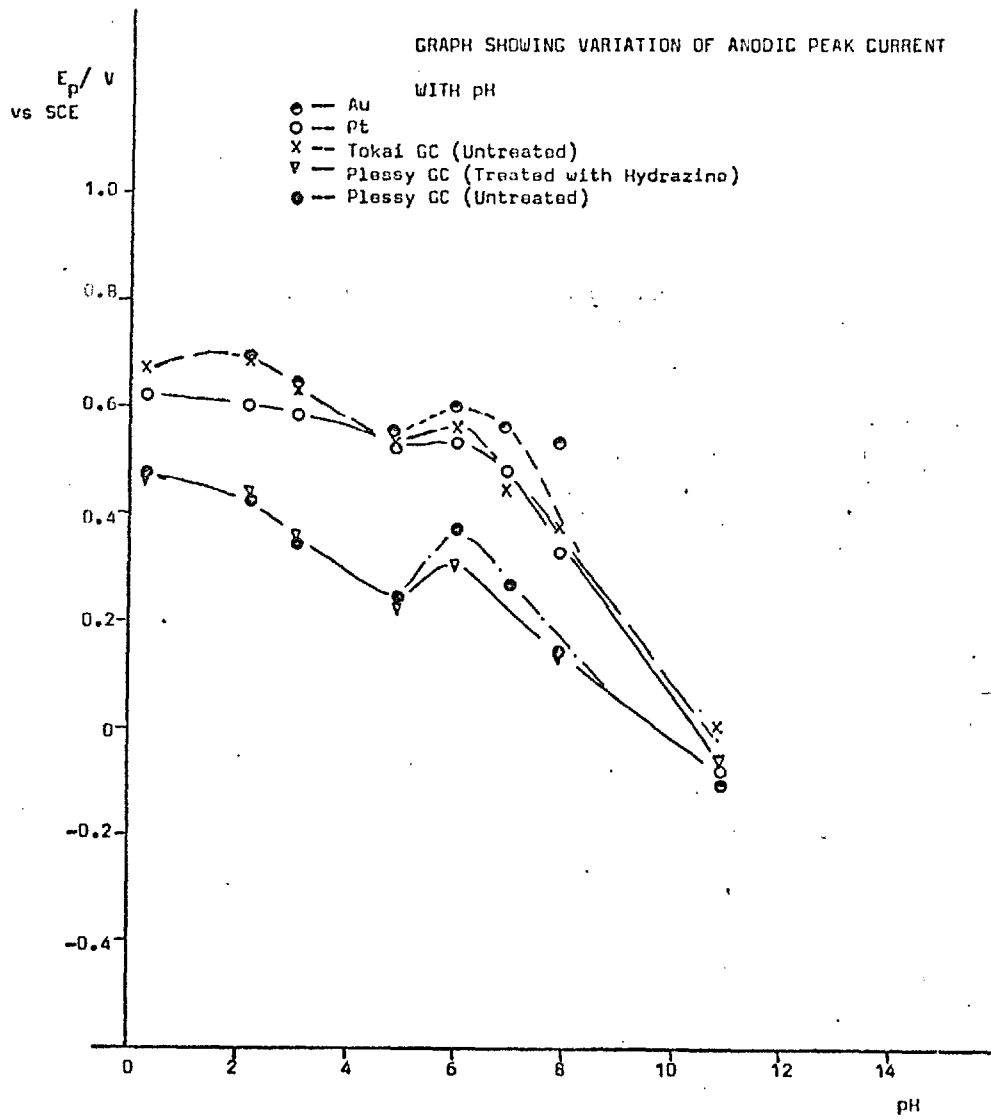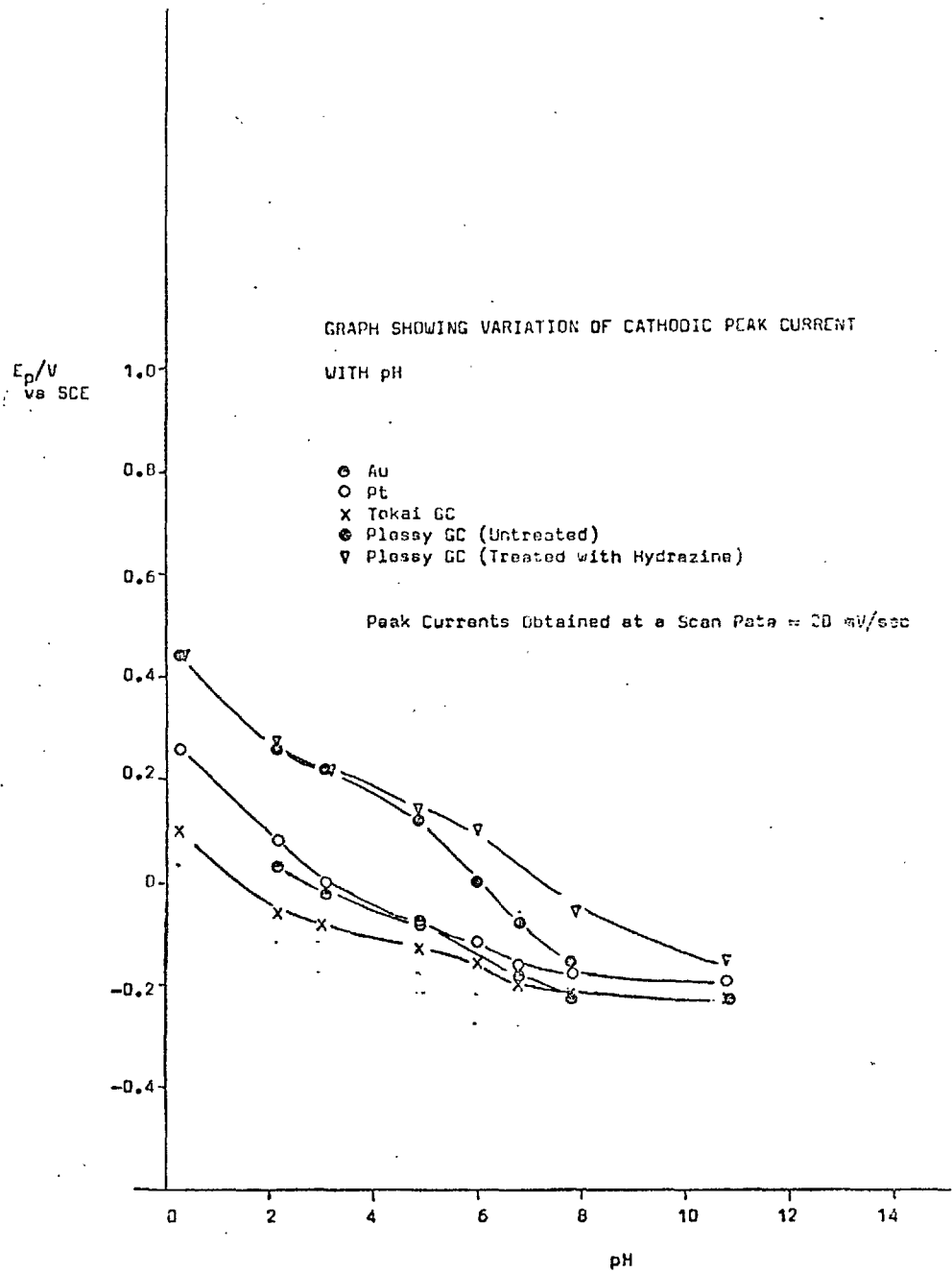
Figure 2-32

Discussion

From the results that have been presented in this chapter it appears as though the chemical pretreatment of glassy carbon surfaces with hydrazine and hydroxylamine greatly enhances the reversibility of the hydroquinone reaction. Additionally, it was found that high surface activity was reflected in loss of hydrogen and oxygen overvoltage.

In the case of the ferrocyanide reaction, chemical pretreatment does not seem to influence the reversibility significantly. In contrast with the hydroquinone reaction however, the reaction shows itself to be reversible on Pt.

Tokai GC, characterized in chapter I as having very little surface activity, seems to give the worst performance of the electrode materials that were tried as both the hydroquinone and ferrocyanide reactions appear to be highly irreversible. Additionally, hydrogen and oxygen overpotentials occur at more negative and positive potentials respectively.

On the basis of these results it is difficult to define any one mechanism by which surface groups enhance the hydroquinone reaction but not the ferrocyanide reaction. Perhaps it is a direct interaction of the surface groups with the reactant. There is also the possibility of resonance tunelling via acceptor states formed in the surface electronic band gap. Surface groups could also alter the double layer characteristics thus enhancing the formation of the transition state.

CHAPTER III   ASPECTS OF FLOWING STREAM ANALYSIS

3.1   Introduction and General Considerations

A wide range of designs and cell geometries have been used for measurements in experimental systems where convective diffusion is the principal mode of mass transport (see Table 3-1). These systems cover both the design and operation of continuous voltammetric sensors and also experimental assemblies such as the rotating disc, used for more theoretical studies of electrode processes.

The primary requirements for continuous monitoring are:

i) well defined electrode geometry and limiting current

ii) high sensitivity and stability

iii) ease of maintenance of working electrode surface

A detailed study (79,80) of many of the electrode designs smmarised in Table 3-1 indicates that the Wall Jet Cell (WJC) is possibly the most versatile design for a wide range of continuous monitoring applications

Electrode Geometry	Equation for i_{lim}
Conical	$i_1 = knFAL^{\frac{1}{2}}CD^{\frac{2}{3}}v^{-1/6}V^{\frac{1}{2}}$
Tubular	$i_1 = knFAL^{\frac{2}{3}}CD^{\frac{2}{3}}V^{\frac{1}{3}}$
Rotating Disc	$i_1 = knFACD^{\frac{2}{3}}v^{-1/6}\omega^{\frac{1}{2}}$
Flat Plate	$i_1 = knFAL^{-\frac{1}{2}}CD^{\frac{2}{3}}v^{-1/6}V^{\frac{1}{2}}$
Wall Jet	$i_1 = knFR^{\frac{3}{4}}a^{-\frac{1}{2}}CD^{\frac{2}{3}}v^{-5/12}V^{\frac{3}{4}}$

Table 3-1 Equations for the limiting current for various
electrode geometries

v = kinematic viscocity, V = flow rate, R = radius, a = inlet diamet

ω = rotation velocity, D = diffusion coef., A = area

83

It can be seen from table 3-1 that whereas for most of the electrode geometries the limiting current depends on the (flow rate)$^{\frac{1}{3}-\frac{1}{2}}$; in the case of the Wall Jet the dependence is to the power $\frac{3}{4}$.

A wall jet describes the flow of a jet of fluid impinging onto a wall placed perpendicular to it and flowing radially over the surface. The first rigorous treatment of this phenomena was due to Glauert (81). Later Yamada and Matsuda (82) used the correlations arrived at by Glauert to define the diffusion current in terms of various hydrodynamic parameters.

Though the correlations of Glauert holds for laminar flow conditions , in the case of turbulent flow the velocity distribution within the boundary layer has been criticized by Spalding (83) and others (84). The error made by Glauert was attributed to neglecting the effect of the wall on the jet. This assumption holds apparantly only in the case of laminar flow and then only after a certain inlet to wall separation (determined emperically).

In this chapter the hydrodynamic parameters of the wall-jet cell are investigated. The approach employed is firstly to derive the equation for the boundary layer thickness and diffusion layer thickness and hence the equation for the limiting current. The equation for boundary layer and the diffusion layer has not been previously derived.

3.12 Convective Diffusion

The considerable problems encountered in the analysis of mass transfer during forced convection electrolysis often makes a rigorous

mathematical treatment difficult. Though this appears to be the
general situation there are particular electrode geometries operating under
laminar flow conditions wherein a complete solution may be obtained.

The mass transfer of a (electroactive) species by convective
diffusion may be described for a three dimensional system by the general
equation (85).

$$\frac{\partial c}{\partial t} = D\left(\frac{\partial^2 c}{\partial x^2} + \frac{\partial^2 c}{\partial y^2} + \frac{\partial^2 c}{\partial z^2}\right) - \left(V_x \frac{\partial c}{\partial x} + V_y \frac{\partial c}{\partial y} + V_z \frac{\partial c}{\partial z}\right) \quad\text{------ (i)}$$

In the particular case of linear mass transfer of a species to a
electrode of fixed geometry, it is possible to obtain a solution
for this equation by setting appropriate initial and boundary conditions.
An important feature of this equation is the distribution
of concentration in the diffusionlayer next to the electrode surface.
In the second group of terms on the right hand side of equation (i),
which describes the rate of change of concentration due to convection,
the solution flow characteristics are embodied in the terms V_x, V_y, and
V_z. These terms often involve complicated velocity distribution
functions.

3.13 The Analogy Between Convective Diffusion and Surface Friction.

While most treatments of the problem of convective diffusion
has involved a solution to equation (i) , it is also possible, in theory,
to obtain an approximate solution by considering the analogy between mass
transfer and momentum transfer.

The flux of mass is given by the equation;

$$j = D \frac{\partial c}{\partial y} \qquad\qquad\text{--------(ii)}$$

85

The flux of momentum is given by the equation;

$$\tau = \rho \nu \frac{\partial v_x}{\partial y}$$ ———— (iii)

Where y is the direction normal to the electrode,
τ = skin friction, and ν =kinematic viscocity.

In terms of mass transfer the equation for the limiting
current may then be given by;

$$i_{lim} = nF j_{max}$$ ———————— (iv)

Where n = number of electrons

& F = Faradays constant

Correspondingly the equation for the limiting current
may be described in terms of the flux of momentum which for an
irrotational fluid is given by (85b);

$$i_{lim} = knFCD^{\frac{2}{3}} \mu^{-\frac{1}{3}} (\int_{x_o}^{x_1} [r_o(x)^3 \tau(x)]^{\frac{1}{2}} dx)^{\frac{2}{3}}$$ ———————— (v)

Where k is a numerical constant and other symbols have their
usual meaning.

3.14 Electrode Geometries used in Flowing Solution Monitoring.

Rigorous mathematical solutions have been derived for i_{lim} for
the following electrode systems; The Conical Electrode (86), Planar
Electrode with solution flowing parallel over the surface with zero
incidence (87), the Tubular Electrode (88), the Rotating Disc Electrode
(89), Ring Disc Electrode (90),   the Wedge Electrode, a Flat Plate
perpendicular to solution flow (91), and the Wall Jet Electrode (92).

Solutions for the last three electrode geometries mentioned
above have been obtained by deriving an equation for the skin friction
and substituting in equation (v) (93,94).

Cell Design

The working cell design is slightly modified from the original wall-jet concept and is in effect a constricted wall-jet with the cell body and working electrode forming a thin layer cell; unlike the original concept where a nozzle was placed close to the electrode surface in a large volume cell.

Two versions of the wall-jet cell have been tried. The first was based on the original design due to Fleet and Little (95); Figure 3-1. Here the cell body was made of 'perspex' and for non aqueous work- of the fluorocarbon plastic Kel-F (Minnesota Mining and Manufacturing USA).

The working electrode consisted of a disc of glassy carbon, encased in a Kel- F body and sealed with 'Araldite' (Ciba Giegy Ltd. UK). Electrical contact was made using a silver loaded epoxy cement to connect a copper lead to the back of the glassy carbon. A Ag/AgCl system served as the reference electrode and was housed in a removable unit, separated from the solution in the cell by a ceramic frit.

In the modified cell design, the wall-jet was made in a ring - disc configuration (figure 3-2) with the reference electrode placed opposite the working electrode. Additionally, two outlets were used in order to enhance uniform flow over the electrode surface. Owing to the different types of glassy carbons used it was difficult to compare the two configurations though it might be said that performance is not enhanced with the modified design.

87
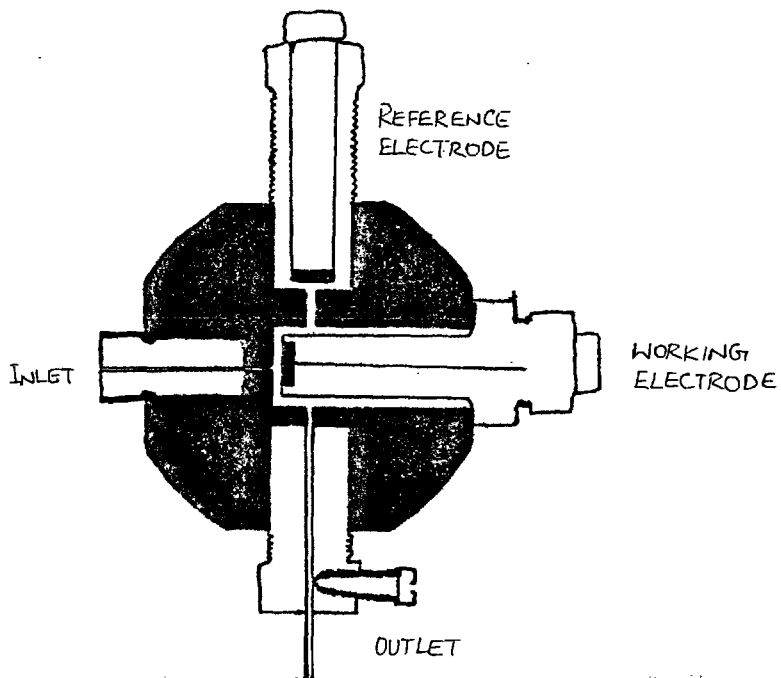
fig. 3-1

The Wall Jet Cell- the original cell
design.
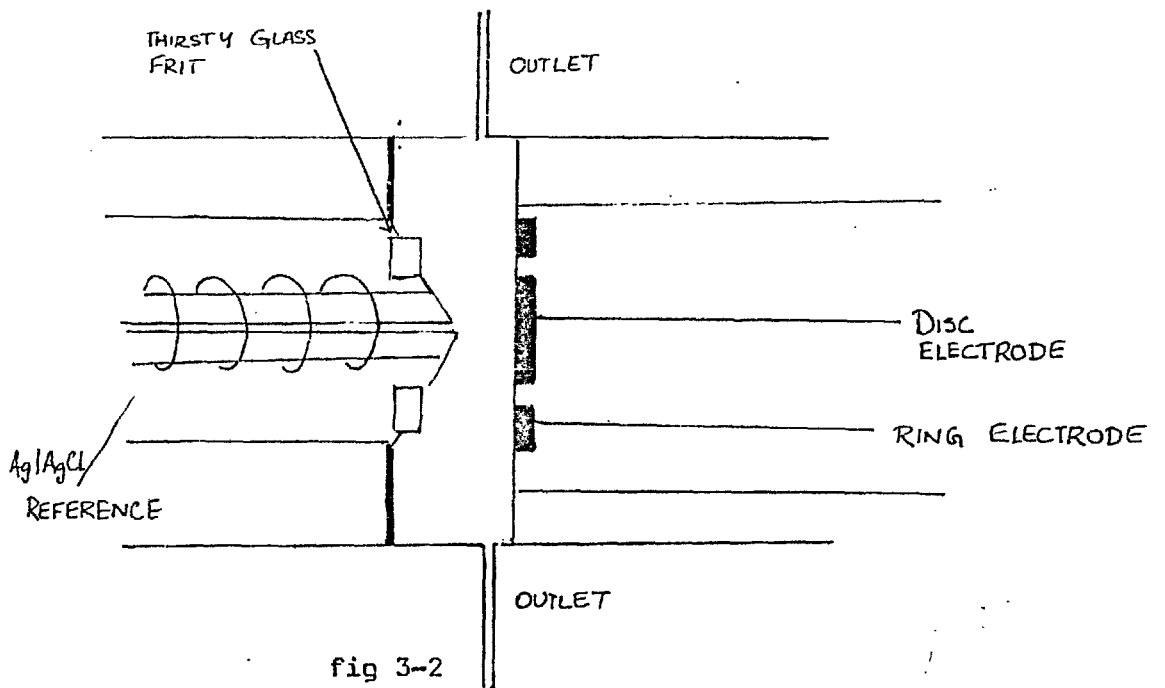
fig 3-2

The Wall Jet Cell - the modified cell
design

3.3 Evaluation of Hydrodynamic Parameters

3.31 Estimation of the Boundary Layer Thickness for a Wall Jet.

When a solution flows over a solid surface, there is a region in the vicinity of the surface where a high velocity gradient exists owing to the viscous properties of the liquid. This region was first described by Prandtl (95) and is termed the Hydrodynamic boundary Layer or the Prandtl Layer. Practically, the Boundary Layer thickness is not defined but is taken as the distance from the surface within which the main change in the flow velocity occurs.

In the simplest case of solution flow, viz. flow parallel to a flat plate with zero incidence,(fig. 3-3) the evaluation of the boundary layer thickness involves the equation of inertia and frictional forces (96). Within the boundary layer, owing to the large shearing forces present, frictional forces are of comparable magnitude to inertia forces.
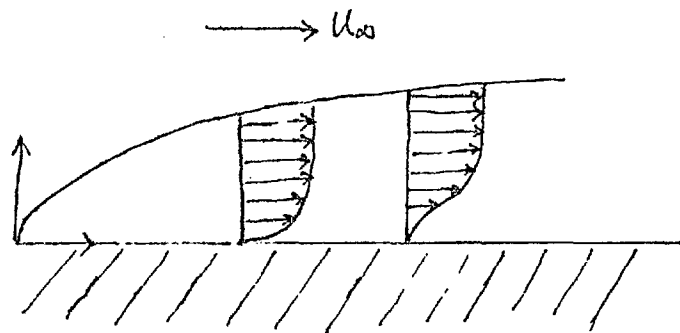
fig. 3-3 Exagerated schematic representation of the Hydrodynamic Boundary Layer formed due to parallel flow over a flat plate.

If the frictional force within the boundary layer is of the order of $\mu U/\delta^2$ (Newton's Law of Friction), where μ = viscocity, U = velocity and δ= the boundary layer thickness, and the inertia force of the order $\rho U^2/L$, where ρ = density of the solution and L = length, equating the two it is possible to obtain a value for the boundary layer

thickness   , given by;

$$\delta \simeq \sqrt{\frac{\nu L}{U_\infty}} \qquad \text{————(vi)}$$

and   for laminar flow (96);

$$\delta = \sqrt{\frac{\nu L}{U_\infty}} \qquad \text{————(vii)}$$

Following this line of argument it is possible to estimate the boundary layer thickness for the Wall Jet.
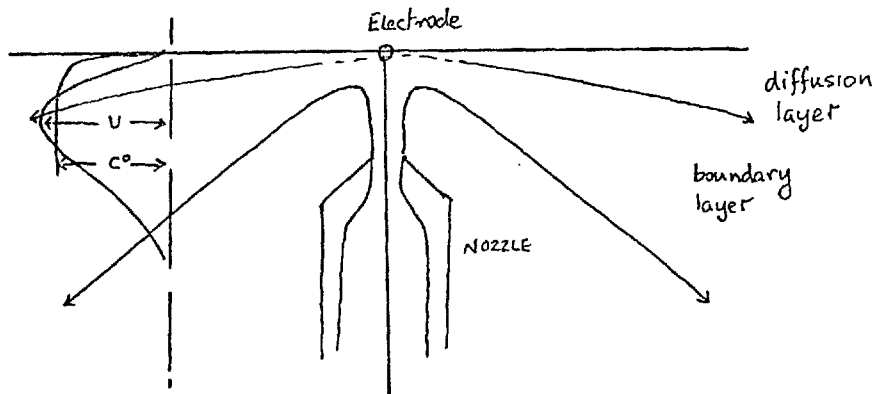
fig 3-4 Schematic representation of the boundary layer formed for a Wall Jet showing the velocity profile within the boundary layer.

The velocity term U in equation vii can be given the maximum value of the radial flow velocity. According to Glauert (81) the radial velocity is given by;

$$u = \left(\frac{15F}{2\nu x^3}\right) f'(\eta) \qquad \text{————(ix)}$$

where $\eta = \left(\frac{135F}{32\,\nu^3 x^5}\right)^{\frac{1}{4}} y \qquad \text{————(x)}$

and F is the flux of exterior momentum flux given by;

$$\int_0^\infty xu \left\{ \int_y^\infty xu^2 dy \right\} dy = \text{constant.}$$

Glauert also indicated that a rough estimate of the term F could be made by;

$$F= \tfrac{1}{2} \text{ (typical velocity) (volume flow per radian)}^2$$

For a jet issuing from a nozzle of diameter a cm with a volume flow rate = Vcc/sec,

$$F= \tfrac{1}{2}k \left(\frac{4V}{2\pi^3} \right) \left(\frac{V^3}{a^2} \right) \quad \text{------} \quad (xi)$$

Where k is a constant =0.4979 (82).

The radial velocity function can be estimated by considering the velocity profile deduced by Glauert (81), given in figure 3-4 below.
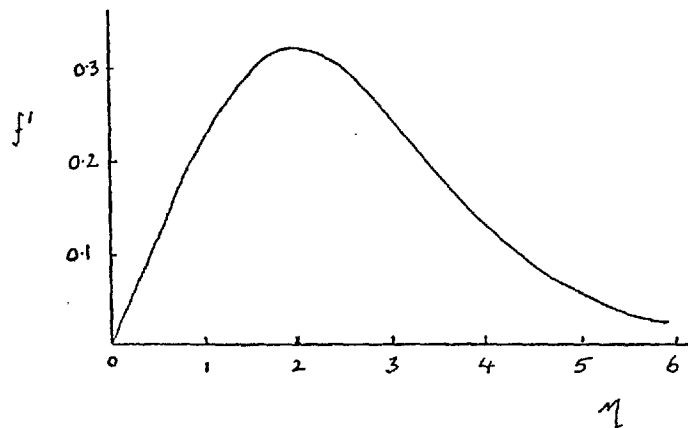
Fig. 3-4 Variation of velocity f'(n) with

·distance from wall as deduced by Glauert.

From fig 3-4 it can be estimated that the maximum value of

$$f'(\eta) = 0.319 \quad \text{----------} (xii)$$

Substituting (xii) and (xi) in (ix) we have the maximum value of the radial velocity u, given by;

91

$$u = (0.319(15/4)^{\frac{1}{2}}(0.84)^2) \left(\frac{v^3}{\pi^3 a^2 v x^3} \right)^{\frac{1}{2}} \text{---------}(\text{xiii})$$

Substituting xiii. in equation vii and simplifying we have δ_{BL}, the boundary layer thickness given by,

$$\delta_{BL} = 7.6\pi^{\frac{3}{4}} a^{\frac{1}{2}} v^{\frac{3}{4}} x^{5/4} \; v^{-\frac{3}{4}} \qquad \text{-------------}(\text{xiv})$$

Owing to the complexity of the velocity profile of the Wall Jet within the boundary layer when compared with the case of parallel flow over a flat plate, it may be more valid to define the hydrodynamic boundary thickness in another sense.

According to Von Karman (97) and Riddiford (98), in the case of the Rotating Disc electrode, the hydrodynamic boundary layer is seen as the layer of liquid dragged by the rotating lamina. In other words the region where the major portion of the tangential and radial velocity profiles is found. The approximate equation for the boundary layer thickness estimated by these workers is given by

$$\delta_{RDE} = 2.8 \left(\frac{v}{\omega} \right)^{\frac{1}{2}} \qquad \text{-------------}(\text{xv})$$

Following this reasoning it is plausible to define the boundary layer thickness for the Wall Jet to be the layer wherein the major portion of the radial velocity profile is contained (see fig. 3-4)

Refering once again to Glauert's velocity profile (fig. 3-5) at $f'(\eta) = 0.025$ - close to the end of the velocity profile, $\eta = 6.$

92

Substituting the value for n in equation x we have;

$$= (\frac{135 \, F}{32 \vartheta^3 x5})^{-\frac{1}{4}} \times 6 \qquad \text{\textemdash\textemdash}(xvi)$$

From equation (xi),

$$F = (\frac{k}{2 \pi^3})(\frac{v^3}{a^2})$$

Substituting in (xvi) and simplifying we have;

$$\delta_{BL} = 5.9\pi^{\frac{3}{4}} a^{\frac{1}{2}} \vartheta^{\frac{3}{4}} x5/4 \, v^{-\frac{3}{4}} \qquad \text{\textemdash\textemdash\textemdash}(xvii)$$

Comparing the two derivations it seen that the numerical coeficient determined by the first method is slightly larger than that obtained by the second. In both cases however, the variable terms have the same expression;

viz.

$$\delta_{BL} \propto a^{\frac{1}{2}} x5/4 \, v^{-\frac{3}{4}}$$

The second derivation is probably based on a more correct interpretation of the boundary layer.

Unlike the case of the Rotating Disc Electrode, where the boundary layer thickness is independent of the disc radius, in the case of the Wall Jet

$$\delta_{BL} \propto x^{5/4}$$, x being measured from the jet axis. Thus the hydrodynamic boundary layer increases rapidly downstream from the jet axis. This is to be compared with the case of the flat plate where

$$\delta_{BL} \propto x^{\frac{1}{2}}$$

3.32 Estimation of the Diffusion Layer Thickness.

For a solution flowing over a solid body there is a region in the immediate vicinity of the surface where a rapidly changing concentration profile is found (96). This region is termed the diffusion layer (see fig. 3-4).

According to Levich (96) the thickness of the diffusion layer given by;

$$\delta_{dl} = (\frac{D}{v})^{\frac{1}{3}} \delta_{bl} \quad\text{------------- (xviii)}$$

where δ_{bl} is the boundary layer thickness.

Substituting for δ_{bl} we have

$$\delta_{dL} = k \pi^{\frac{3}{4}} D^{\frac{1}{3}} a^{\frac{1}{2}} v^{5/12} x^{5/4} v^{-\frac{3}{4}} \quad\text{---------- (xix)}$$

where k is a numerical constant which can be determined from the data of Yamada and Matsuda (82).

3.33 Derivation of the Equation for the Limiting Current.

From Fick's First Law, thr current due to diffusion controlled electrolysis is given by;

$$i = nFAD_{o}(\frac{\partial C_{o}(y)}{\partial y})_{y=0} \quad\text{------(xx)}$$

n = number electrons

F = Faraday's Constant

A = area of electrode

D_{Q} = diffusion coef

If δ_{dl} is the diffusion layer thickness then equation (xx) can be simplified (96) to give an expression for the limiting current given by;

94

$$i_{lim} = \frac{nFAD_0C}{\delta_{dl}} \qquad \text{------- (xxi)}$$

Substituting for δ_{dl} we have;

$$i_{lim} = k'nFD^{\frac{2}{3}}Ca^{-\frac{1}{2}}v^{-5/12}x^{\frac{3}{4}}v^{\frac{3}{4}} \qquad \text{------- (xxii)}$$

Equation (xxii) shows the same form as the one evaluated by Yamada and Matsuda.

3.34 Numerical estimation of k and δ_{dl}.

From Yamada and Matsuda $k' = 1.33$.

Therefore $k = 0.72$.

A more accurate expression for the general equation for the diffusion layer thickness in terms of the hydrodynamic boundary layer thickness may now be obtained. In place of equation (xviii) we have;

$$\delta_{dl} = 0.1 \left(\frac{D}{v} \right)^{\frac{1}{3}} \delta_{bl} \qquad \text{------- (xxiii)}$$

for the oxidation of Ferrocyanide,

$$D = 0.76 \quad 10^{-5} cm^2/sec$$

$$v = 1.0 \quad 10^{-2} cm^2/sec$$

$$x = 1.5 \quad 10^{-1} cm$$

$$\& \; a = 3.0 \quad 10^{-2} cm$$

Substituting these values and that for k in equation (xix) we have;

$$\delta_{dl} = 0.002 \; cm$$

3.35 Discussion

The boundary layer thickness calculated for the Rotating Disk Electrode at intermediate rotation speeds is of the order of a few tenths of a millimeter. The thickness is independent of the disk radius. In the case of the Wall Jet Electrode the thickness increases rapidly from the jet axis. For a disk of radius 1.5mm, the maximum boundary layer thickness occurs at low flow rates (less than 3 cc/min) where δ_{bl} is greater than 1-2mm . At higher flow rates, δ_{bl} reduces to a few tenths of a millimeter- comparable to the RDE.

The diffusion layer thickness δ_{dl} is about 1% of δ_{bl}. Finally the high value for the boundary layer thickness affords an explanation for the variation in the limiting current with inlet distance. This phenomena while having been noted by Yamada and Matsuda (82) has not been looked at in great detail. This is attempted below.

3.4 Experimental Investigation.

3.41 Experimental

Solution flow rates of 0.2- 10.0 cc/min were achieved using a Variopex peristaltic pump (LKB Instruments, London). Use of a simple damping system (see fig 3-9) seemed to give pulse free flow.
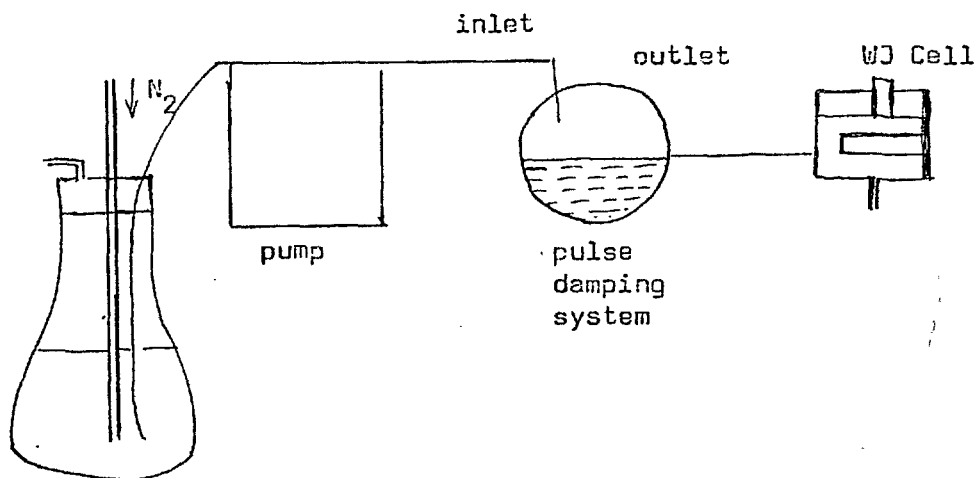
Fig. 3-8

The Experimental Set Up

Chemicals were all of Analar grade and were freshly prepared

for each determination. Solutions were bubbled with purified Nitrogen

for twenty minutes and a Nitrogen atmosphere was kept over the

solution throughout the duration of the experiment.

Current- potential curves were obtained using a PAR 174

polarograph (Princeton Applied Research). Results were obtained both

with the original cell design (fig 3-1) and the modified Ring - Disk cell

(figure 3-2).

3.42 Results and Discussion.

Dependence of i_{lim} on concentration.

Equation (xxii) predicts a linear dependence of the limiting

current on the concentration. This has been found to be true for the

range of flow rates that have been investigated in this work (1 - 3 cc/min)

- see figure 3-9.

Dependence of i_{lim} on Flow Rate.

The dependence of the limiting current on the flow rate is

found to be significantly influenced by the proximity of the jet nozzle

to the electrode surface. Whereas equation (xxii) predicts that the limiting

current is proportional to $V^{\frac{3}{4}}$ (where V is the volume flow rate), it

has been established in this work that this proportionality is obeyed

only after a certain inlet-electrode separation, d. The nominal value of

d is governed by the diameter of the electrode, the flow rate , the solution

viscocity and the geometry of the nozzle body. On closer examination it

is possible to relate this phenomena to the presence of the nozzle body

within the hydrodynamic boundary layer, which in the case of the Wall Jet

is significantly thicker when compared with other electrode geometries.

Figure 3—9

98
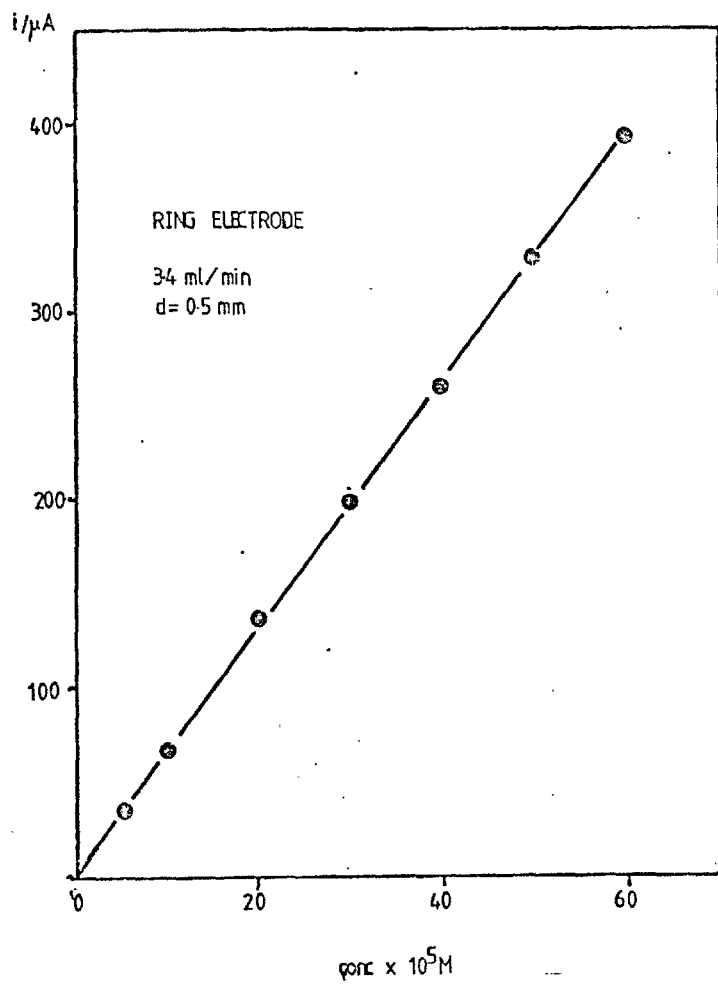
What is believed to happen is that, on account of the large velocity

gradients found   within the boundary layer, shearing forces due

to the interaction of the flowing solution and the body of the nozzle

occur. As a result there is a reduction in the solution momentum and

thus a reduction in momentum mass transfer to the electrode surface.

In electrochemical terms this means that the limiting current is

decreased.
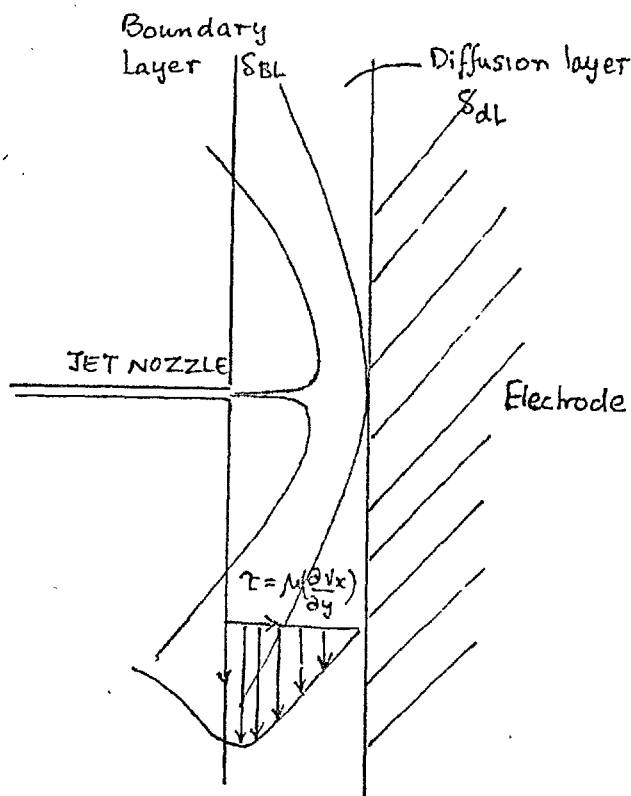
Figure 3- 10

The Effect of the Jet Nozzle Within the

Hydrodynamic Boundary Layer

Some experimental results are now presented: In figure 3-11

we have a plot of $\log i_{lim}$ vs $\log V$ (V = volume flow rate) measured at

an inlet - electrode separation $d = 0.5$ mm. It can be seen that at

Figure 3-11

Plot of $\log i_{lim}$ vs $\log V$

logi/Amp.

Inlet- Electrode separation = 0.5mm

Disc diameter = 3.0mm

slope= 0.78
Mean after 6 runs
= 0.76
Std. deviation = 0.03

Slope = 0.47
Mean after 6 runs = 0.50
Std. deviation. = 0.04

log V/cc sec

100

Figure 3-12

Slope = 0.72

inlet/electrode separation= 3.0mm

5mM Ferrocyanide

Mean slope after 8 runs = 0.73

Std. deviation = .02

GlassyCarbon
Disc Electrode d= 3.0mm

low flow rates (less than 3cc/min) the slope is less than 0.5. As

the flow rate is increased the slope increases to about 0.75

which is the theoretically expected value.

At larger inlet - electrode separations (figures 3.-12)

the theoretical slope of 0.75 is observed both for high and low flow

rates.

The two graphs can be easily explained in terms of the earlier

reasoning; viz. in the case of the first graph, at d = 0.5mm, when the

flow rate is low the jet nozzle is within the boundary layer region. Thus

the slope is reduced. As the flow rate increases however the thickness

of the boundary layer reduces significantly to a value very much less

than 0.5mm . Thus the nozzle body no longer disturbs the solution flow

and the theoretical slope of 0.75 is obtained.

At larger d however, the nozzle being well clear of the

boundary layer, both at high and low flow rates. Thus a constant slope

of about 0.75 is obtained for the entire range of flow rates used in the

experiment. This is shown in the second graph.

Effect of Inlet - Electrode Separation.(d).

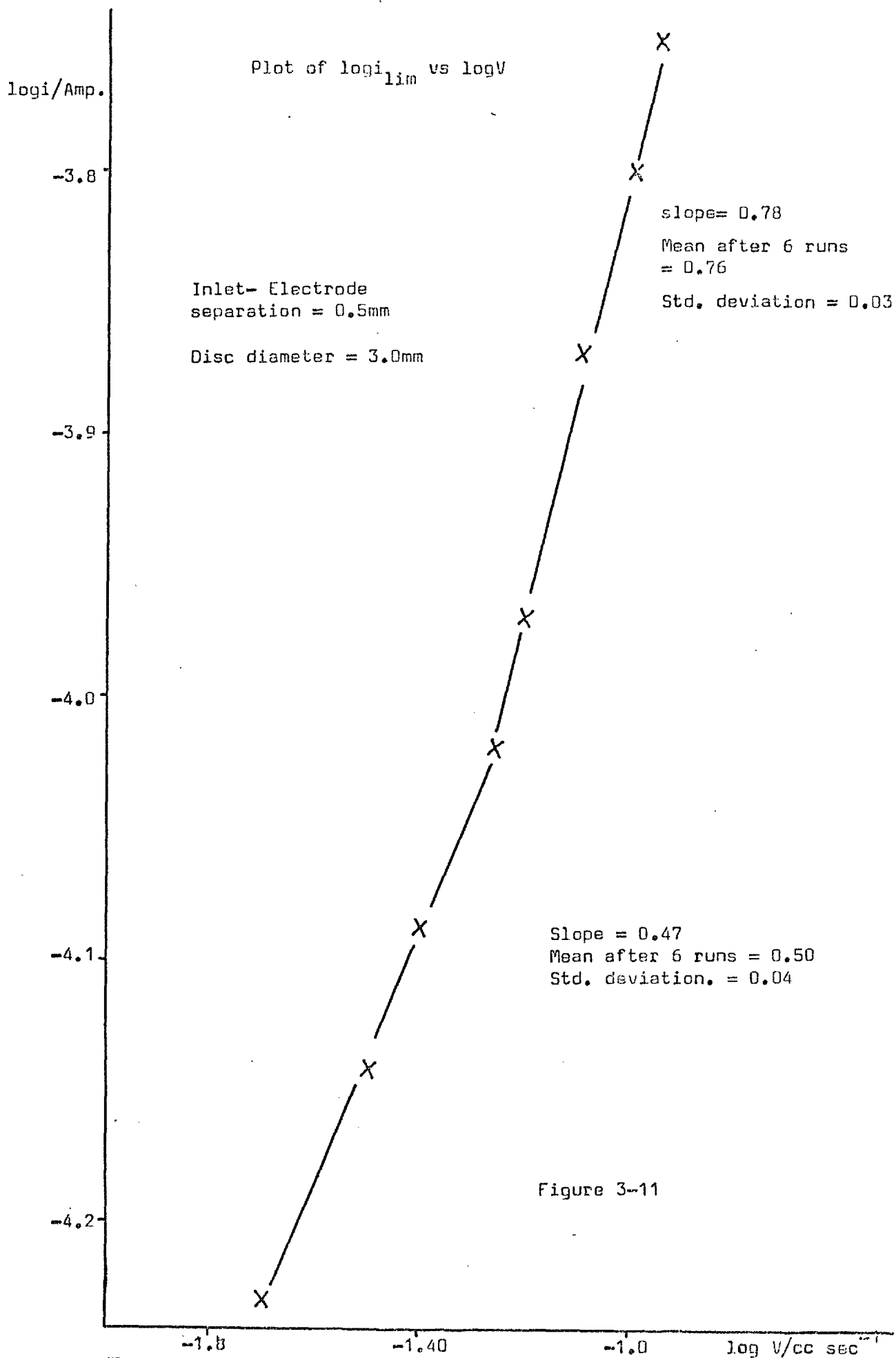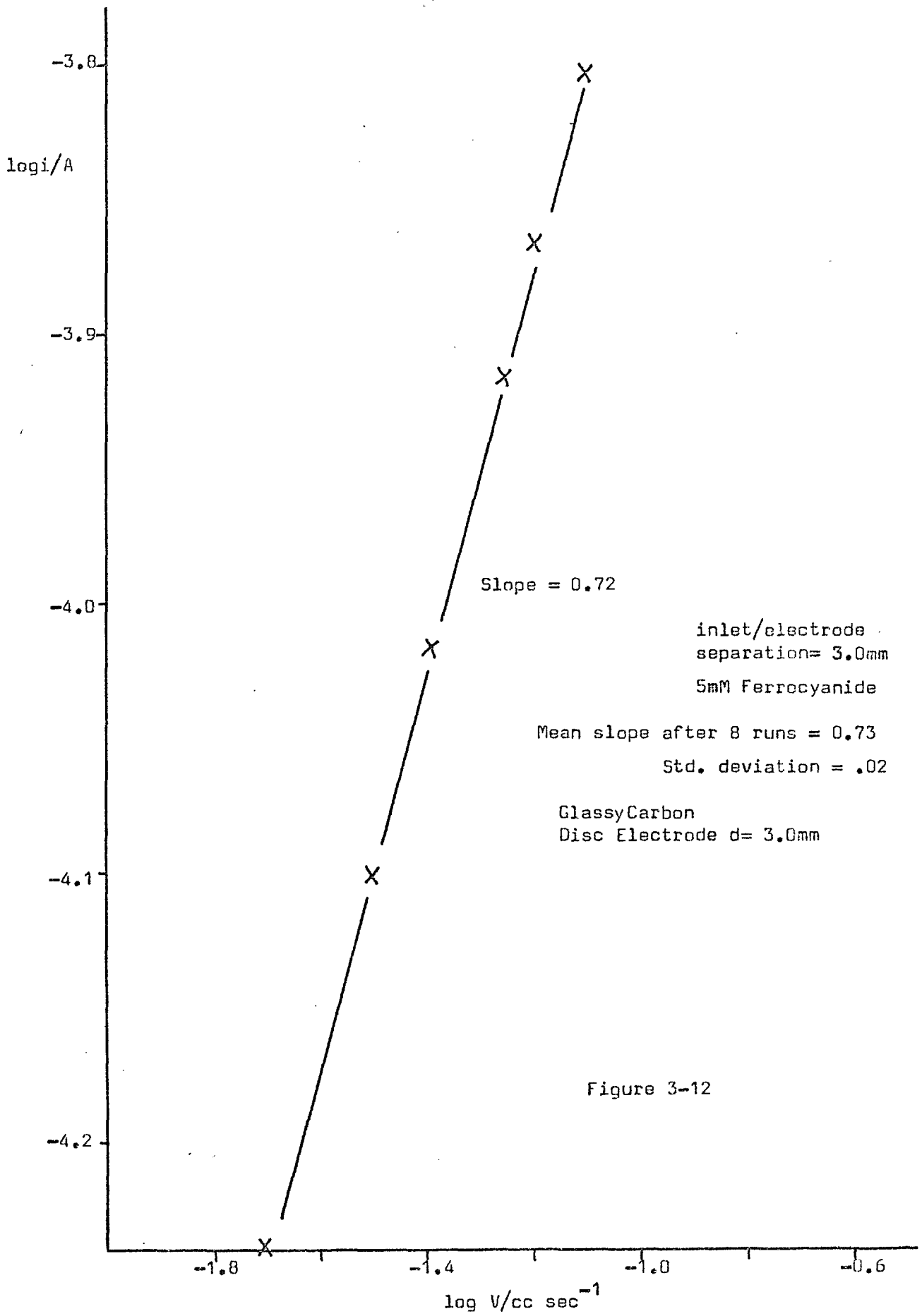It has been stated that the proximity of the nozzle body to

the boundary layer can influence the limiting current. Additionally the

shearing forces resulting from the large velocity gradients within the

layer can be expressed by equation (iv) which relates the skin friction

to the velocity gradient by;

$$\tau(x) = (\partial v_x / \partial y) \mu \quad (\mu = viscocity)$$

From Glauert's velocity profile (figure 3-5) it can be seen

that the velocity gradient changes within the boundary layer; initially

starting with a steep positive gradient, reaching a minimum and then

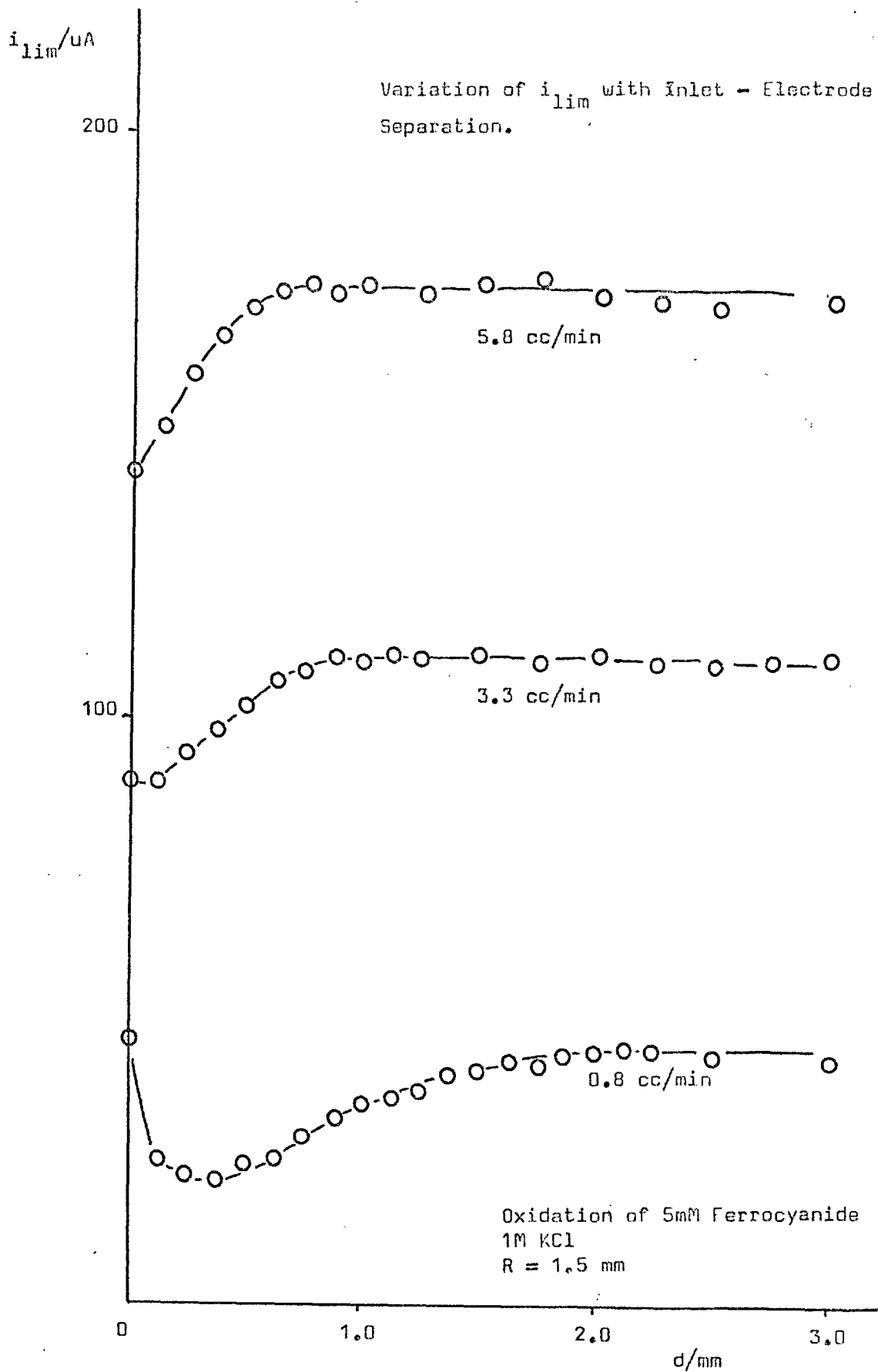a more shallow negative gradient. On this basis we can expect the

Figure 3-13
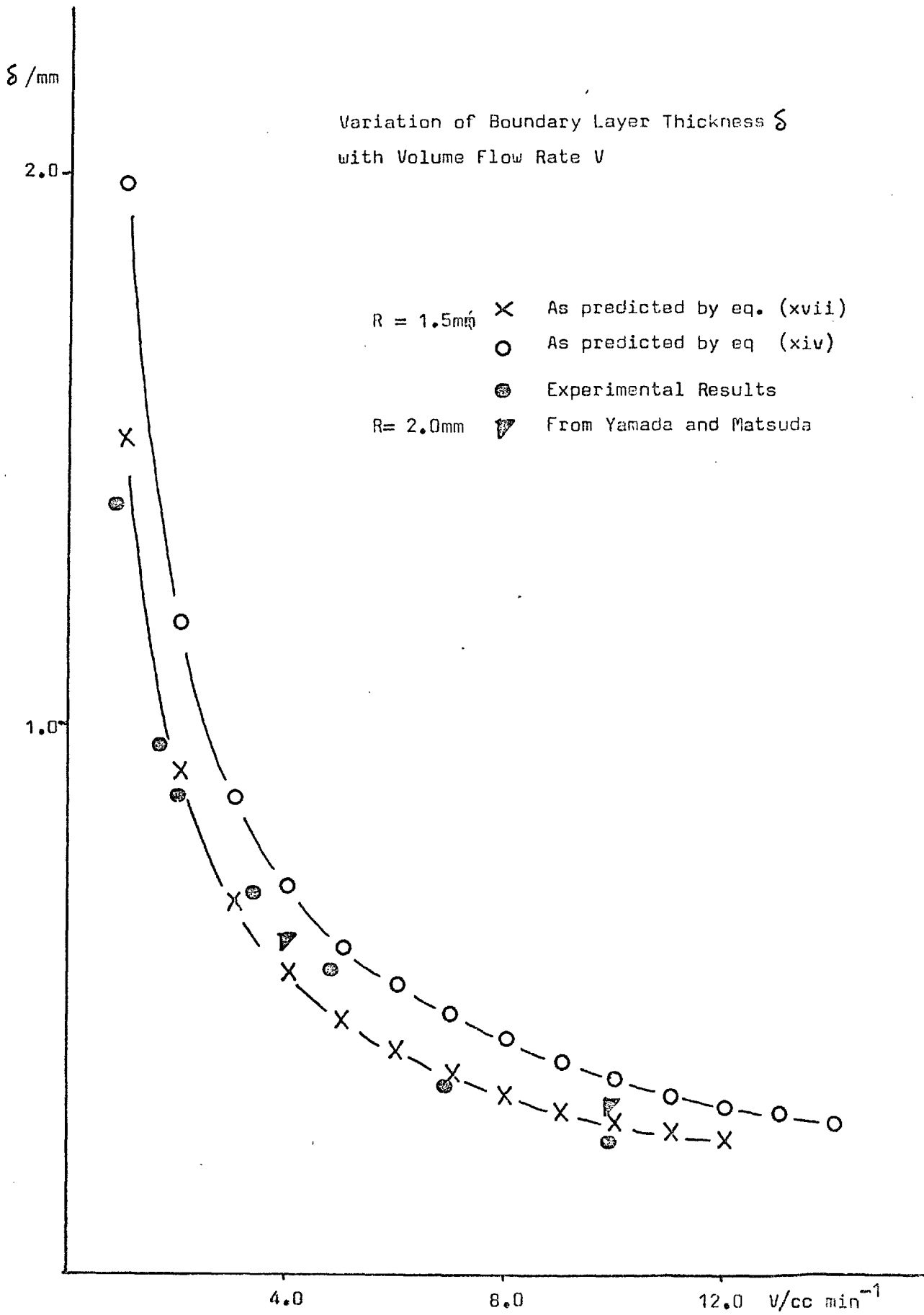
Figure 3-14

104

variation of i_{lim} with d to reflect the velocity profile predicted by Glauert, This in fact is clearly suggested in figure 3-13.

Again it is possible to see a difference in plots for low flow rates and high flow rates. The minimum point on the plots correspond to the maximum of Glauert's velocity profile. At higher flow rates however the minimum is not discernable - probably due to the fact that velocity gradients are much steeper and the boundary layer thickness is quite small.

The point at which the current reaches a limiting value should correspond to the boundary layer thickness. This can be seen in figure 3-14 which gives a plot of the boundary layer thickness δ_{bl} vs flow rate.

3.43 Studies of th Ring Electrode.

The effect of the nozzle in reducing momentum transfer to the electrode is clearly seen in the case of the ring electrode. In the plot of limiting current vs inlet-electrode separation (figure 3-15) i_{lim} decreases rapidly reaches a minimum and then increases. The current should then, following the earlier reasoning, reach a limiting value. Unfortunately limitations in the cell design did not allow varying the inlet - electrode separation to more than 4.5 mm. The high value of δ_{bl} is seen by substituting in equation (xvii) the appropriate values for the hydrodynamic parameters. Thus for a flow rate of 1.05 cc/min, d = 0.7mm.

A plot of the minimum points of the i_{lim} vs d plots reveals a linear relationship. This is unexpected. If the minimum corresponds to the maximum point on Glauerts profile then in accordance with equation (xvii) we should get a curve which reflects a dependence on $V^{-\frac{3}{4}}$ and not V^{-1}

.105

Figure 3-15

106

PLOT OF FLOW RATE vs DISTANCE
AT TRANSITION POINT

Figure 3-16

GRAPH SHOWING VARIATION OF
SLOPE OF logi vs logv PLOTS WITH
DIST. FROM INLET

RING

GLAUERTS
PROFILE

Figure 3-17

107

3.4 ml/min

2.0 ml/min

1.4 ml/min

0.7ml/min

50uA

i-E Curves for the Oxidation
of 5x 10^{-4}M Hydroquinone
Ring Electrode, R= 5.0mm

| 1.2 | 1.0 | 0.8 | 0.6 | 0.4 | 0.2 | 0 |

Scan Rate = 5mV/sec

inlet- electrode separation= 0.5mm

3.4ml/min

2.0ml/min

1.4ml/min

10uA

0.7ml/min

Disc Electrode
R= 2.5 mm

| 1.4 | 1.2 | 1.0 | 0.8 | 0.6 | 0.4 | 0.2 | 0 |

108

Variation of i_{lim} with inlet – electrode separation

Comparism of Ring and Disc Configurations

Measurements made on modified cell design (fig 3-2)

Flow rate =1.6 ml/min
Ring Outer Diameter = 10mm, Inner Diameter = 7mm
Disc Diameter = 5.0mm
Oxidation of .2 mM Ferrocyanide

Disc Electrode

Ring Electrode

i/uA

d/mm

109

Figure 3-18

RING ELECTRODE

SLOPE =0.7

SLOPE=0.43
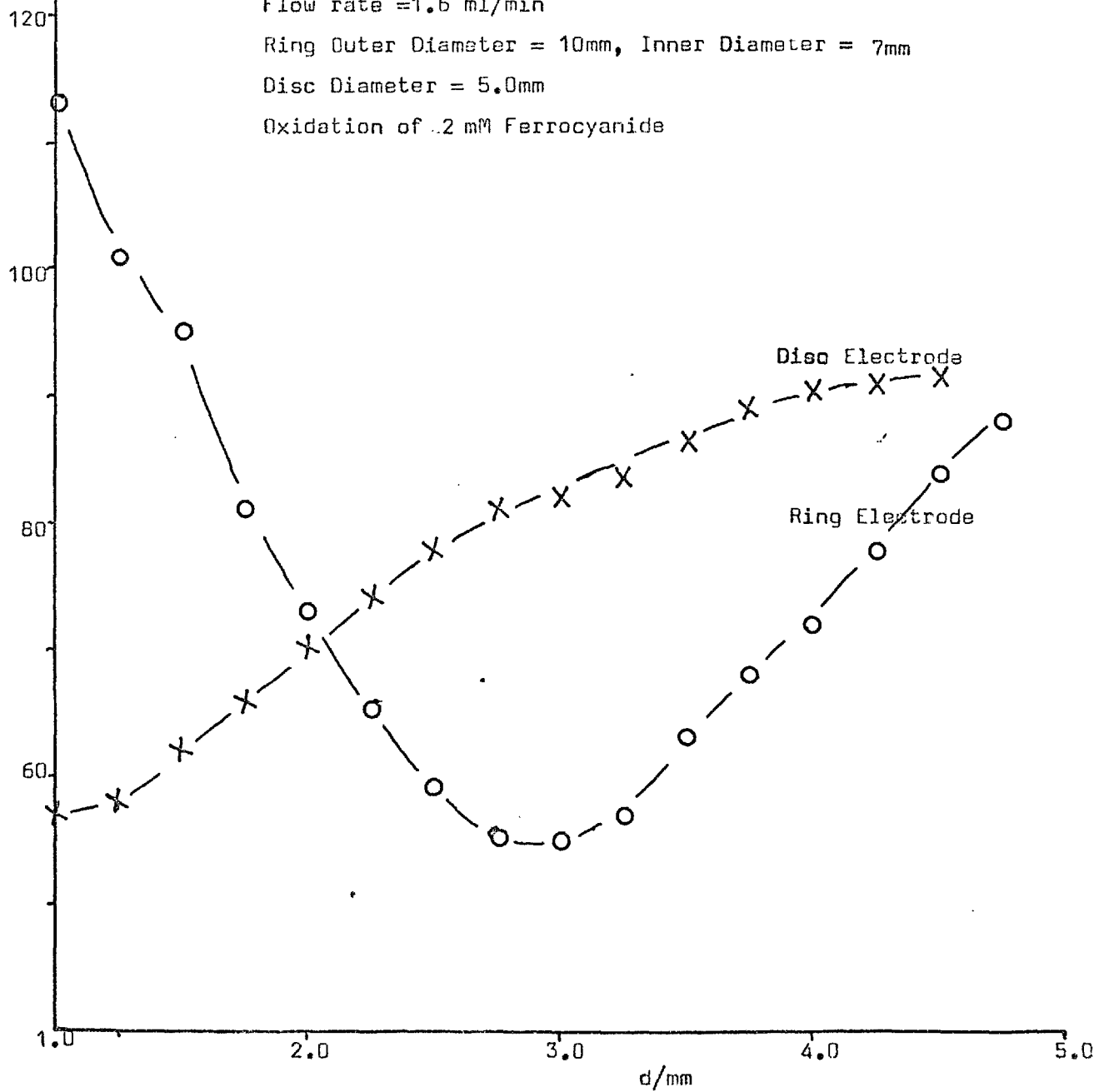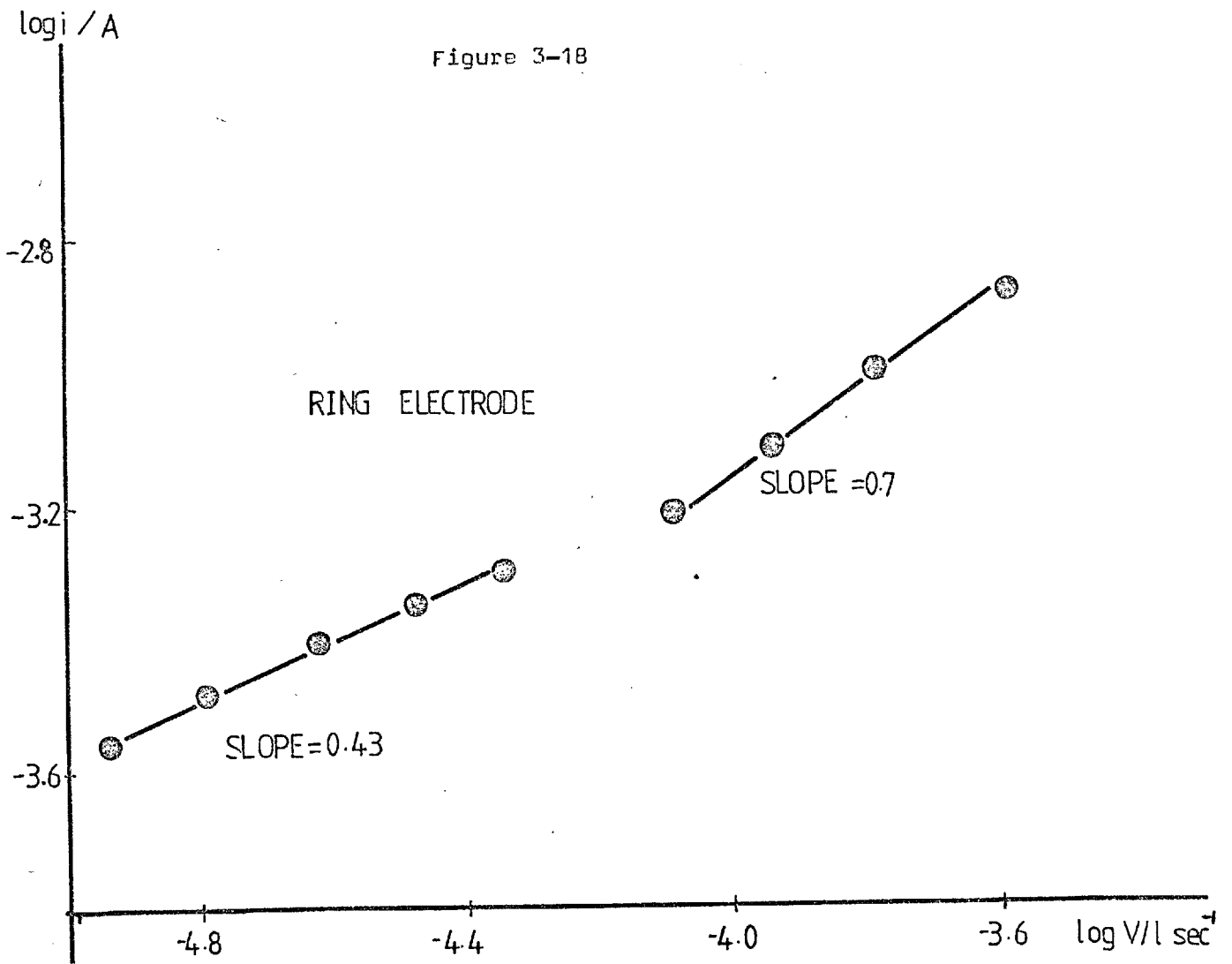
as is shown in figure 3-16. The reason for this anomaly can be attributed to the geometry of the nozzle body (of a convex shape) . Thus the earlier description of the interaction of the nozzle with the flowing solution within the boundary layer is perhaps somewhat simplified and must take into account the nozzle geometry. This does not however change the qualitative argument.

In fact if $\log i_{lim}$ vs $\log V$ slopes are plotted against d, the inlet — electrode separation,an interesting trend is seen which strengthens the above qualitative argument.(see fig. 3-17). At very small d the slope = 0.43. As d is increased the slope rapidly decreases to a minimum of 0.1. This point can be related to the region in the boundary layer where the velocity gradient is a minimum corresponding to the point on Glauert's velocity profile (η_v = 1.9). As the separation is increased further a slope of 0.7 is obtained.

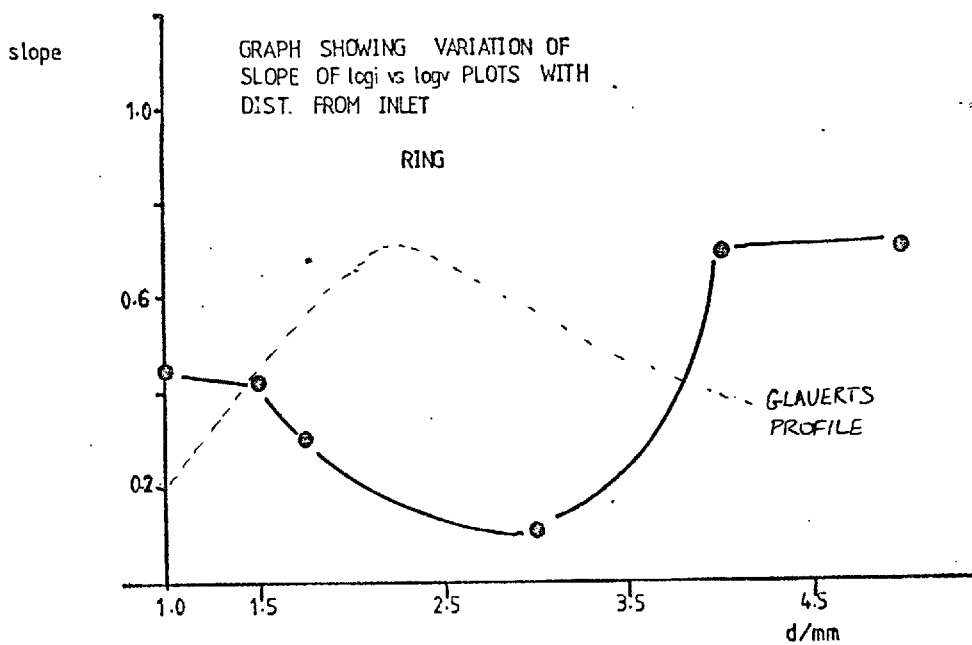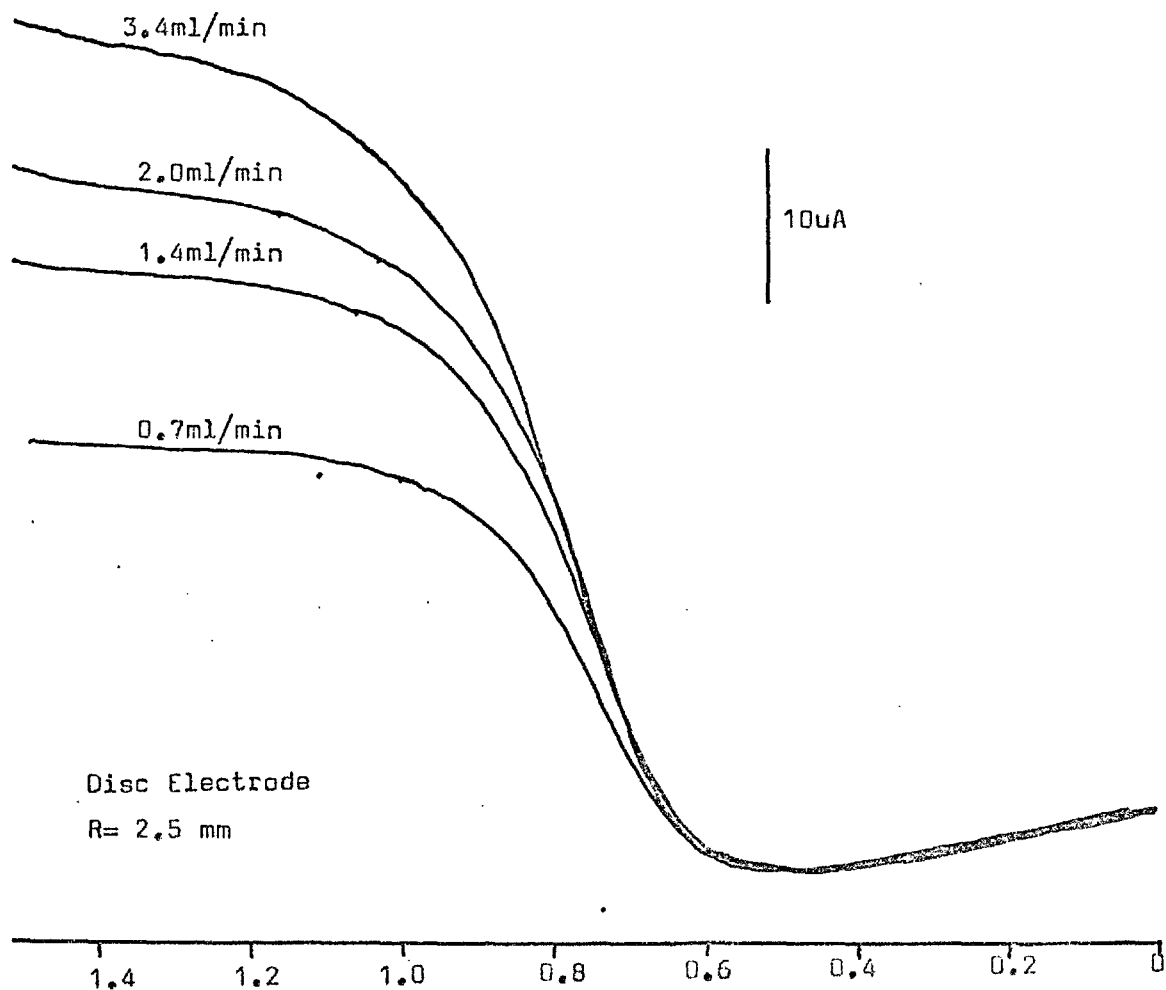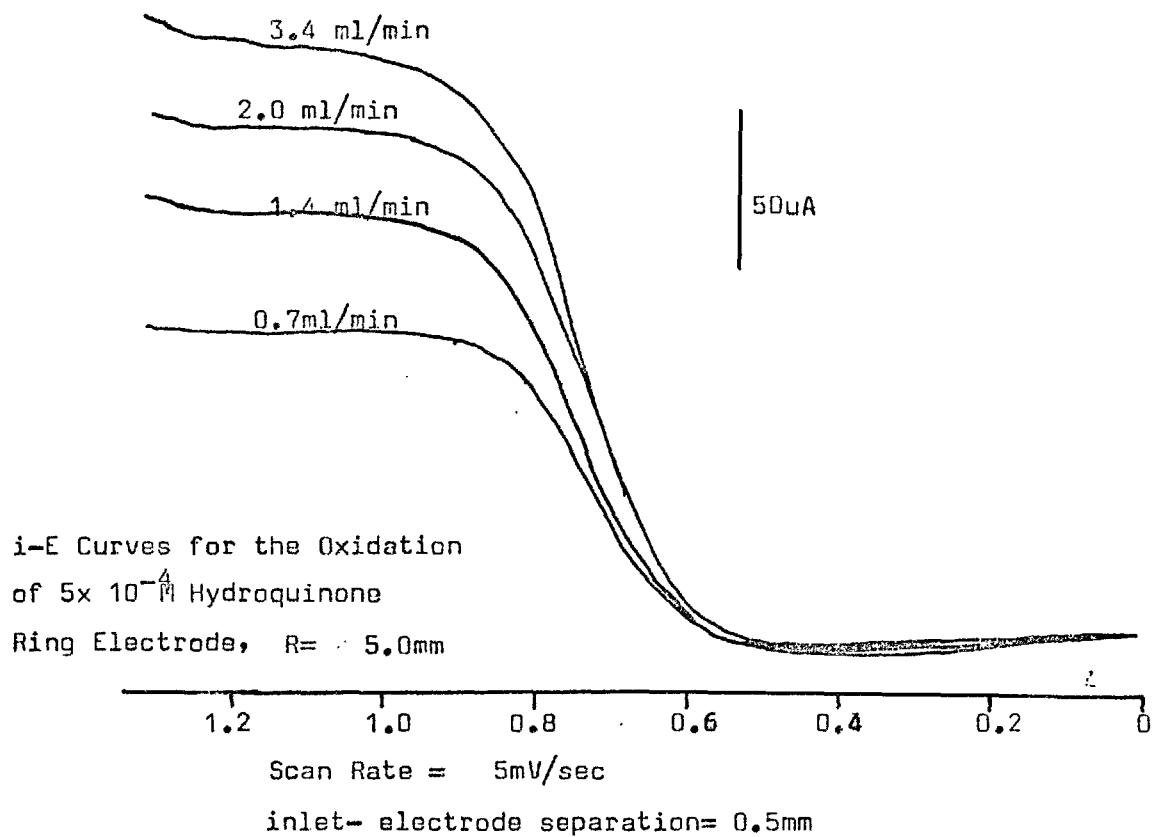Also plotted on figure is the corresponding velocity profile as predicted by Glauert. The correlation between the two plots is reasonable considering the effect of the nozzle geometry. The maximum on Glauerts plot corresponds to the minmum on the experimental plot — which is as would be expected.

Finally in figure 3-18 is a plot of $\log i_{lim}$ vs $\log V$ for the ring electrode. Measurements were made at an inlet to electrode separation of d = 0.5mm.

Hydrodynamic Considerations in HPLC Detection.

In the previous sections, hydrodynamic parameters of the wall jet cell were evaluated by use of Hydrodynamic Voltammetry. In the light of this work, the implications for HPLC, in particular the effect of inlet-electrode separations (d) and flow rate on peak currents and resolution can be examined

3.51 Effect of Flow Rate.

Figure 3-19 gives a plot of $\log i_{peak}$ vs $\log V$ (V= volume flow rate). The slope is about 0.55 for an inlet-electrode separation $d = 0.5$mm. At higher d values the slope is increased to about 0.7 which is consistent with the earlier reasoning.
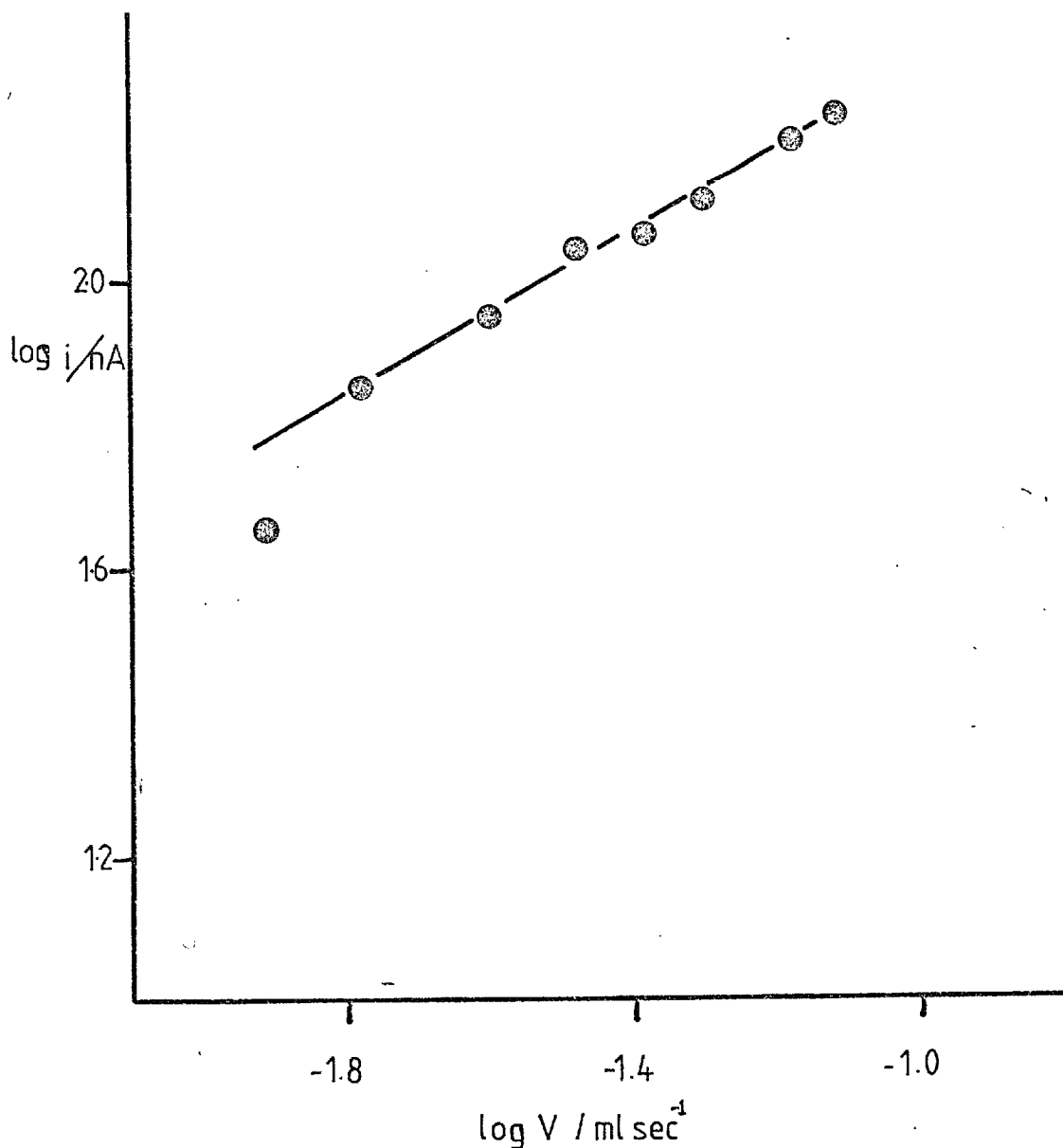
Peak Height vs Flow Rate   L- Dopa
20% Methanol/Water   0.1M KNO_3
ODS Permaphase Column.   Working Electrode Potential = +1.0 V vs Ag/AgCl

Figure 3-19

3.52 Effect of Inlet- Electrode separation.

In considering the effects of varying d we must, as   has been discussed earlier, take into consideration the solution viscosity, flow rate, nozzle geometry etc. The flow rates normally used in HPLC vary between 0.2 - 2.0 ml/ min , which means that the boundary layer thickness will be relatively large and varying d will have a significant influence on the peak current.

Figure 3-20 is a plot of i_{peak} vs d. It can be seen that the current follows the curve predicted for low flow rates. There is no peak broadening with increase in d; this suggests that the jet is fully laminar both before and after striking the wall.

We could thus take the effective dead volume in the case of the Wall Jet Cell to be related to the thickness of the boundary layer. No band spreading would thus be expected as δ_{BL} remains constant regardless of d.

An interesting example of the effect of d on performance is seen in the case of a 'normal phase' separation (see chapter 4) of a mixture of phenols using a Hexane/Ethanol system as the eluent (fig 3-21-3-23). In normal phase separations, the least polar compound elutes first; this is in accordance with the solubility of the compound in the solvent (and thus the mobility).

Comparing the i_{peak} vs d plots most mobile (least polar) compounds (fig. 3-22) and the least mobile (most polar) compunds (fig. 3-23) it can be seen that the response is different. This can be attributed to the larger shearing forces in the case of the latter compounds.

Both plots however reach limiting values at the same d which can be related to the boundary layer thickness δ_{BL}.

113

Variation of Peak Current with Inlet- Electrode Separation.

Flow Rate = 0.4 cc min $^{-1}$
ODS Permaphase Column
10% Methanol/Water Eluent
0.1 M KNO_3
Potential +1.0 V vs Ag/AgCl
Sample: Hydroquinone
            1ng/1ul

Ring Electrode

Figure 3-20

Disc Electrode (R = 2.5mm)
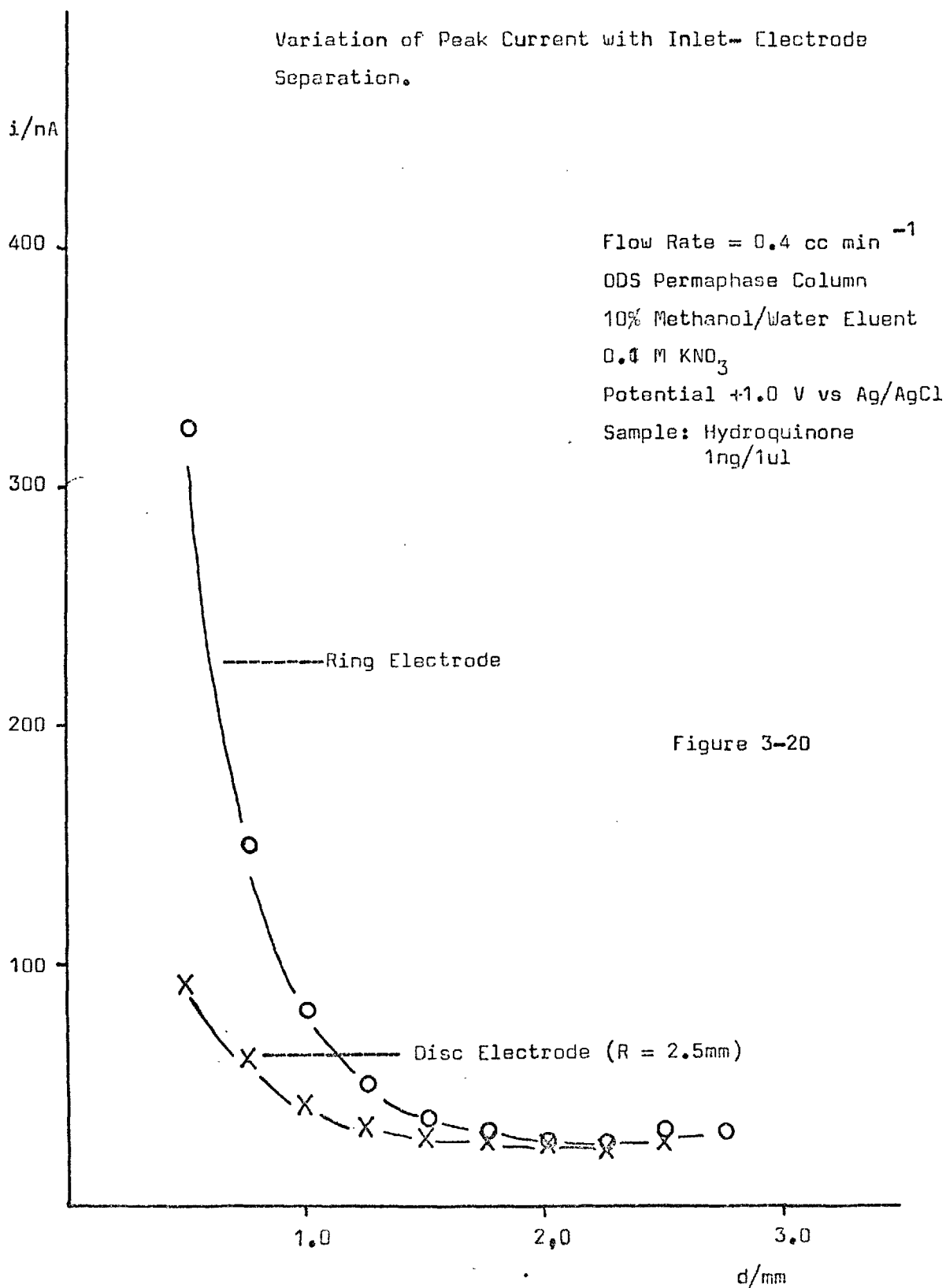
Figure 3-21

Flow Rate = 0.2 ml/min

$E_{applied}$ = 0.8V vs Ag/AgCl

d = 0.125 mm

50 nA
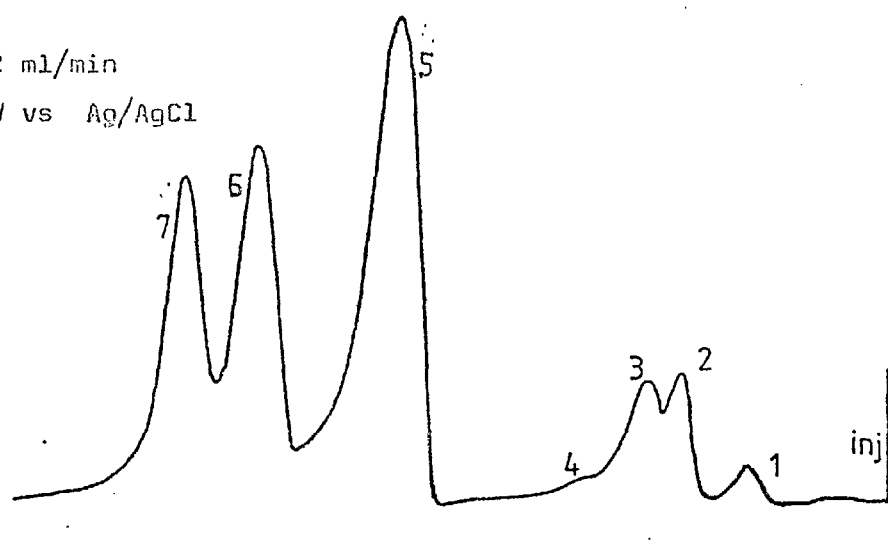
d = 0.375 mm
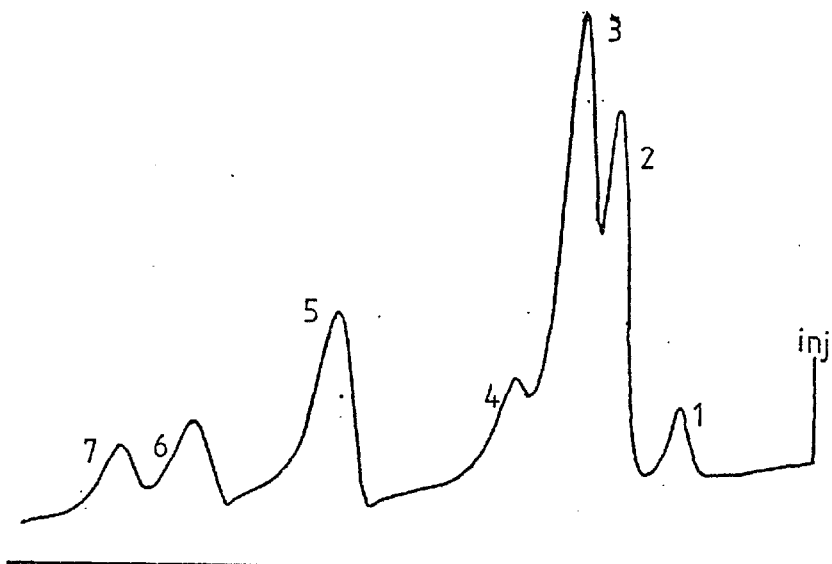
d = 1.125 mm
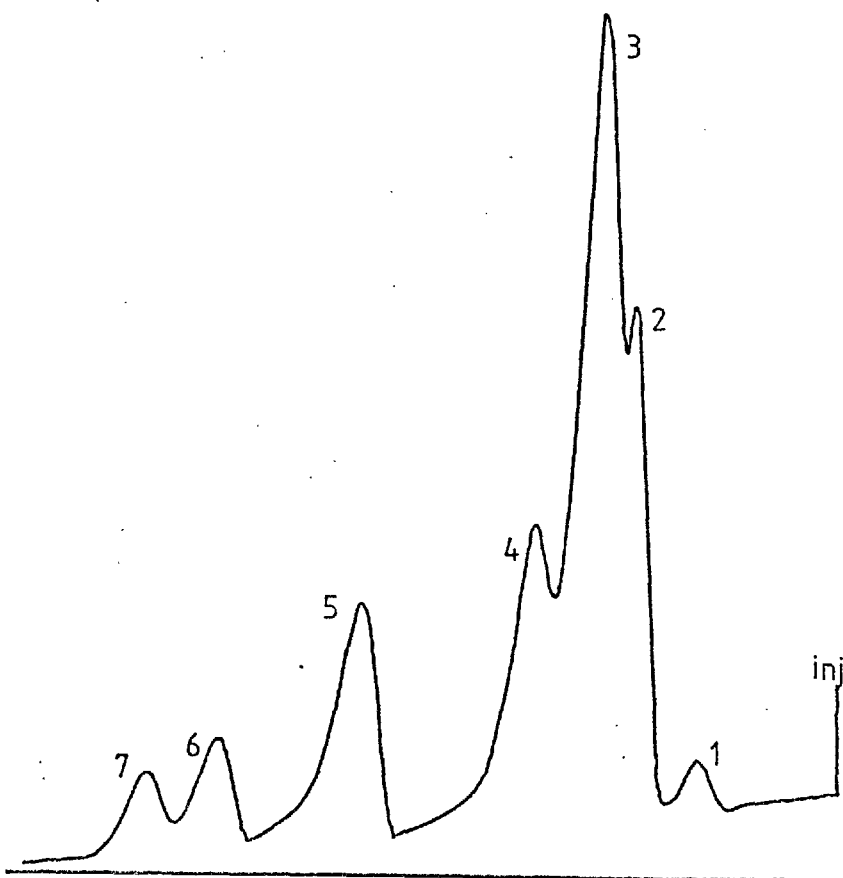
Figure 3-23

Figure 3-22

116
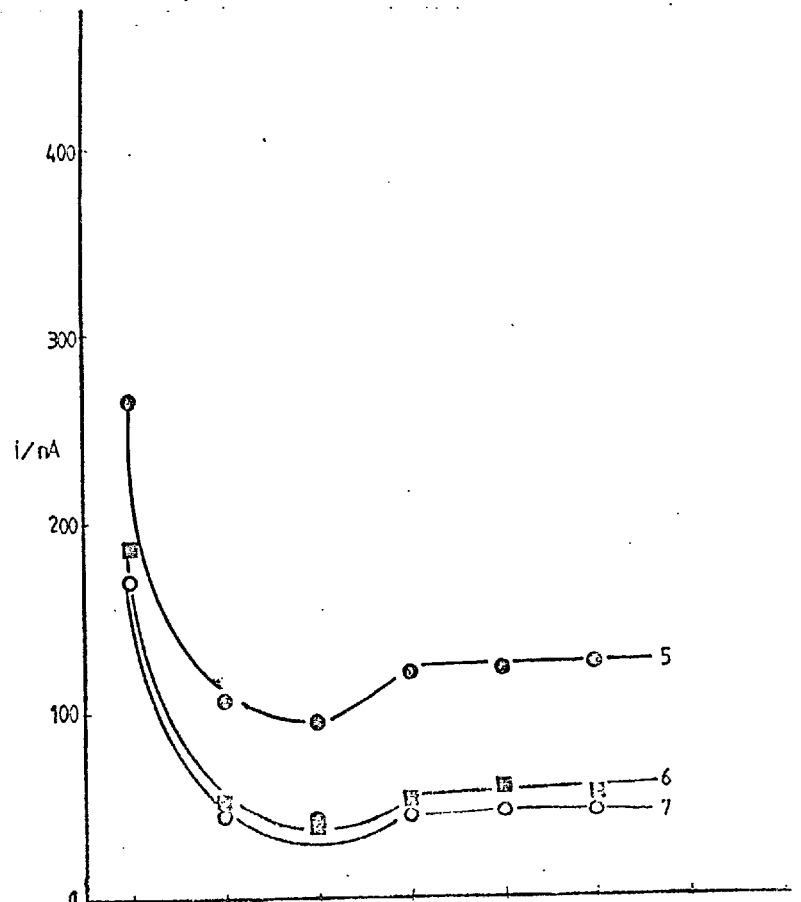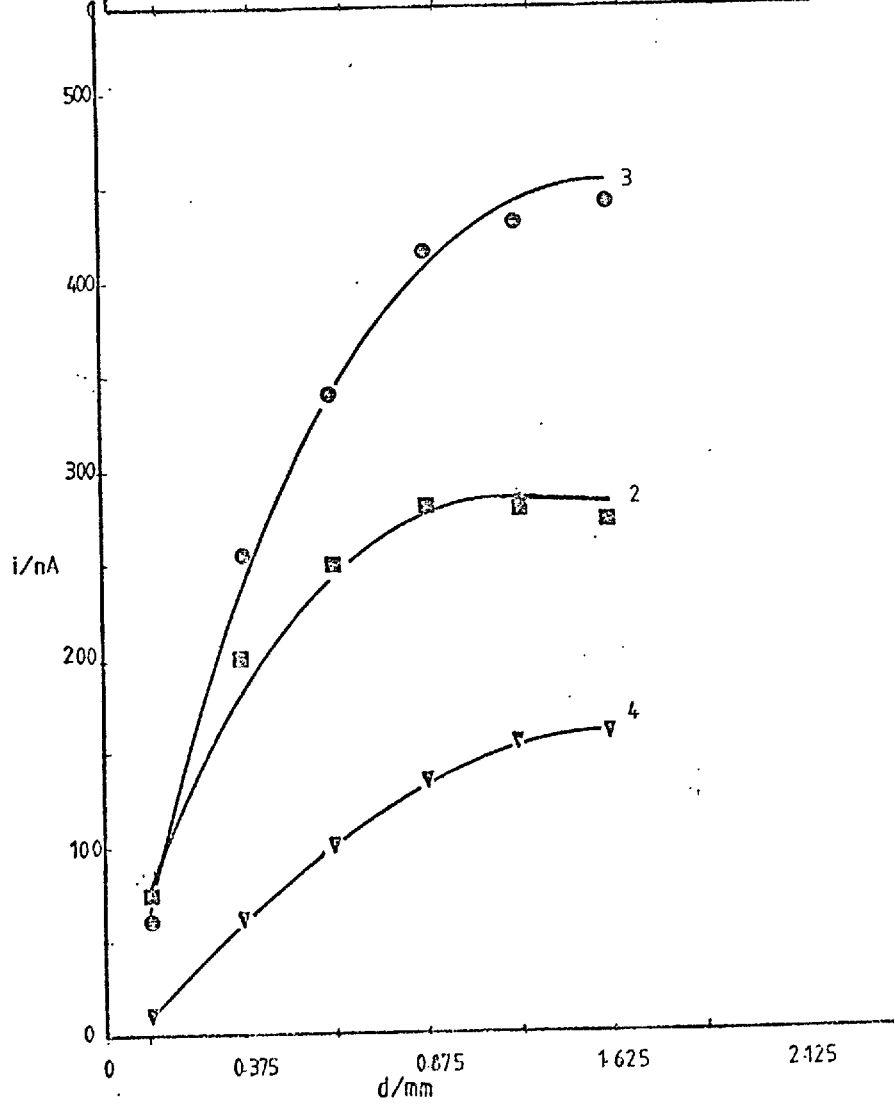
3.5 Turbulent Flow

The study of the transition of fluid characteristics from laminar to turbulent flow forms, together with boundary layer theory, the foundations of modern fliud dynamics. In the case of the wall-jet, the question as to whether flow characteristics are laminar or turbulent is governed by the stability of the jet as it emerges from the nozzle. This in turn depends on the dimensionless Reynolds number ' Re, where

$$Re = Ul/v$$

U= jet velocity in cm/sec

L= nozzle diameter in cm

v= kinematic viscosity

According to experimental findings, a three dimensional jet remains laminar up to a critical Reynolds number, $Re_{critical}$ where $25 < Re < 1000$ (99). the exact value of $Re_{critical}$ depends on the shape of the nozzle. As the Reynolds number is increased beyond $Re_{critical}$, the jet becomes more concentrated and less stable, finally breaking up and becoming turbulent.

For a jet nozzle diameter L = 0.03 cm and v taken as $10^{-2} cm^2/sec$, the Reynolds number can be calculated for the following flow rates:

V cc/min	U cm/sec	Re
1.0	23.5	70
5.0	118.5	495
10.0	235.0	707

In order to be satisfied that flow characteristics of the jet were in fact laminar (in view of the high Reynolds Numbers) a potasium permanganate solution was used to highlight the jet flow pattern.

The jet that was observed(in the flow rate range 1-5cc/min) was found to show distinct laminar properties; namely no evidence of turbulent eddy formation or spreading of the jet stream. In fact it was found that the jet remained of constant width (of the order of the jet nozzle) for a distance greater than 10 cm from the nozzle.

On this basis and the fact that Glauerts assumptions hold, it could be presumed that, at least in the flow rate range 0.5 - 5 cc/min, laminar flow conditions exist in the wall-jet.
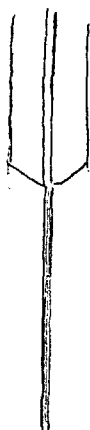
i) a free laminar jet   ii) a free turbulent jet

Figure 3-24

118

CHAPTER IV HIGH PRESSURE LIQUID CHROMATOGRAPHY

4.1 Introduction

High pressure or high performance liquid chromatogaraphy
(HPLC) is probably the most rapidly expanding analytical technique.
Its increasing popularity reflects the steadly growing demands being
made upon separation techniques, mainly in biochemistry, drug analysis
and such areas as environmental pollution monitoring. Additionally,
a deeper understanding of the process of chromatographic separation,
especially more knowledge about the factors that influence equilibria
and the selectivity of separations, has resulted in a more complete
analytical technique, offering numerous ways of automation and a
delicate approach to the separation of different substances.

4.11 Chromatographic Systems

Chromatographic systems can be classified according to the
mechanism governing the distribution equilibrium. By this classification
five basic systems can be defined (100);

i) liquid-solid chromatography

ii) liquid-liquid chromatography

iii) ion exchange chromatography

iv) gel permeation chromatography

v) ion pair partition chromatography

In this work only liquid-solid and ion pair chromatography
were used. These are described in greater detail below.

119

Liquid-Solid Chromatography

Liquid-Solid separation is performed with a liquid mobile phase and a stationary solid surface which 'reversibly' adsorbs the solute; in practice, reversibility depends on the particular solute. The mobile phase is usually a non polar solvent. In some cases it is preferable to use a polar mobile phase and a non polar stationary phase; usually in the form of silica particles chemically bonded with long chain aliphatics. This is termed Reverse Phase Adsorption Chromatography.

In this work all 'normal phase' separations were carried out with silica columns (particle size 10 microns). 'Reverse phase' separations were carried out with'ODS Permaphase' columns (Dupont, particle size 10 microns).

Ion Pair Partition Chromatography

Ion-pair partition chromatography can serve as an alternative to ion exchange (101). Using this technique, separation of ionic substances may be accomplished with a reverse phase column.

Though the exact mechanism has not been substantiated, it is believed that an increase in retention time results due to the formation of ion pairs between counter ions (added to the mobile phase) and the ionic species to be separated (102).

For basic substances alkyl sulphonates are used as the counter ion, and for acidic compounds alkyl ammonium ions are used.
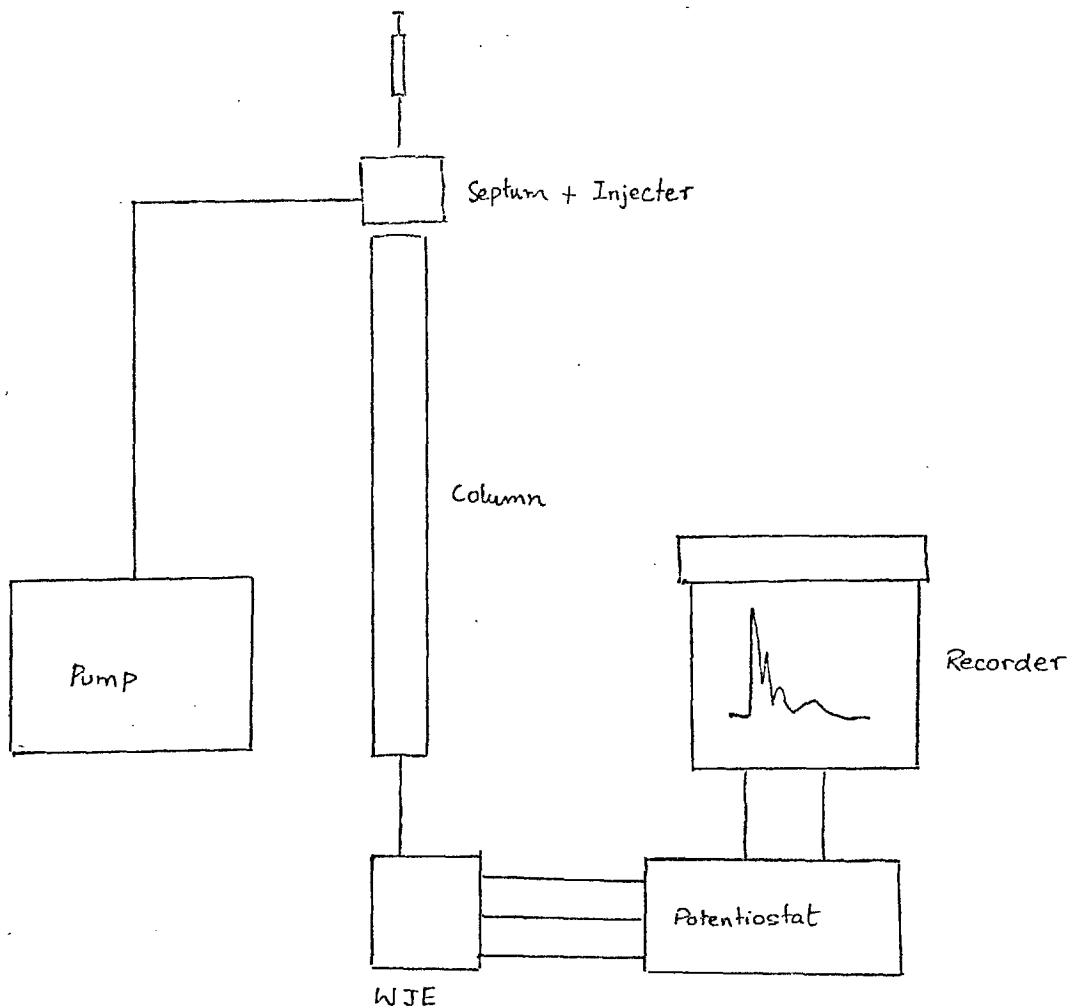
Figure 4-1 The Complete Chromatographic
Set Up.

4.12 Detection Systems

The main drawback to liquid chromatography is the lack of

a universal detector with the same versatility as the Flame Ionisation

Detector (FID) in gas chromatography. The principal problem in liquid

chromatography is that the solute and solvent are similar unlike the

situation in GLC where the mobile phase is generally inert. Consequently,

a wide range of new ideas and principles have been applied to the

design of liquid chromatography detectors.

The criteria for an ideal detector can be listed as follows.

i) high sensitivity

ii) applicable to a large range of compounds

iii) low dead volume

iv) reproducibilty

v) robust

vi) easily maintained

In general whereas 'bulk property' detectors such as the Conductivity Detector (103) and Dielectric Constant Detector (104) fail in points (i) and (iii) , 'Specific Analyte' Detectors such as the Ultra Violet (105), Fluo rescent ‥ ·‐ (106), and Electrochemical Detector (107) are limited by the range of applicability.

4.2 Recent Advances in Electrochemical Detectors

The early history of electrochemical detectors has been almost completely dominated by the Dropping Mercury Electrode (DME) (108). The fundamental problem with these detectors is the construction of a flow through cell having a sufficiently small effective volume. Additionally, the difficulties of handling mercury has contributed to a situation where the use of electrochemical detection was viewed with some reservation though this now rapidly changing.

A number of coulometric cells have been devised using packed tubular electrodes(109), carbon cloth(110),and more recently carbon fibre (111). These designs while having the advantage of 100% effeciency have very large effective volumes and slow response times. Thus coulometric cells would probably only find use for well resolved analyte where there is not any stringent requirements for band spreading.

In a recent review Kissinger (112) highlighted the advent of voltammetric detectors incorporating one of the newer forms of carbon as the working electrode material.The basic feature of these detectors is a

122

geometrically simple cell design with cell volumes of less than

10 microlitres. The main types of carbon used as working electrode

material are carbon paste (113), silicone impregnated graphite (114),

and glassy carbon (115), used in this work. One of the advantages of

glassy carbon is that it is more robust and can be used in non

aqueous solvents. Additionally it has superior electrocatalytic

properties as it has been indicated in Chapter I.

4.3 Ultra Violet vs Electrochemical Detection

In principle it is valid to say that most compounds that

are UV active show some degree of electrochemical activity. In practice

however it is not as straightforward. Several factors have to be taken

into consideration; for instance the potential limits of the electrode

solvent system.

_____ phenothiazines		aldehydes and ketones
		_____
_____ phenols		_____ olefinic
		esters
aromatic hydroxyls _____		_____ ethers
catecholamines		_____ diazo cpds
_____		
_____ quinolins	_____ nitro compounds	
_____ PAH's halogens		
_____		

+1.0	0	−1.0

Table 4-1   E vs SCE

123

In order to determine the full range of compound types

listed in table 4-1 the electrode/solvent system must have a

workable potential range of +1.5V - -2.0 V. In the case of carbon

electrodes in aqueous solutions, the potential range lies between

-0.8 V - +1.5 V vs SCE. The compounds that could be detected are

therefore limited to within this range. If non aqueous solvents

are used however this potential range can be greatly increased.

iii) impure   ii)   i)
     sample containing
     mixture of two

UV

280 nm

isopropyl
phenol

phenol

impurity

WJE

+1.0 V
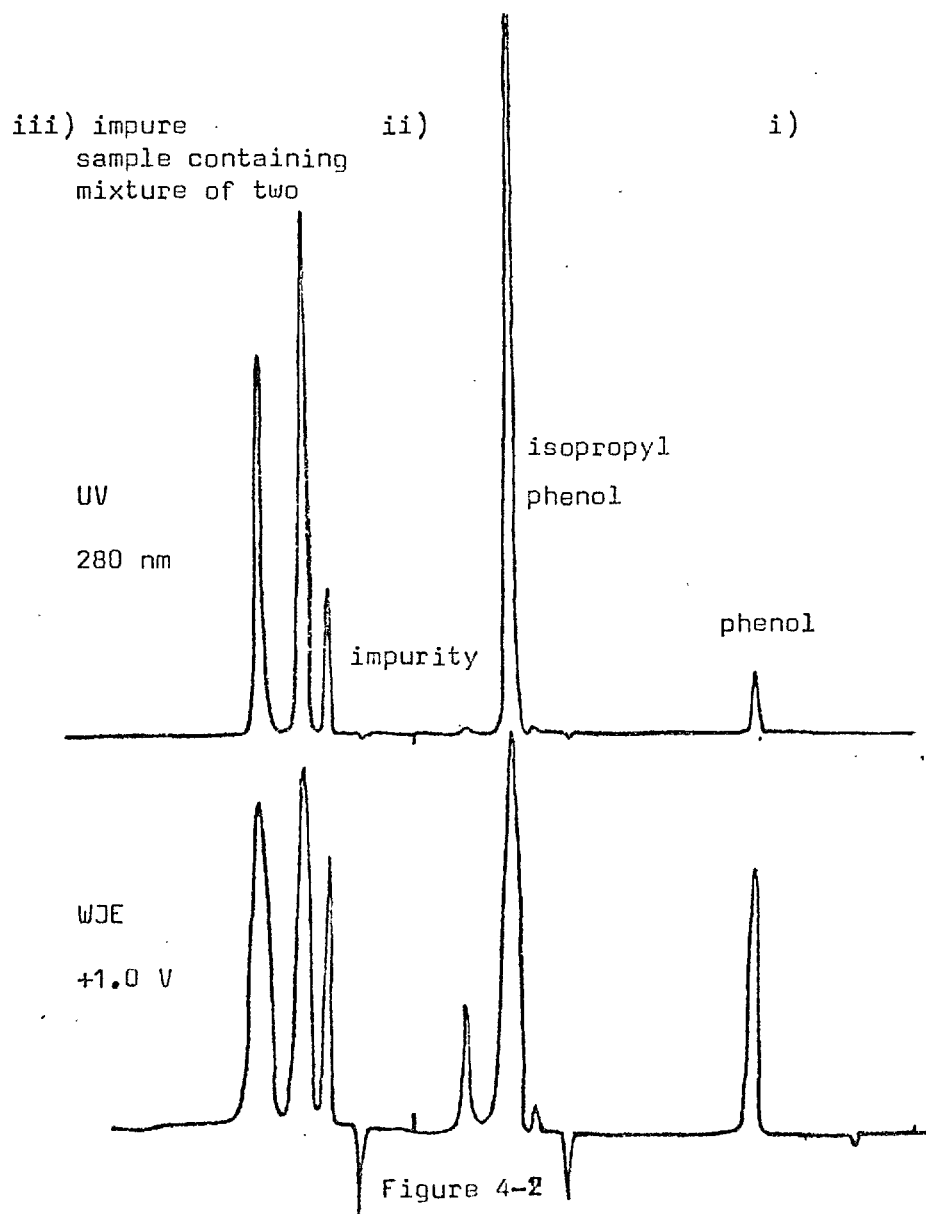
Figure 4-2

In figure 4-2 we have two traces which show the similarity in response of the UV and the WJE for the detection of some phenols separated on a silica column with hexane/ethanol as eluent. The two detectors were placed in series in this determination.

Within the limited potential range available for aqueous solutions there remains a large range of compounds for which electrochemical detection can prove extremely useful. The work on dopamines by Kissinger (116-120) is one good example where electrochemical detection has proved better than UV detection.

There are a number of compounds which, while showing high UV activity, can be determined at lower levels with electrochemical detection. Among these compounds are phenols (. see figure 4-3) and a range of important drugs, including the oestrogen steroids.

Comparism of UV Detection with the Wall Jet Detector -
Sensitivity

Sample: 3 isopropyl phenol 10 ng/5ul injection
Eluent: 73% Hexane/ 27% EtOH / 0.5% Ammonia
Column: Silica

5nA

0.001 abs units

a) Electrochemical WJC   b) UV
Working Potential +1.2 V vs SCE   Wavelength = 280nm
Sensitivty= 50nA f.s.d.   Sensitivty= 0.01 abs. units
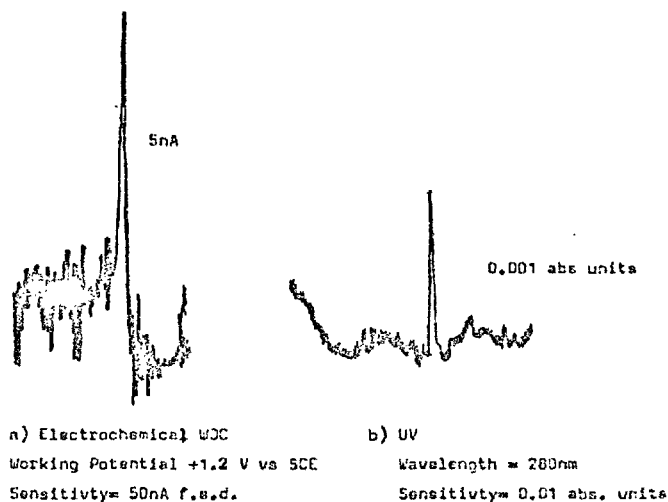
Figure 4-3

SILICA COLUMN
20% EtOH/HEXANE   0.05M TETRABUTYL AMMONIUM
                   FLUOROBORATE
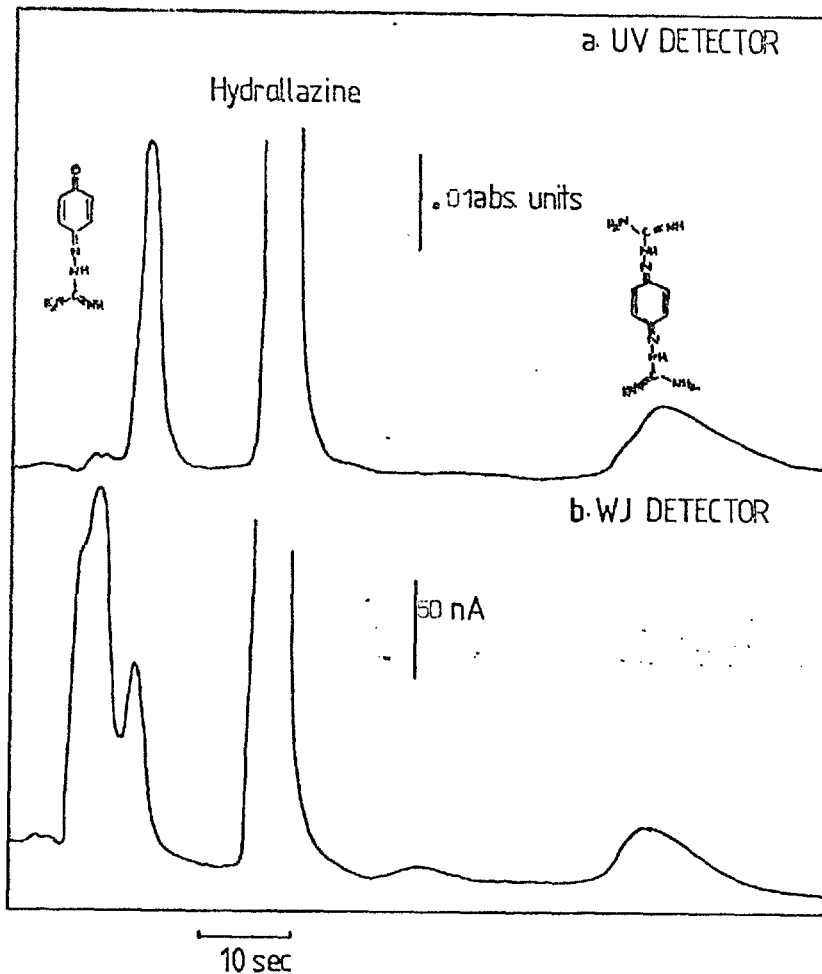
Figure 4-4

The usefulness of electrochemical detection is seen
in figure 4-4 above, which shows traces of hydralazine (a
antihypertensive drug) and its metabolites, determined using the
WJE and UV detectors.

The trace for the WJE shows the presence of impurities
which dont appear in the UV trace.

Figure 4-5

Chromatogram Showing Speed of
Response of the Wall Jet Detector

Sample: 96.5% 2,6 diisopropyl phenol

Eluent: Hexane/Ethanol — 75/25
        + 0.5% Ammonia

Electrolyte: 0.05M $Bu_4N^+ BF_4^-$

Working Potential: +1.2 V vs Ag/AgCl

The well resolved, sharp peaks reflects
the low dead volume (of the thickness
of the hydrodynamic boundary layer).

Additionlly, though the oxidation of the
phenol is an irreversible electrochemical
process, the response is not limited by
kinetics.

2minutes
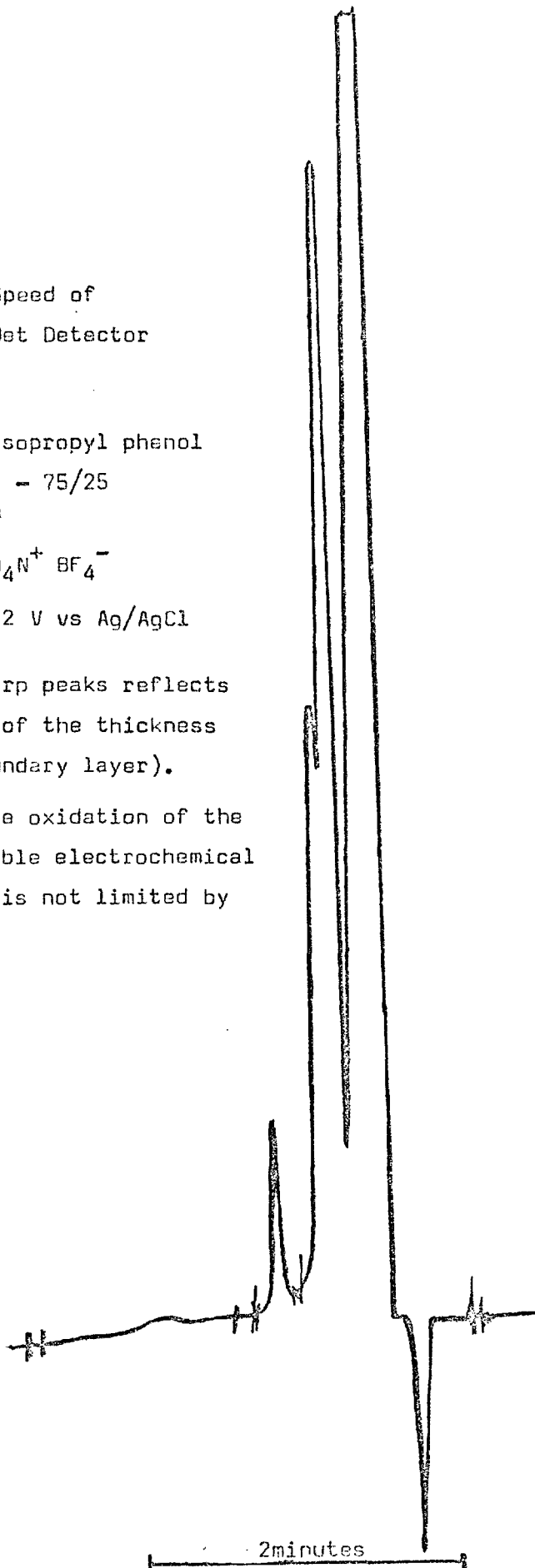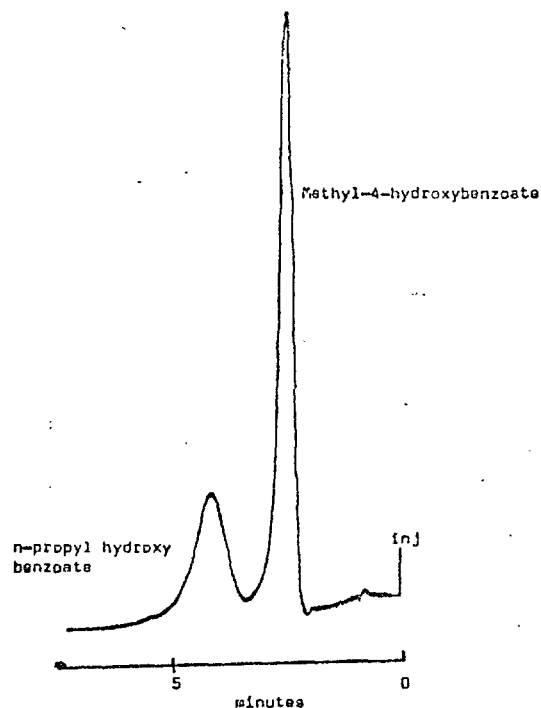
Figure 4-6

Chromatogram of a Mixture of Hydroxybenzoates

50 ng of each in 5 microlitres

Peak shapes are due to chromatographic considerations.

Column: ODS Permaphase
Solvent: 20% MeOH/Water V/V
Electrolyte: 0.1M KNO$_3$

Flow Rate: 1.2 ml/min
Working Potential: +1.2V vs Ag/AgCl Cleaning Potential: -0.2V
Mode: Pulse.

4.4 Non Aqueous Solvents

The efficacy of electrochemical detection for monitoring
non aqueous eluents is one area which workers in the field have
neglected. There is no apparant reason for this state of affairs
especially since there has been considerable interest in non aqueous
electrochemistry in recent years. Whatever the case may be, the

128

result of inactivity in this area has meant that the technique of 'Normal Phase' Liquid -Solid Chromatography has been neglected.

In the present work it is demonstrated that electrochemical detection can be easily used to monitor non aqueous eluents. The prime consideration here is that the eluent should be made conducting. This unfortunately precludes the use of pure solvents of very low dielectric constant (such as Hexane). However mixtures of solvents of low dielectric constant with a small proportion of a higher dielectric solvent can be used. For example mixtures of 85/15 hexane/ethanol are possible.

Non aqueous solvents provide a broad range of dielectric constants, from a value of about 2 in non polar solvents (benzene, dioxane etc.) to as great as 182 (N methyl formamide). Table 4-2 lists some non aqueous solvents which can be used for HPLC coupled with elctrochemical detection.

Solvent	Dielectric Constant
Acetonitrile	35.95
Benzene	2.28
Chloroform	4.81
Dimethyl Sulphoxide	48.9
Dioxane	2.24
Ethanol	25.0
Ethyl Acetate	6.11
Methanol	33.7
Sulfolane	98.7

Table 4-2

Note that for the low dielectric solvents asuitable amount of Ethanol must be added.

EFFECT OF FLOW RATE ON RESOLUTION
ON CHROMATOGRAPHY OF PHENOL MIXTURE
ELUENT: HEXANE / EtOH / NH$_3$ ÷ 70/29.5 / 0.5

25nA

SOLV. FRONT
0.75ml/min

SOLVENT FRONT
0.5 ml/min

para phenylene diamine

p-amino phenol

3 isopropyl phenol

ortho amino phenol

phenol

2,6 di isopropyl phenol

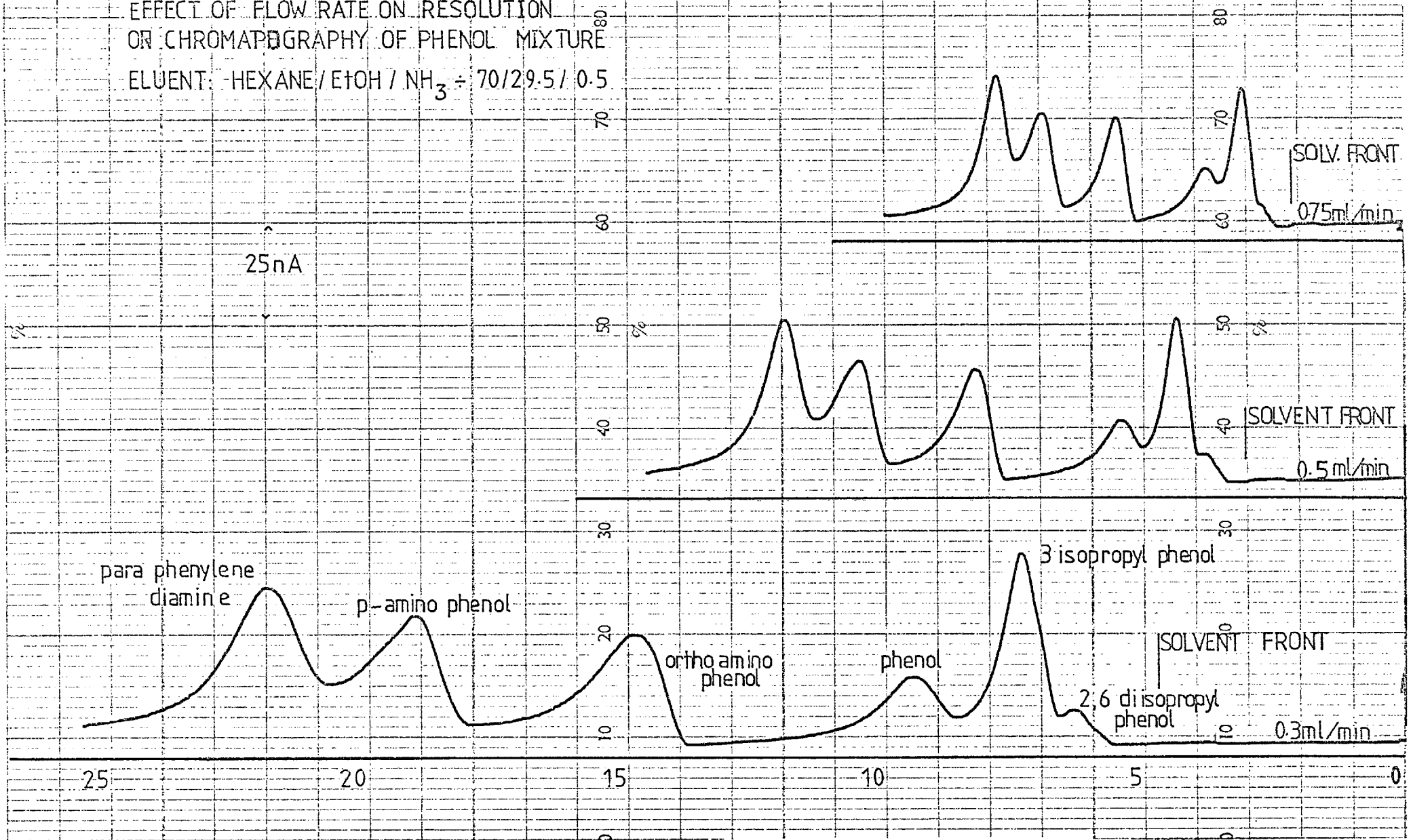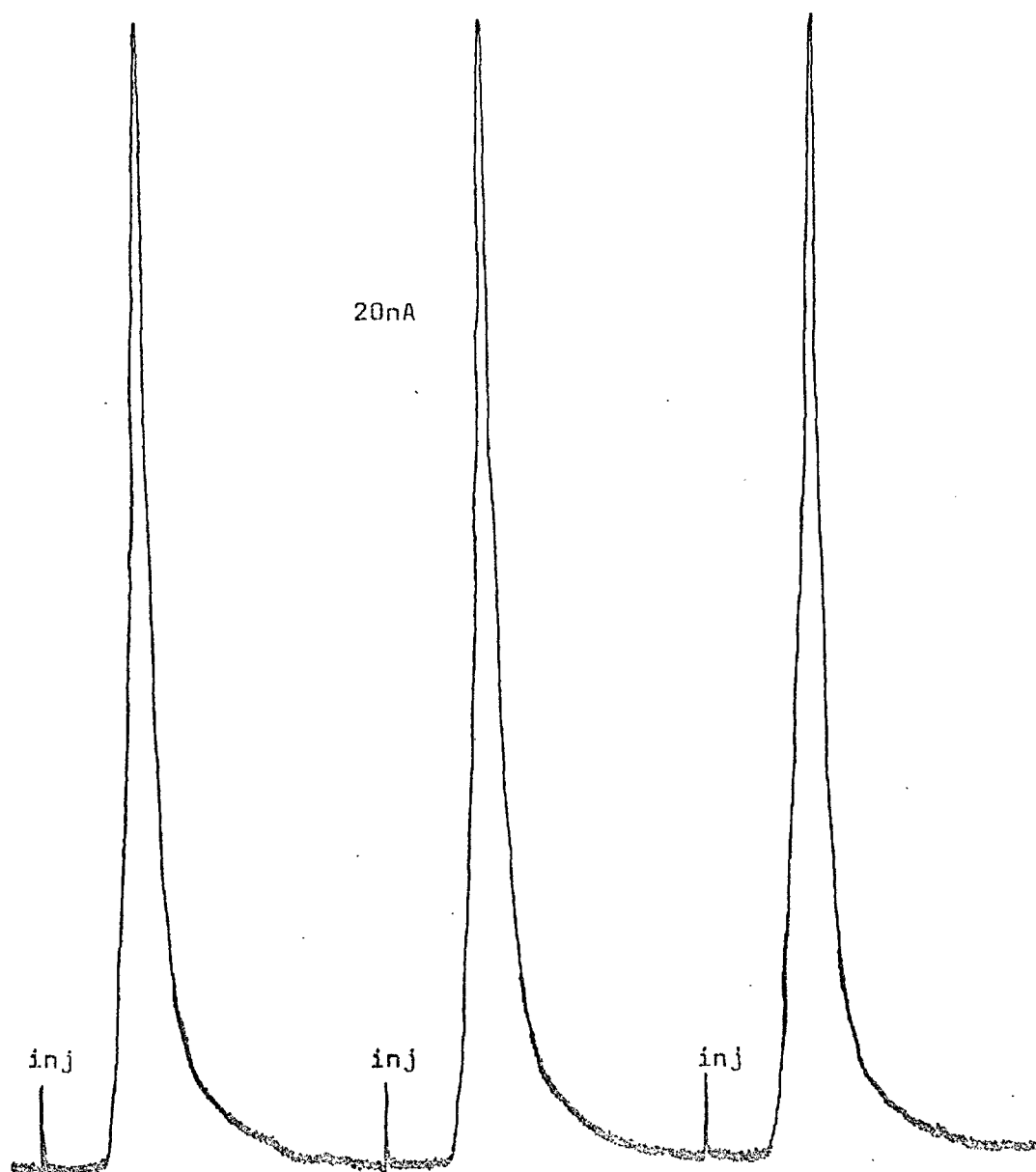SOLVENT FRONT

0.3ml/min

25   20   15   10   5   0

Figure 3-8
Reproducibility

Sample: L Dopa   500pg/5ul injection
Solvent: MeOH/ Water 10% V/V
Flow Rate: 1.5ml/min
Working Potential: +1.2 vs Ag/AgCl
Column: ODS Permaphase

20nA

inj   inj   inj

For the non aqueous work the Silver/Silver Chloride reference
system had to be modified. In place of the saturated KCl solution
hydroxy ethyl cellulose gel impregnated with saturated KCl was used.
This provided a reasonably stable reference system. The use of Agar was
discontinued owing to the formation of solid KCl at the end of the reference
electrode which contributed to high resistance effects. The use of
hydroxy ethyl cellulose seemed to obviate this problem.

4.5 Electrolyte Considerations

The main reason for the addition of supporting electrolyte
is to make the solvent conducting. As such there is no great need to
add excessive supporting electrolyte for reasons of eliminating migration
effects etc. It has been found that electrolyte levels of less than 0.01M
concentrations can be used without any significant adverse effects.
The same points hold for non aqueous solvents.

As the addition of supporting elctrolyte can effect the chrom-
atography due consideration must be given to factors such as ionic strength
and pH. In the case of Reverse Phase Chromatography, except when use of
buffers are warranted, pot asium nitrate was found to be a satisfactory
electrolyte. In the case of Normal Phase Chromatography with non aqueous
eluents tetra alkyl ammonium salts were used. The conductivity of these
salts increases both with the degree of substitution and alkyl substituent.
Tetra butyl ammonium fluoroborate proved the most satisfactory for non
aqueous solvents because of its high solubility and the high conductance
of its solutions. It is easily prepared in large quantities by mixing
teta butyl ammonium bromide and hydrofluoroboric acid (121).

132

4.6 Potential Selection

The use of potential selection is one of the attractive features of electrochemical detection since it is possible, in principle, to pick out one electroactive species in a mixture thus reducing effects of interfering compounds and overlapping peaks.

Figure 4-9 shows the use of potential selection in order to reduce effects of overlapping peaks. The chromatograph is of a sample of pregnancy urine (see section 5-1) separated on a silica column using hexane/ethanol as the eluent.
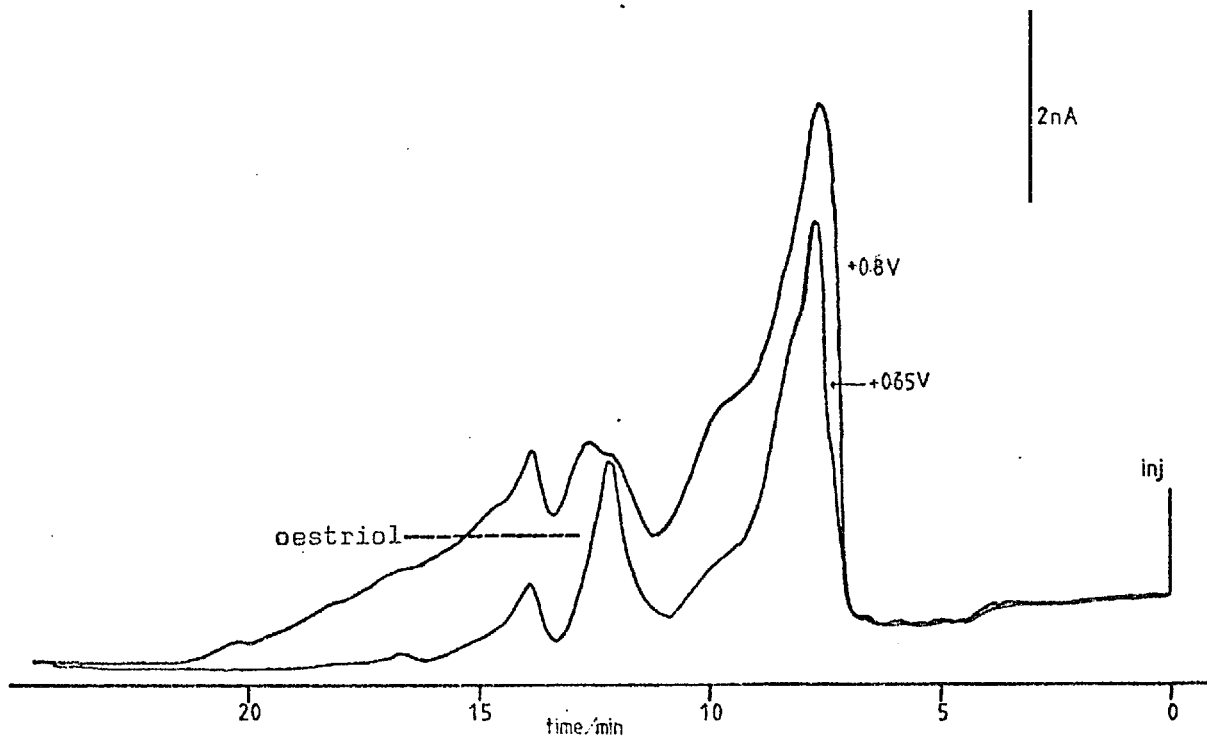
Figure 4-9
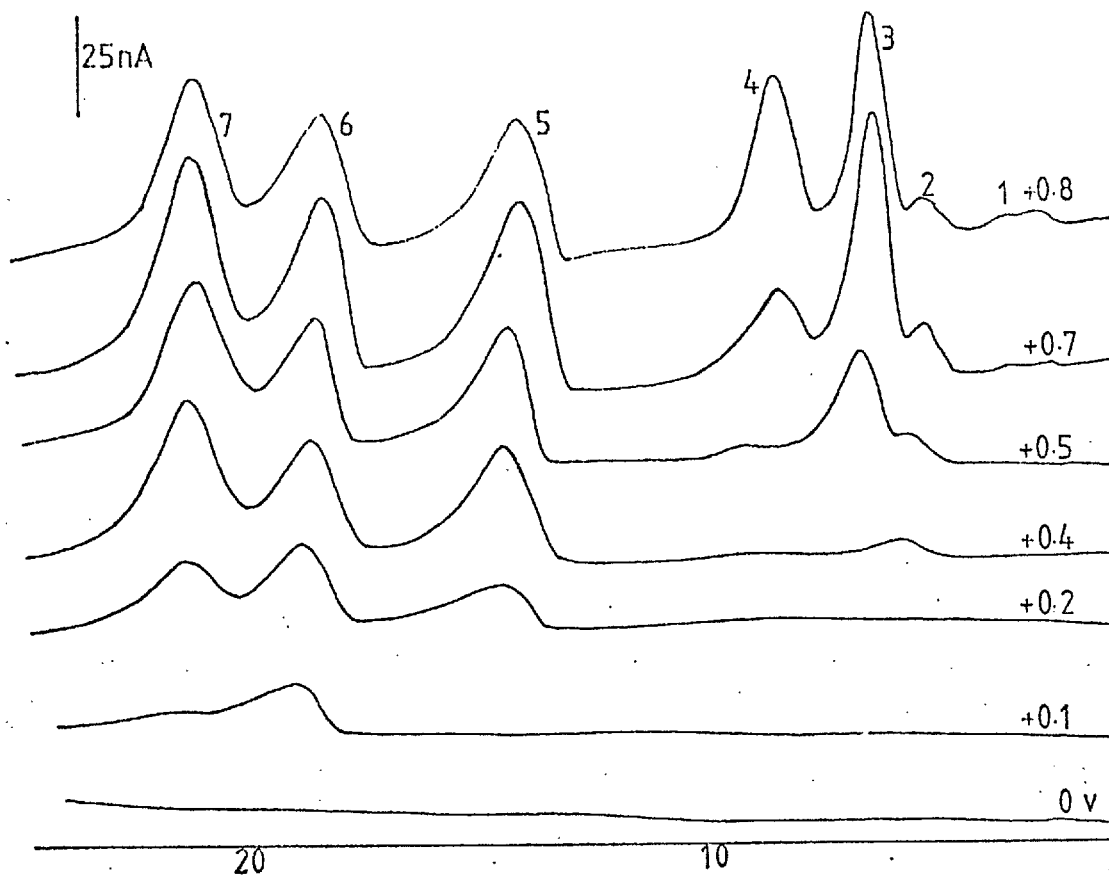
EFFECT OF WORKING ELECTRODE POTENTIAL ON SELECTIVITY   HEXANE/EtOH   70:30

1 SOLVENT FRONT   6 PARA AMINO PHENOL
2 2,6 DIISOPROPYL PHENOL   7 PARA PHEN. DIAMINE
3 3, ISOPROPYL PHENOL
4 PHENOL
5 ORTHO AMINO PHENOL

Figure 3-10

An elegent example of the use of potential selection

is given above (figure 3-10). It can be seen that individual phenols

can be 'selected' quite accurately by varying the potential.

Potentials were measured against a Ag/AgCl reference.

4.7 Indirect Techniques- Post Column Addition

The use of post column addition has a number of applications:

i) to make an electroinactive compound electroactive by the addition of a suitable reagent which by itself shows little electroactivity.

ii) the addition of electrolyte/buffer solutions in oredr to make the eluent conducting . This is of use in cases where change in the eluent pH or ionic strength may adversely affect the chromatography.

Assembly for
Post Column Reagent
Addition
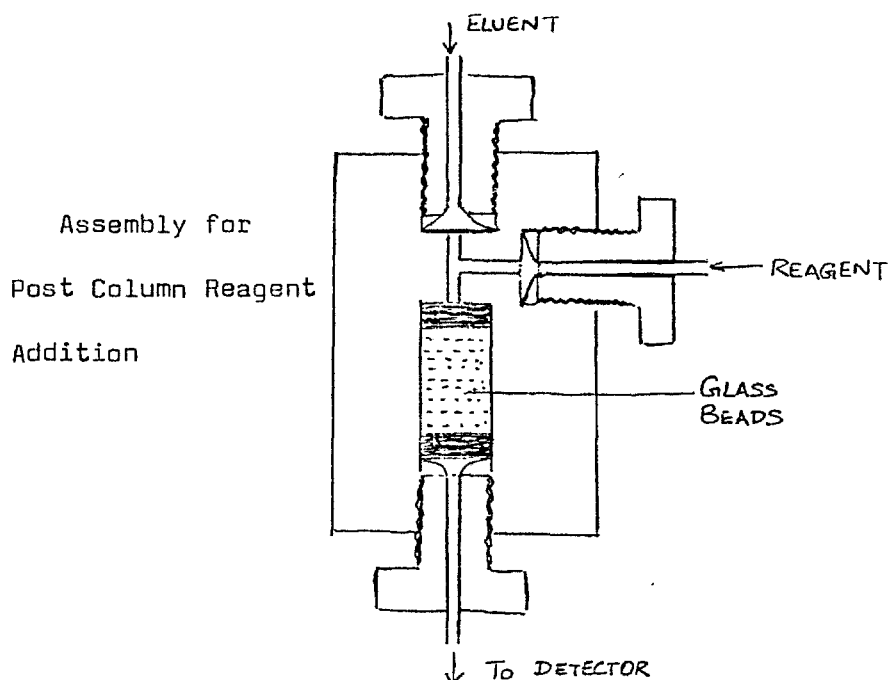
Figure 3-11

iii) the addition of mercury solution for insitu plating of a thin film of mercury on the working electrode surface , thus extending the cathodic potential range.

A good example of the use of post column addition is in the determination of dithio compounds. Oxidation of these componuds can only be accomplished in highly alkaline medium (for example KOH). Figure 3-12 demonstrates this.

I.+ 0.1M KOH

II. + acetate buffer
pH 5.5

-0.3	0.1	0.5	0.9
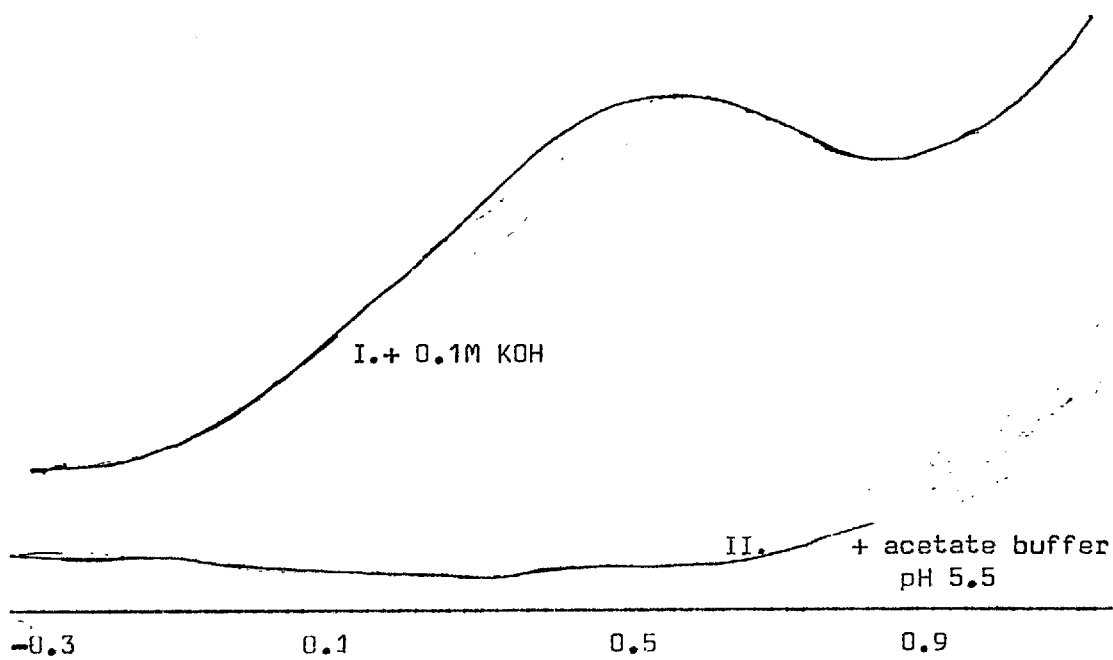
Figure 3-12

Differential Pulse Voltammogram of Ethylene Bis Dithiocarbamate.
Scan Rate = 20 mV/sec.

Glassy Carbon Electrode, previusly polished with diamond paste.

CHAPTER V. BIOMEDICAL APPLICATIONS

5.1 Oestrogen Steroids as an Indication of Feotal Well Being

5.11 The Nature and Role of Oestrogen Steroids

The oestrogens, in combination with other hormones, are responsible for the development and maintenance of the female sex organs. During pregnancy oestrogen levels in the urine and blood increase dramatically (up to a thousand times more than normal) (122), declining rapidly after delivery or feotal death. For this reason there is considerable interest in measuring levels of oestrogens as an indication of feotal well being especially in high risk pregnancies where need for early delivery may occur.

The three main oestrogens that are produced at increased levels during pregnancy are oestrone, oestradiol, and oestriol. A number of other oestrogens are believed to be secreted at lower levels.

Apart from serving a vital function during pregnancy, it has been observed that oestrogens play a part in determining the aging process in man (123). The monitoring of oestrogens could therefore provide information as to the breakdown of vital human functions as a result of aging.

5.12 Methods of Determining Urinary Oestrogens

Among the techniques that have been used for determining urinary oestrogens the most popular has been a colourimetric assay of total oestrogens (124,125). More recently the use of prior separation, in particular HPLC, has been advocated as a means of eliminating the substantial interference caused by a number of drugs commonly used in the treatment of pregnancy cases.

OH

HO

Oestradiol

OH

OH

HO

Oestriol

O

HO
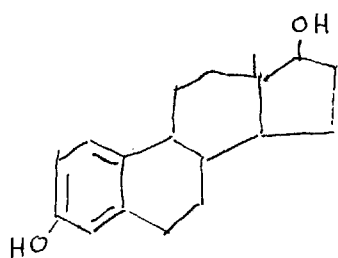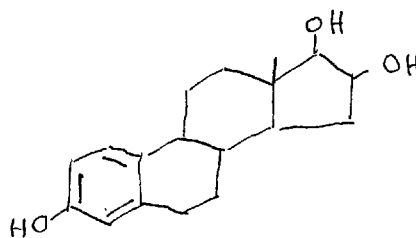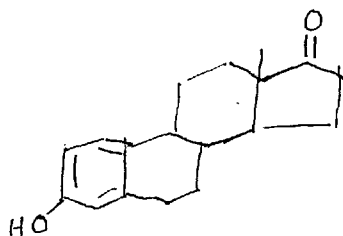
Oestrone

figure (5-1)

The most succesful example of the use of of prior separation

is due to Huber et. al. (126). Here use was made of Liquid- Liquid

High Pressure Chromatogaraphy coupled with UV detection; analysis

times of less than 15 minutes were quoted.

5.13 Choice of Separation Technique.

Oestrogen Steroids are of medium polarity, with a tendancy

towards lipophilicity owing to their large hydrocarbon skeleton. As a

result Adsorption Chromatography with solvents of low polarity prevail in

the field. However , use of Reverse Phase (127) and Liquid- Liquid

Chromatography (128) has also proved succesful.

In this work it was found that use of Reverse Phase separation

(ODS Permaphase column; water/methanol eluent) did not give the resolution

that was required to separate the large number of interfering compounds

that seemed to be present in the sample . Additionally,it was found that

as many of these compounds were of high polarity, they eluted with the solvent As a result it was decided that Normal Phase Adsorption Chromatography would be the most suitable. Mixtures of Hexane and Ethanol served as the low polarity solvent system.

5.14 Sample Preparation.

Oestrogens can be extracted from Urine by exploiting the weakly acidic nature of the A ring phenolic group. As oestrogens are normally secreted as sulphate and glucorinidase conjugates hydrolysis with a concentrated acid solutionis required (129). The full procedure is given below and is adapted from Huber et. al. (130).

Four millilitres of Urine samplewas refluxed for one hour with 1 ml of concentrated hydrchloric acid. After cooling Oestrogens were extracted into ether (3x 20 mls) followed by a sodium carbonate wash (pH 10). The ether was then evaporated and the residue was disolved in 1ml ethanol.

Urine samples were taken at the last trimester of pregnancy and stored in a freezer prior to ues.

5.15 Results and Discussion.

i) Calibration Curves and Reproduciblity.

Figure 5-2 gives calibration curve for oestriol, separated on an ODS column. It can be seen that within the given range, the plot is linear.

In order to test for reproducibility of extraction and detection, standard additions were made to fresh male urine samples (male urine contains neglegible levels of Oestrogens). The oestriol content was then determined after extraction, following 5-14. Table 5-1 shows that results are quite reproducible.
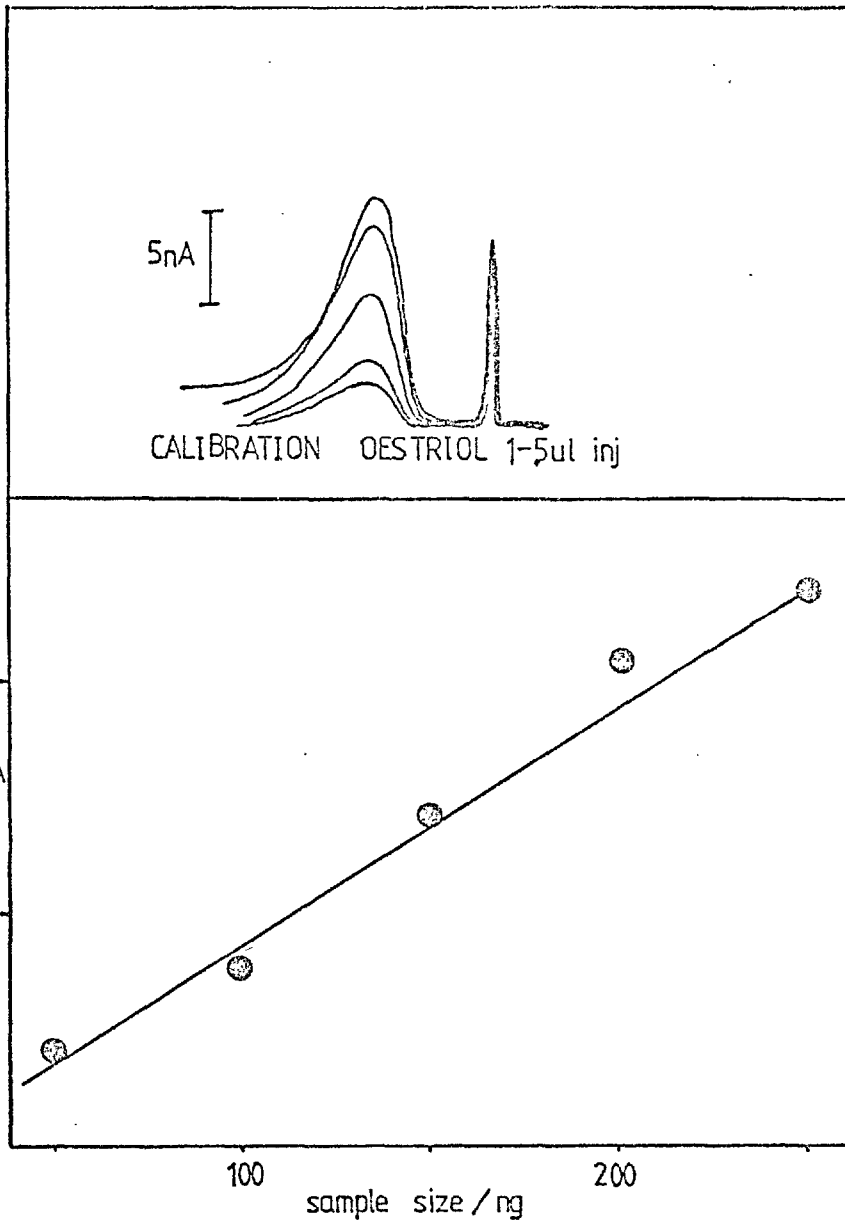
Figure 5-2

Working Conditions: $E_{applied}$ = +1.2 V vs Ag/AgCl

Eluent = 20% MeOH/H_2O/0.1M KNO_3

Flow Rate = 0.5 ml/min

Table 5-1

Accuracy and Precision of Extraction and

Chromatography

(Extraction of Oestriol Added to Male Urine + 2% EtOH)

Extraction Conditions

pH	Temperature	Added	Found
4.3	20°C	mg/100cc	mg/100cc
		1.5	1.5
		1.5	1.4
		1.5	1.4
		1.6	1.5

% Recovery   = 95%

ii) Separation of urine samples on an ODS Permaphase column

For the sake of comparism use of reverse phase separation is given (see figures 5-3 and 5-4). As it can be seen, most of the polar constituents are eluted on the solvent front . A few of the : polar compounds expected in the sample did not elute at all at low methanol/ water ratios. This suggests the need for gradient elution.

iii) Separation by Normal Phase Adsorption Chromatography.

Chromatograms obtained by normal phase separation are given in figures 5-5 - 5.7. These can be seen to be a significant improvement from the previous ones by reverse phase separation. The chromatograms also compare very favourably with those obtained by Huber (130) by Liquid-Liquid Chromatography. Table 5-2 gives the amounts of Oestriol present in the samples as quoted by Middlesex Hospital where use of a colourimetric technique was used.

Name	Figure no.	Amount of Oestriol
Newman	5.5	95nmole/ml
Webb	5.6	138nmole/ml
Potonius	5.7	52nmole/ml

Table 5-2

Though it was initially proposed to measure simply the levels of oestriol in order to have a quick method of determining the state of the foetus, it was found that the relative levels of the other oestrogens may serve to give further information.From figures 5-5 - 5-7 it can be seen that as the estriol levels increase the relative oestrone and oastriol levels decrease. This trend is clearly shown in figure 5-8.

i) Newman 95 nmole/ml

ii) Webb 138 nmole/ml

iii) Potonius 52nmole/ml
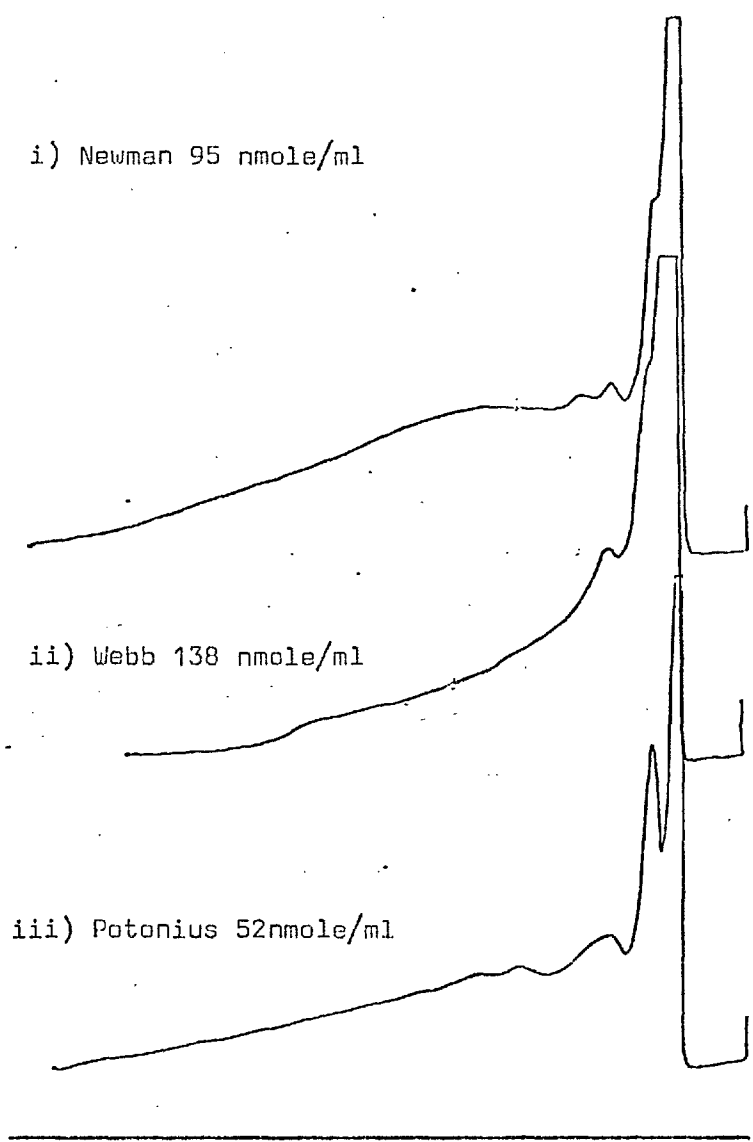
Figures 5-3 — 5-4

Separation of hydrolysed pregnancy urine samples on ODS Permaphase

Eluent: MeOH/ H_2O — 30/70 0.1M KNO_3

$E_{applied}$ = 1.2 V vs Ag/AgCl

Flow Rate = 0.8ml/min

Figure 5-6
Webb 138 nmole / ml

2nA

inj
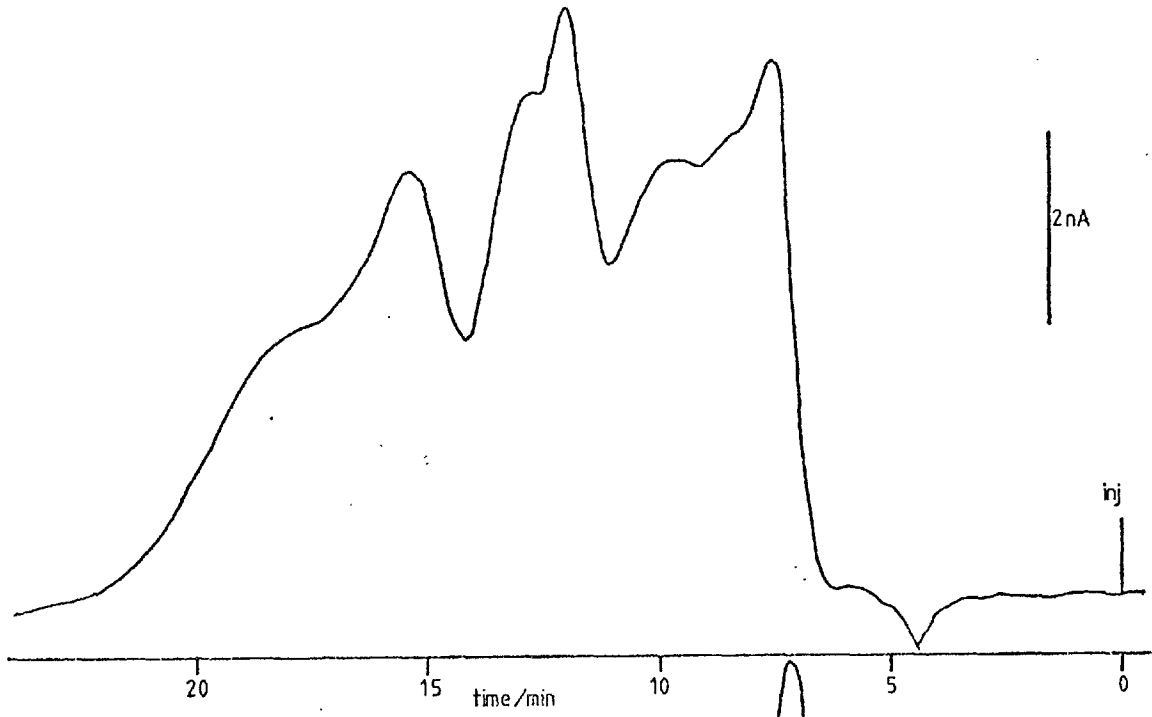
Figure 5-5
Newman 95 nmole/ml

estrone
diol

estrone

2nA

inj

estrone
triol

STD

Potonius 52 nmole/ml

Figure 5-7

inj

Figure(5-8)

Graph showing variation of relative
Estriol/Estrone levels with Estriol concentration.

Ratio of
peak heights
Estriol/ Estrone

Quoted Estriol Levels umol/l
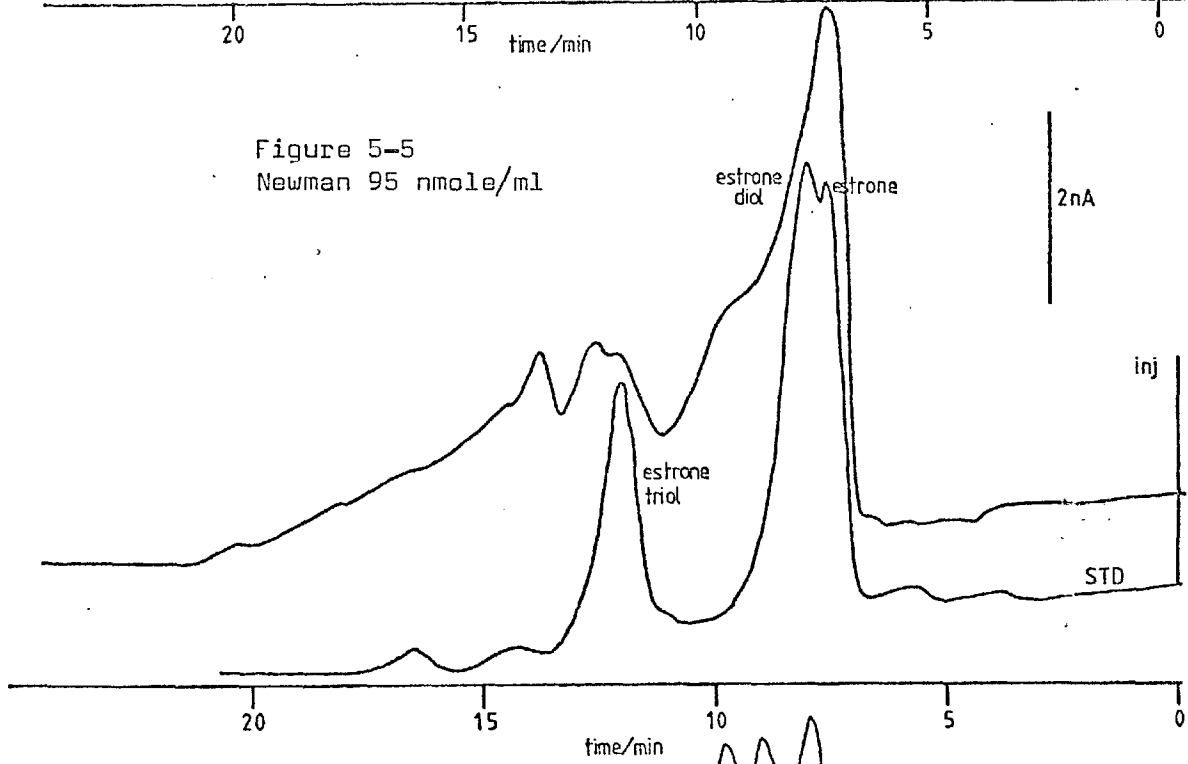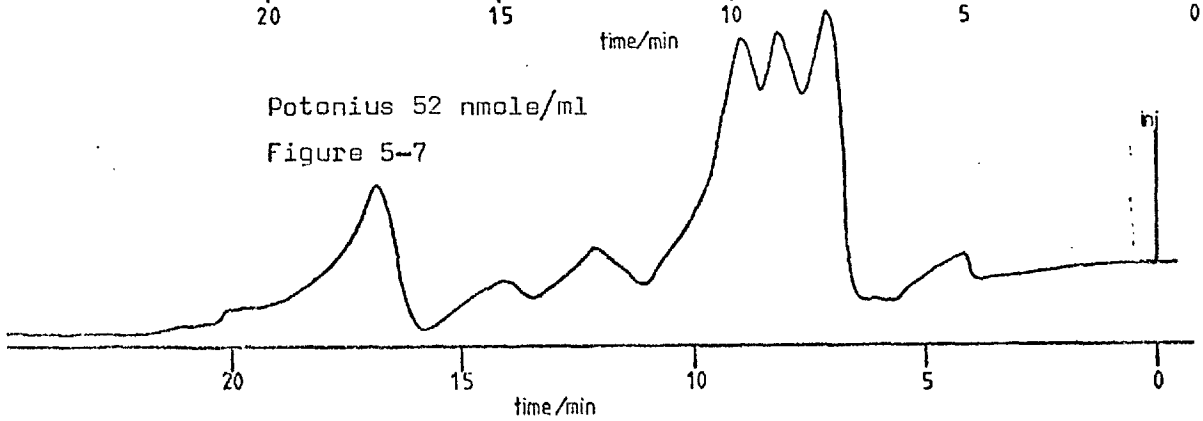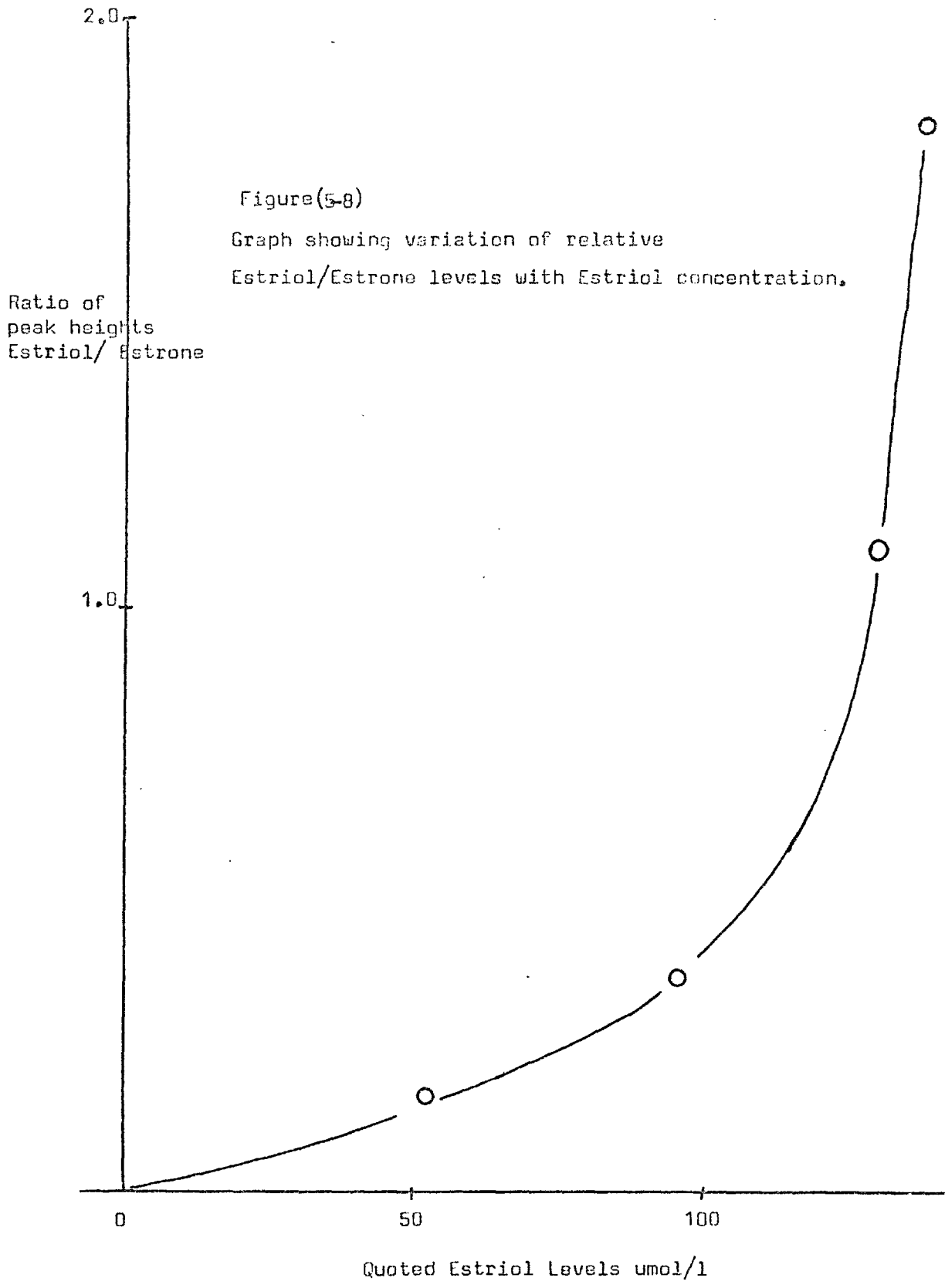
5.2 Ascorbic Acid by Ion Pair Partition Chromatography

5.21 Introduction

The determination of ascorbic acid by ion-pair partition chromatography has been described as a good alternative to ion exchange (131) . Kissinger (132) has shown that electrochemical detection coupled with ion exchange chromatography is ideally suited for determining very low levels of ascorbic acid. In this work ion pair partition chromatography is combined with electrochemical detection to determine ascorbic acid at very low levels.

5.22 Experimental

Preparation of Eluent

To the methanol/water eluent 0.005 M tetrabutylammonium bromide was added and the solution stirred for 5 minutes. The solution was then filtered through a 0.45 micron filter. A fresh solution was prepared for each set of runs.

Tetraethyl ammonium bromide was also tried as the counter ion but this gave significantly less retention times when compared with the tetrabutyl salt.

Results and Discussion

In figure 5-9a we have a chromatogram of a 10ng sample of ascorbic acid injected with 5 ul methanol. It can be seen that the compound elutes on the solvent front.

Addition of 0.005 M tetrabutylammonium bromide increases the retention time significantly, as it is shown in the figure below (5-9b).

Figure 5-9 a

Working Potential: +1.0 V vs Ag/AgCl

Column: ODS Permaphase

Eluent: 30/70 MeOH/H_2O 0.1M KNO_3

10ng/5ul MeOH
Ascorbic Acid

10 nA

inj

0   1   2   3   time/ minutes

10 nA

Figure 5-9 b

Ascorbic Acid

10 ng

Eluent: MeOH/H_2O :30/70
         + 0.005 M
         tetrabultyl ammonium
         bromide

inj

0   1   2   3

time/ minutes
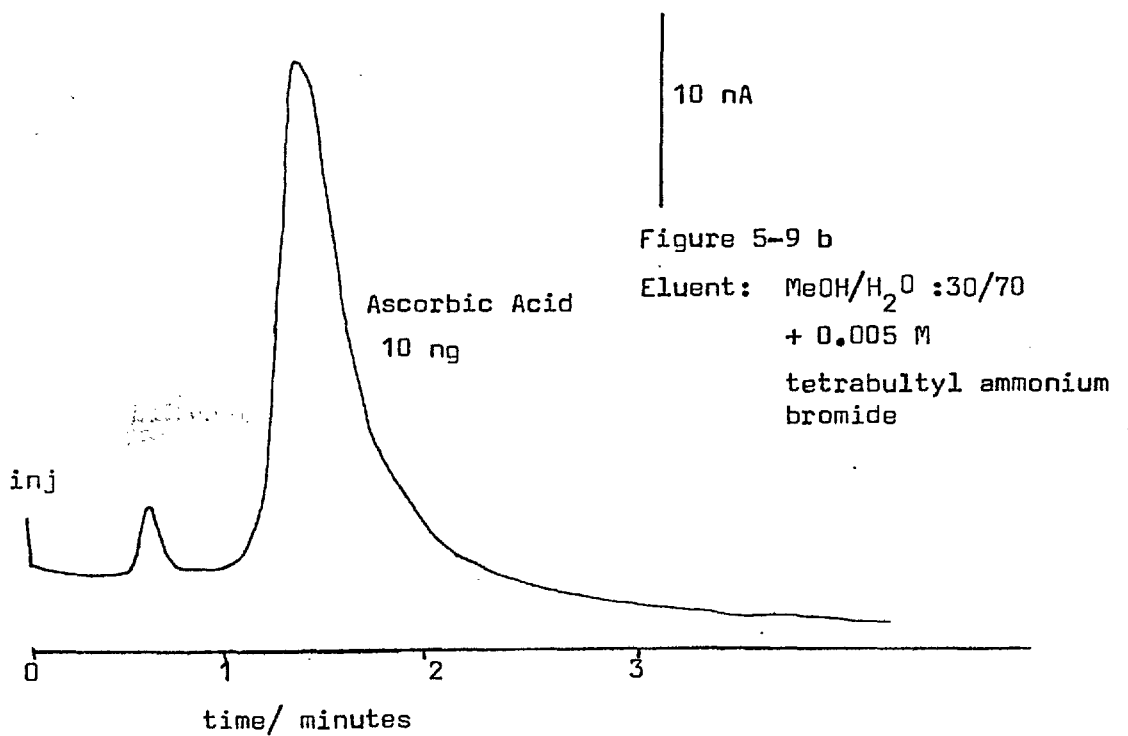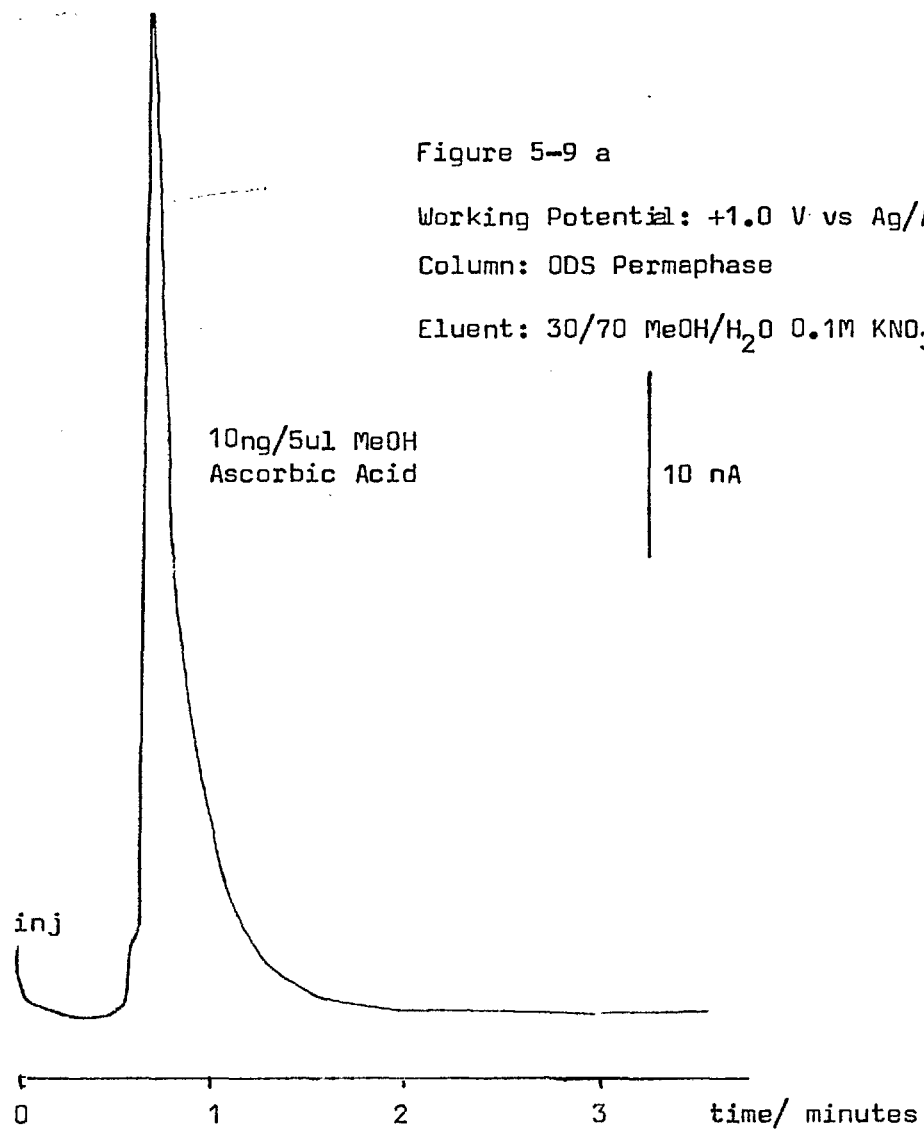
5.3 Determination of Some Important Drugs and Their Metabolites

5.31 Introduction

The analysis of drugs and their metabolites is the area
where HPLC has found the greatest usage. Though most drugs show
UV activity, there are quite a number which can be determined at
significantly lower levels by electrochemical detection.

This section presents a summary of the results obtained
for the determination of a range of drugs and their metabolites. As
the experimental procedure has already been described in some detail
only the basic parameters for each analysis will be presented.

5.32   Central Nervous System Depressants (Hypnotics and   Sedatives)

Drug	Column	Eluent	$E_{applied}$	Detection Limit
Barbituric Acid	ODS Permaphse	20% MeOH/H_2O	+1.3 V	10ng
Valium	"	"	"	10ng
Phenothiazine	"	"	+1.0 V	500pg

The site of oxidation of phenothiazine is probably the
nitrogen. The primary electrode reaction being a one electron transfer
to form the cation radical (133).

phenothiazine
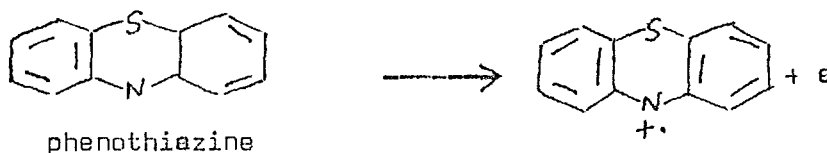
5.33 Central Nervous System Stimulants

(Antidepressants)

Caffeine

Caffeine which is widely used as a respiratory stimulant (134), was chosen as an example of this class of compounds. It is a constituent of coffee and tea.

The structure of the molecule is shown below. It is possible that the site of oxidation is nitrogen attached to the methyl group; the primary electrode reaction being again a 1 e transfer to form the cation radical. However on the basis of some studies by Dryhurst and Elving on adenine (135) it is more likely that the overall process is a two electron process as given below:
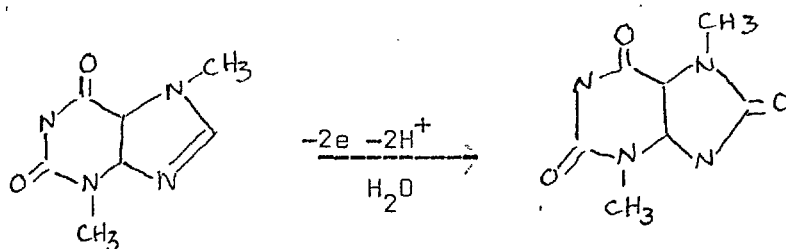
Compared with phenothiazine, the detection limit is somewhat les; about 1ng for the same working conditions.

5.34 Analgesics

Pain can be relieved by general anesthetics, local anesthetics or by various drugs which act on the central nervous system without producing general anesthesia. The best known of these are morphine and derivatives.
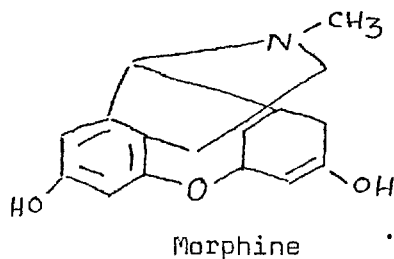
Morphine

The electro-oxidation of morphine has recently been reported to be reversible process involving the phenolic group (136).

In this work narcotine, an important constituent of opium and a derivative of morphine (137) was determined at a level of less than 100 picograms. The working potential was +1.3 V vs Ag/AgCl.

5.35 Body Temperature and Antipyretics Analgesics

These drugs serve to reduce body temperature by inducing perspiration (137). Compounds in this group include asprin and paracetamol.

OH

NHCOCH₃
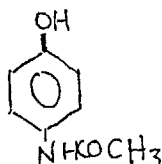
Paracetamol

Detection limits for these compounds were less than 100 pico grams (see figure 5-11).

5.36 Antihypertensive Drugs

Hydralazine

Commonly used to reduce hypertension. Detection limits obtained with the WJE were compared with the UV detector (figure 5-12 - 5-13). It was found that the WJE was at least ten times more sensitive.

SK &F Drugs

A range of nitrogen heterocyclic drugs manufactured by SK&F (England) were determined. These compounds are used as anti-hypertensive drugs.
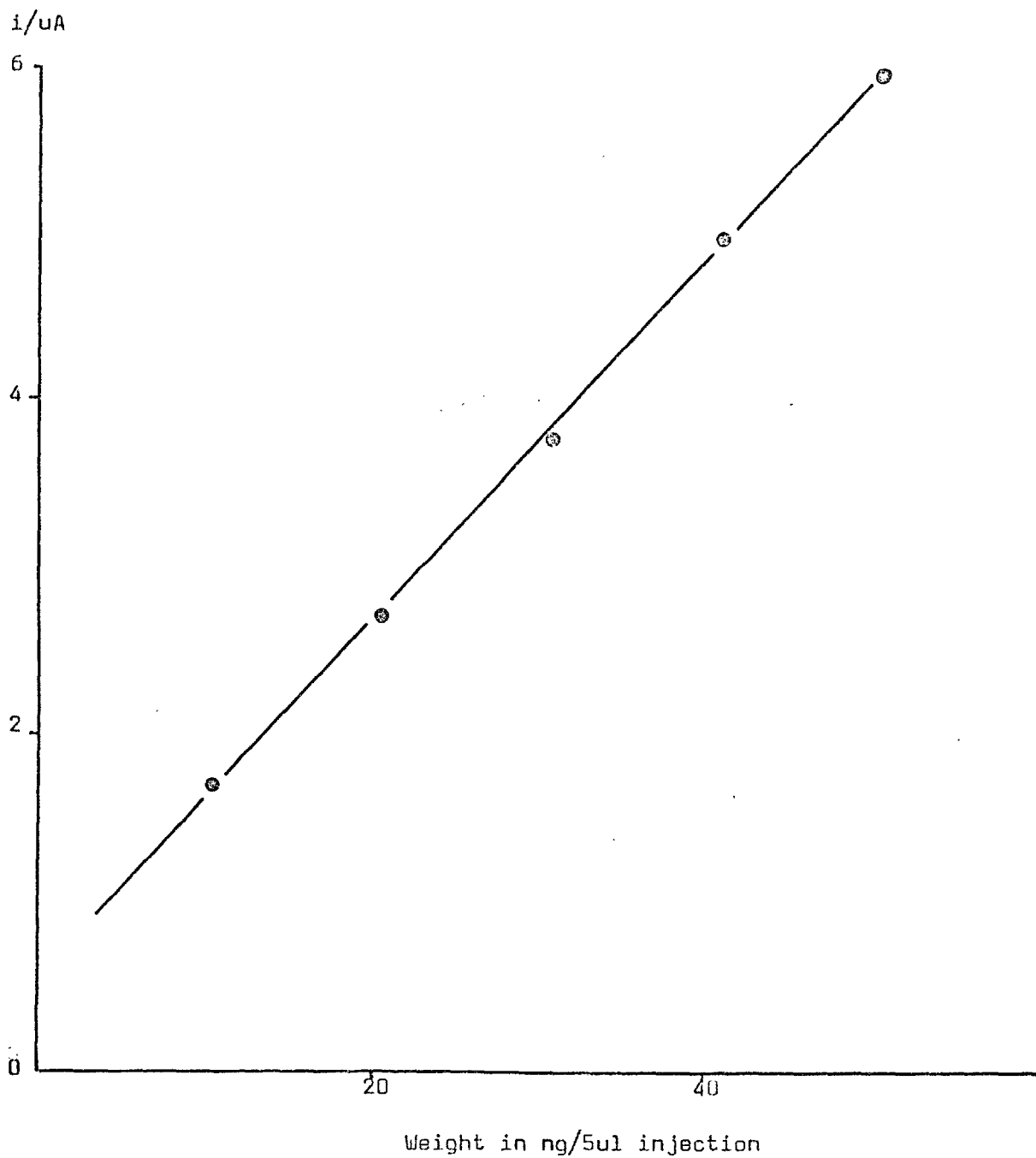
Figure 5-11   Calibration curve for Paracetamol

Column: ODS Permaphase

Eluent: MeOH/Water 0.1M KNO$_3$

Working Potential: +1.0 V VS Ag/AgCl

a.) Wall Jet Detector Trace
   Working Potential =+ 1.2 V vs Ag/AgCl

40nA

b.) UV Trace
Wavelength = 370nm

0.1 abs units
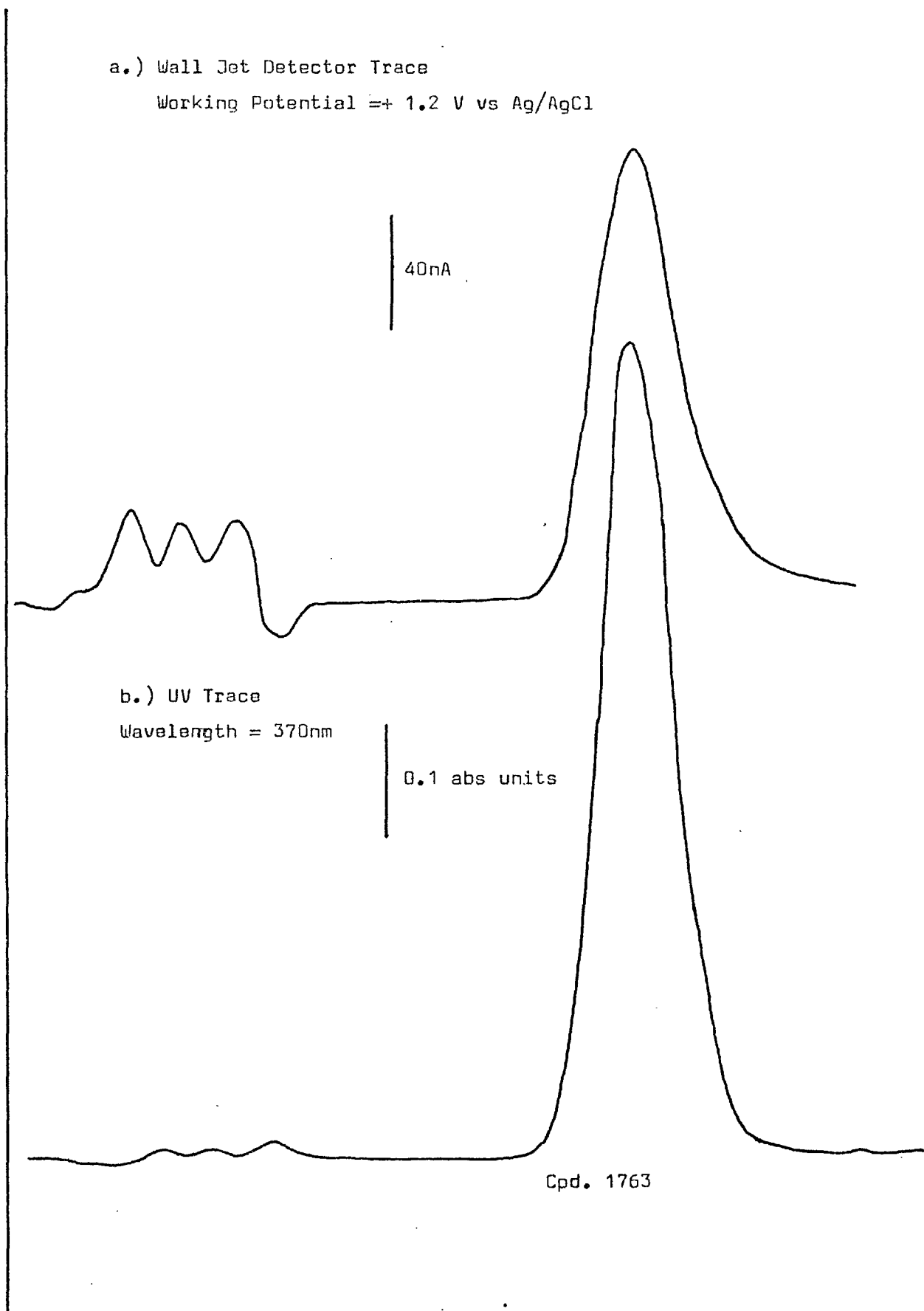
Cpd. 1763

Figure (12) Separation of Cpd.1763(ICI) — a heterocyclic nitogen
drug similar to Hydralazine.
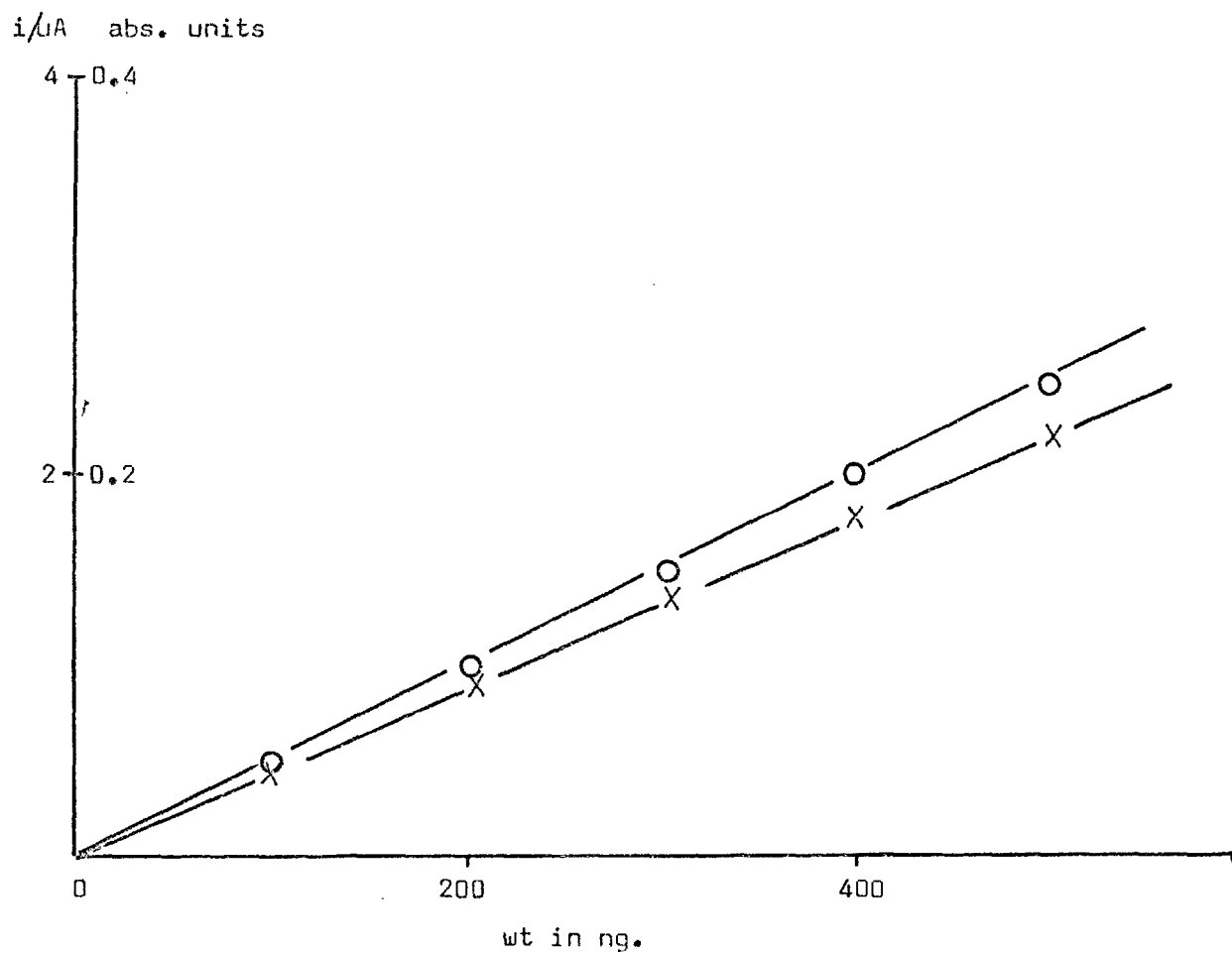
Figure 5-13   Calibration Curve for Hydralazine

Eluent— acetonitrile/Ethanol

O —   Wall Jet Detector; Working Potential= + 1.0 V vs Ag/AgCl

X —   Ultra Violet Detector;   Wavelength = 260nm
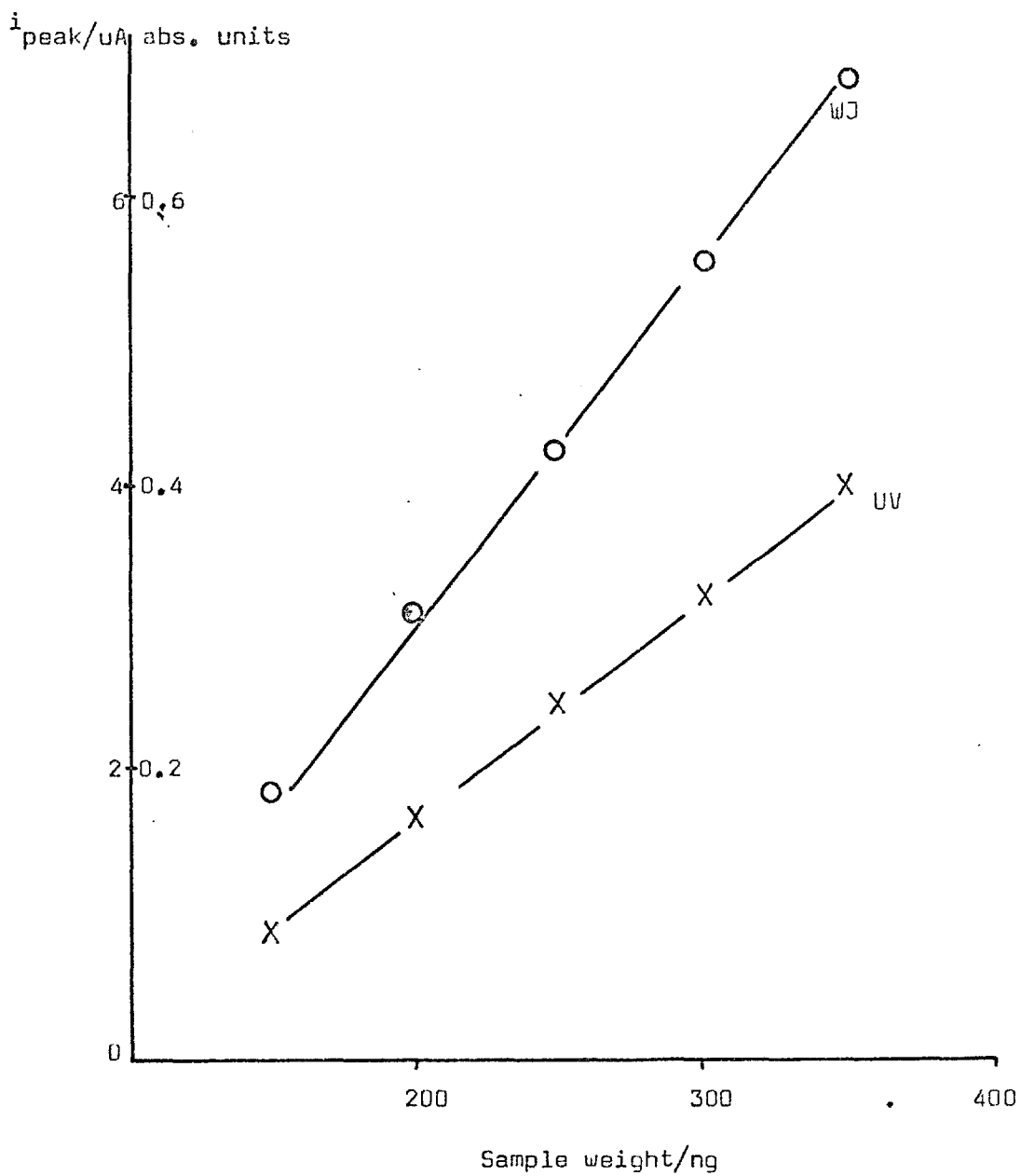
Figure (14) Callibration for impure sample of Hydralazine
(Plots do not pass through origin)

Silica Column
Acetonitrile/Ethanol Eluent

153

50nA

Separation of some
Antihypertensive drugs
(SK & f)

Column: ODS PERMAPHASE

Eluent: 30% MeOH/ Water

Working Potential: + 1.0 V
vs Ag/AgCl

$X = CF_3, CH_3$

154

25nA

0   25   50

t/minutes
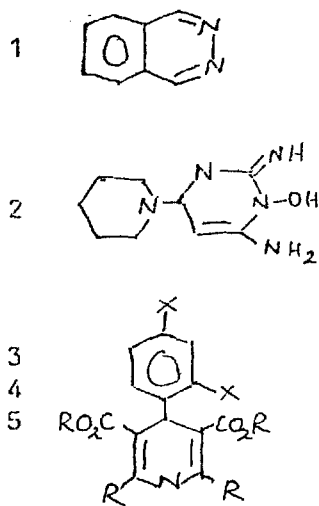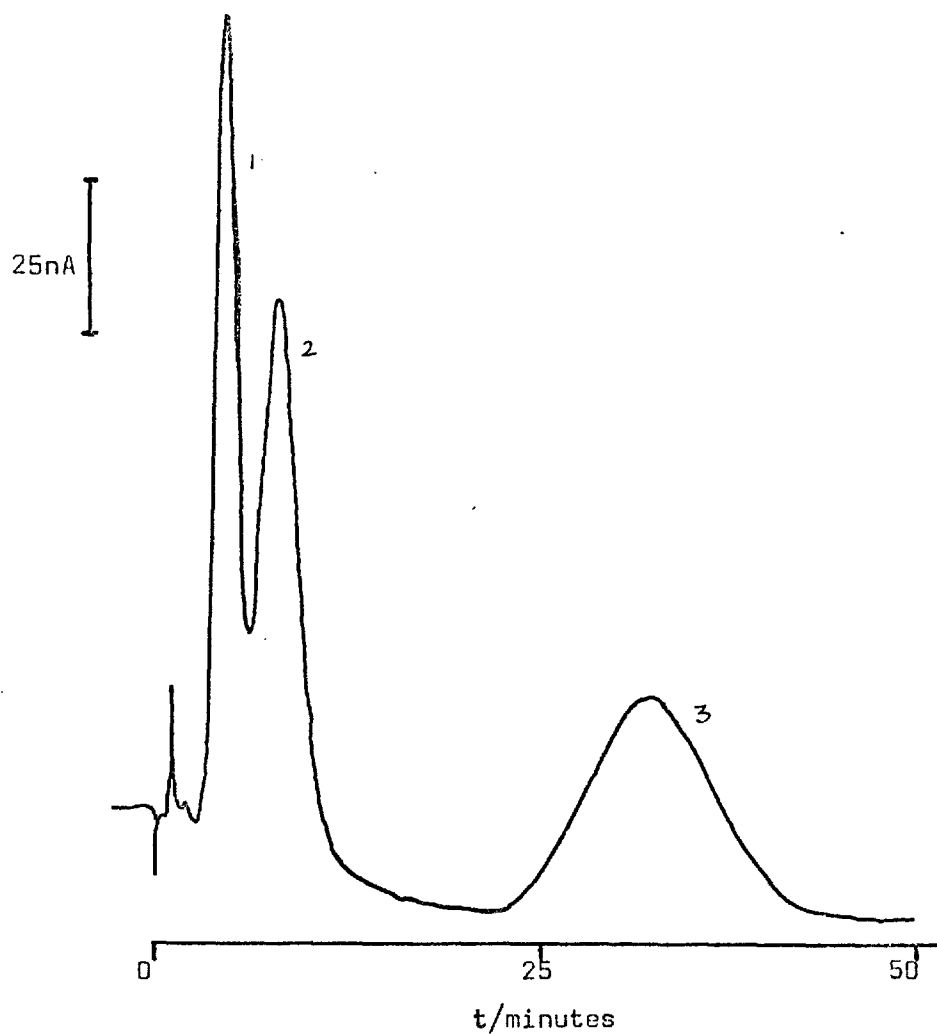
Figure (16)   Separation of some Antihypertensive Drugs (SK&F)

ODS Permaphase

25% MeOH/ Water

CHAPTER VI.   ENVIRONMENTAL ANALYSIS

6.1 Introduction

The increasing public awareness of the harmful effects
of environmental pollution and its consequences has resulted in
more severe legislation and an increase in   · technical activity in
the field of pollution monitoring and control. As the list of
potentially toxic substances increases with each year, new techniques
have to be devised to monitor (very often) trace amounts of these
substances. Addititionally, the Threshold Limit Value (TLV) of toxic
compounds are being decreased at regular intervals. This adds to the
problem of analysis. Fortunately for analytical chemists, most toxic
substances have a high electronic activity. As a result they are easily
determined by spectroscopic and electroanalytical techniques.

Although electroanalytical techniques have already found
significant usage in the analysis of trace heavy metals and
organometallics(138-142), the area of organic pollutants has been
neglected owing to the complex nature of the mixtures in which they
occur. This often necessitates time consuming extraction procedures.
In this context, the use of the separation capabilities of HPLC
coupled with electrochemical detection affords a means of determining
trace amonts of organics even in complex matrices with minimum.
sample preparation.

In this chapter the wall-jet cell is used to determine a
number of organic pollutants at levels of less than 100 picograms.
These include catechol and the poly nuclear aromatic hydrocarbons
which are known carcinogens.

6.2 Constituents of Cigarette Smoke Condensate

Intensive research in a number of countries in the last decade have confirmed that cigarette smoking is the major cause of lung cancer (143). Among compounds that have been found in cigarette the following are the most common (144).

i) Nicotine   v) Cresol (ortho, meta and para)

ii) Benz(a)pyrene   vi) m & p Ethyl Phenol

iii) Catechol

iv) Phenol

Though it is believed that the major cancer causing agent is benzo(a)pyrene, phenols, in particular catechol have been identified as possible carcinogens.

Owing to the difficulties of isolating benzo(a)pyrene it was decided in this work to determine only phenols and nicotine, which can be extracted by exploiting their acidic and basic character respectively.

6.21 The Electrochemistry of Phenols

Phenols are easily oxidised at carbon electrodes. The mechanism depends on the particular solvent system being used and the pH. According to Vermellion and Pearl (145) two different mechanisms are possible in aqueous solution:

i) a 2 electron loss from the unionised phenol to give a phenoxonium ion at low pH

ii) the removal of 1 electron from the phenoxide anion to give a phenoxy radical at high pH

In non aqueous solvents phenols are practically unionised and the initial electrode reaction could be given as follows:

157

CH3—⟨ring⟩—OH C(CH3)3 / C(CH3)3   —2e→   H+ + [CH3—⟨ring⟩—O+ C(CH3)3 / C(CH3)3 ↕ CH3 + ⟨ring⟩ =O C(CH3)3 / C(CH3)3 ↕ CH3—⟨ring⟩ =O C(CH3)3 / C(CH3)3]
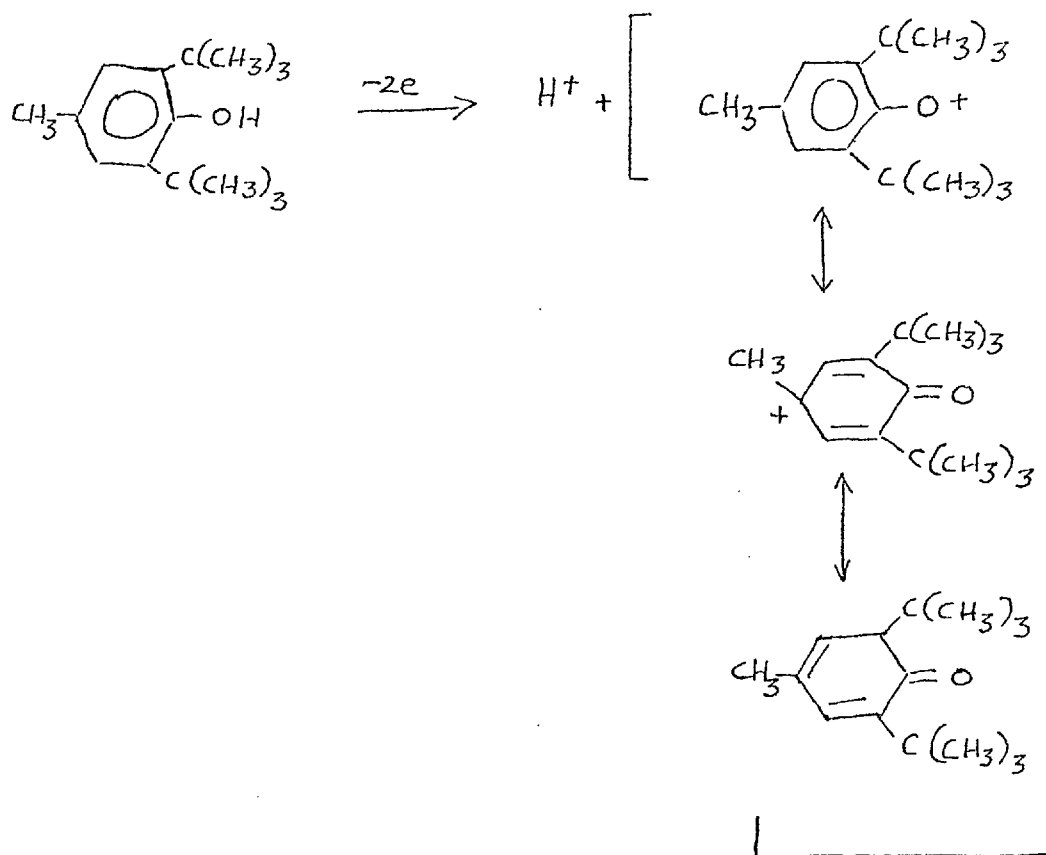
When a base is added to the solution the half wave

potential is shifted to a much lower value and the wave height is

approximately halved (146).

The reaction now involves a one electron transfer.

⟨ring⟩—O⁻ ⇌ −e [⟨ring⟩—O· ↔ ⟨ring⟩=O with ·H ↔ H· ⟨ring⟩=O]
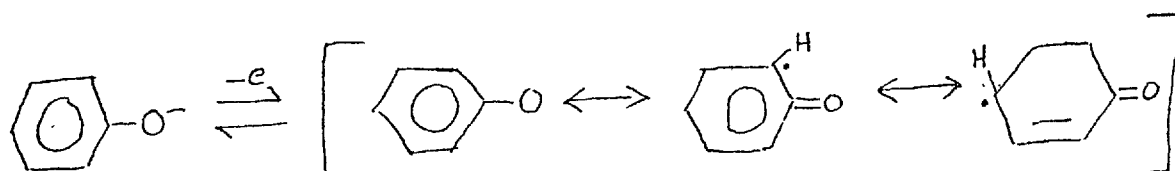
6.22 Sample preparation.

The determination of constituents of cigarette smoke presents considerable difficulties owing to the large number of compounds present, varying greatly with respect to polarity, structure etc... It was therefore essential that a preliminary extrction procedure be developed in order to isolate compounds of particular interest.

In this work phenols and nicotine were extracted by exploiting the acidic character of the former and the basic character of the latter. The complete extrection scheme is presented in the following page.

Smoke condensate samples were obtained by means of a twenty channel 'smoking machine' at the Laboratory of the Government Chemist London WC2 . Smoke condensate was collected onto a fibre glass flter pads placed at the end of each channel. A total of five cigarettes were 'smoked' onto each filter pad.

6.23 Chromatographic Considerations.

The more polar/phenols are most easily separated by Normal- Phase Liquis Solid Chromatography. This is partly due to the high sorption energy towards alumina and silica. Factors which influence separations are the ⁻ number of hydroxyl groups in the phenol molecule, their mutual positions and the presence of other functional groups.

In this work a six inch slica column was used with Hexane/ Ethanol mixtures serving as the low polarity eluent.

159

SMOKE CONDENSATE

(2Filter pads, 10 Cigarrettes)

i) Et$_2$O / 0.1M HCl

ii) Cross Wash Et$_2$O with 0.1M HCl

HCl (+ Nicotine) layer   Et$_2$O layer (+ Phenols)

i) 1M NaOH   0.1M NaOH

ii) Et$_2$O x3

Et$_2$O layer   Aqueous layer   Discard
                                                        Et$_2$O layer

i) Evaporate   i) Cool

ii) Dissolve residue   ii) 1M HCl
    in 5ml EtOH
                               iii) Et$_2$O x 4

HPLC   Et$_2$O layer

                               i) 2x H$_2$O- Discard

                               ii) Dry with Na$_2$SO$_4$

                              iii) Evaporate and dissolve
                                   in 5 ml EtOH

                               HPLC

ACID EXTRACT
OF CIGARETTE SMOKE CONDENSATE
SILICA COLUMN

ELUENT - HEXANE / EtOH / NH$_3$ - 70 / 29·5 / 0·5
WORKING POTENTIAL - +0·7 V vs Ag / AgCl

NICOTINE

SOLVENT
FRONT

2·5 nA

25   20   15   10   5

t/min

BASIC EXTRACT
OF CIGARETTE SMOKE
ADSORPTION CHROMATOGRAPHY
SILICA COLUMN
ELUENT: HEXANE/EtOH/NH$_3$ SOL$^-$ 70/29.5/0.5
WORKING POTENTIAL: +0.7 V vs Ag/AgCl

2.5nA

CATECHOL

PHENOL

CRESOL

SOLVENT
FRONT

inj.

t/min

25   20   15   10   5   0

162

6.3 Polynuclear Aromatic Hydrocarbons (PAH's)

Formed as the result of decomposition of petroleum and
other natural products polynuclear aromatic hydrocarbons constitute
a major pollution problem (147-150). Several of these compounds
have been listed as extremely active carcinogens (151,152).
Carcinogenic activity is apparantly related to binding of the PAH
with DNA and RNA strands.

All the highly carcinogenic PAH's show a high degree
of electroactivity. In this context electrochemical detection
coupled with HPLC seems suited for the purpose of analysis of these
compounds.

6.31 The Electrochemistry of PAH's
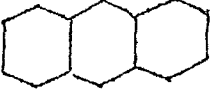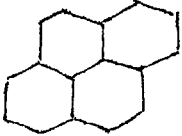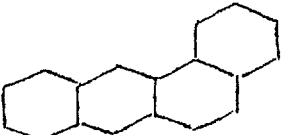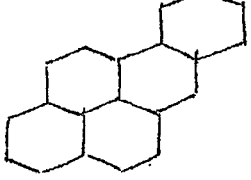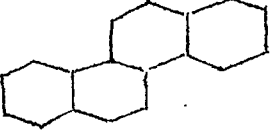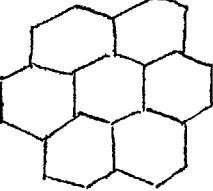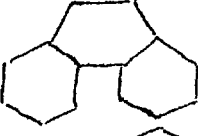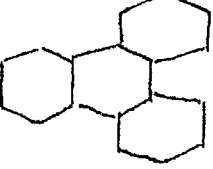
The oxidation of PAH's initially involves the formation of
a cationic radical(153-156):

$$Ar \longrightarrow Ar^{+}_{\bullet} + e$$
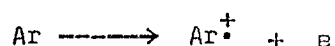
The stability of the radical depends to a great extent
on the degree of delocalisation and substitution. In the step
preceding electron transfer, it is believed that the hydrocarbons
adsorb on the electrode surface. Finally, as the cation radical is
very reactive as an electrophile or proton donar it reacts with
nucleophiles.

For the oxidation of 9,10 diphenyl anthracene the following
reaction pathway has been suggested (156):

$$DPA \xrightarrow{-e} DPA^{+}_{\bullet} \xrightarrow{\text{mass transfer}} DPA^{+}_{\bullet} \text{ (bulk)}$$
at electrode

Nu

$$DP\overset{\bullet}{A}---Nu^{+} \xrightarrow{-e} DPA^{+}---Nu^{+}$$

163
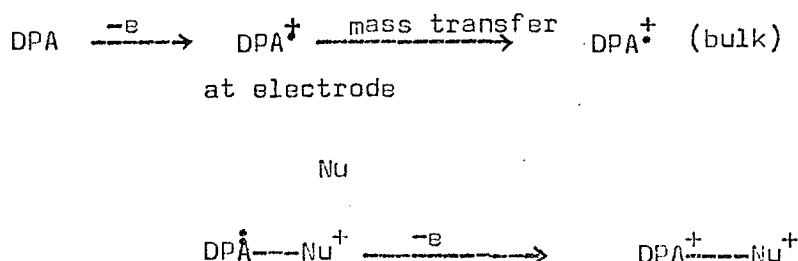
PAH	STRUCTURE	$E_{\frac{1}{2}}$	Carcinogenic Activity
anthracene		0.84	
pyrene		0.86	++
benz(a) anthraceme		0.92	+++
benzo(a) pyrene		0.76	+++
chrysene		1.13	+
coronene		1.23	
phenanthrene		1.23	
triphenelene		1.46	

E vs Ag^+ (157)

+ weakly active, ++ active, +++ strongly active

Table 6-1

6.32 Chromatographic Considerations

Alkyl substituted polyaromatic hydrocarbons are separated using silica (158) or alumina (159) columns. Useful results have also been obtained by exclusion chromatography (160) and liquid-liquid systems. In all these cases the presence of alkyl side chains causes diminuation in retention.

The liquid chromatography of unsubstituted PAH's in the reverse phase mode gives good separation.(161). In contrast with normal-phase LC, where retention depends largely on the interaction between the aromatic π electrons and polar functional groups in the stationary medium. Reverse phase LC of these compounds is more dependent on their limiting solubility in the polar mobile phase.

The limited solubility of PAH's in aqueous medium however causes problems with the electrochemistry.

Figure 6-3 shows the effect of water on the anodic voltammogram of anthracene. It can be seen that as the water content increases the oxidation peak decreases, finally disappearing at 30% H_2O.

The next figure (6-4) shows how the use of aqueous eluents diminishes the chromatographic peak height. Anthracene, which is more soluble in the aqueous eluent then benzopyrene, shows a smaller increase in the peak current. when the eluent is changed to pure acteonitrile with $LiClO_4$ as the supporting electrolyte.

From the above considerations therfore, reverse-phase separation is not the best technique for PAH determination if electro-chemical detection is to be used. A more suitable technique would probably be exclusion chromatography. Unfortunately a suitable column was not available to demonstrate this.

I $CH_3CN/0.1M$ $LiCLO_4$

II 0.1% H_2O

III 20% H_2O

IV 30% H_2O

V vs SCE
(scan rate = 20mV/sec)
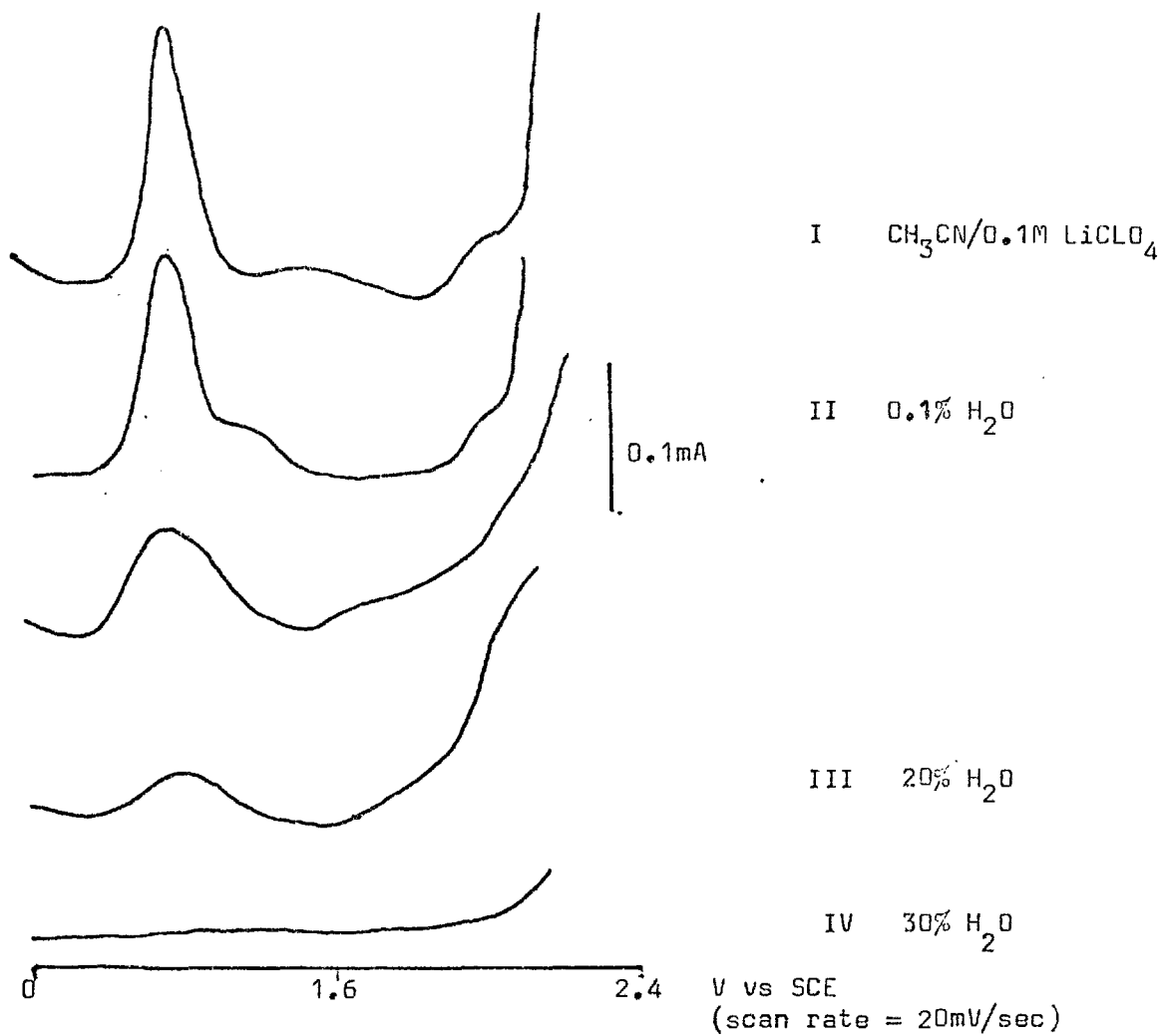
DIFFERENTIAL PULSE VOLTAMMOGRAMS SHOWING EFFECT OF H_2O

ON THE OXIDATION OF ANTHRACENE
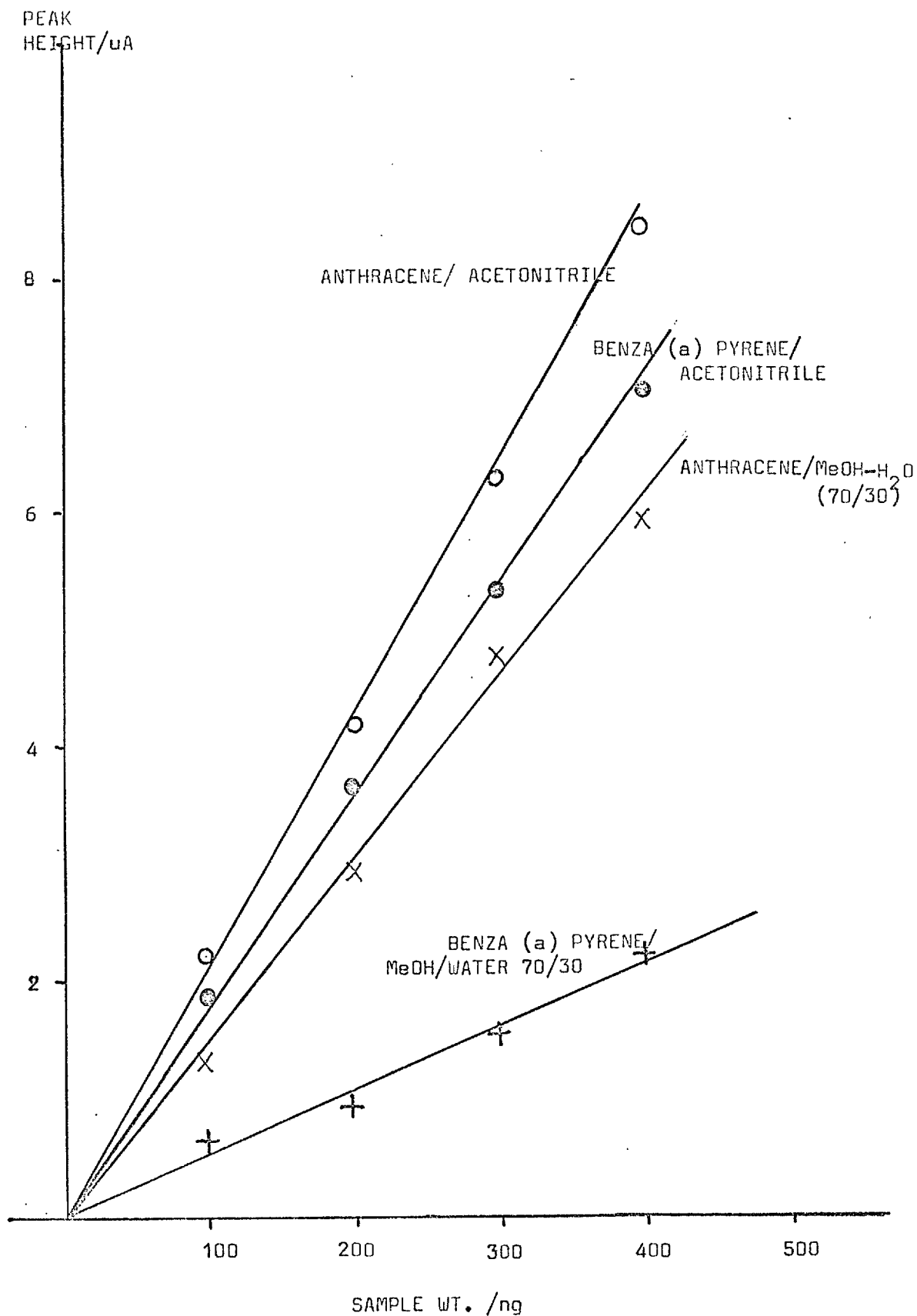
PEAK
HEIGHT/uA

ANTHRACENE/ ACETONITRILE

BENZA (a) PYRENE/
ACETONITRILE

ANTHRACENE/MeOH-H_2O
(70/30)

BENZA (a) PYRENE/
MeOH/WATER 70/30

SAMPLE WT. /ng
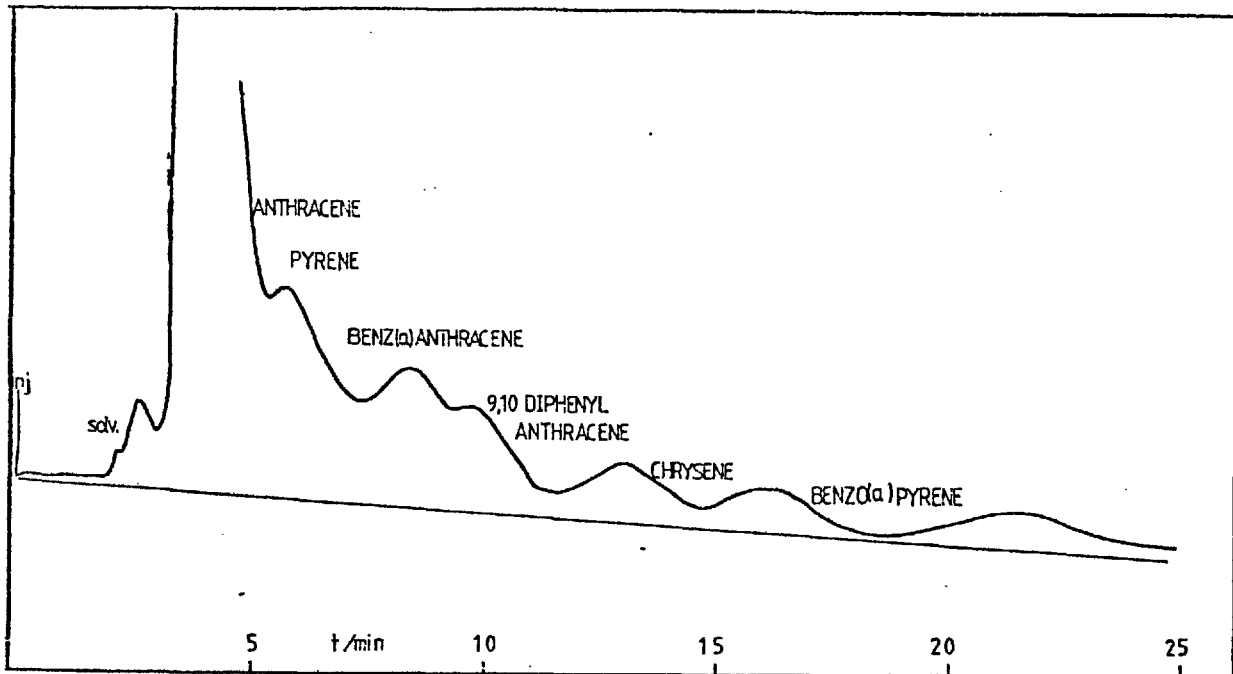
Figure 6-4a

In the above figure we have a reverse phase separation of some PAH's. It can be seen that anthracene has a very much higher response than the other PAH's.

The use of acetonitrile as part of the eluent mixture improves the response of the other PAH's; this is seen in figure 6-5. The quantity of anthracene was a third of the other PAH's.

Figure 6-6 shows an example of the use of potential selection. This once again demonstrates the utility of this technique. One specific use of potential selection is the determination of benzo(a)pyrene,the most carcinogenic PAH, in complex matrices such as sludge and soot. Theses matrices contain a large number of substances with highly anodic oxidation potentials. Benzo(a)pyrene having a low oxidation potential (see table 6-1) can thus be easily be determined.

100nA

ANTHRACENE

SOLVENT

TRIPHENELENE

9, 10 DIBENZANTHRACEENE

+1.5 V

+1.3 V

+1.0 V

+0.6 V

0   5   10

t/min

170
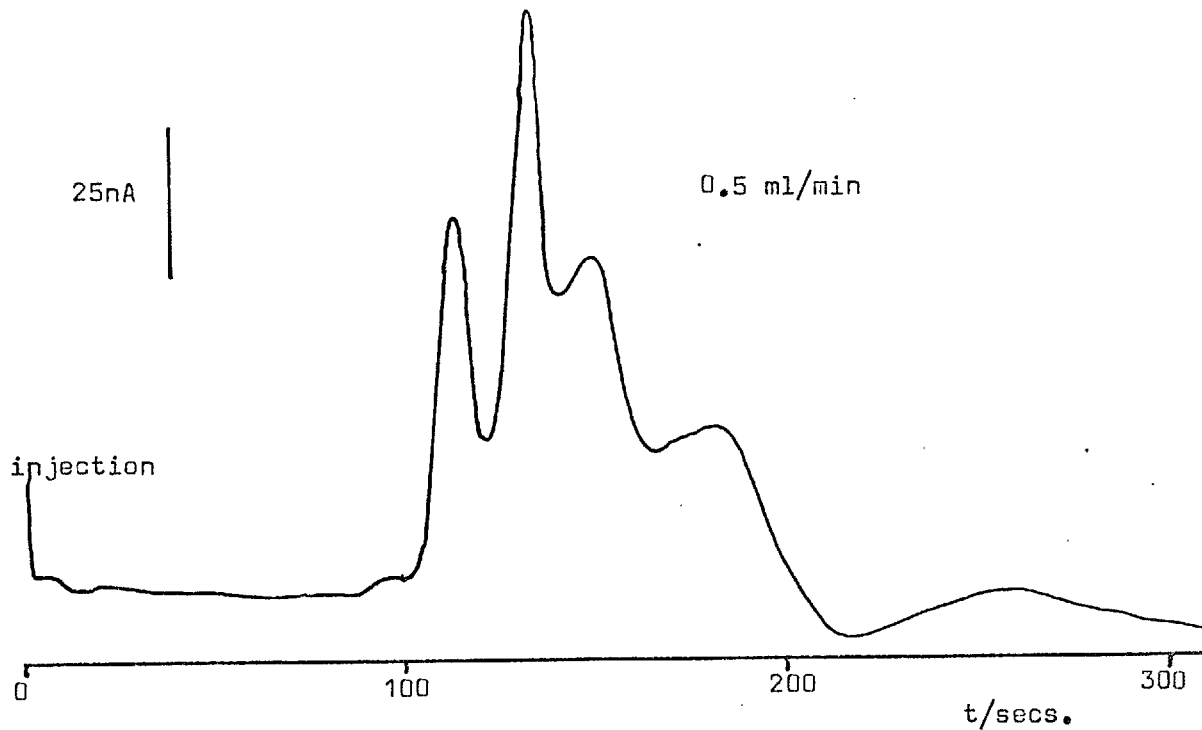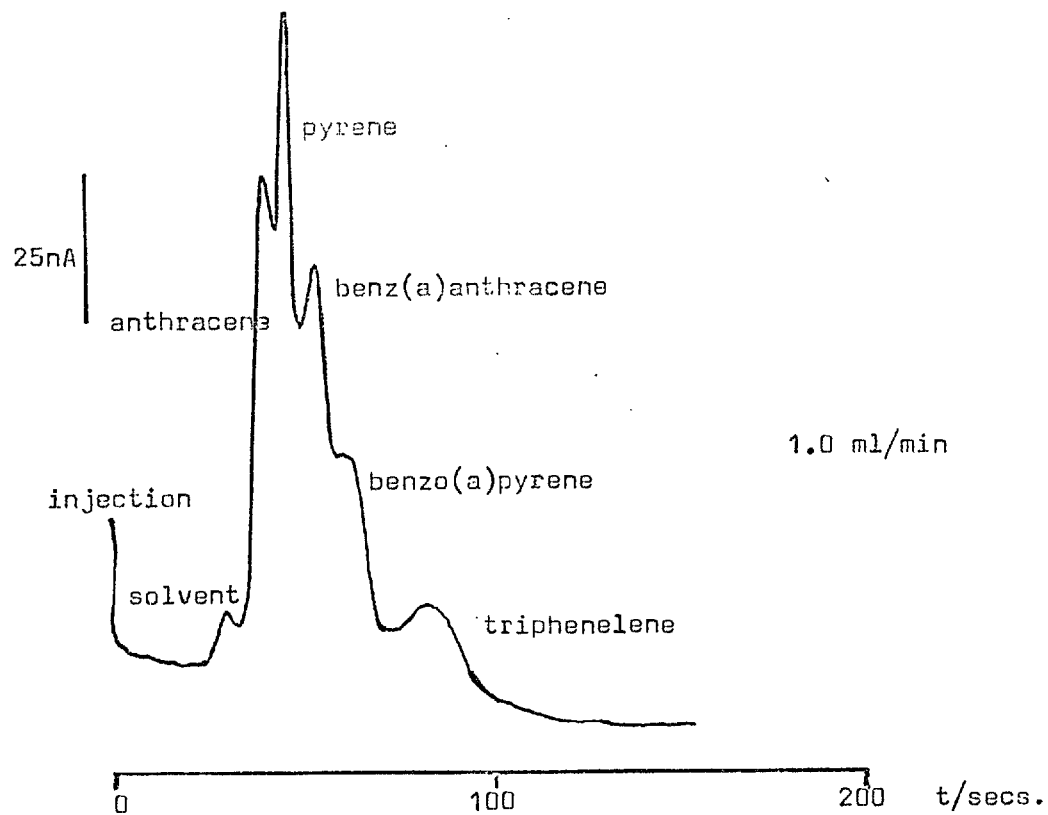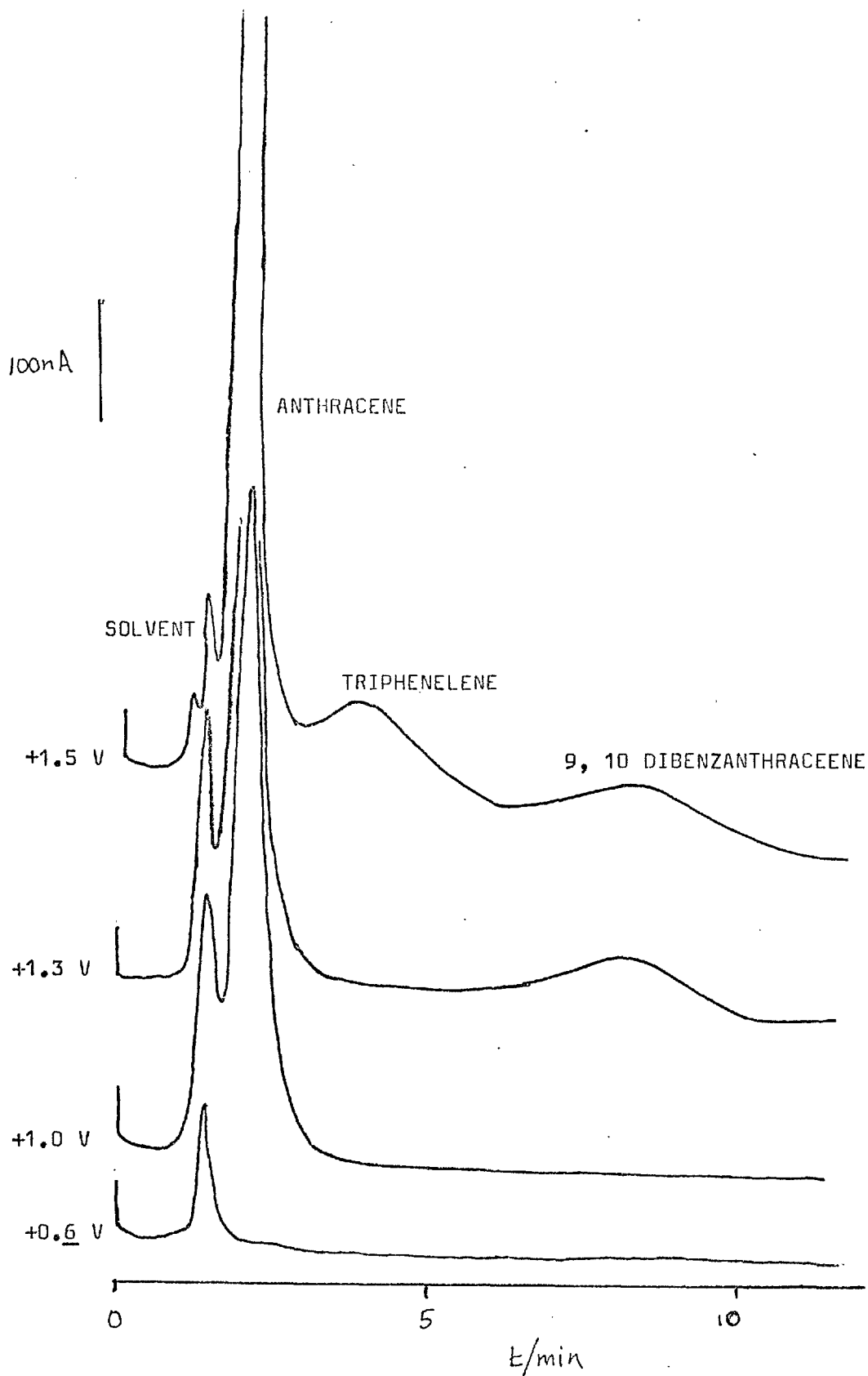
SUGGESTIONS FOR FURTHER WORK

The work that has been presented in chapters I and II has

shown how the electrocatalytic properties of glassy carbon can be altered

by chemical modification of the surface. Obviously this work has been

only a preliminary study; what is required is a more sophisticated

approach to chemical pretreatment. as well as more experimental work

on the influence of pretreatment on a greater variety of electrode

processes than has been given here.

In chapter III it was established that the wall-jet cell,

of the design configuration used in this work, is hydrodynamically,a

well defined system. Apart from its more obvious continuous monitoring

applications, it could be also used for more theoretical kinetic studies.

For instance, a ring-disk configuration could be used to study

electrochemically generated intermediates (as has been done with the

rotating ring disk electrode). The advantage of the wall-jet cell is

that cah be used for 'on line' kinetic studies; for example, of substances

in a reaction vessel.

Finally , the use of the wall-jet cell in HPLC has only

covered a limited number of applications. There still remains a large

range of compounds that can be determined. One area which has not been

looked at in great depth is post column derivatization; this requires

more work.

REFERENCES

1. W.L. Reynolds and R.W. Lumnry,   Mechansims of Electron Transfer Ronald Press 1966 US.

2. R. Parsons,   Modern Aspects of Electrochemistry, Vol. 1, Butterworths, London, 1969.

3. A.N. Frumkin,   J. Colloid Sci., 1 (1946) 290.

4. J. OM. Bockris and A.K.N. Reddy,   Modern Electrochemistry Vol. 2, Macdonald London, 1970.

5. S. Yamada and H. Sato,   Nature (London), 193 (1962) 261.

6. A.I. Scott,   Quart Rev., (London) 19 (1965) 1.

7. D.H. Evans,   Accounts of Chem. Res., 10 (1977) 313.

8. T.M. Florence,   J. Electroanal. Chem., 27 (1970) 273.

9. T. Berger,   PhD Thesis, London 1975.

10. M. Butcha and L.J. Papa,   J. Chromatogr. Sci., 14 (1976) 213.

11. J.F. Alder, P.O. Kane and B. Fleet,   J. Electronal. Chem., 30 (1971) 427.

12. M. Brezina and A. Hofmanova,   Collec. Czech. Chem. Common., 38 (1973) 985.

13. M. Stulikova and F. Vydra,   J. Electroanal. Chem., 38, (1972) 349.

14. R.J. Taylor and A.A. Humffray,   J. Electroanal. Chem. 42 (1973) 347.

15. J.C. Lewis, B. Redfern and F.C. Cowlard,   Solid State Electronics, 6 (1963) 251.

16. F.C. Cowlard and J.C. Lewis,   J. Material Science, 2 (1967) 507.

17. J.P. Randin and E. Yeager,   J. Electrochem Soc., 118 (1971) 711.

18. J.P. Randin and E. Yeager,   J. Electroanal. Chem. 36 (1972) 257.

19. G.R. Hennig,   Progr. Inorg. Chem., 1 (1961) 143.

20. A.R. Ubbelohde and F.A. Lewis,   Graphite and its Crystal Compounds, Oxford Univ. Press, London 1960.

21. T. Tsuzuku and K. Saito, Jap. J. Appl. Phys. $\underline{9}$ (1966) 738.

22. J.P. Randin and E. Yeager, J. Electroanal. Chem., $\underline{58}$ (1975) 323.

23. P.R. Wallace, Phys, Rev. $\underline{71}$ (1947) 622.

24. R.E. Panzer and P.J. Elving, Electrochim. Acta. $\underline{20}$ (1975) 635

25. H.P. Boehm, E. Diel, W.Heck and R. Sappok, Angew Chem. Int. Ed. $\underline{3}$ (1964) 669.

26. G.R. Hennig, Proc. Conf. Carbon, $\underline{1}$ (1961) 143.

27. V.A. Garten and D.E. Weiss, Australian J. Chem., $\underline{10}$ (1957) 309.

28. A. Dodson and V.J. Jennings, Anal. Chim Acta., $\underline{72}$ (1974) 205.

29. D. Laser and M. Ariel, J. Electroanal. Chem.,$\underline{52}$ (1974) 291.

30. G. Mamantov, D.R. Freeman, F.J. Miller and H.E. Zittell, J. Electroanal. Chem. $\underline{9}$ (1965) 305.

31. J.V. Hallum and H.V. Donshel, J. Phys. Chem.,$\underline{62}$ (1958) 1502.

32. R.E. Panzer and P.J. Elving, J. Electrochem. Soc.,$\underline{119}$ (1972) 864.

33. J.S. Mattson and H.B. Mark Jr., J. Colloid and Interfac. Sci., $\underline{31}$ (1969) 131.

34. B.D. Epstein, E, Dalle Molle and J.S. Mattson, Carbon,$\underline{9}$ (1971) 609.

35. J. Dolezal and K. Stulik, J. Electroanal. Chem.,$\underline{17}$ (1968) 87.

36. H.P. Boehm, Advan. Catalysis,$\underline{16}$ (1966) 179.

37. H.P. Boehm and M. Voll, Carbon,$\underline{8}$ (1970) 227.

38. K.F. Blurton, Electrochim. Acta,$\underline{18}$ (1973) 869.

39. K.F. Blurton, P. Greenberg, H.G. Oswin and D.R. Rutt, J. Electrochem. Soc., $\underline{119}$ (1972) 539.

40. S. Gilman, Electroanal. Chem., A.J. Bard Ed. Marcel Dekker, NY,1967.

41. R. Thacker and J.P. Hoare, J. Electroanal. Chem.,$\underline{30}$ (1970) 14.

42. S.E.S El. Wakked and S₉H. Emra, J. Chem. Soc. (1952) 461.

43. J.P. Hoare, Advances in Electrochem. and Electrochemical Eng. P. Delahay and C.W. Tobias Ed.,Vol. 6,1967.

44. J.F. Evans and T. Kuwana,   Anal. Chem. <u>49</u> (1977) 1632.

45. W.J. Albery,   Electrode Kinetics, Clarendon Press, Oxford, 1975.

46. J.M. Hale,   Reactions of Molecules at Electrodes, Ed. N.S. Hush, J. Wiley and Sons, London, 1971.

47. H. Gerischer,   Discussions of the Faraday Soc., Intermediates in Electrochem. Reactions., (1973) 7.

48. H. Gerischer,   Ann. Rev. Physical Chem., <u>12</u> (1961) 227.

49. K.J. Vetter   Electrochemical Kinetics, Academic Press, N Y, 1967.

50. S.D. Argarde and E. Gileadi,   Electrosorption, E. Gileadi Ed., Plenum Press, N Y, 1967.

51. H. Gerischer,   Advances in Electrochem. and Electrochemical Eng., Vol.1, Interscience, 1961.

52. H. Gersicher,   Z. Physik. Chem., <u>27</u> (1961) 48.

53. A.K. Vijh,   Electrochemistry of Metals and Semiconductors , Marcel Dekker, N.Y., 1973.

54. F.C. Anson,   J. Amer. Chem. Soc. <u>81</u> (1959) 1554.

55. D.G. Davis,   Talanta,   <u>3</u> (1960) 335.

56. V.I. Vaselovskii and T.I. Borisova,   Zh. Fiz. Khim. <u>27</u> (1953) 1195.

57. M. Fleschman, K. Korinek and D. Pletcher,   J. Electroanal. Chem. <u>31</u> (1971) 39.

58. M. Fleishman, K. Korinek and D. Pletcher,   J. Chem. Soc. Perkin Trans. II, (1972) 1392.

59. R.W. Coughlin and F.S. Ezra,   Environ. Sci. Technol. <u>2</u>(1968) 291.

60. P.L. Walker Jr., L.G. Austin and J.J. Tietjen,   Chemistry and Physics of Carbon,   RL. Walker Ed. <u>1</u> (1965) 328.

61. R.E. Parker and R.N. Adams,   Anal. Chem. <u>28</u> (1956) 828.

62. R.H. Wopschall and I. Shain,   Anal. Chem. <u>39</u> (1967) 1514.

63. H.L. Piette, P. Ludwig and R.N. Adams,   Anal. Chem. 34 (1962) 916.

64. R.C. Snowdon,   J. Phys. Chem., 15 (1911) 797.

65. P.T. Kissinger,   Interface, 20 (1977) 2.

66. D.S. Villars,   J. Amer. Chem. Soc., 70 (1948) 3655.

67. P.R. Moses and R.J. Murray,   J. Amer. Chem. Soc. 98 (1976) 7435.

68. C.M. Elliot and R.W. Murray,   Anal. Chem., 48 (1976) 1247.

69. R.G. Clem,   Anal. Chem., 47 (1975) 1778.

70. H. Hart and R.D. Schultz,   Lab Manual for Organic Chemistry,
Houghton Mifflin and Co., Boston, 1967.

71. J. Kaoryta, J. Dvorak and V. Bohackova,   Electrochemistry,
Methuen and Co., London, 1970.

72. R. Parsons,   Trans. Faraday Soc., 54 (1958) 1035.

73. W.J. Blaedel and R.A. Jenkins,   Anal. Chem. 46 (1974) 1952.

74. L. Antrop,   Theoretical Electrochemistry, MIR Publishers,
Moscow, 1972.

75. R.A. Marcus,   J. Phys. Chem. 67 (1973) 853.

76. R.N. Adams,   Electrochemistry at Solid Electrodes,
Marcel Dekker, 1969.

77. A. Sevcik,   Collection, Czech. Chem. Commun.,
13 (1948) 349.

78. J.E.B. Randles,   Trans. Faraday Soc. 44 (1948) 327.

79. S. Das. Gupta   PhD Thesis, London Univ. 1975.

80. C.J. Little,   PhD Thesis, London Univ., 1974.

81. M.B. Glauert,   J. Fluid Mech. 1 (1956) 625.

82. J. Yamada and H. Matsuda,   J. Electroanal. Chem. 44 (1973) 189.

83. D.B. Spalding,   A.R.C. Report No. 25925, (1964).

84. A. Sicalla,   Aircraft Eng., Vol. 30131, (1958).

85. P. Delahay,   New Instrumental Methods in Electrochemistry,

Interscience, N.Y. 1954.

86. J. Jordan, R.A. Javick and W.E. Ranz,   J. Amer. Chem. Soc.,

80, (1959) 3846.

87. V.G. Levich,   Discussions Faraday Soc., 1 (1947) 37.

88. L.N. Klatt and W.J. Blaedel,   Anal. Chem., 40 (1968) 512.

89. V.G. Levich,   Acta. Physichim. URSS 17 (1942) 257.

90. J. Yamada and H. Matsuda,   J. Electroanal. Chem. 30 (1971) 271.

91. H. Matsuda and J. Yamada,   J. Electranal. Chem., 30 (1971) 261.

92. J.S. Bazau, S.L. Marchiano, J.J. Podesta and A.J. Arvia,

Electrochim. Acta. 12 (1967) 809.

93. H. Matsuda,   J. Electroanal. Chem., 16 (1948) 153.

94. B. Fleet and C.J. Little,   J. Chromatogr. Sci. 12 (1974) 747.

95. L. Prandtl,   Phys. Zeit. 11 (1910) 1072.

96. V.G. Levich,   Physico-Chemical Hydrodynamics,

Prentice Hall, N J, 1963.

97. T. Von. Karman,   Z. Angew Math Mech., 1 (1921) 233.

98. A.C. Riddiford,   Advan. Electrochem. and Electrochemical

Eng. 4 (1966) 47.

99. G. Birchoff and G.H. Zarruntonello,   Jets, Wakes and Cavities,

Academic Press N.Y. 1957.

100. L.R. Snyder and J.J. Kirkland,   Introduction to Modern Liquid

Chromatography,   John Wiley and Sons, 1974.

101. J.H. Knox and J. Jurand,   J. Chromatogr. 125 (1976) 39.

102. Paired Ion Chromatography,   Waters Assoc. Bulletin, Dec. 1975.

103. J. Polesuk, D.G. Howery,   J. Chromatogr. Sci. 11 (1973) 226.

104. M.N. Munk,   J. Chromaotogr. Sci. 8 (1970) 491.

105. J.J. Kirkland,   Anal. Chem., 40 (1968) 391.

106. J.J. Kirkland,   Analyst 99 (1974) 859.

107. J. Bland,   PhD Thesis London Univ. 1976.

108. J.G. Koen, JFK Huber, H. Popper, and G. den Boef,

J. Chromatogr. Sci. 8 (1970) 192.

109. D.C. Johnson and J. Larochelle,   Talanta, 20 (1973) 959.

110. Y. Takata and G. Muto,   Anal. Chem. 45 (1973) 1864.

111. S. Das Gupta,   PhD Thesis, London Univ. 1975.

112. P.T. Kissinger,   Review Anal. Chem. 49 (1977).

113. R.N. Adams,   Anal. Chem. 30 (1958) 1576.

114. M. Varadi, Zs. Feher and E. Pungor,   J. Chromatogr., 90 (1974) 259.

115. C.J. Little,   PhD Thesis, London Univ, 1975.

116. P.T. Kissinger, R.M. Riggin, R.L. Alcorn and L.D. Rau,

Biochem. Med., 13 (1975) 299.

117. W,D. Slaunwhite, L.A. Pachla, D.L. Wenke, and P.T. Kissinger,

Clin. Chem.,21 (1975) 1427.

118. P.T. Kissinger, C.J. Refshauge, R. Dreiling and R.N. Adams,

Anal. Lett. 6 (1973) 465.

119. L.J. Felice and P.T. Kissinger,   Anal. Chem. 48 (1976) 794.

120. P.T. Kissinger, L.J. felice, R.M. Riggin and L.A. Pachla,

Clin. Chem., 20 (8) (1974) 992.

121. H.O. House, E. Feng and N.P. Peet,   J. Org. Chem.,36 (1971)2371.

122. F. Spielman, M.A. Goldberger and R.T. Frank, J. Amer. Med Assoc.

101 (1933) 266.

123. J. Stevens, Middlesex Hospital, London, Personal Communication.

124. S.L. Cohen,   J. Clin. Endocrinol. Metab.,
26 (1966) 994.

125. M.G. Coyle and J.B. Brown,   J. Obstet. Gynoecol. Brit.
Commonwealth, 70 (1963) 225.

126. B. Neher,   Steroid Chromatography, Elsevier, Amsterdam, 1964.

127. Applied Science Labs, Application Sheets.

128. R.A. Henry, J.A. Schmitt and J.F. Dietkman,   J. Chromatogr. Sci.,
9 (1971) 513.

129. W.S. Bauld,   Biochem. J.,59 (1955) 294.

130. J.F.K Huber, J.AR. J. Hulsman and C.A.M. Meijers,   J. Chromatogr.,
62 (1971) 79.

131. J.H. Knox and J. Jurand,   J. Chromatogr.,125 (1976) 39.

132. L.A. Pachla and P.T. Kissinger,   Anal. Chem. 48 (1976) 364.

133. R. F. Nelson,   Technique of Electrorganic Synthesis Part II,
Norman Weinberg Ed. , John Wiley and Sons, 1975.

134. A.S.V. Burgen and J.F. Mitchell,   Gaddums Pharmacology,
Seventh Edition, Oxford Medical Publications, London 1972.

135. G. Dryhurst and P.J. Elving,   J. Electrochem. Soc. 115 (1968) 1014.

136. B. Proksa and L Molnar,   Anal. Chim. Acta., 97 (1978) 149.

137. E.F. Domino,   Ann. Rev. Pharmacol., 6 (1962) 217.

138. H. Siegerman and G. O'Dom,   Amer. Lab. June 1972.

139. N.B. Fouzder,   PhD Thesis, London Univ.,1975.

140. D. Jagner and L. Kryger,   Anal. Chim. Acta. 80 (1975)255.

141. R,W. Andrews and D.C. Johnson,   Anal. Chem., 48 (1976) 1056.

142. W.J Settineri and L.D. McKeever,   Tehnique of Electroorganic,
Synthesis Part II, N. Weinberger Ed., John Wiley and Sons, 1975.

143. The Consequences of Smoking,   U S Dept. of Health, Education

and Welfare Publication, 1973.

144. Tobacco Smoke Chemistry Project, Dept. of Health Publication

July 1976.

145. F.J. Vermillion Jr. and I.A. Pearl,   J. Electrochem. Soc. 111 (1964)

1392.

146. S.D. Ross, M. Finklestein and E.J. Rudd,   Anodic Oxidation,

Academic Press 1975.

147. V.L. Snoeyink and W.J. Weber,   Environ. Sci. Technol. 1 (1967) 228.

148. M.L. Lee and R.A. Hites,   Anal. Chem., 48 (1976) 1890.

149. G.M. Janim, K. Johnston and W.Z. Zielinski,   Anal. Chem. 47 (1975) 670.

150. R.F. Severson, M.E. Snook, R.F. Arrendale and O.T. Chortyk,

Anal. Chem. 48 (1976) 1866.

151. Chemical and Engineering News,   Sept.1977, pg. 4.

152. E. Clar,   Polycyclic Hydrocarbons, . Academic Press n y, 1964.

153. W.G. Neikam and M.M. Desmond,   J. Electrochem. Soc. 111 (1964) 1190.

154. R. Zahradnik and V. Parkanyi,   Talanta 12 (1965) 1289.

155. J.W. Loveland and G.R. Dimeler,   Anal. Chem. 33 (1961) 1196.

156. L. Eberson and K. Nyberg,   J. Amer. Chem. Soc. 88 (1966) 1686.

157. J.F. Coetzee, G.H. Kazi and J.C. Spurgeon,   Anal. Chem. 48 (1976) 2171.

158. R.B. Sleight,   J. Chromatogr. 83 (1973) 31.

159. J.H. Weber and H.H. Oelert,   Separ. Sci. 5 (1970) 669.

160. H. J. Klimisch,   Z- Anal. Chem., 264 (1973) 275.

161. M.A. Fox and S.W. Staley,   Anal. Chem., 48 (1976) 992.